

**A SYNTHETIC, SPECTROSCOPIC AND MAGNETIC SUSCEPTIBILITY STUDY OF
SELECTED MAIN GROUP AND TRANSITION METAL FLUORO COMPOUNDS**

By

M. SHAH ROSHAN CADER

M.Sc., The University of British Columbia, 1986

A THESIS SUBMITTED IN PARTIAL FULFILLMENT OF
THE REQUIREMENTS FOR THE DEGREE OF
DOCTOR OF PHILOSOPHY

in

THE FACULTY OF GRADUATE STUDIES
(Department of Chemistry)

We accept this thesis as conforming
to the required standard

THE UNIVERSITY OF BRITISH COLUMBIA

April, 1992

© M.S.R. CADER, 1992

In presenting this thesis in partial fulfilment of the requirements for an advanced degree at the University of British Columbia, I agree that the Library shall make it freely available for reference and study. I further agree that permission for extensive copying of this thesis for scholarly purposes may be granted by the head of my department or by his or her representatives. It is understood that copying or publication of this thesis for financial gain shall not be allowed without my written permission.

Department of CHEMISTRY

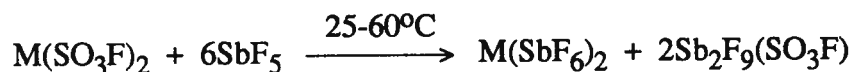
The University of British Columbia
Vancouver, Canada

Date OCTOBER 7, 1992

ABSTRACT

This study was initiated in order to synthesize, and where appropriate, to investigate the magnetic properties of selected main group and transition metal cationic complexes, all stabilized by weakly basic fluoro anions derived either from the Brønsted superacids HSO_3F and HSO_3CF_3 , or the Lewis acids SbF_5 and AsF_5 .

Of the preparative reactions, the solvolysis of metal(II) fluorosulfates in excess SbF_5 according to:



with $\text{M}=\text{Ni}$, Pd , Cu , Ag or Sn , is found to be a useful synthetic route to the corresponding divalent hexafluoro antimonates. The products, as their precursors, are characterized as CdCl_2 -type layered polymeric compounds. Relevant vibrational (Raman and IR), electronic and ^{119}Sn -Mössbauer spectra as well as magnetic susceptibility measurements and X-ray powder data are reported. Several compounds prepared by this method display unusual features: $\text{Pd}(\text{SbF}_6)_2$ is, like its fluorosulfate precursor, paramagnetic with the Pd^{2+} ion in a $^3\text{A}_{2g}$ ground state. $\text{Ag}(\text{SbF}_6)_2$, unlike its paramagnetic blue valence isomer, is diamagnetic and nearly white in color, and is formulated as the mixed valency complex $\text{Ag}(\text{I})[\text{Ag}(\text{III})(\text{SbF}_6)_4]$. The $\text{Cu}(\text{SbF}_6)_2$ compound also contains, in addition to Cu^{2+} ions, small quantities of $\text{Cu}(\text{I})$ and $\text{Cu}(\text{III})$ ions. Both $\text{Ni}(\text{SbF}_6)_2$ and $\text{Pd}(\text{SbF}_6)_2$ exhibit temperature dependent low magnetic moments, indicative of antiferromagnetic exchange. $\text{Pd}(\text{SbF}_6)_2$ also displays very weak ferromagnetism below $\sim 10\text{K}$.

The $\text{Sn}(\text{SbF}_6)_2$ product from the above synthesis, and its precursor $\text{Sn}(\text{SO}_3\text{F})_2$, react with excess 1,3,5-trimethylbenzene (mesitylene or mes) to give the π -arene adducts $\text{Sn}(\text{SbF}_6)_2 \cdot 2\text{mes}$ and $\text{Sn}(\text{SO}_3\text{F})_2 \cdot \text{mes}$ in high yield. The adducts are characterized by elemental analysis and infrared spectra. The adduct formation is followed by ^{119}Sn Mössbauer spectroscopy. It is found that only tin(II) compounds with large, weakly nucleophilic anions are capable of forming mesitylene complexes, while SnCl_2 , SnF_2 , and stannocene do not give any indication of adduct formation under similar reaction conditions.

The divalent fluorosulfates $\text{Ni}(\text{SO}_3\text{F})_2$, $\text{Pd}(\text{SO}_3\text{F})_2$ and $\text{Ag}(\text{SO}_3\text{F})_2$, precursors to the $\text{M}(\text{SbF}_6)_2$ compounds, and the mixed valency $\text{Pd}(\text{II})[\text{Pd}(\text{IV})(\text{SO}_3\text{F})_6]$, as well as their corresponding trifluoromethylsulfate derivatives $\text{Ni}(\text{SO}_3\text{CF}_3)_2$, $\text{Pd}(\text{SO}_3\text{CF}_3)_2$ and $\text{Ag}(\text{SO}_3\text{CF}_3)_2$, investigated for their magnetic behavior by susceptibility studies down to ~ 4 K, show significant magnetic exchange, and except in $\text{Ag}(\text{SO}_3\text{CF}_3)_2$, the onset of magnetic exchange becomes observable at low temperatures. The fluorosulfates are found to exhibit strong ferromagnetism below ~ 11 K, whereas the trifluoromethylsulfates behave as antiferromagnets with the spin interactions noted over a wider temperature range. The maximum magnetic susceptibilities of $\text{Ni}(\text{SO}_3\text{F})_2$, $\text{Pd}(\text{SO}_3\text{F})_2$ and $\text{Ag}(\text{SO}_3\text{F})_2$ indicate saturation magnetization, and hence for these compounds field dependent maximum magnetic moments are obtained in the temperature range ~ 5 to 10.5 K. Maxima in the susceptibility vs. temperature plots are noted for the antiferromagnets $\text{Pd}(\text{SO}_3\text{CF}_3)_2$ and $\text{Ag}(\text{SO}_3\text{CF}_3)_2$ at ~ 4 and ~ 13 K respectively. Unlike in the corresponding divalent antiferromagnetic fluorides, no spin canting is detected in the trifluoromethylsulfates at lower temperatures.

Magnetic susceptibility measurements to ~ 4 K are also carried out for the main group molecular cations within $\text{O}_2^+[\text{AsF}_6]^-$, $\text{Br}_2^+[\text{Sb}_3\text{F}_{16}]^-$ and $\text{I}_2^+[\text{Sb}_2\text{F}_{11}]^-$. The data are interpreted utilizing previous results from photoelectron spectroscopy, known crystal structures, magnetic studies on the superoxide ion and the ozonide ion, and in the case of $\text{O}_2^+[\text{AsF}_6]^-$, previous ESR studies.

The magnetic properties of the three materials are quite different. $\text{Br}_2^+[\text{Sb}_3\text{F}_{16}]^-$ obeys Curie-Weiss law between 80 and 4 K. The magnetic moment decreases slightly from $2.04 \mu_{\text{B}}$ at room temperature to $1.93 \mu_{\text{B}}$ at 4 K. $\text{I}_2^+[\text{Sb}_2\text{F}_{11}]^-$ exhibits relatively strong antiferromagnetic coupling with a maximum in χ_{M} observed at -54 K. The magnetic moment (corrected for TIP) decreases from $1.92 \mu_{\text{B}}$ at 124 K to $0.41 \mu_{\text{B}}$ at 4 K. Experimental susceptibilities for this compound over the temperature range 300-4 K have been compared to values calculated using three different theoretical models for extended chains of antiferromagnetically coupled paramagnetic species. $\text{O}_2^+[\text{AsF}_6]^-$ exhibits Curie-Weiss behavior over the temperature range 60-2 K. The magnetic moment, uncorrected for TIP, varies from $1.63 \mu_{\text{B}}$ at 80 K to $1.17 \mu_{\text{B}}$ at 2 K, and the presence of weak antiferromagnetic coupling in this material is suggested.

TABLE OF CONTENTS

	Page
ABSTRACT	ii
LIST OF TABLES	ix
LIST OF FIGURES	xi
LIST OF SYMBOLS	xiii
ACKNOWLEDGEMENTS	xiv
CHAPTER 1	
INTRODUCTION	1
1.1 General Introduction	1
1.2 The Lewis Acid SbF_5	3
1.2.1 Physical and Chemical Properties	3
1.2.2 Cationic Derivatives	4
1.3 The Transition Metal Fluorosulfates and Trifluoromethyl-sulfates	9
1.4 Post-Transition Metal Arene Π -Compounds	13
1.5 Magnetic Measurements	16
1.6 Objectives of this Study	20
References	22
CHAPTER 2	
GENERAL EXPERIMENTAL	27
2.1 Introduction	27
2.2 Chemicals	27
2.2.1 Purification Methods	29
2.2.2 Synthetic Methods	29

	Page	
2.3	Apparatus	31
2.3.1	Reaction Vessels	33
2.3.2.	SbF ₅ Storage-bridge Vessel	33
2.3.3	S ₂ O ₆ F ₂ - Addition Trap	33
2.3.4	Pyrex Vacuum Line	37
2.3.5	Metal Vacuum Line	37
2.3.6	Dry Atmosphere Box	37
2.4	Instrumentation and Methods	38
2.4.1	Infrared Spectroscopy	38
2.4.2	Raman Spectroscopy	38
2.4.3	Nuclear Magnetic Resonance Spectroscopy	38
2.4.4	Electronic Spectroscopy	39
2.4.5	Mössbauer Spectroscopy	39
2.4.6	X-ray Photoelectron Spectroscopy	39
2.4.7	Magnetic Susceptibility Measurements	40
2.4.8	X-ray Powder Diffractometry	41
2.4.9	Differential Scanning Calorimetry (DSC)	41
2.4.10	Elemental Analyses	42
	References	42
CHAPTER 3	METAL(II) HEXAFLUORO ANTIMONATES M(SbF₆)₂, M(II) = Sn(II), Ni(II), Pd(II), Cu(II) AND Ag(II)	43
3.1	Introduction	43
3.2	Experimental	46
3.2.1	General Synthetic Scheme to M(SbF ₆) ₂	46
3.2.2	Physical Properties and Analyses	47
3.2.2a	Cu(SbF ₆) ₂	48

	Page
3.2.2b Pd(SbF ₆) ₂	48
3.2.2c β-Ag(SbF ₆) ₂	48
3.2.3 Alternate Synthetic Route to β-Ag(SbF ₆) ₂	48
3.3 Results and Discussion	49
3.3.1 Synthesis	49
3.3.2 Vibrational Spectra	55
3.3.3 Electronic Spectra	62
3.3.4 Magnetic Susceptibility Measurements	66
3.3.5 X-ray Photoelectron Spectra	82
3.3.6 Attempted Synthesis of Au(SbF ₆) ₂	83
3.4 Conclusion	85
References	87
CHAPTER 4	
MESITYLENE ADDUCTS OF TIN(II) FLUORO COMPOUNDS, Sn(SO₃F)₂·C₉H₁₂ and Sn(SbF₆)₂·2C₉H₁₂	90
4.1 Introduction	90
4.2 Experimental	93
4.2.1 Synthesis	93
4.2.1a Synthesis of Sn(SO ₃ F) ₂ ·1,3,5-(CH ₃) ₃ C ₆ H ₃	93
4.2.1b Synthesis of Sn(SbF ₆) ₂ ·2[1,3,5(CH ₃) ₃ C ₆ H ₃]	94
4.3 Results and Discussion	95
4.3.1 Synthesis	95
4.3.2 ¹¹⁹ Sn Mössbauer Spectra	99
4.3.3 Infrared spectra	101
4.4 Conclusion	108
References	108

		Page
CHAPTER 5	A LOW TEMPERATURE MAGNETIC STUDY OF THE MOLECULAR CATIONS O₂⁺, Br₂⁺ AND I₂⁺	111
5.1	Introduction	111
5.2	Experimental	112
5.3	Results and Discussion	113
5.3.1	Synthesis	114
5.3.2	Magnetic Measurements	118
5.3.3	Br ₂ ⁺ [Sb ₃ F ₁₆] ⁻	118
5.3.4	O ₂ ⁺ [AsF ₆] ⁻	126
5.3.5	I ₂ ⁺ [Sb ₂ F ₁₁] ⁻	130
5.4	Conclusion	136
	References	137
CHAPTER 6	MAGNETIC EXCHANGE IN M(II) SULFONATES, M(II) = Ni(II), Pd(II) AND Ag(II)	141
6.1	Introduction	141
6.2	Experimental	144
6.3	Results and Discussion	144
6.3.1	Ferromagnetism of M(II) fluorosulfates Ni(SO ₃ F) ₂ , Pd(SO ₃ F) ₂ , Pd(II)[Pd(IV)(SO ₃ F) ₆] and Ag(SO ₃ F) ₂	145
6.3.2	Antiferromagnetism of M(II) trifluoromethylsulfates Ni(SO ₃ CF ₃) ₂ , Pd(SO ₃ CF ₃) ₂ and Ag(SO ₃ CF ₃) ₂	163
6.4	Conclusion	176
	References	178
CHAPTER 7	SUMMARY AND GENERAL CONCLUSIONS	181
APPENDIX A		185
APPENDIX B		194

LIST OF TABLES

		Page
Table 1.1:	Solid Polyhalogen Cationic Derivatives of SbF_5	5
Table 1.2:	Solid Binary Transition Metal Derivatives of SbF_5	6
Table 2.1:	Chemicals Used Without Purification	28
Table 3.1:	Vibrational Spectra of $\text{Ni}(\text{SbF}_6)_2$, $\text{Pd}(\text{SbF}_6)_2$ and $\text{Cu}(\text{SbF}_6)_2$	56
Table 3.2:	Vibrational Spectra of the Two Valence Isomers of $\text{Ag}(\text{SbF}_6)_2$	57
Table 3.3:	Electronic Transitions and Ligand Field Parameters for $\text{Ni}(\text{SbF}_6)_2$, $\text{Pd}(\text{SbF}_6)_2$ and Related Compounds	64
Table 3.4:	Low Temperature Magnetic Data of $\text{Ni}(\text{SbF}_6)_2$	67
Table 3.5:	Low Temperature Magnetic Data of $\text{Pd}(\text{SbF}_6)_2$	68
Table 3.6:	Low Temperature Magnetic Data of $\text{Cu}(\text{SbF}_6)_2$	69
Table 3.7:	Magnetic Moment Data of $\text{Ni}(\text{SbF}_6)_2$ for the Temperature Range ~80 to 295 K	75
Table 4.1:	^{119}Sn Mössbauer Parameters of Relevant Tin(II) Compounds at 80 K	100
Table 4.2:	Infrared Bands of Liquid Mesitylene and Bands Attributed to Mesitylene in the Adducts $\text{Sn}(\text{SO}_3\text{F})_2 \cdot \text{mes}$ and $\text{Sn}(\text{SbF}_6)_2 \cdot 2\text{mes}$	104
Table 4.3:	Infrared Frequencies for $\text{Sn}(\text{SO}_3\text{F})_2$ and $\text{Sn}(\text{SbF}_6)_2$ and Bands Attributed to the Anions in the Mesitylene Adducts $\text{Sn}(\text{SO}_3\text{F})_2 \cdot \text{mes}$ and $\text{Sn}(\text{SbF}_6)_2 \cdot 2\text{mes}$	106
Table 5.1:	Magnetic Data of $\text{Br}_2^+[\text{Sb}_3\text{F}_{16}]^-$	119
Table 5.2:	Magnetic Data of $\text{I}_2^+[\text{Sb}_2\text{F}_{11}]^-$ and $\text{O}_2^+[\text{AsF}_6]^-$	120
Table 5.3:	Structural and Spectroscopic Information on $\text{O}_2^+[\text{AsF}_6]^-$, $\text{I}_2^+[\text{SbF}_{11}]^-$, $\text{Br}_2^+[\text{Sb}_3\text{F}_{16}]^-$ and the corresponding Ions O_2^+ , Br_2^+ and I_2^+	121
Table 6.1:	Low Temperature Magnetic Data of $\text{Ni}(\text{SO}_3\text{F})_2$	146
Table 6.2:	Low Temperature Magnetic Data of $\text{Pd}(\text{SO}_3\text{F})_2$	147
Table 6.3:	Low Temperature Magnetic Data of $\text{Pd}(\text{II})[\text{Pd}(\text{IV})](\text{SO}_3\text{F})_6]$	148
Table 6.4:	Low Temperature Magnetic Data of $\text{Ag}(\text{SO}_3\text{F})_2$	149
Table 6.5:	Magnetic Data of $\text{Ni}(\text{SO}_3\text{F})_2$ for the Temperature Range 291 to 79 K	150

	Page
Table 6.6: Magnetic Parameters of $\text{Ni}(\text{SO}_3\text{F})_2$, $\text{Pd}(\text{SO}_3\text{F})_2$, $\text{Pd}(\text{II})[\text{Pd}(\text{IV})(\text{SO}_3\text{F})_6]$ and $\text{Ag}(\text{SO}_3\text{F})_2$	151
Table 6.7: Experimental and Calculated Saturation Magnetic Susceptibilities of $\text{Ni}(\text{SO}_3\text{F})_2$, $\text{Pd}(\text{SO}_3\text{F})_2$, $\text{Pd}(\text{II})[\text{Pd}(\text{IV})(\text{SO}_3\text{F})_6]$ and $\text{Ag}(\text{SO}_3\text{F})_2$	157
Table 6.8: Magnetic Data of $\text{Ag}(\text{SO}_3\text{CF}_3)_2$ for the Temperature Range 304 to 4 K	164
Table 6.9: Low Temperature Magnetic Data of $\text{Pd}(\text{SO}_3\text{CF}_3)_2$	165
Table 6.10: Low Temperature Magnetic Data of $\text{Ni}(\text{SO}_3\text{CF}_3)_2$	166
Table 6.11: Magnetic Data of $\text{Ni}(\text{SO}_3\text{CF}_3)_2$ for the Temperature Range 292 to 80 K	167

LIST OF FIGURES

	Page
Figure 2.1: Apparatus for Preparing $S_2O_6F_2$	30
Figure 2.2: Typical Pyrex Reaction Vessels	32
Figure 2.3: Vacuum Filtration Apparatus	34
Figure 2.4: Kel-F Tubular Reactor	35
Figure 2.5: SbF_5 Storage-bridge Vessel	36
Figure 3.1: Raman Spectrum of β - $Ag(SbF_6)_2$	58
Figure 3.2: Crystal Structure of α - $Ag(SbF_6)_2$	60
Figure 3.3: Spin Allowed Electronic Transitions from $^3A_{2g}$ Ground Term for Pd^{2+} and Ni^{2+} (d^8) in Octahedral Ligand Field	63
Figure 3.4: Magnetic Moment vs. Temperature of $M(SbF_6)_2$, $M = Ni, Pd$ and Cu	70
Figure 3.5: Magnetic Moment vs. Temperature of $Ni(SbF_6)_2$	74
Figure 3.6: Magnetic Moment vs. Temperature of HF-Treated $Cu(SbF_6)_2$	80
Figure 3.7: Magnetic Moment vs. Temperature of SbF_5 -Treated $Cu(SbF_6)_2$	81
Figure 4.1: ^{119}Sn Mössbauer Spectrum of $Sn(SbF_6)_2 \cdot 2\text{mes}$ at 77 K	102
Figure 5.1: Magnetic Moment vs. Temperature of $Br_2^+[Sb_3F_{16}]^-$, $I_2^+[Sb_2F_{11}]^-$ and $O_2^+[AsF_6]^-$	122
Figure 5.2: Inverse Susceptibility vs. Temperature of $O_2^+[AsF_6]^-$ and $Br_2^+[SbF_3F_{16}]^-$	123
Figure 5.3: Crystal Structure of $Br_2^+[Sb_3F_{16}]^-$	125
Figure 5.4: Energy Level Diagram of the Dioxygenyl Ion with the σ and π -Bonding 2p Orbitals	127
Figure 5.5: Crystal Structure of $I_2^+[Sb_2F_{11}]^-$	131
Figure 5.6: Magnetic Susceptibility vs. Temperature of $I_2^+[Sb_2F_{11}]^-$	132
Figure 6.1: Proposed Structure of $Pd(SO_3F)_2$	143
Figure 6.2: Inverse Susceptibility vs. Temperature of $Ni(SO_3F)_2$	152
Figure 6.3: Inverse Susceptibility vs. Temperature of $Pd(SO_3F)_2$, $Pd(II)[Pd(IV)(SO_3F)_6]$ and $Ag(SO_3F)_2$	154
Figure 6.4: Magnetic Susceptibility vs. Temperature of $Pd(SO_3F)_2$ at 7501 and 9625 G	155

	Page
Figure 6.5: Magnetic Susceptibility vs. Temperature of Pd(II)[Pd(IV)(SO ₃ F) ₆] at 7501 and 9625 G	156
Figure 6.6: Magnetic Moment vs. Temperature of Pd(SO ₃ F) ₂ and Ag(SO ₃ F) ₂	159
Figure 6.7: Magnetic Moment vs. Temperature of Pd(SO ₃ CF ₃) ₂	170
Figure 6.8: Magnetic Susceptibility vs. Temperature of Pd(SO ₃ CF ₃) ₂	171
Figure 6.9: Magnetic Moment vs. Temperature of Ni(SO ₃ CF ₃) ₂ and Ni(SO ₃ F) ₂	173

LIST OF SYMBOLS

N	=	Avogadro's number
k	=	Boltzmann's constant
T	=	Absolute temperature
g	=	Lande splitting factor
J	=	Exchange coupling constant
D	=	Zero-field splitting parameter
λ	=	Spin-orbit coupling constant
Dq	=	Ligand field splitting parameter
B	=	Racah parameter (interelectronic repulsion parameter)
μ_B or β	=	Bohr magneton
$\mu_{s.o}$	=	Spin only magnetic moment
μ_{eff}	=	Effective magnetic moment
χ_M	=	Molar magnetic susceptibility
χ_M^{corr}	=	Molar magnetic susceptibility corrected for diamagnetism
C_m	=	Curie constant
θ	=	Weiss constant
G	=	Magnetic field in Gauss
ΔE_Q	=	Quadrupole splitting
δ	=	Isomer shift

ACKNOWLEDGEMENTS

It has been a rewarding experience to work under the supervision of Professor F. Aubke. His guidance and encouragement were invaluable during the course of this work, and for this I extend my sincere gratitude and thanks to him. I also wish to thank Professor R.C. Thompson for his constructive and valuable collaboration in this study over the past few years.

Many thanks are also due to my co-workers Dingliang Zhang, Germaine Hwang, Fred Mistry and Walter Cicha for their pleasant friendship and enlightening discussions. Tom Otieno and Martin Ehlert are thanked for their kind assistance in obtaining the magnetic measurements. Thanks are also due to the members of the mechanical, glassblowing, and electronic shops for their technical expertise. I am also indebted to Mr. P. Borda for his microanalytical services. Special thanks are extended to Germaine Hwang for proof-reading this thesis and Rani Theeparajah for the excellent work done in typing the manuscript.

Finally I would like to express my sincere thanks to my family for their kind understanding and words of encouragement throughout my years of graduate study.

DEDICATED

TO MY MOTHER

J.B.A. CADER

CHAPTER 1

INTRODUCTION

1.1 General Introduction

The synthesis and physical study of solid compounds where unusual metal and non-metal cations are stabilized by weakly coordinating fluoro anions is an area of research which has grown steadily over the last two decades, and is the primary focus of this dissertation. In recent years, there has been an increasing interest shown both by chemists and physicists in the synthetic and solid state properties of these rare cationic complexes, often obtainable only as derivatives of strong Brönsted (protonic) fluoroacids or Lewis acids (1, 2). The use of a wide array of physical methods including various magneto-chemical techniques to characterize these compounds has permitted structure-property relationships to be understood in detail and has also provided rational approaches to the synthesis of new and unusual materials.

The types of compounds which have been studied in this thesis are varied, and range from main group non-metallic molecular cationic complexes to inorganic and organometallic coordination polymers, where the organometallic polymers are π -arene adducts of the post-transitional metal Sn(II) fluoro derivatives. The molecular cations and the transition metal coordination polymers have been investigated for their magnetic properties to obtain information on the ground state electronic structure as well as to detect any magnetic exchange interactions between the paramagnetic centers (particularly at low temperature) in the respective compounds. Furthermore, spectroscopic and structural data (where available) have been utilized in the interpretation of the magnetic behavior observed for the compounds.

The inorganic and organometallic polymers synthesized in this study contain fluoroanions such as SbF_6^- and SO_3F^- , which are usually generated in superacidic media. Strong protonic fluoroacids and superacids have been used extensively as reaction media, solvents and synthetic reagents in both inorganic and organic syntheses (1). The role of these acids and their anions in the synthesis and stabilization of unusual cations is of significance to this work, since all the fluoro compounds studied here have anions which are derived from either the protonic fluoroacids HSO_3F and HSO_3CF_3 or the Lewis acids SbF_5 and AsF_5 . Consequently, the corresponding anions of interest SO_3F^- , SO_3CF_3^- , SbF_6^- , $\text{Sb}_2\text{F}_{11}^-$, $\text{Sb}_3\text{F}_{16}^-$ and AsF_6^- are all poorly coordinating, weakly nucleophilic anions, well capable of stabilizing a variety of electrophilic cationic centers either in solid compounds or in solutions.

These fluoro anions are in general non-oxidizable and are reasonably resistant toward reduction and, when coordinating to transition metals, act as monodentate as well as bidentate or tridentate ligands, usually with bridging, rather than chelating configurations. The coordinating ability of the fluorosulfate SO_3F , and the trifluoromethylsulfate SO_3CF_3 groups has been discussed relatively recently by Lawrence (3), and the generation and stabilization of various halogen and interhalogen cations in protonic fluoroacids and superacids has been reviewed in the past by Gillespie and Morton (4), and many years later by Shamir (5).

It is generally agreed that the anions mentioned above are all very weakly basic and have high group electronegativities. For a number of dimethyltin(IV) compounds of the type $(\text{CH}_3)_2\text{SnX}_2$ (X = a fluoro or fluoroxy anion) with linear or near linear C-Sn-C groupings and bidentate bridging anions, the ^{119}Sn Mössbauer parameters suggest the following order of anion basicity: $\text{F}^- > \text{SO}_3\text{CH}_3^- > \text{SO}_3\text{CF}_3^- \approx \text{SO}_3\text{F}^- > \text{AsF}_6^- > \text{SbF}_6^- \approx \text{Sb}_2\text{F}_{11}^-$ (6).

These general concepts mentioned briefly above will now be discussed in some detail in the following sections to provide the necessary background information for the extended study.

1.2 The Lewis Acid SbF_5

1.2.1 Physical and Chemical Properties

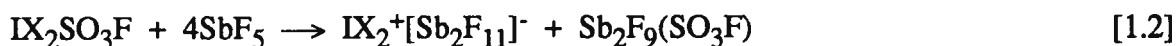
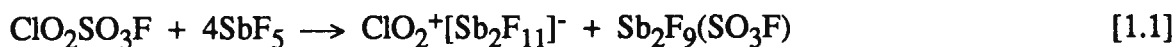
Antimony(V) fluoride, SbF_5 , is generally regarded as the strongest molecular Lewis acid (7). It is a very viscous (460 cP at 20°C) (8), colorless liquid, with a specific gravity of 3.145 g/cm^3 at 15°C. It has a relatively high melting point (8.3°C) and a high boiling point (142°C) (1a), compared to the Lewis acid AsF_5 (mp = -80°C, bp = -53°C). This suggests a considerable degree of association for the molecule, and vapor density measurements indicate aggregates corresponding to $(\text{SbF}_5)_3$ at 150°C and $(\text{SbF}_5)_2$ at 250°C (9). The polymeric structure of the liquid SbF_5 has been established by ^{19}F -NMR spectroscopy (10), and is found to have a *cis*-fluorine bridged framework in which each antimony atom is surrounded by six fluorine atoms in an octahedral arrangement. In the solid state, SbF_5 is tetrameric with octahedral coordination achieved again by *cis*-bridging fluorine atoms (11).

Antimony pentafluoride is a good oxidizing and a moderately strong fluorinating agent. As shown by conductometric, cryoscopic, and related acidity measurements, it appears that SbF_5 is by far the strongest Lewis acid known, and hence is preferentially used in preparing stable metallic as well as non-metallic cationic derivatives. For the purpose of comparison, the following order of acidity can be assigned for a series of Lewis acids (1a): $\text{SbF}_5 > \text{AsF}_5 > \text{TaF}_5 > \text{BF}_3 > \text{NbF}_5 > \text{PF}_5$. For their anions, the basicity is expected to increase in nearly the same order from SbF_6^- to PF_6^- . Moreover, SbF_5 also shows a remarkable ability to coordinate to protonic fluoroacids such as HF, HSO_3F and HSO_3CF_3 , resulting in vastly enhanced acidity for the conjugate superacid systems, where many types of unusual cations have been observed as stable species.

1.2.2 Cationic Derivatives

Cation formation in SbF_5 or in its conjugate superacid solutions is not restricted to metallic species only, but occurs with equal frequency among non-metals such as halogen and polyhalogen derivatives (4,5). In most instances SbF_5 has proven to be an excellent fluoride-ion acceptor, and the hexafluoro anion SbF_6^- or polyanions of the type SbF_6^- . $(\text{SbF}_5)_n$, $n = 1$ or 2 , are readily formed. Some selected solid polyhalogen and binary transition metal cationic species stabilized by such anions are listed in Tables 1.1 and 1.2. Extensive research has been carried out in our laboratory to study the possible extension of this fluoride-ion acceptor ability of SbF_5 to include a similar "fluorosulfate-ion transfer" via the solvolysis of fluorosulfate compounds in SbF_5 (12-15).

The solvolysis process was initially used in our group to synthesize non-metallic cations (12,13,15), and later for the preparation of the dimethyltin(IV) cation $(\text{CH}_3)_2\text{Sn}^{+2}$ (16):



(X = Cl or Br)

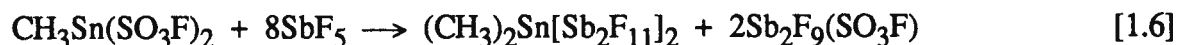
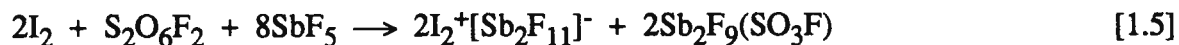
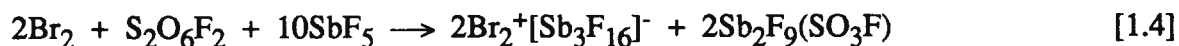
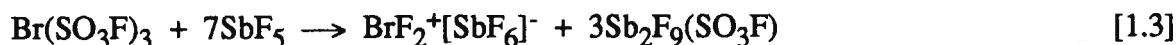


Table 1.1: Solid Polyhalogen Cationic Derivatives of SbF₅

Compound	Synthesis	Reference
Cl ₃ ⁺ [SbF ₆] ⁻	Cl ₂ + ClF + SbF ₅ in HF	4
Br ₂ ⁺ [Sb ₃ F ₁₆] ⁻	Br ₂ + BrF ₅ + SbF ₅	17
	Br ₂ + S ₂ O ₆ F ₂ + SbF ₅	15
I ₂ ⁺ [Sb ₂ F ₁₁] ⁻	I ₂ + SbF ₅ in SO ₂	18
	I ₂ + S ₂ O ₆ F ₂ + SbF ₅	15
ClF ₂ ⁺ [SbF ₆] ⁻	ClF ₃ + SbF ₅	19
BrF ₂ ⁺ [SbF ₆] ⁻	BrF ₃ + SbF ₅	20
	Br(SO ₃ F) ₃ + SbF ₅	15
IF ₂ ⁺ [SbF ₆] ⁻	IF ₃ + SbF ₅	21
ICl ₂ ⁺ [Sb ₂ F ₁₁] ⁻	ICl ₂ SO ₃ F + SbF ₅	13
IBr ₂ ⁺ [Sb ₂ F ₁₁] ⁻	IBr ₂ SO ₃ F + SbF ₅	13
ClF ₄ ⁺ [SbF ₆] ⁻	ClF ₅ + SbF ₅ in HF	22
BrF ₄ ⁺ [Sb ₂ F ₁₁] ⁻	BrF ₅ + SbF ₅	22
IF ₄ ⁺ [SbF ₆] ⁻	IF ₅ + SbF ₅	8
BrF ₆ ⁺ [Sb ₂ F ₁₁] ⁻	BrF ₅ + Kr ₂ F ₃ SbF ₆	23
IF ₆ ⁺ [Sb ₂ F ₁₁] ⁻	IF + SbF ₅	24

Table 1.2: Solid Binary Transition Metal Derivatives of SbF₅

Compound	Synthesis	Reference
Cr(SbF ₆) ₂	CrF ₂ + SbF ₅ in HF	25
Mn(SbF ₆) ₂	Mn + SbF ₅ in SO ₂	26
Fe(SbF ₆) ₂	FeF ₂ + SbF ₅ in HF	25
	Fe + SbF ₅ in SO ₂	26
Co(SbF ₆) ₂	CoF ₂ + SbF ₅ in HF or SO ₂	25
	Co + SbF ₅ in SO ₂	26
Ni(SbF ₆) ₂	NiF ₂ + SbF ₅ in HF	25
	Ni + SbF ₅ in SO ₂	26
	Ni + SbF ₅ + F ₂	27
Ag(SbF ₆) ₂	AgF ₂ + SbF ₅ in HF	25
Zn(SbF ₆) ₂	ZnF ₂ + SbF ₅ in HF	25
Cd(SbF ₆) ₂	CdF ₂ + SbF ₅ in HF	25
Hg ₃ (Sb ₂ F ₁₁)	Hg + SbF ₅ in SO ₂	28

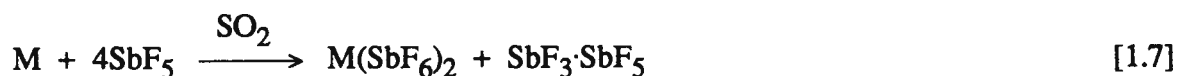
Two of the above halogen cations synthesized by the solvolysis route, i.e. $\text{Br}_2^+[\text{Sb}_3\text{F}_{16}]^-$ and $\text{I}_2^+[\text{Sb}_2\text{F}_{11}]^-$, are investigated in this work for their magnetic properties by low temperature magnetic susceptibility measurements. This improved preparative method (15) provides a simple and straightforward route to sufficiently large quantities of very pure paramagnetic Br_2^+ and I_2^+ compounds, and hence is of value in magnetic studies where highly pure materials are desired. It is interesting to note that in Table 1.1, $\text{Br}_2^+[\text{Sb}_3\text{F}_{16}]^-$ and $\text{I}_2^+[\text{Sb}_2\text{F}_{11}]^-$ are the only two solid polyhalogen cation derivatives that are paramagnetic.

The volatile components formed in these solvolysis reactions ($\text{SbF}_4(\text{SO}_3\text{F})$ and more frequently $\text{Sb}_2\text{F}_9(\text{SO}_3\text{F})$ where SbF_5 is in an excess) can be removed easily in a dynamic vacuum (14), facilitating the isolation of pure solid products in very high yield. In this study, the solvolysis method is extended to divalent transition metal fluorosulfates as well.

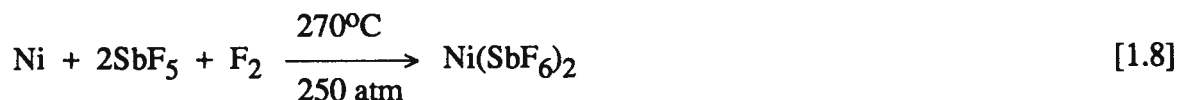
The polyhalogen derivatives of SbF_5 listed in Table 1.1 are generally accepted to be of ionic structure, although there is evidence that in most of them some secondary cation-anion interaction of various degrees does exist. Single crystal X-ray studies performed on two compounds of interest to this study, i.e. $\text{Br}_2^+[\text{Sb}_3\text{F}_{16}]^-$ and $\text{I}_2^+[\text{Sb}_2\text{F}_{11}]^-$, support an ionic formulation since the cation-anion contacts are rather long, although shorter than the sum of the van der Waals radii, indicating a very small cation-anion interaction (17,18).

Interestingly, the shortest $\text{I}\cdots\text{F}$ contact distance in $\text{I}_2^+[\text{Sb}_2\text{F}_{11}]^-$ is almost the largest cation-anion contact observed in a series of $\text{Sb}_2\text{F}_{11}^-$ derivatives with the following cations of decreasing contacts: $\text{SbCl}_4^+ > \text{I}_2^+ > \text{XeF}_3^+ > \text{Br}_2^+ > \text{BrF}_4^+$. This decreasing distance indicates an increase in the acidity for the cations (18). The Sb-F (terminal) distances in $\text{Br}_2^+[\text{Sb}_3\text{F}_{16}]^-$ and $\text{I}_2^+[\text{Sb}_2\text{F}_{11}]^-$ (1.83 Å and 1.85 Å) are similar to those observed in SbF_6^- derivatives like $\text{ClF}_2^+[\text{SbF}_6]^-$ and $\text{BrF}_2^+[\text{SbF}_6]^-$, namely 1.84 Å and 1.835 Å respectively (19,20).

The transition metal hexafluoroantimonates listed in Table 1.2 are, in most reported instances, formulated as metal difluoride adducts of the parent acid SbF_5 , and are of the type $\text{MF}_2 \cdot 2\text{SbF}_5$ (25). This formulation is derived from a common synthetic route where the metal difluoride is reacted with SbF_5 , usually in the presence of anhydrous HF or SO_2 to yield the desired product. However, alternative structural forms like $\text{M}(\text{SbF}_6)_2$ and $\text{MF}(\text{Sb}_2\text{F}_{11})_2$ are also possible for these products. When other preparative methods such as the oxidation of metals by SbF_5 in SO_2 (26) or metal fluorination with F_2 in the presence of SbF_5 (27) are used, the resulting products are conveniently formulated as $\text{M}_x(\text{SbF}_6)_y$:



where $\text{M} = \text{Mn}, \text{Fe}$ or Ni



In the case of cobalt, reaction [1.7] reportedly leads to the ternary $\text{CoF}(\text{SbF}_6)_2$ (26), whereas mercury is converted to $\text{Hg}_3(\text{Sb}_2\text{F}_{11})$ (28).

It is significant to note here that all the above routes to transition metal hexafluoroantimonates have various limitations and complications. Metal oxidation by F_2 at elevated temperature may lead to higher oxidation state compounds, whereas oxidation by SbF_5 may not be a suitable method for metals with higher oxidation potentials than provided for by the $\text{Sb(V)}/\text{Sb(III)}$ couple. In addition, the quantitative separation of the solid byproduct $\text{SbF}_3 \cdot \text{SbF}_5$ from the main product may prove to be difficult (29), and consequently, impure materials are isolated as reaction products. Even the more versatile synthetic method of fluoride abstraction from MF_2 by SbF_5 (25) could lead to compounds of the type $\text{MF}(\text{Sb}_2\text{F}_{11})$, a structural isomer of the binary $\text{M}(\text{SbF}_6)_2$, due to an incomplete breakup of the MF_2 lattice.

Some structural information on the transition metal derivatives of SbF_5 (Table 1.2) has been reported. For the Mn, Fe and Ni compounds obtained from SbF_5 in SO_2 (26), magnetic moment values at room temperature appear to indicate octahedral coordination for the metal centers. Based on vibrational and X-ray powder data, $\text{Ni}(\text{SbF}_6)_2$, which is synthesized from the high temperature fluorination of nickel in SbF_5 (27), is shown to be related to the LiSbF_6 structure by the occupation of only every second octahedral Li^+ site with Ni^{2+} , leading to a layer type structure. Furthermore, a crystal structure has been reported for the paramagnetic (*vide infra*) $\text{Ag}(\text{SbF}_6)_2$ (25), where the Ag^{2+} ion is located in a tetragonally elongated octahedral environment, which in turn implies a layer structure with tridentate bridging SbF_6^- moiety for the compound. Except for the observed distortion due to the Jahn-Teller effect, the reported structure appears to be consistent with the proposed structure of the above mentioned $\text{Ni}(\text{SbF}_6)_2$ compound (27).

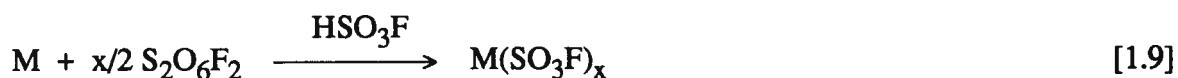
1.3 Transition Metal - Fluorosulfates and Trifluoromethylsulfates

The transition metal sulfonates studied in this work can be considered as derivatives of the strong protonic fluoroacids fluorosulfuric acid (HSO_3F) and trifluoromethylsulfuric acid (HSO_3CF_3). The two acids rank among the strongest known protonic acids (1,3,7). Consequently, the corresponding anions SO_3F^- and SO_3CF_3^- behave as weakly coordinating ligands, and are well suited to stabilize many unusual transition metal (as well as main group) cations. Compared to other poorly coordinating anions like perchlorate (ClO_4^-) or tetrafluoroborate (BF_4^-), the SO_3F^- and SO_3CF_3^- ions are arguably the most stable and non-oxidizing species available for synthetic purposes (3). Interestingly, almost all the transition metal trifluoromethylsulfate compounds are made by the solvolysis of suitable metal salts in an excess of HSO_3CF_3 , and include many metal fluorosulfates as precursors (30,31). Therefore, it is appropriate to examine first the syntheses and properties of transition metal fluorosulfates (particularly the derivatives of electron rich metals) in some detail.

Fluorosulfate chemistry displays many parallels to halogen chemistry, and the fluorosulfate group may be viewed as a pseudohalide. Hence, the synthetic methods used in the preparation of the fluorosulfates have striking parallels to those used in the synthesis of halides, with the necessary modifications.

Two synthetic methods in general have been used to prepare a large number of transition metal fluorosulfate derivatives: (a) solvolysis of a corresponding metal salt such as MCl_2 , MSO_4 or $M(RCOO)_2$ in excess HSO_3F , and (b) the oxidation of a metal with the strongly oxidizing and fluorosulfonating reagent bis(fluorosulfonyl)peroxide, $S_2O_6F_2$ (32,33) in the presence or absence of HSO_3F .

Solvolysis is almost exclusively the route of choice for the synthesis of 3d-block metal(II) fluorosulfates (34,35), whereas metal oxidation by $S_2O_6F_2$ yields a variety of electron rich 4d- and 5d-metal fluorosulfates, in particular $Pd(II)[Pd(IV)(SO_3F)_6]$ (36), $Ag(SO_3F)_2$ (37), $Pt(SO_3F)_4$ (38) and $Au(SO_3F)_3$ (39) according to:



where $x = 2, 3$ or 4

A major advantage to the use of the $S_2O_6F_2/HSO_3F$ reagent combination in metal oxidation is that precursors, in the form of fine metal powders, are available in high purity for all the transition metals, and consequently, very pure products can be isolated after the removal of the excess reagents in a dynamic vacuum. Furthermore, some noble metal fluorosulfates such as $Pd(SO_3F)_2$ (36), $Pt(SO_3F)_4$ (40) and $Au(SO_3F)_3$ (40) are also prepared by the oxidation of the respective metals by bromine monofluorosulfate, $BrSO_3F$ (41). However, the use of $BrSO_3F$

instead of $S_2O_6F_2/HSO_3F$ in the synthesis of binary metal fluorosulfates offers no real advantage, primarily as $S_2O_6F_2$ is initially required to synthesize $BrSO_3F$.

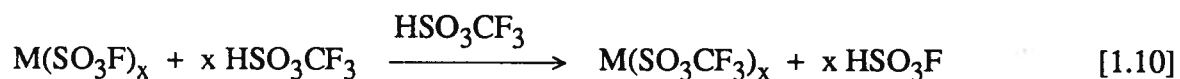
For these transition metal fluorosulfates, only a single molecular structure, that of gold(III) fluorosulfate, which was obtained by single crystal X-ray diffraction, has been reported so far (42). The compound is a dimer and contains both monodentate and symmetrically bridging bidentate fluorosulfate groups. Unfortunately, the polymeric nature of most transition metal fluorosulfates and their resulting lack of volatility and solubility in HSO_3F or other suitable solvents have prevented the formation of single crystals, and hence structural evidence rests largely on vibrational spectra and magnetic properties.

Fluorosulfates of the type $M(SO_3F)_2$ appear to belong to a single structural type, derived from the $CdCl_2$ layer structure, with one exception - the mixed valency $Au(I)[Au(III)(SO_3F)_4]$ (43). The O-tridentate bridging fluorosulfate group in $M(SO_3F)_2$ results in MO_6 -coordination polyhedra within the layer structure. Regular octahedra are found for $M = Fe, Co, Ni, Pd, Zn, Cd$ and Hg (35,36,44), while the symmetry of the SO_3F group appears to be reduced for $M = Mn, Cu$ and Ag (35,37), with Jahn-Teller distortions expected for Cu^{2+} and Ag^{2+} . This structure type is also postulated for the divalent metal trifluoromethylsulfates $Fe(SO_3CF_3)_2$ (45), $Co(SO_3CF_3)_2$ (46), $Pd(SO_3CF_3)_2$ (30) and $Cu(SO_3CF_3)_2$ (46), and also extends to divalent pre-transition and post-transition metal SO_3F^- , $SO_3CF_3^-$ and $SO_3CH_3^-$ derivatives as well. The only two molecular structures reported so far for this type of compounds are that of $Sn(SO_3F)_2$ (47a) and $Ca(SO_3CH_3)_2$ (47b). For the transition metal $M(SO_3R)_2$ type compounds with $R = F, CF_3$ or CH_3 , electronic spectra and magnetic data, where reported, confirm the structural conclusions reached.

A greater structural diversity is encountered for binary fluorosulfates of the general composition $M(SO_3F)_3$. The dimeric structure of $[Au(SO_3F)_3]_2$ (42) and the mixed-valency

Pd(II)[Pd(IV)(SO₃F)₆] (36) are clear exceptions. The mixed valency formulation follows the precedent of PdF₃ (48) and is supported by the magnetic behavior and the synthesis and structural characterization of bimetallic compounds of the types Pd(II)[M(IV)(SO₃F)₆] (M = Pt or Sn) and Ba[Pd(IV)(SO₃F)₆] (49). The fluorosulfate group appears to bond strongly to the M(IV) metal center and coordinates weakly to M(II), in an "anisobidentate" bonding mode. Therefore, it seems that where the SO₃F (and the SO₃CF₃ or SO₃CH₃) group functions as a polydentate ligand, a bridging configuration is observed, resulting in stable solids, often viewed as coordination polymers. Moreover, the versatile coordinating ability of the fluorosulfate group, which may function as a mono-, bi-, or tri-dentate ligand leads to the stabilization of metal ions in high, intermediate, and low oxidation states.

In contrast to the large number of binary transition metal fluorosulfate compounds reported, only a small number of trifluoromethylsulfate derivatives are known. Almost all the M(SO₃CF₃)_x species are made by the solvolysis of suitable metal salts in an excess of HSO₃CF₃. In the solvolysis of M(SO₃F)_x in HSO₃CF₃ (30,31), the reaction initially proceeds according to:



where x = 2 or 3, M = Mn, Pd, Ag or Au

However, the by-product HSO₃F and the reactant HSO₃CF₃ undergo a degradation reaction and produce a series of products (50,51) which do not appear to interfere in the isolation of the trifluoromethylsulfates (30). As mentioned above, for the divalent iron, cobalt and copper derivatives a layered lattice structure involving hexacoordinated metal centers has been suggested on the basis of vibrational and electronic spectra, as well as magnetic and Mössbauer data (45,46). In a manner similar to the SO₃F groups discussed previously, the

SO_3CF_3 groups act as bridging tridentate ligands in these compounds.

Although the solvolysis of transition metal fluorosulfates in excess trifluoromethylsulfuric acid, which is a generally applicable method, should allow the synthesis of a comparatively large number of SO_3CF_3 compounds (30), only limited use has been made of this synthetic possibility. The principal reasons for this are threefold: (a) As discussed in Section 1.1, the SO_3CF_3 group has a basicity comparable to that of the SO_3F group. An extended synthetic approach is not fruitful where compounds with similar properties and molecular structures result, as is often the case. (b) With vibrational spectroscopy used as a principal method of structural analysis, the coincidence of SO_3 and CF_3 stretching modes in SO_3CF_3^- causes a greater complexity, making vibrational assignments and structural conclusions frequently uncertain and ambiguous. (c) The S—C linkage in HSO_3CF_3 and its derivatives is sensitive to oxidative cleavage (30), and hence the acid's use in the synthesis of high-valent metal derivatives with a good oxidizing potential, is not advisable. However, the S-C linkage, unlike the S-F bond, is hydrolytically stable and hence chemistry in aqueous medium is possible with HSO_3CF_3 .

There are nevertheless a number of interesting cases where metal trifluoromethylsulfates display fundamentally different magnetic properties from the corresponding fluorosulfates, as will be discussed in Chapter 6 of the text.

1.4 Post-Transition Metal Arene π -Compounds

Both main group and transition metal organometallic π -complexes have been studied extensively, and a very large number of compounds have appeared in the chemical literature in this field over the past few years alone. In this discussion, however, the emphasis is placed on the relatively rare post-transition metal arene π -complexes. In terms of bonding, these

compounds differ significantly from most of the transition metal π -compounds for three principal reasons (52):

- (a) Metals of the post-transition series contain no partially filled or empty valence d subshells of comparable energy to those of the π orbitals of arene ligands. As a result, the π electron density of the ligand can be transferred only to a very small extent to the s or p type orbitals of the metal.
- (b) The filled d subshells of the metals are usually of much lower energy than the antibonding π^* orbitals of the arene ligand. Consequently, unlike the transition metal counterparts, back-donation from the d electrons to effect synergic bonding is not observed in post transition π -complexes.
- (c) The effective atomic number rule, which is so useful in transition metal carbonyls and arene and Cp derivatives, is rendered ineffective and inapplicable in the case of post transition metal derivatives.

The consequence of factors (a) and (b) is a weak metal ligand interaction, leading to compounds which are not as varied as the transition metal π -complexes. The study of neutral arene-metal complexes with the post transition metals in recent times has included the elements Ga, In, Tl, Sn, Pb, and Bi (53). However, these studies indicate that the π -interactions with the elements above the fourth period are very weak, resulting in reduced hapticity from a desired η^6 to η^3 or η^2 (53).

Studies by Schmidbaur et al. (54) have concentrated on neutral arene complexes of univalent gallium, indium and thallium, which directly follow the d block elements. Both mono and bis(arene) complexes have been synthesized and characterized, and among these is the

mixed mono and bis(arene) thallium complex, $[(\text{Mes})_6\text{Tl}_4][\text{GaBr}_4]_4$, whose crystal structure was also solved. This complex is actually a skeletal framework of tetrameric $\text{Tl}_4(\text{GaBr}_4)_4$, with one or two mesitylene molecules alternately coordinated to the Tl^+ cations. In the Mes-Tl^+ unit, the Tl^+ is located directly above the face of the ring, implying η^6 coordination. A similar structure was also found for the gallium analogue (55) $[\text{Mes}]_4\text{Ga}[\text{GaCl}_4]_4$, indicating that, although weak, π -interactions do exist with univalent Group 13 metals.

It is significant to note that in the above studies it was found that the complex salts TlAlCl_4 , TlAlBr_4 and TlGaCl_4 all dissolved in hot benzene to give colorless crystals upon cooling. However, when dried under a stream of dry N_2 , the benzene content of the crystals steadily decreased, implying very weak π coordination of the benzene ligand to the Tl center. Apparently, only the mesitylene ligand afforded a dry, isolable product. Strauss et al. (56) have also synthesized Tl-Mes complexes such as $[\text{Tl}(\text{OTeF}_5)(\text{Mes})_2]_2$, but found that this compound also loses all traces of the weakly bound arene ligands under N_2 atmosphere or *in vacuo*. Therefore, it appears that the high lability of these arene ligands makes synthesis and purification a very delicate task, even though the synthesis itself is relatively simple (i.e., arene addition to a suitable substrate).

It is apparent from the above studies that the electronic configuration $nd^{10}(n+1)s^2$ plays a particularly important role in the metal's affinity for arene ligands. In view of this, the next logical step is to explore the divalent Group 14 elements (which have the same electronic configuration) to investigate their affinities for arene ligands. In fact, the synthesis and structure of the arene $\text{M}(\text{II})$ complexes $(\text{C}_6\text{H}_6)\text{M}(\text{AlCl}_4)_2 \cdot (\text{C}_6\text{H}_6)$, $\text{M}=\text{Pb}(\text{II})$ or $\text{Sn}(\text{II})$, have been reported by Amma and co-workers (57,58). The X-ray crystallographic study of the compounds reveals a polymeric chain structure, with a benzene ring weakly bound in a η^6 manner to the $\text{M}(\text{II})$ center. In this thesis, the synthesis and characterization of arene adducts of divalent tin fluoro derivatives which contain the weakly coordinating SbF_6^- and SO_3F^- ligands will be considered.

1.5 Magnetic Measurements

Magnetic susceptibility measurements, when recorded as a function of temperature, provide primarily information regarding the nature of the ground state of the paramagnetic ions. The extent of the information that can be obtained is related to the accuracy of the measurements, the range of temperature over which the measurements are carried out, as well as to the purity of the samples used. The magnitude and temperature dependence of the magnetic moment data of magnetically dilute systems are determined by several factors such as ground state occupancy and degeneracy, crystal field symmetry, spin-orbit coupling and electron-delocalization effects. The theory of magnetic susceptibilities of paramagnetic molecular species and transition metal complexes is well covered in several texts (59). In magnetically concentrated systems, the factors mentioned above are also present, and any magnetic interaction is superimposed upon these single-ion phenomena. Furthermore, it is now recognized that magnetic exchange interactions are not at all uncommon in inorganic compounds, even where magnetic dilution (usually at room temperature) appears at first sight to be dominant. It is for this reason that magnetic susceptibility measurements should be performed, where possible, over as wide a temperature range as possible.

Qualitatively, magnetic exchange interactions may be thought of as arising from unpaired spin densities on neighbouring paramagnetic centers, being aligned either parallel or anti-parallel to each other, resulting in ferromagnetism or antiferromagnetism respectively. Magneto-structural relationships emphasize the importance of such factors as the stereochemistry around the paramagnetic center, the efficiency of orbital overlap which may be direct or via a superexchange pathway, the geometry of the bridging anions, the types of substituents on the bridging group and the nature of any nonbridging groups. The theoretical aspects of magnetic exchange phenomena and the models used to interpret the empirical data have been the subject of extensive investigations (60).

The main group molecular complexes and several of the transition metal derivatives studied in this work for their magnetic properties contain unusual paramagnetic cations in the solid state, which are stabilized by weakly basic fluoroanions. Nearly all the previous magnetic measurements on the molecular cations and the divalent sulfonates have been carried out at higher temperatures only, where in most instances, magnetic exchange interactions are not detected.

The halogen cations I_2^+ and Br_2^+ are shown to have $^2\Pi_{3/2g}$ ground states with the first excited states $^2\Pi_{1/2g}$ at approximately 5100 and 2800 cm^{-1} above the ground state, respectively, both in the gas phase (61) and in solution (15). The magnetic moment in both cases is expected to be independent of temperature due to the absence of thermally accessible excited states, and predicted to have a value of $2.0 \mu_B$ at higher temperatures, in analogy to the μ_{eff} of the NO molecule, discussed by van Vleck several years ago (62):

$$\mu_{eff} = 2[(1 - e^{-x} + xe^{-x})/(x + xe^{-x})]^{1/2} \quad [1.11]$$

where $x = \lambda/kT$.

λ = Spin-orbit coupling constant

k = Boltzmann's constant

T = Absolute temperature

In an earlier report, Gillespie and Milne (63) showed the magnetic moment of I_2^+ in a solution of HSO_3F to be $2.0 \pm 0.1 \mu_B$. Kemmitt et al. (64) reported a magnetic susceptibility study on $(SbF_5)_2I$, a material thought to contain the I_2^+ cation, and found magnetic moments that ranged from $2.25 \mu_B$ at room temperature to $2.05 \mu_B$ at 100 K. Considering the uncertainty in the chemical composition of the material, not much significance could be attached to these values. A later work from our group, where the $I_2^+[Sb_2F_{11}]^-$ and $[Br_2^+][Sb_3F_{16}]^-$ compounds

were synthesized by an improved method (15), indicated the possible existence of antiferromagnetic interaction between the I_2^+ cations, with μ_{eff} values of 2.15 and 1.68 μ_B at 295 and 81 K respectively. Furthermore, the Br_2^+ species was found to be magnetically dilute in the temperature range 297 to 80 K, and a magnetic moment close to 2.0 μ_B was obtained for the compound (15). This is in contrast to a previous study, where a room temperature μ_{eff} value of 1.6 μ_B had been reported for the Br_2^+ derivative (17).

In contrast to the I_2^+ and Br_2^+ cations, the dioxygenyl cation O_2^+ (with ground state $^2\Pi_{1/2g}$ and first excited state $^2\Pi_{3/2g}$ at $\sim 1480\text{ cm}^{-1}$ above ground state) investigated in this work has been the subject of several previous magnetic studies (65-68). The O_2^+ cation can be prepared by a variety of methods, and is stabilized in the solid state by various fluoroanions, leading to complexes like $O_2^+[PtF_6]^-$ (69), $O_2^+[BF_4]^-$ (70), $O_2^+[AsF_6]^-$ (71), and $O_2^+[SbF_6]^-$ (71). The magnetic behavior of $O_2^+[PtF_6]^-$ over the temperature range 77-298 K has been postulated to be similar to that of NO, and the magnetic moment was reported as 1.57 μ_B at room temperature (65). A magnetic moment of 1.66 μ_B has been found for the $O_2^+[SbF_6]^-$ compound (68b), and a value of 1.70 μ_B for $O_2^+[BF_4]^-$ (68a). Two previous studies on $O_2^+[AsF_6]^-$ down to 4 K give contradictory results. The study by Grill et al. (67) indicates no magnetic ordering of the O_2^+ cations down to 4 K, whereas weak $O_2^+ \cdots O_2^+$ interaction is suggested in the work of DiSalvo et al. (66).

Even though in all the above studies the μ_{eff} values reported for the O_2^+ salts fall well below the spin only value of 1.73 μ_B , no satisfactory reason has been given so far to explain this curious phenomenon. It appears, however, that sample purity and identity play an important role in the interpretation of magnetic data of the O_2^+ salts.

Several transition metal sulfonate derivatives studied here for their magnetic properties contain paramagnetic cations in unusual coordination environments. As in PdF_2 (48), in

$\text{Pd}(\text{SO}_3\text{F})_2$ (36) and $\text{Pd}(\text{SO}_3\text{CF}_3)_2$ (30) compounds, the Pd(II) ions (d^8) with $^3A_{2g}$ ground states are located in octahedral environments, a situation found only in some of their cationic and anionic derivatives. Similarly, the two silver derivatives $\text{Ag}(\text{SO}_3\text{F})_2$ (37) and $\text{Ag}(\text{SO}_3\text{CF}_3)_2$ (31) investigated in this work have remained, in addition to the AgF_2 compound (72), the only simple binary compounds of Ag(II) with a d^9 configuration.

Previous magnetic susceptibility measurements down to ~ 80 K on $\text{Pd}(\text{SO}_3\text{F})_2$, " $\text{Pd}(\text{SO}_3\text{F})_3$ " and $\text{Ag}(\text{SO}_3\text{F})_2$ indicated that these fluorosulfate derivatives were relatively magnetically unconcentrated in that temperature range with μ_{eff} values of 3.34, 3.45 and 1.92 μ_B respectively (36,37). Furthermore, their susceptibilities followed the Curie-Weiss law with positive Weiss constants. The trifluoromethylsulfate derivative $\text{Ag}(\text{SO}_3\text{CF}_3)_2$ was found to be an antiferromagnetic compound, with χ_{max} at ~ 138 K (31).

Only two other binary fluorosulfate and trifluoromethylsulfate derivatives, $\text{Ir}(\text{SO}_3\text{F})_4$ (73) and $\text{Fe}(\text{SO}_3\text{CF}_3)_3$ (45), are known up to now to be magnetically concentrated. However, unlike in $\text{Ag}(\text{SO}_3\text{CF}_3)_2$, the magnetic moments obtained for $\text{Ir}(\text{SO}_3\text{F})_4$ are only slightly below the calculated values, suggesting weak antiferromagnetic coupling down to ~ 80 K (73). The $\text{Fe}(\text{SO}_3\text{CF}_3)_3$ compound is magnetically more concentrated than the iridium species, exhibiting magnetic moments which are significantly less than the expected values, and which also decrease with decreasing temperature, although no maximum is detected in the susceptibility curve down to ~ 80 K (45). As in the cases of palladium and silver derivatives mentioned above, no low temperature magnetic data are available for these complexes.

The antiferromagnetic coupling observed in all the above mentioned sulfonates is not unusual for magnetically concentrated transition metal fluoro compounds, since antiferromagnetism, rather than ferromagnetism, appears to be the more common type of magnetic exchange interaction among the majority of these compounds (59). Moreover, in most instances

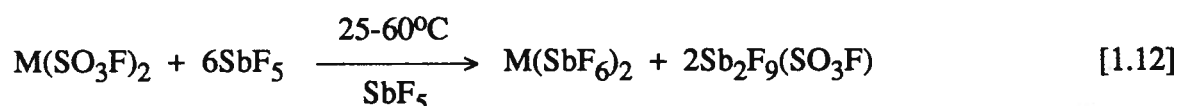
these antiferromagnetic transition metal fluoro derivatives contain small monoatomic ligands (59b,c), whereas the sulfonate coordination polymers studied in this work are composed of the much larger polyatomic SO_3F^- and SO_3CF_3^- ligands.

1.6 Objectives of this Study

The research work presented in this thesis can be categorized into two general, but inter-related sections: (A) Synthesis and characterization of divalent metal coordination polymers, and (B) Magnetic susceptibility studies on unusual main group and transition metal cations. The specific types of research relevant to these two sections are summarized below.

(A) Synthesis and Characterization

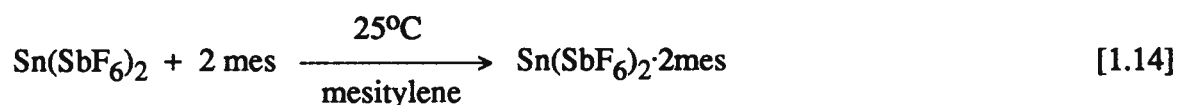
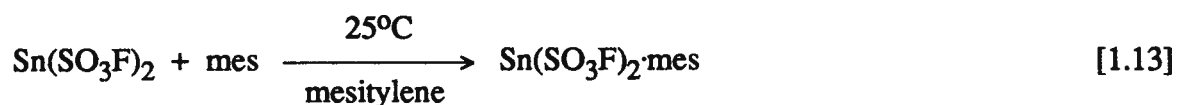
- (i) The solvolysis of main group fluorosulfate derivatives in the Lewis acid SbF_5 was extended in the present study to include the transition metal fluorosulfates according to:



Where M = Ni, Pd, Cu, Ag or (Sn)

The ready availability of the $\text{M}(\text{SO}_3\text{F})_2$ precursors, the low oxidation potential of SbF_5 , and the easy removal of the volatile byproduct $\text{Sb}_2\text{F}_9(\text{SO}_3\text{F})$, as well as mild reaction conditions and the possibility of using glass vessels as reactors were all positive factors in choosing the above solvolysis preparation. The divalent metal hexafluoro antimonates obtained were characterized, where appropriate, by elemental analysis, vibrational, electronic and ^{119}Sn Mössbauer spectra, and magnetic susceptibility measurements.

- (ii) The favorable properties of 1,3,5-trimethylbenzene (mesitylene) as a π -adduct ligand and the possible participation of the lone pair electrons of the Mössbauer nuclide Sn in the +2 state in bonding by being donated to the antibonding π^* ligand orbitals are contributing factors in the syntheses of the post-transition metal Sn(II) arene adducts according to:



(mes = mesitylene)

The adducts isolated were characterized by elemental analysis, infrared and ^{119}Sn -Mössbauer spectra.

(B) Magnetic Susceptibility Studies

- (i) Low temperature magnetic susceptibility measurements down to ~4 K were performed on $\text{O}_2^+[\text{AsF}_6]^-$, $\text{Br}_2^+[\text{Sb}_2\text{F}_{16}]^-$ and $\text{I}_2^+[\text{Sb}_2\text{F}_{11}]^-$, in order to compare the magnetic behavior of the three cations. These paramagnetic homonuclear derivatives seem to be the only three stable and isolable cations formed by non-metals that are suitable for solid state magnetic studies. The two dihalogen cations I_2^+ and Br_2^+ were investigated for possible exchange interactions, and the dioxygenyl cation O_2^+ was studied here to explain its observed low magnetic moment values. Furthermore, the application of van Vleck's theory of molecular paramagnetism to solid state cations was also examined.
- (ii) Several Group 10 and Group 11 divalent transition metal sulfonate compounds were considered in this study as likely materials to exhibit magnetic exchange interactions.

The metal fluorosulfates $\text{Pd}(\text{SO}_3\text{F})_2$, " $\text{Pd}(\text{SO}_3\text{F})_3$ " and $\text{Ag}(\text{SO}_3\text{F})_2$, previously described as relatively magnetically dilute down to ~ 80 K, were re-investigated down to ~ 4 K for their low temperature magnetic properties. The nickel(II) fluorosulfate, $\text{Ni}(\text{SO}_3\text{F})_2$ was, however, measured in the temperature range ~ 291 to 2 K. The corresponding trifluoromethylsulfate derivatives $\text{Ni}(\text{SO}_3\text{CF}_3)_2$, $\text{Pd}(\text{SO}_3\text{CF}_3)_2$ and $\text{Ag}(\text{SO}_3\text{CF}_3)_2$ were similarly studied for their variable temperature magnetic susceptibilities. The last two compounds were measured at low temperatures, whereas the $\text{Ni}(\text{SO}_3\text{CF}_3)_2$ complex was studied in the extended temperature range ~ 292 to 2 K.

References

- 1.a) G.A. Olah, G.K.S. Prakash, and J. Sommer, "Superacids", John Wiley and Sons, New York, 1985.
- b) T.A. O'Donnell, Chem. Soc. Rev., **16**, 1 (1987).
2. P. Hagemuller (Ed.), "Inorganic Solid State Fluorides", Academic Press, New York, 1985.
3. G.A. Lawrence, Chem. Rev., **86**, 17 (1986).
4. R.J. Gillespie and M.J. Morton, Quart. Rev. Chem. Soc., **25**, 553 (1971); and M.T.P. International Review of Science, Inorg. Chem., Ser. 1, Vol. 3, Butterworths, London, 1972.
5. J. Shamir in "Structure and Bonding", Eds. J.D. Dunitz, J.B. Goodenough, P. Hemmerich, J.A. Ibers, C.K. Jorgensen, J.B. Neilands, D. Reinen, and R.J.P. Williams, vol. 37, Springer-Verlag, Berlin, pp 141-210, 1979.
6. S.P. Mallela, S. Yap, J.R. Sams, and F. Aubke, Inorg. Chem., **25**, 4327 (1986).
7. P.-L. Fabre, J. Devynek, and B. Tremillon, Chem. Rev., **82**, 591 (1982).
8. A.A. Woolf and N.N. Greenwood, J. Chem. Soc., 2200 (1950).

9. E.E. Ainsley, R.D. Peacock, and P.L. Robinson, Chem. Ind., 1117 (1951).
- 10.a) E.L. Muetterties and W.D. Phillips, Adv. Inorg. Chem. Radiochem., 4, 234 (1962).
- b) G.J. Hoffman, B.F. Holder, and W.L. Jolly, J. Phys. Chem., 62, 364 (1958).
11. A.J. Edwards and P. Taylor, Chem. Comm., 1376 (1971).
12. P.A. Yeats and F. Aubke, J. Fluorine Chem., 4, 243 (1974).
13. W.W. Wilson, J.R. Dalziel, and F. Aubke, J. Inorg. Nucl. Chem., 37, 665 (1975).
14. W.W. Wilson and F. Aubke, J. Fluorine Chem., 13, 431 (1979).
15. W.W. Wilson, R.C. Thompson, and F. Aubke, Inorg. Chem., 19, 1489 (1980).
16. S.P. Mallela, S. Yap, J.R. Sams, and F. Aubke, Rev. Chim. Minerale, 23, 572 (1986).
- 17.a) A.J. Edwards, G.R. Jones, and R.J.C. Sills, Chem. Comm., 1527 (1968).
- b) A.J. Edwards and G.R. Jones, J. Chem. Soc., A2318 (1971).
18. C.G. Davies, R.J. Gillespie, S.R. Ireland, and J.M. Sowa, Can. J. Chem., 52, 2048 (1974).
- 19.a) F. Seel and O. Detmer, Z. Anorg. Allg. Chem., 301, 113 (1959).
- b) A.J. Edwards and R.J.C. Sills, J. Chem. Soc., A2697 (1970).
- 20.a) A.J. Edwards and G.R. Jones, Chem. Comm., 1304 (1967).
- b) A.J. Edwards and G.R. Jones, J. Chem. Soc., A1467 (1969).
- c) K.O. Christe and C.J. Schack, Inorg. Chem., 9, 2296 (1970).
- 21.a) M. Schmeisser and W. Ludovici, Z. Naturforsch., 20b, 602 (1965).
- b) M. Schmeisser, W. Ludovici, D. Naumann, P. Sartori, and E. Scharf, Chem. Ber., 101, 4214 (1968).
22. K.O. Christe and W. Sawodny, Inorg. Chem., 12, 2879 (1973).
- 23.a) R.J. Gillespie and G.J. Schrobilgen, Inorg. Chem., 13, 1230 (1974).
- b) K.O. Christe and R.D. Wilson, Inorg. Chem., 14, 694 (1975).
24. F.A. Hohorst, L. Stein, and E. Gebert, Inorg. Chem., 14, 2233 (1975).
25. D. Gantar, I. Leban, B. Frlec, and J.H. Holloway, J. Chem. Soc. Dalton Trans., 2379 (1987).

26. P.A.W. Dean, J. Fluorine Chem., 5, 499 (1975).
27. K.O. Christe, W.W. Wilson, R.A. Bougon, and P. Charpin, J. Fluorine Chem., 34, 287 (1987).
28. B.D. Cutforth, C.G. Davies, P.A.W. Dean, R.J. Gillespie, P.R. Ireland, and P.K. Ummat, Inorg. Chem., 12, 1343 (1973).
29. L. Kolditz, Adv. Inorg. Chem. Radiochem, 7, 1 (1965).
30. S.P. Mallela, J.R. Sams, and F. Aubke, Can. J. Chem., 63, 3305 (1985).
31. P.C. Leung, K.C. Lee, and F. Aubke, Can. J. Chem., 57, 326 (1979).
32. F.B. Dudley and G.H. Cady, J. Am. Chem. Soc., 79, 513 (1957).
33. R.A. DeMarco and J.M. Shreeve, Adv. Inorg. Chem. Radiochem., 16, 109 (1974).
34. A.A. Woolf, J. Chem. Soc., A355, (1967).
35. C.S. Alleyne, K.O. Mailer, and R.C. Thompson, Can. J. Chem., 52, 336 (1974).
36. K.C. Lee and F. Aubke, Can. J. Chem., 55, 2473 (1977).
37. P.C. Leung and F. Aubke, Inorg. Chem., 17, 1765 (1978).
38. K.C. Lee and F. Aubke, Inorg. Chem., 23, 2124 (1984).
39. K.C. Lee and F. Aubke, Inorg. Chem., 18, 389 (1979).
40. W.M. Johnson, R. Dev, and G. Cady, Inorg. Chem., 11, 2260 (1972).
41. F. Aubke and R.J. Gillespie, Inorg., Chem., 7, 599 (1968).
42. H. Willner, S.J. Rettig, J. Trotter, and F. Aubke, Can. J. Chem., 69, 391 (1991).
43. H. Willner, F. Mistry, G. Hwang, F.G. Herring, M.S.R. Cader, and F. Aubke, J. Fluorine Chem., 52, 13 (1991).
44. S.P. Mallela and F. Aubke, Can. J. Chem., 62, 382 (1984).
45. J.S. Haynes, J.R. Sams, and R.C. Thompson, Can. J. Chem., 59, 669 (1981).
46. A.L. Arduini, M. Garnett, R.C. Thompson, and T.C.T. Wong, Can. J. Chem., 53, 3812 (1975).
- 47.a) D.C. Adams, T. Birchall, R. Faggiani, R.J. Gillespie, and J.E. Vekris, Can. J. Chem., 69, 2122 (1991).

- b) F. Charbonnier, R. Faure, and H. Loiseleur, Acta Cryst., **B33**, 1478 (1977).
48. N. Bartlett and P.R. Rao, Proc. Chem. Soc., 393 (1964).
49. K.C. Lee and F. Aubke, Can. J. Chem., **57**, 2058 (1979).
50. G.A. Olah and T. Ohyama, Synthesis, **5**, 319 (1976).
51. R.E. Nofle, Inorg. Nucl. Chem. Lett., **16**, 195 (1980).
52. H. Schmidbaur, Angew. Chem. Int. Ed. Engl., **24**, 893 (1985).
53. H. Schmidbaur, W. Bublak, B. Huber, and G. Muller, Angew. Chem. Int. Ed. Engl., **3**, 26 (1987).
54. H. Schmidbaur, W. Bublak, J. Riede, and G. Muller, Angew. Chem. Int. Ed. Engl., **5**, 24, (1985).
55. H. Schmidbaur, U. Thewalt, and T. Zafirooulos, Z. Naturforsch., **B39**, 1642 (1984).
56. S.H. Strauss, M.D. Nairot, and O.P. Andersen, Inorg. Chem., **25**, 3850 (1986).
57. E.L. Amma, P.F. Rodesiler, and M.S. Weininger, Inorg. Chem., **18**, 751 (1979).
58. P.F. Rodesiler, Th. Auel, and E.L. Amma, J. Am. Chem. Soc., **97**, 7405 (1975).
- 59.a) R.J. Myers, "Molecular Magnetism and Magnetic Resonance Spectroscopy", Prentice Hall Inc., Englewood Cliffs, New Jersey, 1973.
- b) E.A. Boudreaux and L.N. Mulay (Ed.), "Theory and Applications of Molecular Paramagnetism", John Wiley and Sons, New York, 1976.
- c) R.L. Carlin, "Magnetochemistry", Springer-Verlag, Berlin, 1986.
- 60.a) W.E. Hatfield, W.E. Estes, W.E. Marsh, M.W. Pickens, L.W. ter Haar, and R.R. Weller in "Extended Linear Chain Compounds", Ed. J.S. Miller, Vol. 3, Plenum Press, New York, pp. 43-50, 1983.
- b) A.P. Ginsberg, Inorg. Chim. Acta. Rev., **5**, 45 (1971).
- c) C.J. O'Connor, Prog. Inorg. Chem., **29**, 203 (1982).
61. A.B. Cornford, D.C. Frost, C.A. McDowell, J.L. Ragle, and I.A. Stenhouse, J. Chem. Phys., **54**, 2651 (1971).

62. J.H. van Vleck, "Electric and Magnetic Susceptibilities", Oxford University Press, London, 1932.
63. R.J. Gillespie and J.B. Milne, Inorg. Chem., **5**, 1577 (1966).
64. R.D.W. Kemmitt, M. Murray, V.M. McRae, R.D. Peacock, M.C.R. Symons, and T.A. O'Donnell, J. Chem. Soc., **A862** (1968).
65. N. Bartlett and S.P. Beaton, Chem. Comm., 167 (1966).
66. F.J. DiSalvo, W.E. Falconer, R.S. Hutton, A. Rodriguez, and J.V. Waszczak, J. Chem. Phys., **62**, 2575 (1975).
67. A. Grill, M. Schieber, and J. Shamir, Phys. Rev. Lett., **25**, 747 (1970).
- 68.a) V.I. Belova, V. Ya. K. Syrkin, D.V. Bantov, and V.F. Sukhoverkhov, Russ. J. Inorg. Chem., (Engl. Trans.), **16**, 772 (1971).
b) V.I. Belova, V. Ya. Rosolovskii, and E.K. Nikitina, Russ. J. Inorg. Chem., (Engl. Trans.), **16**, 772 (1971).
69. N. Bartlett and D.H. Lohmann, J. Chem. Soc., 5253 (1962).
70. J.N. Keith, I.J. Solomon, I. Sheft, and H.H. Hyman, Inorg. Chem., **7**, 230 (1968).
71. D.E. McKee and N. Bartlett, Inorg. Chem., **12**, 2738 (1973).
72. P. Fischer, G. Roullet, and D. Schwarzenbach, J. Phys. Chem. solids, **32**, 1641 (1971).
73. K.C. Lee and F. Aubke, J. Fluorine Chem., **19**, 501 (1982).

CHAPTER 2

GENERAL EXPERIMENTAL

2.1 Introduction

This chapter will deal with general experimental techniques, chemical sources, purification procedures and the syntheses of starting materials used in this study. Specific synthetic procedures will be described in the appropriate chapters.

Since most of the compounds involved in this work are extremely hygroscopic, they had to be handled in an environment free of moisture. Hence, standard vacuum line techniques were employed for the transfer of volatile liquids, and less volatile liquids and solids were manipulated inside an inert atmosphere dry box. All reactions were performed inside well ventilated fumehoods.

Reactions were monitored by weight where possible, and the removal of volatile materials *in vacuo* was usually done at room temperature. However, where liquids with low vapor pressures like SbF_5 or HSO_3F were involved, elevated temperatures had to be used even under vacuum conditions.

Fluorolube grease type 25-10M (Halocarbon Corporation) was used to lubricate ground glass connections to maintain vacuum tight conditions.

2.2 Chemicals

Some chemicals were used without purification as received, and these are listed in Table

2.1, along with their sources and purities. The other chemicals used were purified or synthesized according to the methods described below.

Table 2.1: Chemicals Used Without Purification

Chemical	Source	Purity (%)
Ag, -100 mesh	Alfa	99.95
Au, -20 mesh	Alfa	99.99
Pd, -60 mesh	Alfa	99.95
Pt, -60 mesh	Alfa	99.90
Sn, -100 mesh	Alfa	99.99
I ₂	Fisher	99.9
CuF ₂	Alfa	99.5
AgF ₂	Aldrich	98.0
SnF ₂	Matheson	98.0
AgSbF ₆	Aldrich	98.0
AsF ₅	Ozark Mahoning	reagent grade
HF	Matheson	reagent grade
SnCl ₂	BDH	reagent grade
KI	Fisher	99.95
CaH ₂	BDH	reagent grade
NaC ₅ H ₅	Aldrich	2.0 M solution in THF

2.2.1 Purification Methods

- (a) SbF_5 , obtained from Ozark Mahoning, was purified (1) first by purging the crude liquid of most HF by bubbling dry N_2 through in a 500 mL two-necked Pyrex flask fitted with a gas inlet tube and Drierite guard tube. Subsequent purification was done by repeated distillation, first at atmospheric pressure in a stream of dry N_2 and later *in vacuo*.
- (b) HSO_3F , from Orange County Chemicals, was purified by double distillation in a Pyrex apparatus under a counter flow of dry N_2 at atmospheric pressure (2). The constant boiling fraction at 162-163°C was collected into Pyrex storage vessels.
- (c) HSO_3CF_3 , from Aldrich, was purified by repeated vacuum distillation and stored in Pyrex vessels for synthetic use.
- (d) Br_2 , from Aldrich, was stored in a Pyrex vessel containing P_2O_5 to exclude moisture and KBr to remove Cl_2 .
- (e) Mesitylene (1,3,5-Trimethylbenzene), obtained from Aldrich, was dried over CaH_2 for one week and distilled *in vacuo* prior to use.

2.2.2 Synthetic Methods

- (a) Bis(fluorosulfonyl) peroxide, $\text{S}_2\text{O}_6\text{F}_2$, was prepared in one to two kilogram quantities by the reaction of SO_3 and F_2 , using AgF_2 as catalyst and N_2 as carrier gas (3). The synthesis was carried out at ~180°C in a flow reactor made of Monel metal (Figure 2.1). The crude liquid product was condensed into Pyrex vessels, cooled to -78°C with dry ice.

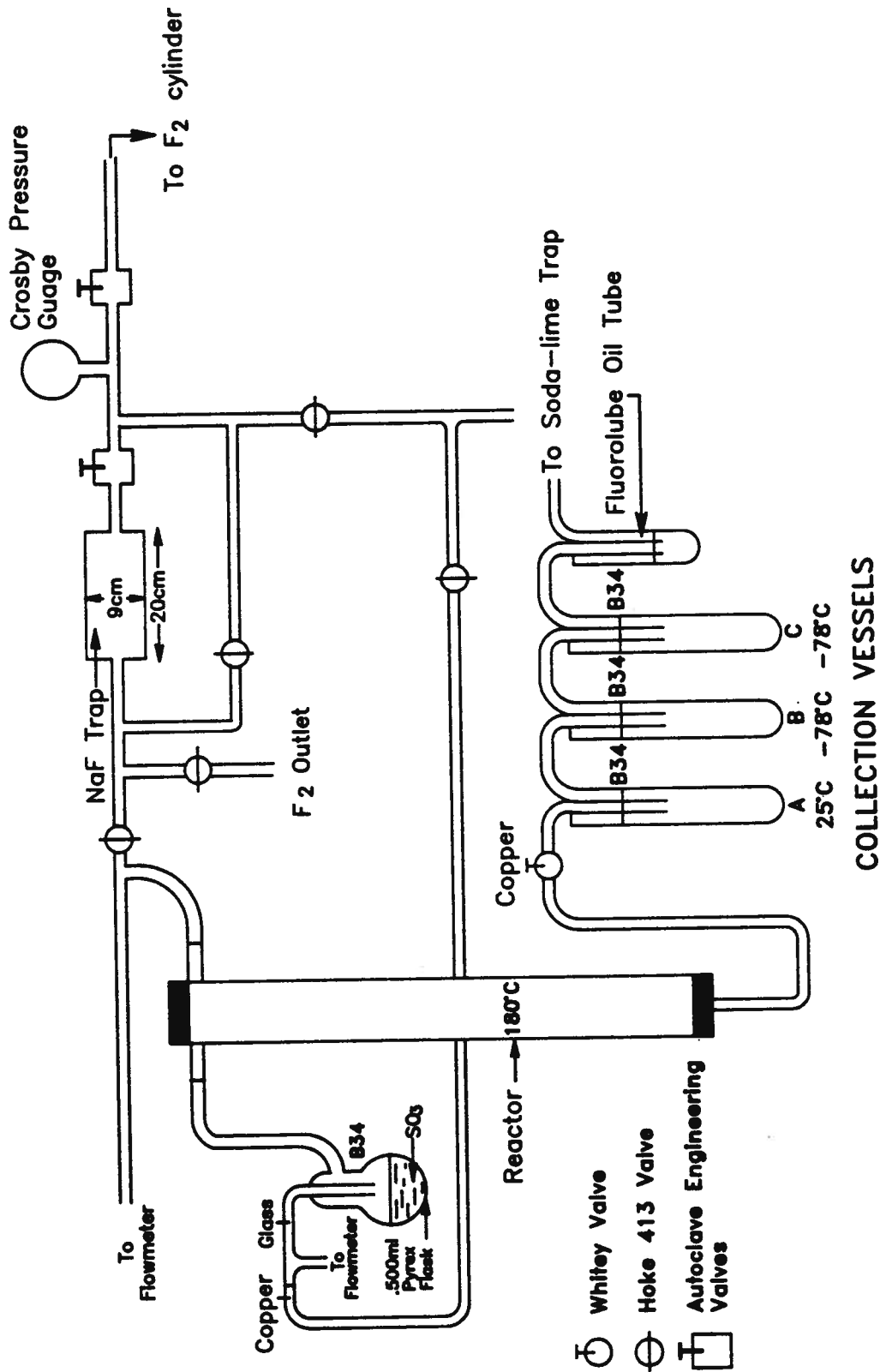


Figure 2.1: Apparatus for Preparing $S_2O_6F_2$

Most of the potentially explosive byproduct FSO_3F was removed by intermittently warming the product to room temperature and cooling down to -78°C . Further purification was achieved by pumping on the product overnight at -78°C to remove any residual FSO_3F . Unreacted SO_3 was removed by extracting the crude $\text{S}_2\text{O}_6\text{F}_2$ with concentrated H_2SO_4 in a separatory funnel. A product obtained by this route may contain a small amount of disulfuryl difluoride, $\text{S}_2\text{O}_5\text{F}_2$, which has no effect on the synthetic reactions, except where a stoichiometric amount of $\text{S}_2\text{O}_6\text{F}_2$ is required. The purified colorless liquid was vacuum distilled into large (500-1000 mL) one-part Pyrex storage vessels equipped with Kontes Teflon stem stopcocks. The purity of the reagent was checked by both IR and ^{19}F -NMR spectroscopy.

- (b) BrSO_3F was synthesized by reacting Br_2 with a slight excess of $\text{S}_2\text{O}_6\text{F}_2$ (4) in a long stem one-part Pyrex reactor. The excess $\text{S}_2\text{O}_6\text{F}_2$ was required to remove any unreacted Br_2 from the liquid product. The BrSO_3F obtained by this method can be vacuum distilled directly from the Pyrex vessel when required.

2.3 Apparatus

2.3.1 Reaction Vessels

One part glass Pyrex reactors of 25-100 mL capacity were used when solid products could be isolated by removing the volatiles *in vacuo*. These round bottom reactors were fitted with Kontes Teflon stem stopcocks and had side arms extending to B10 ground glass cones (Figure 2.2(a)). If high pressures were anticipated during reactions, 3 mm thick-wall rather than 2 mm normal wall vessels were employed.

To facilitate the isolation of products by filtration, two-part reactors made from 50-100

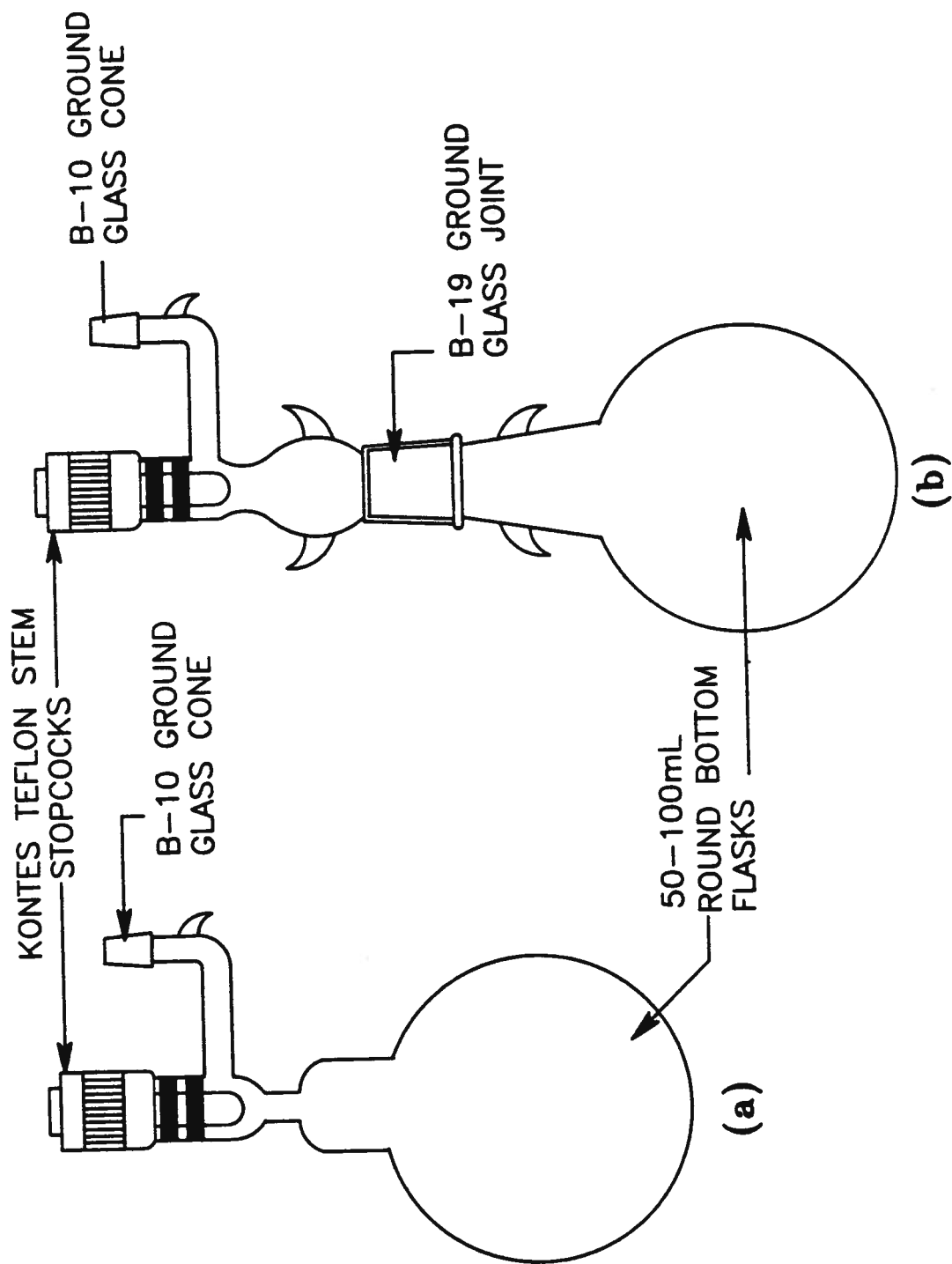


Figure 2.2: Typical Pyrex Reaction Vessels
 (a) One Part Reactor
 (b) Two Part Reactor

mL round bottom flasks were utilized (Figure 2.2(b)). A typical reactor consisted of a round bottom flask with a B19 ground glass cone fitted with a "drip lip" to trap possible grease-contaminated liquids. The corresponding adaptor top had a Kontes Teflon stem stopcock between the B19 socket and a B10 cone. During reaction work-up, the adaptor could be substituted by an appropriate equipment - such as a vacuum filtration apparatus, seen in Figure 2.3. The design of the filter was adopted from the one described by Shriver (5).

A Kel-F tubular reactor (Figure 2.4) was employed for syntheses involving liquid HF. The Kel-F tube (2 cm o.d. and 1.2 cm i.d.; obtained from Argonne National Laboratory, USA) was held by a Monel top adaptor equipped with a Whitey valve (type 1KS4-316) which could be fitted to a metal vacuum line.

2.3.2. SbF_5 - Storage-bridge Vessel

The purified liquid SbF_5 was stored in a dual purpose one-part Pyrex container as shown in Figure 2.5. The two Kontes Teflon stem stopcocks and B10 ground glass joints made it feasible for the vessel to be attached to a glass vacuum line and a Pyrex reactor simultaneously. SbF_5 could then be distilled directly from the storage vessel into the reactor via the side arm extension.

2.3.3 $\text{S}_2\text{O}_6\text{F}_2$ - Addition Trap

Where exact amounts of $\text{S}_2\text{O}_6\text{F}_2$ had to be used, a 1.00 or 4.00 mL graduated pipet equipped with an overflow bulb and fitted on top with a Kontes Teflon stem stopcock was employed. The side arm of the trap ended in a B10 ground glass cone, which could be connected to a Pyrex T-shaped bridge for the transfer of $\text{S}_2\text{O}_6\text{F}_2$. Determination of the precise amount of $\text{S}_2\text{O}_6\text{F}_2$ used was obtained by weight difference.

Figure 2.3: Vacuum Filtration Apparatus

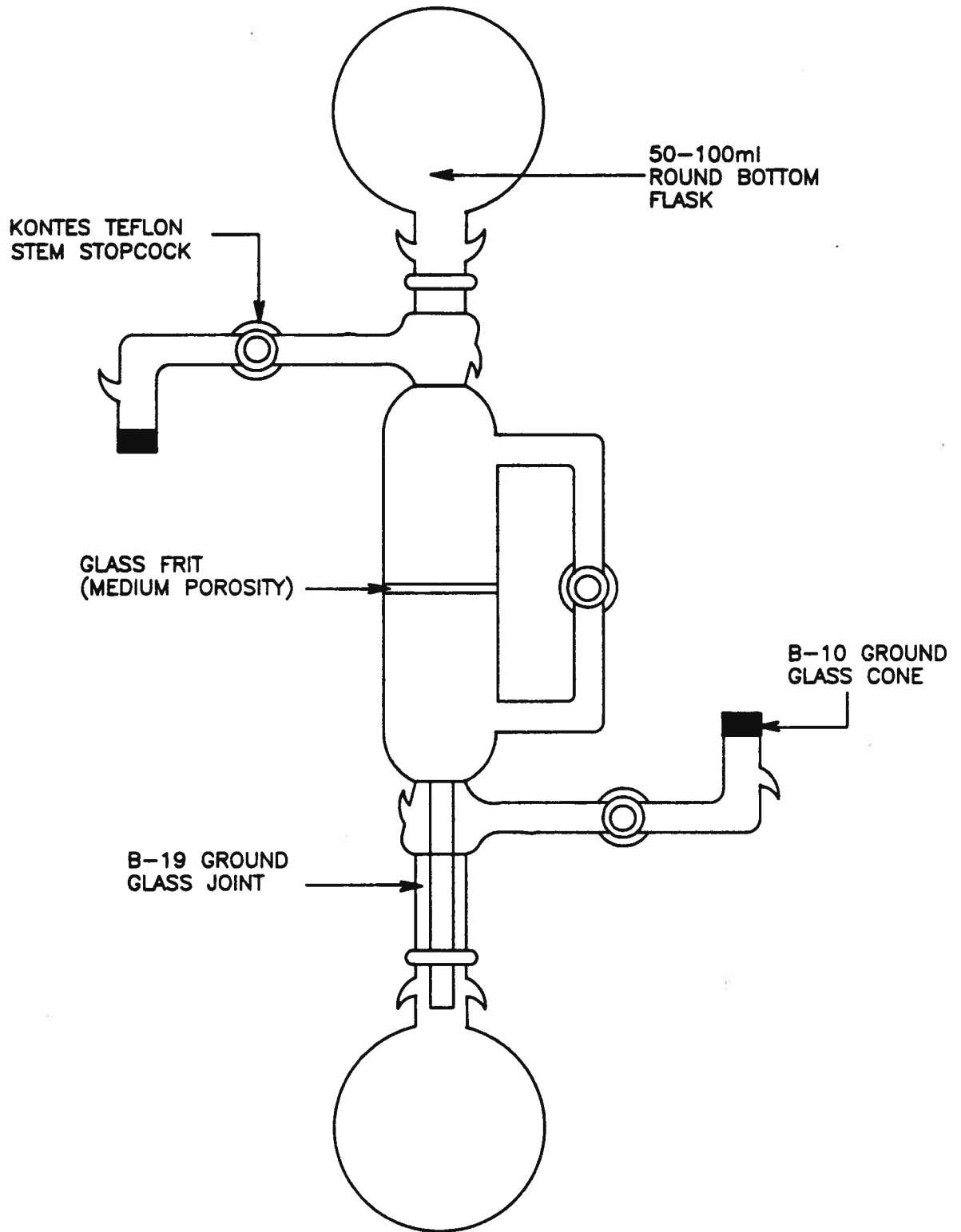


Figure 2.4: Kel-F Tubular Reactor

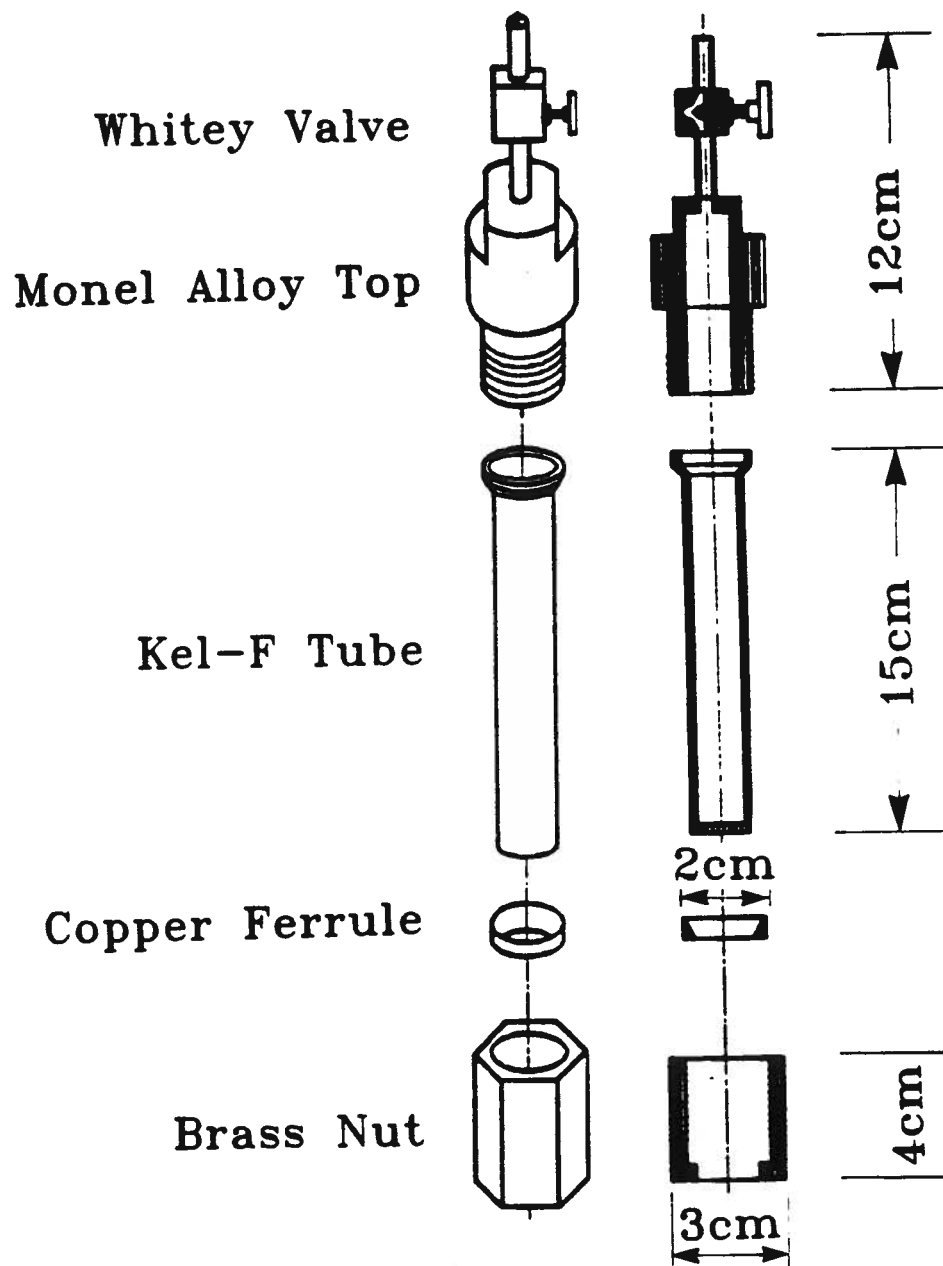
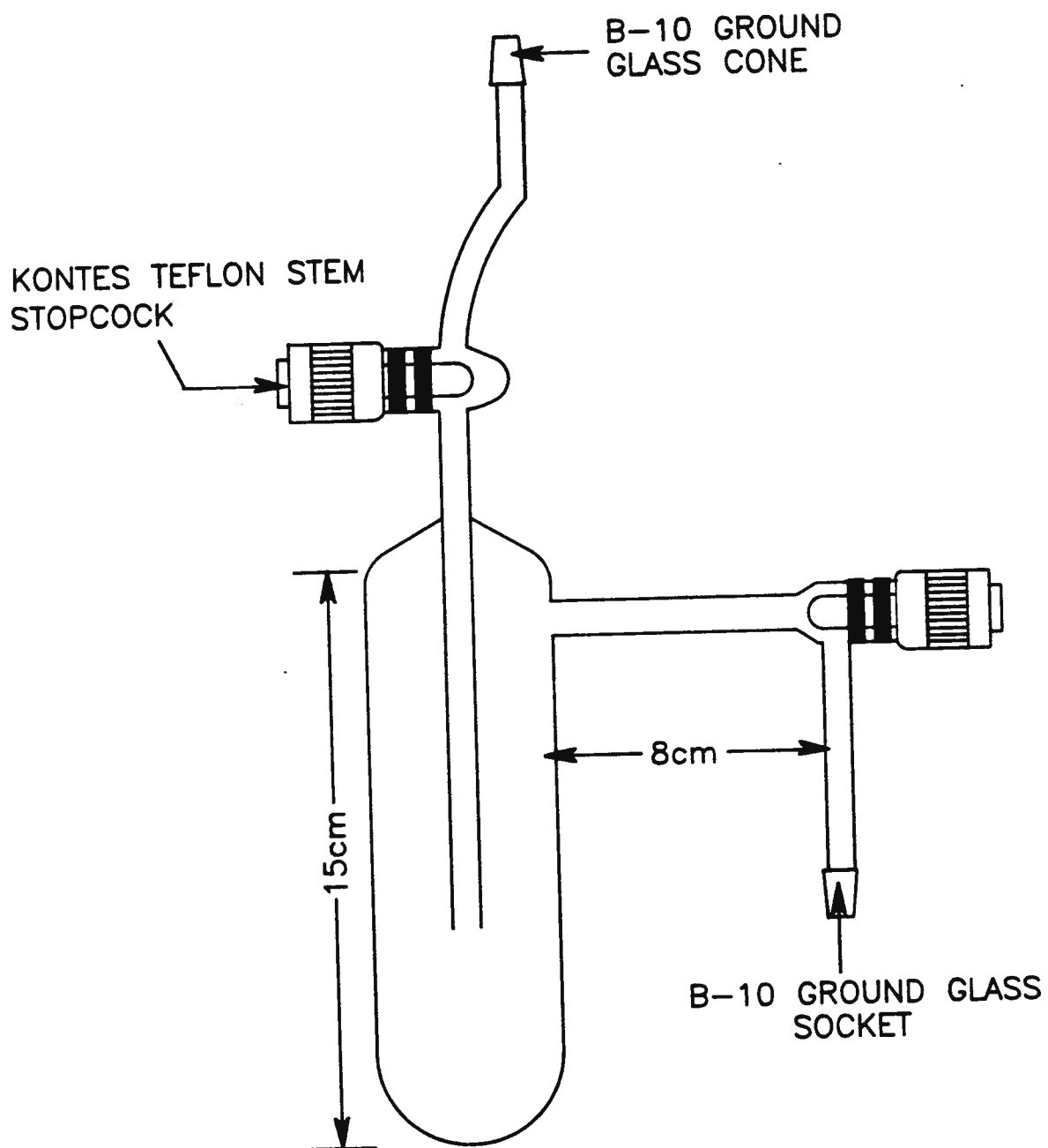


Figure 2.5: SbF₅-Storage-bridge Vessel



2.3.4 Pyrex Vacuum Line

A general purpose glass vacuum line, consisting of five Kontes Teflon stem stopcocks with B10 ground glass sockets, was used. The manifold was approximately 60 cm long, and a detachable safety trap, cooled with liquid N₂, was placed between the manifold and the vacuum pump to protect the pump from volatile corrosive materials. Typical vacuum generated on this line was about 10⁻² torr.

2.3.5 Metal Vacuum Line

For the reactions involving liquid HF, a metal vacuum line was used. It was operated in a manner similar to that of the Pyrex line. The metal manifold was constructed using 6 cm o.d. Monel tubing equipped with Whitey valves (type 1KS4-316), and connected to a liquid N₂ cooled safety trap via a Teflon adaptor.

2.3.6 Dry Atmosphere Box

Hygroscopic solids and low volatility liquids were manipulated inside a Vacuum Atmosphere Corporation "Dri-Lab" Model DL-001 SG dry box, filled with K-grade N₂ gas. The removal of moisture inside the dry box was accomplished by circulating the nitrogen over molecular sieves located in the "Dri-Train" Model HE-493. The molecular sieves were periodically regenerated by heating in a stream of 10% H₂ mixed with N₂. Fresh P₂O₅ was also kept inside the dry box to exclude any residual moisture.

2.4 Instrumentation and Methods

2.4.1 Infrared Spectroscopy

Room temperature IR spectra were recorded using three types of spectrometers: (a) Nicolet 5DX FT-IR, (b) Perkin Elmer 1710 FT-IR, and (c) Perkin Elmer 598.

Samples were run on thin solid films pressed between AgCl or AgBr windows, with transmission ranges down to ~ 400 and ~ 250 cm^{-1} respectively. The high reactivity of the compounds studied precluded the use of mulling agents or other window materials. Samples were prepared inside the dry box and the spectra were recorded immediately after removing the samples from the box. Spectra of gaseous samples were recorded using a glass cell of 10 cm path length, fitted with AgBr windows and a Kontes Teflon stem stopcock. All spectra were calibrated with a polystyrene reference.

2.4.2 Raman Spectroscopy

Raman spectra were obtained with a Spex Ramalog 5 Spectrophotometer equipped with a Spectra Physics 164 argon ion laser, using the 514.4 nm green line as the excitation wavelength. Solid samples were packed in the dry box into melting point capillaries, temporarily sealed with Fluorolube grease and then immediately flame-sealed.

2.4.3 Nuclear Magnetic Resonance Spectroscopy

The FT-NMR spectra were obtained on a Varian XL-300 multinuclear spectrometer, with the following operating frequencies and external references: (a) ^1H = 300 MHz, TMS; (b) ^{19}F = 282.231 MHz, CFCl_3 . The solutions were either loaded into 5 mm NMR tubes inside the

dry box or, in the case of volatile liquids, transferred via a static vacuum into NMR tubes fitted with B10 ground glass cones and then flame sealed. Low temperature spectra were recorded by cooling the probe with liquid N₂ and controlling the temperature with a high precision thermocouple.

2.4.4 Electronic Spectroscopy

Solid state electronic spectra in the near infrared and visible regions (4,000 to 30,000 cm⁻¹) were recorded on a Cary 14 spectrophotometer. Samples were prepared in the dry box, and run as mulls in either SbF₅ or Fluorolube oil as mulling agent in a Teflon cell fitted with quartz windows of 2.5 cm diameter. The absorbance level was adjusted with neutral density filters. Nujol mull spectra in the UV-visible range (12,000 to 50,000 cm⁻¹) were run on a Hewlett Packard 8452-A diode array spectrophotometer using the same Teflon Cell described above.

2.4.5 Mössbauer Spectroscopy

The ¹¹⁹Sn Mössbauer spectra were recorded on a constant acceleration spectrometer (6). Data counts were accumulated on a Tracer-Northern TN-1706 multichannel analyzer, linked to the mainframe computer via an IBM-PC. The γ -ray source used was Ba¹¹⁹SnO₃, and the Doppler Velocity Scale was calibrated with an iron foil absorber and a ⁵⁷Co source. The chemical shifts were measured relative to SnO₂.

2.4.6 X-ray Photoelectron Spectroscopy

X-ray photoelectron spectra were recorded with a Varian IEE-15 spectrometer using Al K α X-rays of 1486.6 eV energy. The detachable XPS sample probe was taken inside the dry

box where powdered samples were thinly dusted onto 2 cm length 3M Scotch tapes, which were wrapped around the sample slugs. The carbon $1S_{1/2}$ binding energy peak at 284.0 eV was used as a calibrant in all the measurements. The chemical shift is taken as the difference between the measured binding energy of a peak and that of the chosen standard atomic peak for a given energy level. The accuracy of the measurements is estimated to be ± 0.1 eV.

2.4.7 Magnetic Susceptibility Measurements

Variable temperature magnetic susceptibility measurements from ~ 2.0 -124 K were made using a Princeton Applied Research Model 155 Vibrating Sample Magnetometer, internally calibrated with ultrapure nickel (7). Temperature equilibration was obtained using a Janis Research Company Model 153 Cryostat and a Princeton Applied Research Model 152 Cryogenic temperature controller. Accurately weighed samples of ~ 200 -300 mg were loaded into Kel-F capsules inside the dry box and sealed with epoxy resin.

Temperature measurements were taken with a chromel vs. Au-0.02% Fe thermocouple, located in the sample holder immediately above the sample. The thermocouple was calibrated using the known susceptibility vs. temperature behavior of tetramethylethylenediammonium tetrachlorocuprate (II) and checked with mercury tetrathiocyanatocobaltate (II). From the scatter in data points of four different calibrations, the temperatures are estimated to be accurate to $\pm 1\%$ over the range studied. Thermocouple potentials were measured using a Fluke 8200A digital voltmeter. Magnetic fields of 7501, 9225, and 9625 G were employed, and set to an accuracy of 0.5%, and measured with a F.W. Bell Inc. Model 620 Gaussmeter. The accuracy of the susceptibility values is estimated to be $\pm 1\%$.

A Gouy balance, equipped with a Mettler AE 163 balance was used in the temperature range ~ 80 -300 K to measure the susceptibility of some compounds. Samples were packed in a

Pyrex tube containing an air-tight Teflon cap. Measurements were made in a nitrogen atmosphere at a field strength of 8000G and HgCo (NCS)₄ was again used as a calibrant. The accuracy of the susceptibility values obtained by this method is estimated as $\pm 5\%$. Corrections were made for the diamagnetic contribution of the holders and the molar susceptibilities were corrected for diamagnetism using the following values (8) (units of $10^{-6} \text{ cm}^3 \text{ mol}^{-1}$): SO₃F⁻ 40; SO₃CF₃⁻ 46; SbF₆⁻ 80; Sb₃F₁₆⁻ 218; Sb₂F₁₁⁻ 149; AsF₆⁻ 72; O₂⁺ 7; Br₂⁺ 61; I₂⁺ 89; Ni²⁺ 11; Pd²⁺ 25; Pd⁴⁺ 18; Cu²⁺ 11; Ag²⁺ 24.

2.4.8 X-ray Powder Diffractometry

X-ray powder diffraction patterns were obtained using a RU 200B series Rigaku Rotating Anode Diffractometer operating at 12 KW maximum power output. The Diffractometer detected Cu K_α target radiation through a 200 μm nickel filter with a horizontal-type NaI Scintillator probe. A horizontal goniometer was used for the rotating anode. The diffractometer was interfaced with a DMax/B computer system driven by an IBM PS/2. The peak-finding program was provided by Rigaku.

Finely powdered samples were put on two sided 3M Scotch tapes attached to glass slides and protected from moisture by sealing the samples with plastic film. All preparations were carried out inside the dry box and samples were analyzed as soon as they were removed from the dry box.

2.4.9 Differential Scanning Calorimetry (DSC)

DSC studies were performed using a Mettler DSC-20 cell interfaced with a Mettler TC10 TA processor and a Swiss Matrix printer. Finely powdered samples of approximately 2-4 g were sealed into aluminum pans and mounted on the measuring cell, under a dry N₂ flow

rate of 50 ml/min. The samples were scanned through a temperature range of 35 to 450°C with 4°C per minute increments.

2.4.10 Elemental Analyses

Carbon, hydrogen and some of the sulfur analyses were performed by Mr. Peter Borda of this Department. All other elemental analyses were carried out by the Analytische Laboratorien, Gummersbach, Germany.

References

- 1.a) W.W. Wilson and F. Aubke, J. Fluorine Chem., **13**, 431 (1979).
- b) W.W. Wilson, R.C. Thompson, and F. Aubke, Inorg. Chem., **19**, 1489 (1980).
2. J. Barr, R.J. Gillespie, and R.C. Thompson, Inorg. Chem., **3**, 1149 (1964).
- 3.a) J.M. Shreeve and G.H. Cady, Inorg. Synth., **7**, 124 (1963).
- b) G.H. Cady, Inorg. Synth., **11**, 155 (1967).
4. F. Aubke and R.J. Gillespie, Inorg. Chem., **7**, 599 (1968).
5. D.F. Shriver, "The Manipulation of Air Sensitive Compounds", McGraw Hill Book Co., New York, 1969.
6. J.R. Sams and T.B. Tsin, Inorg. Chem., **14**, 1573 (1975).
7. J.S. Haynes, K.W. Oliver, S.J. Rettig, R.C. Thompson, and J. Trotter, Can. J. Chem., **62**, 891 (1984).
8. Landolt-Börnstein, Numerical data and functional relations in Science and Technology, Vol. 2, Magnetic properties of coordination and organometallic compounds, Springer-Verlag, Berlin, 1966.

CHAPTER 3

METAL(II) HEXAFLUORO ANTIMONATES $M(\text{SbF}_6)_2$,

$M(\text{II}) = \text{Sn}(\text{II}), \text{Ni}(\text{II}), \text{Pd}(\text{II}), \text{Cu}(\text{II}) \text{ AND } \text{Ag}(\text{II})$

3.1 Introduction

Antimony(V) fluoride, SbF_5 , is commonly regarded as the strongest molecular Lewis acid (1). Conversely the anions SbF_6^- and the related $\text{Sb}_2\text{F}_{11}^-$ are extremely weak nucleophiles (2), capable of stabilizing a wide range of electrophilic cations, both in solid compounds and in HF-SbF_5 superacid solution (3).

The objective of this study was the synthesis and characterization of SbF_6^- salts formed by divalent metal cations. The synthetic route chosen was the solvolysis of metal fluorosulfates in liquid SbF_5 according to the general route:



with $M = \text{Sn}, \text{Ni}, \text{Pd}, \text{Cu}, \text{ or } \text{Ag}$.

Early work by Gillespie and Rothenbury (4), and a subsequent investigation by our group (5) into the antimony-fluoride-fluorosulfate system, form the basis for this synthetic reaction. The byproduct $\text{Sb}_2\text{F}_9\text{SO}_3\text{F}$ which is the most volatile component in this system, facilitates the ready removal of the SO_3F - group from the reaction mixture.

As mentioned previously in Chapter 1, initial uses of the solvolysis reaction in SbF_5 have involved the stabilization of non-metallic cations, such as ClO_2^+ (6), a series of triatomic inter-

halogen cations (7), or the dihalogen cations Br_2^+ and I_2^+ (8) (see Chapter 4) in solid compounds. Use of this method in the synthesis of the first stage graphite salt C_8SbF_6 (9) and stabilization of the dimethyltin(IV) cation as $(\text{CH}_3)_2\text{Sn}(\text{Sb}_2\text{F}_{11})_2$ (10) illustrate its versatility.

There has been a variety of alternative methods used for the synthesis of hexafluoroantimonates of divalent metals, and two of the compounds discussed here ($\text{Ni}(\text{SbF}_6)_2$ (11,12) and $\text{Sn}(\text{SbF}_6)_2$ (13)) had been prepared when this study was started. All methods have the use of SbF_5 in common, even though the routes vary. Metal oxidation either by elemental fluorine or by SbF_5 in SO_2 solution has allowed the synthesis of $\text{Ni}(\text{SbF}_6)_2$ (11,12) as well as $\text{Fe}(\text{SbF}_6)_2$ and $\text{Mn}(\text{SbF}_6)_2$ (12). However, there are obvious limitations to this approach. Where higher oxidation states are accessible, direct fluorination may result in oxidation beyond the +2 state, unless the reaction conditions are well understood and carefully controlled. Oxidation by SbF_5 fails for metal with higher oxidation potentials than provided for by the Sb(V)/Sb(III) couple (Appendix A-1). Quantitative separation of the reduced product, solid $\text{SbF}_3 \cdot \text{SbF}_5$, may prove to be difficult, and mixed fluoride-hexafluoroantimonates like $\text{CoF}(\text{SbF}_6)$ (12) may form instead.

Fluoride abstraction from MF_2 by SbF_5 in SO_2 or anhydrous HF may be a more versatile synthetic method (13,14), but here another problem surfaces: the MF_2 lattice could be incompletely broken up under the reaction conditions. This can lead to the formation of $\text{MF}(\text{Sb}_2\text{F}_{11})$, a structural isomer of $\text{M}(\text{SbF}_6)_2$, and consequently chemical analysis becomes inconclusive. When moving from ionic SbF_6^- to coordinated SbF_6^- in these compounds, vibrational spectra become more complex and are less readily interpreted. As a consequence, formulation as $\text{MF}_2 \cdot 2\text{SbF}_5$ is employed in a recent publication for materials obtained in this manner (14).

There is a fair amount of evidence for the existence of cations of the type $[\text{MF}]^+$, $[\text{M}_2\text{F}_3]^+$, and $[\text{MF}^+]_n$ when AsF_6^- is used as a counter anion (15,16), and a crystal structure

obtained on $\text{AgF}_2 \cdot \text{AsF}_5$ (17) shows a chain-type cation $[\text{AgF}^+]_n$ with AsF_6^- as counter anion. In $\text{AgF}_2 \cdot 2\text{SbF}_5$ however, a true Ag^{2+} appears to be present and the crystal structure supports its formulation as $\text{Ag}(\text{SbF}_6)_2$ (14).

The advantages of using the $\text{M}(\text{SO}_3\text{F})_2$ - excess SbF_5 solvolysis method as a viable synthetic route to metal(II) hexafluoro antimonates are summarized below:

- (i) $\text{M}(\text{SO}_3\text{F})_2$ precursors are readily available either from the solvolysis of SnCl_2 or NiCl_2 , or the corresponding Ni(II) or Cu(II) benzoates or other carboxylates in HSO_3F (18), or by the use of $\text{S}_2\text{O}_6\text{F}_2$ in the case of $\text{Pd}(\text{SO}_3\text{F})_2$ (19) and $\text{Ag}(\text{SO}_3\text{F})_2$ (20).
- (ii) In all instances further oxidation by SbF_5 appears unlikely, since higher oxidation states for the metals cannot be achieved with the potential provided for only by the Sb(V)/Sb(III) couple.
- (iii) Vibrational spectra allow monitoring of the reaction by probing the absence of SO_3F^- vibrations. All the vibrational bands due to SbF_6^- appear below $\sim 750 \text{ cm}^{-1}$, whereas SO_3F^- stretching vibrations are present well above this value (see Appendix A-2).
- (iv) Reactions can be carried out under mild conditions in glass vessels and followed by weight. This also facilitates detection of any color changes that may occur during the reaction process.

The reasons for the preparation and selection of these five $\text{M}(\text{SbF}_6)_2$ compounds for this study, with $\text{M} = \text{Sn}, \text{Ni}, \text{Pd}, \text{Cu},$ or Ag are two-fold:

- (i) To avoid structural ambiguities of the type observed above, it became necessary to

obtain a ^{119}Sn Mössbauer spectrum on a sample of $\text{Sn}(\text{SbF}_6)_2$ prepared by a different route and to compare it to the spectrum reported previously (13). Furthermore, it was found previously that the SbF_6^- and $\text{Sb}_2\text{F}_{11}^-$ anions allow a close approach to the true $(\text{CH}_3)_2\text{Sn}^{2+}$ cation (10) on account of their low nucleophilicity. The same anions, it is felt, also permit the closest approach to a true Sn^{2+} cation. In both instances, ^{119}Sn -Mössbauer spectroscopy can be effectively employed.

- (ii) Significant ferromagnetism was observed at low temperature in the fluorosulfates of Pd^{2+} and Ag^{2+} (Chapter 6, also ref. 21) with a weaker manifestation of this interesting coupling phenomenon seen also in the analogous $\text{Ni}(\text{SO}_3\text{F})_2$ compound. However, surprisingly the $\text{Cu}(\text{SO}_3\text{F})_2$ compound is magnetically dilute to low temperatures (see Chapter 6). Therefore it is of interest to study the magnetic properties of the four corresponding transition-metal SbF_6^- derivatives at temperatures below 80 K.

Since $\text{Ni}(\text{SbF}_6)_2$ had been obtained previously by all three methods (11,12,14) discussed above, its formation by solvolysis in liquid SbF_5 is viewed as a test case. A final point of interest concerns the nickel(II) and palladium(II) compounds. The Pd^{2+} and Ni^{2+} ions in the fluorosulfate are located in an octahedral coordination environment which is unusual for Pd^{2+} , and as a result paramagnetic $\text{Pd}(\text{II})$ and $\text{Ni}(\text{II})$ with $^3\text{A}_{2g}$ ground state is found in both $\text{Ni}(\text{SO}_3\text{F})_2$ and $\text{Pd}(\text{SO}_3\text{F})_2$. It is expected that similar paramagnetic ions are present in the corresponding $\text{Ni}(\text{SbF}_6)_2$ and $\text{Pd}(\text{SbF}_6)_2$ compounds as well.

3.2 Experimental

3.2.1 General Synthetic Scheme to $\text{M}(\text{SbF}_6)_2$

The fluorosulfates $\text{Ni}(\text{SO}_3\text{F})_2$ (18), $\text{Cu}(\text{SO}_3\text{F})_2$ (18), $\text{Sn}(\text{SO}_3\text{F})_2$ (18), $\text{Pd}(\text{SO}_3\text{F})_2$ (19),

and $\text{Ag}(\text{SO}_3\text{F})_2$ (20) were all synthesized according to published methods.

A general synthetic method was applied to the solvolysis reactions in liquid SbF_5 . Approximately 500 mg of the $\text{M}(\text{SO}_3\text{F})_2$ compound was transferred inside the inert-atmosphere box into a preweighed reaction vessel, and ~10 mL of freshly purified SbF_5 was added subsequently by vacuum distillation. The reaction vessel was warmed up, initially to room temperature, and subsequently to 50-60°C in an oil bath. Detailed temperatures and reaction times are given below.

Only the reactions of $\text{Pd}(\text{SO}_3\text{F})_2$ (purple → light-grey) and $\text{Ag}(\text{SO}_3\text{F})_2$ (black-brown → yellow-green → off-white) involved perceptible color changes of the solid reactant and the mixture remained heterogeneous throughout. The initially very viscous antimony(V) fluoride became less viscous after about 24 h and the mixture could be stirred effectively with a magnetic stirrer. Volatiles were removed in a dynamic vacuum. A sample of $\text{Ni}(\text{SbF}_6)_2$, made from Ni and SbF_5 by fluorinating with F_2 (11), was obtained from Dr. Karl O. Christe of Rocketdyne, U.S.A.

3.2.2 Physical Properties and Analyses

Both $\text{Ni}(\text{SbF}_6)_2$ (11,12,14) and $\text{Sn}(\text{SbF}_6)_2$ (13) are known compounds. Their identities were ascertained by weight and by infrared spectroscopy. Formation of both $\text{Ni}(\text{SbF}_6)_2$ and $\text{Sn}(\text{SbF}_6)_2$ required reaction times of 14 and 2 days at 60 and 50°C, respectively. The IR frequencies observed for $\text{Ni}(\text{SbF}_6)_2$ are listed in Table 3.1. For $\text{Sn}(\text{SbF}_6)_2$ the following IR bands were found (estimated intensities are in parentheses): 700 (s, sh), 678 (s), 648 (s), 620 (m), 595 (ms), 571 (ms), 520 (m, sh), 477 (m), 432 (w).

3.2.2a $\text{Cu}(\text{SbF}_6)_2$

Reaction time 10 days, reaction temperature 50°C , white hygroscopic solid that is thermally stable up to 210°C .

Anal. Calcd. for $\text{CuSb}_2\text{F}_{12}$: Cu, 11.88; Sb, 45.51; F, 42.61%.

Found: Cu, 11.65; Sb, 45.75; F, 42.47. Total: 99.87%.

3.2.2b $\text{Pd}(\text{SbF}_6)_2$

Reaction time 14 days, reaction temperature 50°C , light-grey solid, very hygroscopic and thermally stable up to 250°C .

Anal. Calcd. for $\text{PdSb}_2\text{F}_{12}$: Pd, 18.62; Sb, 42.14; F, 39.45%.

Found: Pd, 18.35; Sb, 41.90; F, 39.18. Total: 99.43%.

3.2.2c $\beta\text{-Ag}(\text{SbF}_6)_2$

Reaction time 10 days, reaction temperature 25°C , creamy white, hygroscopic solid, melts at $180\text{-}182^\circ\text{C}$ to clear liquid.

Anal. Calcd. for $\text{AgSb}_2\text{F}_{11}$: Ag, 19.25; Sb, 43.45; F, 37.25%.

Calcd. for $\text{AgSb}_2\text{F}_{12}$: Ag, 18.62; Sb, 42.03; F, 39.35%.

Found: Ag, 18.65; Sb, 42.30; F, 39.06. Total: 100.01%.

3.2.3 Alternate Synthetic Route to $\beta\text{-Ag}(\text{SbF}_6)_2$

Two other preparative methods for $\beta\text{-Ag}(\text{SbF}_6)_2$ using the silver compounds AgSbF_6 and AgF_2 as precursors are shown below:

- a) 0.323 g of AgSbF_6 was allowed to react with an excess of $\text{S}_2\text{O}_6\text{F}_2$ at room temperature. The color of AgSbF_6 changed immediately from white to black-brown. The excess $\text{S}_2\text{O}_6\text{F}_2$ was removed *in vacuo* and subsequently replaced by an excess of SbF_5 . The mixture was kept at room temperature for 2 days, then heated at 60°C for 2 h. A white solid of the composition $\text{Ag}(\text{SbF}_6)_2$ was isolated by removing the excess SbF_5 *in vacuo* and identified by its IR spectrum.
- b) 0.436 g (2.99 mmol) of AgF_2 was loaded inside the dry box into a Kel-F reactor together with 4.50 g (20.8 mmol) of SbF_5 . About 6.5 mL anhydrous HF was distilled into this mixture *in vacuo*. After warming to room temperature under magnetic stirring, a light-yellow solid formed immediately. The solution's initial color was light blue, which faded quickly. Removal of all volatiles yielded again a compound corresponding to the composition $\text{Ag}(\text{SbF}_6)_2$ as a cream-colored solid.

3.3 Results and Discussion

3.3.1 Synthesis

As noted previously (6-10), solvolysis reactions of fluorosulfates in a large excess of SbF_5 proceed smoothly and frequently without any color change of the solid reactant. Hence, rather long reaction times are chosen to ensure complete conversion. Two indications that a reaction takes place are a noticeable decrease in the viscosity of SbF_5 after about one day, and a slight increase in the vapor pressure above the reaction mixture. Both observations may be attributed to the formation of $\text{Sb}_2\text{F}_9(\text{SO}_3\text{F})$ (7).

To reduce the viscosity even further in order to stir the heterogeneous mixture more effectively, slightly elevated reaction temperatures are chosen. Removal of all volatiles

proceeds easily in a dynamic vacuum, with the reaction flask at room temperature.

It is noteworthy that after pumping overnight, the correct weight for $M(\text{SbF}_6)_2$ is obtained. Previous use of this synthetic method (6-8,10) had in all instances led to products where molecular cations are stabilized by $\text{Sb}_2\text{F}_{11}^-$, and in one case (8) even by $\text{Sb}_3\text{F}_{16}^-$. For the spherical, less electrophilic M^{2+} cations, SbF_6^- appears to be the more suitable counter anion allowing formation of layered materials, as discussed below. In any event, neither product weights on isolation, nor chemical analyses, nor vibrational spectra give any indication of $\text{Sb}_2\text{F}_{11}^-$ containing intermediates or by-products.

Of the resulting compounds, $\text{Ni}(\text{SbF}_6)_2$ (11) and $\text{Sn}(\text{SbF}_6)_2$ (13) are identified by their weights and their previously reported IR spectra. The ^{119}Sn Mössbauer spectrum of $\text{Sn}(\text{SbF}_6)_2$ shows a single broad line ($\Gamma = 1.35 \text{ mm s}^{-1}$) caused by unresolved quadrupole splitting. The isomer shift is found at 4.39 mm s^{-1} relative to SnO_2 , in excellent agreement with the previously reported value (13).

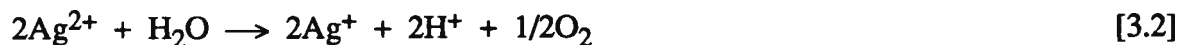
The solvolysis of $\text{Ag}(\text{SO}_3\text{F})_2$ is expected to lead to the recently reported blue form of $\text{Ag}(\text{SbF}_6)_2$ since solutions of Ag^{2+} in HF are deep blue in color. The X-ray diffraction study had revealed a true Ag^{2+} ion in a distorted octahedral environment (14). However, in this study the course of the solvolysis and the final product obtained are unanticipated. The initial black-brown color of $\text{Ag}(\text{SO}_3\text{F})_2$ quickly disappears and a greenish-blue solid slowly changes to yellow in color. Ultimately a cream-colored, diamagnetic solid is isolated, which melts at $\sim 180^\circ\text{C}$ without decomposition to a clear, colorless liquid.

The magnetic behavior, the color, and the observed lack of solubility in anhydrous HF (22) suggest the possible presence of univalent silver in the resulting yellow compound. An alternative formulation of the reaction product as $\text{AgSb}_2\text{F}_{11}$ is, however, not supported by the

weight change during reaction, a complete chemical analysis (see experimental section), the vibrational spectrum, or the chemical behavior of the material. Furthermore, with paramagnetic divalent silver well established in $\text{Ag}(\text{SO}_3\text{F})_2$ (20), the other reactant, the Lewis acid SbF_5 , can hardly be regarded as a reducing agent. A possible reductive decomposition of the reaction product appears unlikely, since besides excess SbF_5 , $\text{Sb}_2\text{F}_9(\text{SO}_3\text{F})$ is the only volatile product formed during the reaction process.

The chemical behavior of the white $\text{Ag}(\text{SbF}_6)_2$ is not consistent with the presence of Ag^+ in the reaction product. Unlike other silver(I) salts, the material will not undergo further oxidation by $\text{S}_2\text{O}_6\text{F}_2$ in the presence or the absence of HSO_3F . In contrast, AgSbF_6 is immediately oxidized by $\text{S}_2\text{O}_6\text{F}_2$ alone, to give a black-brown solid, with an increase in weight consistent with the composition $\text{Ag}(\text{SbF}_6)(\text{SO}_3\text{F})$. Subsequent solvolysis of this material in SbF_5 proceeds in an identical manner to the solvolysis of $\text{Ag}(\text{SO}_3\text{F})_2$, suggesting a viable alternative synthetic route to the white diamagnetic $\text{Ag}(\text{SbF}_6)_2$.

Strong evidence for the presence of silver in an oxidation state higher than +1 comes from the hydrolysis of $\text{Ag}(\text{SbF}_6)_2$ in aqueous KI solution. The reaction proceeds very vigorously and I_2 and O_2 (where the latter evolves with rapid bubbling) are produced. Formation of I_2 may in part be due to oxidation by Sb(V) in an acidic environment (23), but evolution of O_2 can only be caused by Ag(II) or Ag(III) ((24), also Appendix A-1):



and



In summary, all evidence suggests that the material obtained in the solvolysis of

$\text{Ag}(\text{SO}_3\text{F})_2$ in SbF_5 is $\beta\text{-Ag}(\text{SbF}_6)_2$, a valence isomer of the previously reported $\alpha\text{-Ag}(\text{SbF}_6)_2$ (14).

Attempts were made to synthesize the α -form using the published method (14), where AgF_2 was reacted with SbF_5 in anhydrous HF according to:



These syntheses are only partially successful if a slight excess of SbF_5 (ratio $\text{SbF}_5:\text{AgF}_2 = 2.32$) over the stoichiometric amount is used. Even here a fair amount of solid $\beta\text{-Ag}(\text{SbF}_6)_2$ forms in addition to a blue solution, from which crystalline $\alpha\text{-Ag}(\text{SbF}_6)_2$ is obtained by slow evaporation of the volatiles. When a larger excess of SbF_5 is used ($\text{SbF}_5:\text{AgF}_2 = 6.01$), $\beta\text{-Ag}(\text{SbF}_6)_2$ is the only product. The blue color of the HF solution quickly fades within an hour. Removal of the HF and the excess SbF_5 yields pure $\beta\text{-Ag}(\text{SbF}_6)_2$.

It seems that formation of $\alpha\text{-Ag}(\text{SbF}_6)_2$ in HF represents an acid-base titration with both the cation $\text{Ag}^{2+}_{(\text{solv})}$ and the final product $\alpha\text{-Ag}(\text{SbF}_6)_2$ stable in, and isolable from, anhydrous HF. Similar behavior is reported for all other transition-metal hexafluoro antimonates of the $\text{M}(\text{SbF}_6)_2$ or $\text{MF}_2 \cdot 2\text{SbF}_5$ type (14). On the other hand, $\beta\text{-Ag}(\text{SbF}_6)_2$ is insoluble in anhydrous HF, suggesting structural differences.

The observed diamagnetism of the compound is best explained by assuming a mixed-oxidation-state compound of the composition $\text{Ag}(\text{I})\text{Ag}(\text{III})(\text{SbF}_6)_4$. To account for the diamagnetism, Ag^{3+} should be in a square planar, or at least in a tetragonally elongated, octahedral environment while Ag^+ would be located in a tetragonally compressed, nearly linear coordination environment. Argentic oxide, AgO , represents a precedent, according to neutron diffraction studies on this compound (25). The black-brown color, also found for the recently reported

oxides Ag_2O_3 (26) and Ag_3O_4 (24), is seemingly common to binary oxides and oxysalts of di- or trivalent silver, e.g. the sulfonates $\text{Ag}(\text{SO}_3\text{F})_2$ (20) or $\text{Ag}(\text{SO}_3\text{CF}_3)_2$ (27), and may possibly be due to a charge transfer transition (28). In contrast, alkali metal salts containing the $[\text{AgF}_4]^-$ ion are reported to be yellow (25,29), while AgF_2 and many $\text{Ag}(\text{III})$ fluoro derivatives are blue (30), just like $\alpha\text{-Ag}(\text{SbF}_6)_2$ (14).

It appears, then, that all the observations mentioned above support formulation of the β -form as $\text{Ag}(\text{I})\text{Ag}(\text{III})(\text{SbF}_6)_4$; however, the inability to oxidize Ag^+ further with $\text{S}_2\text{O}_6\text{F}_2$ is not consistent with an ionic formulation as silver(I) tetrakis(hexafluoroantimonato)argentate(III), $\text{Ag}^+[\text{Ag}(\text{SbF}_6)_4]^-$.

No report has been published so far of any other valence isomeric pair of the $\text{Ag}(\text{II})$ vs. $\text{Ag}(\text{I})\text{Ag}(\text{III})$ type. The above mentioned AgO is reported to be $\text{Ag}(\text{I})\text{Ag}(\text{III})\text{O}_2$ (25), but a true $\text{Ag}(\text{II})\text{O}$ appears to be still missing. However, the crystal structure of Ag_3O_4 (24) shows both $\text{Ag}(\text{II})$ and $\text{Ag}(\text{III})$ in square planar coordination sites, and mixed oxidation-state compounds of the type $\text{Pd}(\text{II})\text{Pd}(\text{IV})\text{X}_6$, with $\text{X} = \text{F}$ (31) or SO_3F (19), are known for palladium, the neighboring element in the 4d series, with $\text{Pd}(\text{III})\text{X}_3$ so far unknown. Little is known, at least with regard to structure, about the paramagnetic red-brown compound AgF_3 (32). The mixed valency formula $\text{Ag}(\text{II})\text{Ag}(\text{IV})\text{F}_6$ has been proposed but the product may still contain some impurities (33).

Observations made during the course of this study suggest that $\alpha\text{-Ag}(\text{SbF}_6)_2$ may be irreversibly converted to the β -valence isomer. This conversion occurs at room temperature, if SbF_5 is present in an excess, either in the presence or absence of HF . It is therefore not surprising that all the attempts made to synthesize pure $\alpha\text{-Ag}(\text{SbF}_6)_2$ from AgF_2 and SbF_5 in anhydrous HF (14) produce $\beta\text{-Ag}(\text{SbF}_6)_2$ as well, as an insoluble precipitate in addition to the blue solution. Removal of the solvent at -78°C in a dynamic vacuum affords a mixture of the two valence isomers.

Heating the isomeric mixture allows transformation to the pure β -form. Following this conversion by differential scanning calorimetry indicates two endothermic events, a sharp peak at 100°C, and a broad peak at 139-140°C. The latter peak coincides with the melting point, where a colorless liquid forms. The β -form melts at ~180°C, consistent with differential scanning calorimetry. Absence of the peak at 100°C suggests interpretation of this thermal event as a phase transition from α -Ag(SbF₆)₂ to β -Ag(SbF₆)₂.

It seems likely that electron transfer between two Ag²⁺ ions to give Ag⁺ and Ag³⁺ is mediated by an antimony(V) fluoro species (SbF₅ or SbF₆⁻). Considering the observations made regarding the relative stability of the two valence isomers, it is surprising that β -Ag(SbF₆)₂ has not been reported while the α -form has.

The solvolysis of Pd(SO₃F)₂ in SbF₅, on the other hand, does not appear to change the electronic structure of the Pd²⁺ ion (31,34). The electronic spectra and magnetic susceptibility data clearly show that in Pd(SbF₆)₂, the palladium ion, like in its parent compound, remains as a paramagnetic Pd²⁺ species. However, in Cu(SbF₆)₂, the solvolysis product of Cu(SO₃F)₂, identification of all the copper ions as purely divalent may not be possible. Magnetic measurements taken on Cu(SbF₆)₂ also indicate, as in the case of β -Ag(SbF₆)₂, mixed valency although to a more limited extent. This is discussed in more detail in Section 3.3.4, which deals with magnetic studies.

It is of interest to note here that this solvolysis behavior leading to unexpected mixed valent products is exhibited by the two transition metal precursor compounds Cu(SO₃F)₂ and Ag(SO₃F)₂ with "Jahn-Teller ions", i.e. Cu²⁺ and Ag²⁺ (d⁹).

3.3.2 Vibrational Spectra

The infrared spectra obtained for $\text{Ni}(\text{SbF}_6)_2$, $\text{Pd}(\text{SbF}_6)_2$, $\text{Cu}(\text{SbF}_6)_2$, and $\beta\text{-Ag}(\text{SbF}_6)_2$, together with the Raman spectra for the last two compounds, are summarized in Tables 3.1 and 3.2. Also included are the previously reported Raman spectra for $\text{Ni}(\text{SbF}_6)_2$ (11) and $\alpha\text{-Ag}(\text{SbF}_6)_2$ (14) as well as an approximate band description, also proposed previously (11). However, this description pertains only to the Ni^{2+} , Pd^{2+} , and Cu^{2+} compounds in Table 3.1. The Raman spectrum of $\beta\text{-Ag}(\text{SbF}_6)_2$ is illustrated in Figure 3.1. Attempts to obtain a Raman spectrum of $\text{Pd}(\text{SbF}_6)_2$ result in partial sample decomposition. Apparently the excitation line of the Ar^+ laser falls within ν_2 of the electronic spectrum of $\text{Pd}(\text{SbF}_6)_2$.

Agreement with the IR and Raman spectra previously reported for $\text{Ni}(\text{SbF}_6)_2$ (11) is very good with only a minor exception: an IR band at 585 cm^{-1} attributed to ν_{as} out of phase for bridging SbF_3 group is not observed in this study. This band does not have a counterpart in the Raman spectrum, and may be spurious. The band description in Table 3.1 has been amended slightly. There is only a partial comparison possible with the vibrational spectra reported for $\text{NiF}_2 \cdot 2\text{SbF}_5$ (14). The limited number of bands listed, six Raman and four IR bands with five non-coincidences, suggests an incomplete listing. Nevertheless, the Raman bands reported for $\text{NiF}_2 \cdot 2\text{SbF}_5$ (14) are all observed with similar relative intensities in the Raman spectrum of $\text{Ni}(\text{SbF}_6)_2$ (11). Since the reported X-ray powder data have the principle lines in common (11,14; see also Appendix A-3), it is reasonable to conclude that the two compounds are identical.

This is possibly not the case for $\text{Cu}(\text{SbF}_6)_2$ reported here, and $\text{CuF}_2 \cdot 2\text{SbF}_5$ (14). Very intense Raman and IR bands at 725 cm^{-1} (see Table 3.1) are apparently not observed for $\text{CuF}_2 \cdot 2\text{SbF}_5$ (14). However, the case for polymorphism as evidenced by magnetic measurements (see Section 3.3.4) is by no means as strong as in the case of the two forms of $\text{Ag}(\text{SbF}_6)_2$.

Table 3.1: Vibrational Spectra of Ni(SbF₆)₂, Pd(SbF₆)₂, and Cu(SbF₆)₂

Ni(SbF ₆) ₂ ^{a) Ra. b)} Δν [cm ⁻¹] Int.	Ni(SbF ₆) ₂ IR ν [cm ⁻¹] Int.	Pd(SbF ₆) ₂ IR ν [cm ⁻¹] Int.	Cu(SbF ₆) ₂ IR ν [cm ⁻¹] Int.	Cu(SbF ₆) ₂ Ra Δν [cm ⁻¹] Int.	Approximate Band Description for M(SbF ₆) ₂ ; M = Ni, Pd or Cu
742 (1)	738 vs	730 s, sh	729 s	725 (65)	ν _{as} SbF ₃ ^t out of phase
717 (12)	721 s, sh	716 vs	707 vs, b	721 (70)	ν _{as} SbF ₃ ^t in phase
710 (44)	710 vs	698 s	672 s	709 (18)	ν _{sym} SbF ₃ ^t out of phase
674 (100)	672 m	667 ms	665 m	671 (100)	ν _{sym} SbF ₃ ^t in phase
				657 (22)	
618 (5)	631 m	630 m	633 m		ν _{as} SbF ₃ ^b out of phase
	621 m, sh	615 ms	617 m	620 (4)	ν _{sym} SbF ₃ ^b out of phase
568 (2)	573 s	570 m	556 ms	592 (8)	ν _{as} SbF ₃ ^b in phase
	560 w, sh	550 w, sh			
511 (2)	521 mw	522 ms	496 m		ν _{sym} SbF ₃ ^b in phase
			465 m	450 (8)	
348 (0+)	350 w, sh	345 m		395 (7)	M...F-Sb stretching
322 (5)	330 w	335 m, sh		335 (11)	
308 (24)	310 w	~300 w		305 (19)	
299 (25)	295 w	285 w		295 (26)	Sb-F deformation modes
272 (3)				270 (29)	

Abbreviations: s = strong, m = medium, w = weak, v = very, sh, = shoulder,

b = broad, as = asymmetric, sym = symmetric, t = terminal, b = bridging

a) Additional bands at 246, 220 and 198 cm⁻¹ and shoulders at 172, 146, and 130 cm⁻¹

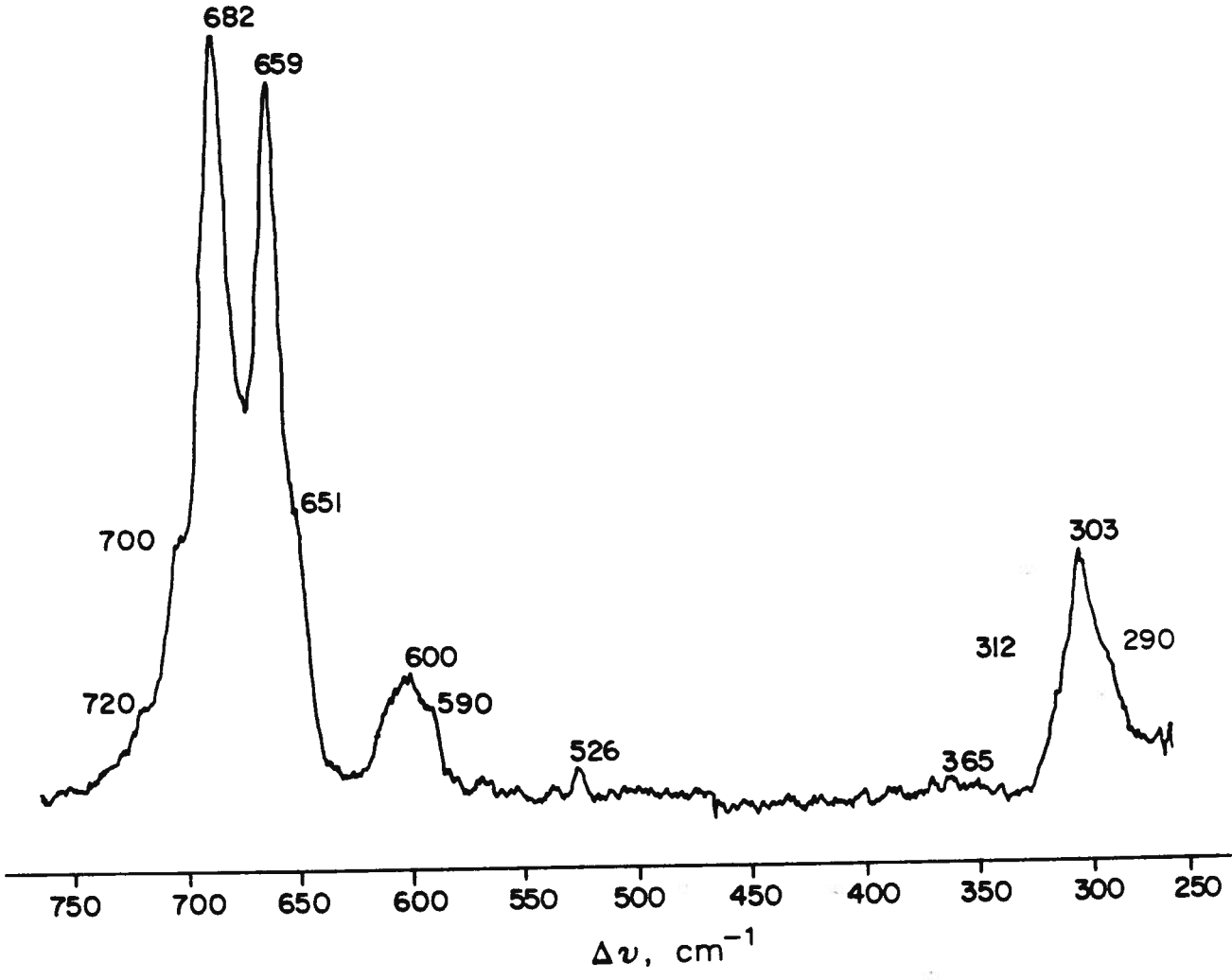
b) Ref. 14

Table 3.2: Vibrational Spectra of the Two Valence Isomers of $\text{Ag}(\text{SbF}_6)_2$

$\beta\text{-Ag}(\text{SbF}_6)_2$ Ra $\Delta\nu[\text{cm}^{-1}]$ Int.	$\beta\text{-Ag}(\text{SbF}_6)_2$ IR $\nu[\text{cm}^{-1}]$ Int.	$\alpha\text{-Ag}(\text{SbF}_6)_2$ Ra ^{a)} $\Delta\nu[\text{cm}^{-1}]$ Int.	$\alpha\text{-Ag}(\text{SbF}_6)_2$ IR ^{a)} $\nu[\text{cm}^{-1}]$ Int.	Approximate Band Description
720 sh (12)	719 s, sh			
700 sh (33)	692 vs		692 vs	SbF ⁺ stretching
682 (100)	673 s	668 (100)	668 ms	
659 (93)	654 s	658 (75)	640 m	
651 sh (30)				
600 (16)	602 m	600 (37) 580 (31)	583 w	SbF ^b stretching
526 (4)	515 vw 490 ms	552 (20)	554 w 496 w	
365 (1)	368 mw 357 w, sh			M...FSb stretching
312 sh (13)				SbF deformation
303 (32)	301 sh			
290 (18)	283 s 278 s	290 (37)		

a) Ref. 14.

Figure 3.1: Raman Spectrum of $\beta\text{-Ag}(\text{SbF}_6)_2$

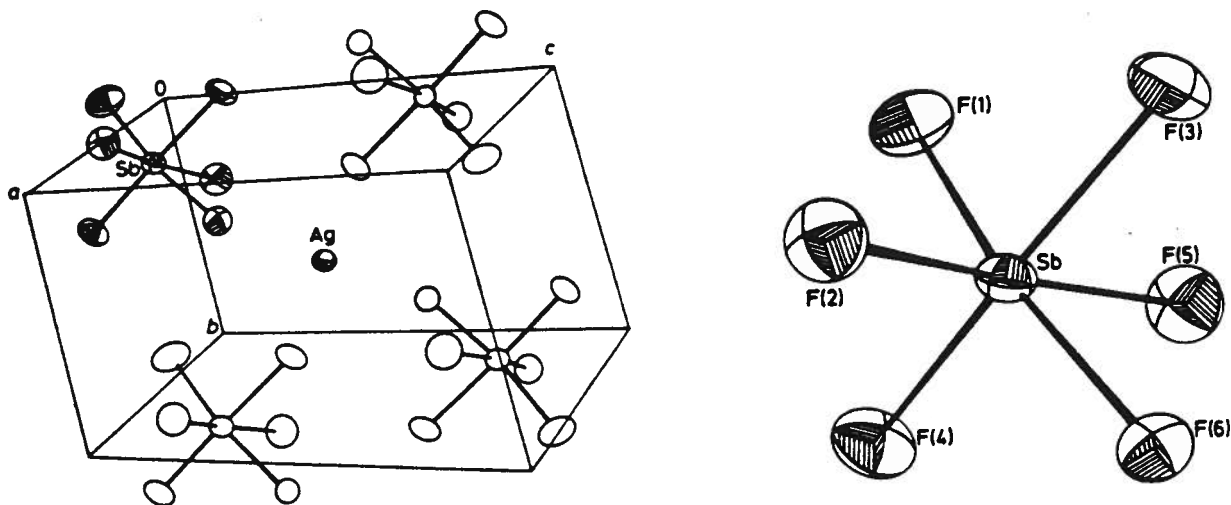


The available structural information on $M(\text{SbF}_6)_2$ compounds facilitates a discussion of the vibrational data shown in Table 3.1. A common CdCl_2 -type layer structure is proposed for $\text{Ni}(\text{SbF}_6)_2$, based on X-ray powder diffraction data (11), and evident for $\alpha\text{-Ag}(\text{SbF}_6)_2$ from the X-ray single crystal diffraction study (14) (Figure 3.2). The structure for $\text{Ni}(\text{SbF}_6)_2$ is deduced, starting from the well known LiSbF_6 structure (35) by placing Ni^{2+} into every second, nearly octahedral Li^+ site (11). In $\alpha\text{-Ag}(\text{SbF}_6)_2$, Ag^{2+} is situated in a tetragonally elongated octahedral site (Figure 3.2(c)), resulting in almost square planar coordination, similar to the coordination in AgF_2 (36). SbF_6^- acts as a tridentate bridging group (Figure 3.2(b)), with the bridging fluorines, F^b , and the terminal fluorines, F^t , in *fac*-octahedral positions. Unlike the SbF_3^b unit, the corresponding SbF_3^t -trigonal pyramid is remarkably regular with two $d_{\text{Sb-F}^t} \sim 1.836 \text{ \AA}$ and one slightly longer at 1.846 \AA .

The vibrational assignment for $\text{Ni}(\text{SbF}_6)_2$ by Christe et al. (11), adopted here in this study, suggests a useful subdivision into $\nu\text{Sb-F}_3^t$ stretching modes found above $\sim 660 \text{ cm}^{-1}$ and $\nu\text{Sb-F}_3^b$ below $\sim 635 \text{ cm}^{-1}$. Each set is further divided into symmetric and asymmetric in-phase and out-of-phase modes. The basic difference between both sets, SbF_3^b and SbF_3^t , is that the former belong to a filled, and the latter to an unoccupied octahedral hole in the $M(\text{SbF}_6)_2$ -layer structure.

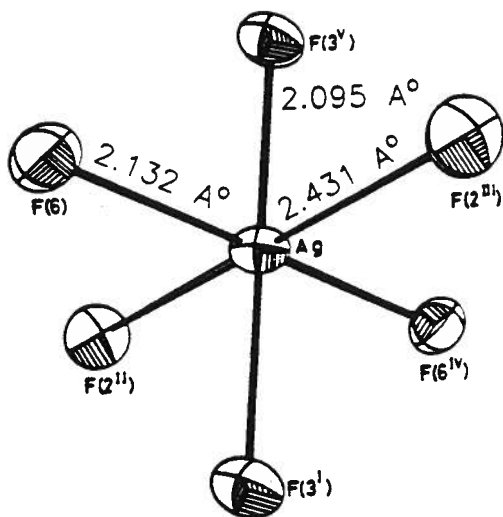
The data summarized in Table 3.1 for $M(\text{SbF}_6)_2$ with $M = \text{Ni}, \text{Pd},$ and Cu , show indeed a common group of four strong vibrations, some small band splittings for $\text{Cu}(\text{SbF}_6)_2$ notwithstanding, which are assigned as $\nu_{\text{Sb-F}^t}$ vibrations. Most prominent among them is a Raman band at $\sim 670 \text{ cm}^{-1}$, which is clearly the strongest band in the respective spectra. Interestingly, this band is found as well for a number of additional $M(\text{SbF}_6)_2$ compounds with $M = \text{Mg}, \text{Zn}, \text{Fe}, \text{Co},$ and Cu (14), in the same position, and always of the highest intensity. This is not unexpected, since the reported X-ray powder diffraction data had indicated the existence of two structurally related triads, consisting of the hexafluoro antimonates of $\text{Mg}, \text{Zn},$ and Ni , and those

Figure 3.2: Crystal Structure of α -Ag(SbF₆)₂ (Ref. 14)



(a) The Unit Cell

(b) ORTEP view of [SbF₆]⁻ anion



(c) ORTEP view of Ag²⁺ environment

of Fe, Co, and Cu (14). However, the structural differences between the two triads appear to be so small that they do not seriously affect the positions of the ${}^{\nu}\text{Sb-F}_3^{\text{t}}$ bands. In the Raman data, the 670 cm^{-1} band is attributed to a symmetric in-phase Sb-F_3^{t} stretching mode, which suggests a common SbF_3^{t} grouping in both triads as well as in $\text{Cu}(\text{SbF}_6)_2$ reported in this work. A corresponding IR band of medium intensity is observed in all instances as well. This band is found for $\text{Pd}(\text{SbF}_6)_2$ at 667 cm^{-1} . In addition, there is a close correspondence between $\text{Ni}(\text{SbF}_6)_2$ and $\text{Pd}(\text{SbF}_6)_2$ in both IR band positions and intensities to suggest isostructural compounds.

The remaining $\text{M}(\text{SbF}_6)_2$ compounds reported by Gantar et al. (14) with $\text{M} = \text{Cr, Pb, and Cd}$, differ slightly in both vibrational spectra and X-ray powder diffraction data. The highest intensity Raman band is now found at about 650 cm^{-1} . Even for these compounds, as for all the others (14), formulation as $\text{M}(\text{SbF}_6)_2$ is suggested. None of the vibrational data reported here or published previously (11,14) suggest the presence of the anion $\text{Sb}_2\text{F}_{11}^-$, by comparison to published precedents (13,37,38).

The vibrational data for both forms of $\text{Ag}(\text{SbF}_6)_2$ in Table 3.2 show interesting differences. Both have two very intense Raman bands, rather than one, in the ${}^{\nu}\text{Sb-F}_3^{\text{t}}$ region, at 668 and 658 cm^{-1} for $\alpha\text{-Ag}(\text{SbF}_6)_2$ and at 682 and 659 cm^{-1} for the β form (see Figure 3.1). In each case the band with the largest Raman shift also has the highest intensity, and yet in spite of the incomplete band listing for $\alpha\text{-Ag}(\text{SbF}_6)_2$, there appears to be some structural similarity between the two forms. Only a rather general band description is suggested, because there may be some band overlap for $\beta\text{-Ag}(\text{SbF}_6)_2$, while the listing for the α -form appears, as stated above, to be incomplete.

The distorted layer structure formed for $\alpha\text{-Ag}(\text{SbF}_6)_2$ with all tetragonally elongated octahedral holes occupied by Ag^{2+} , and concomitant tetragonally compressed, vacant sites

(14) provide a suitable model for the valence isomer as well. Regular occupation of half of the compressed holes by Ag^+ and half of the elongated holes by Ag^{3+} would allow retention of the layer structure, where Ag^+ achieves linear and Ag^{3+} square planar coordination. Conversely, two types of vacant sites are formed with two sets of Sb-F^t vibrations and different band positions for the Sb-F^b stretching modes as well, consistent with observations.

3.3.3 Electronic Spectra

Electronic mull spectra were recorded for the nickel and palladium hexafluoroantimonates, and it appears based on these spectra that the solvolysis of $\text{Ni}(\text{SO}_3\text{F})_2$ and $\text{Pd}(\text{SO}_3\text{F})_2$ in SbF_5 does not lead to a change in the electronic structures of Ni^{2+} and Pd^{2+} ions. The resulting compounds $\text{Ni}(\text{SbF}_6)_2$ and $\text{Pd}(\text{SbF}_6)_2$, like their precursors, are paramagnetic (Section 3.3.4). It is therefore not surprising that the magnetic results and the vibrational spectra point to octahedrally coordinated Ni(II) and Pd(II) in $\text{Ni}(\text{SbF}_6)_2$ and $\text{Pd}(\text{SbF}_6)_2$.

These two compounds show similar three-band electronic spectra, which can be attributed to d-d transitions. Although no extinction coefficients were obtained to support the assignment due to the insolubility of the compounds in a suitable solvent, it seems that the ligand field parameters Dq and B derived from such an assignment are very reasonable, particularly in comparison to the reported Dq and B values of the two parent compounds $\text{Ni}(\text{SO}_3\text{F})_2$ (39) and $\text{Pd}(\text{SO}_3\text{F})_2$ (19).

The electronic ground term for a d^8 ion in an octahedral ligand field is $^3A_{2g}$ and three spin allowed d-d transitions to the excited triplet-terms are expected. The energy level diagram for a d^8 ion in an octahedral field is given in Fig. 3.3. The band positions of the observed electronic spectra and the calculated ligand field parameters of $\text{Ni}(\text{SbF}_6)_2$, $\text{Pd}(\text{SbF}_6)_2$, $\text{Ni}(\text{SO}_3\text{F})_2$ (39) and $\text{Pd}(\text{SO}_3\text{F})_2$ (19) are listed in Table 3.3. It seems that the agreement in band

Figure 3.3: Spin Allowed Electronic Transitions from ${}^3A_{2g}$ Ground Term for Pd^{2+} and Ni^{2+} (d^8) in Octahedral Ligand Field

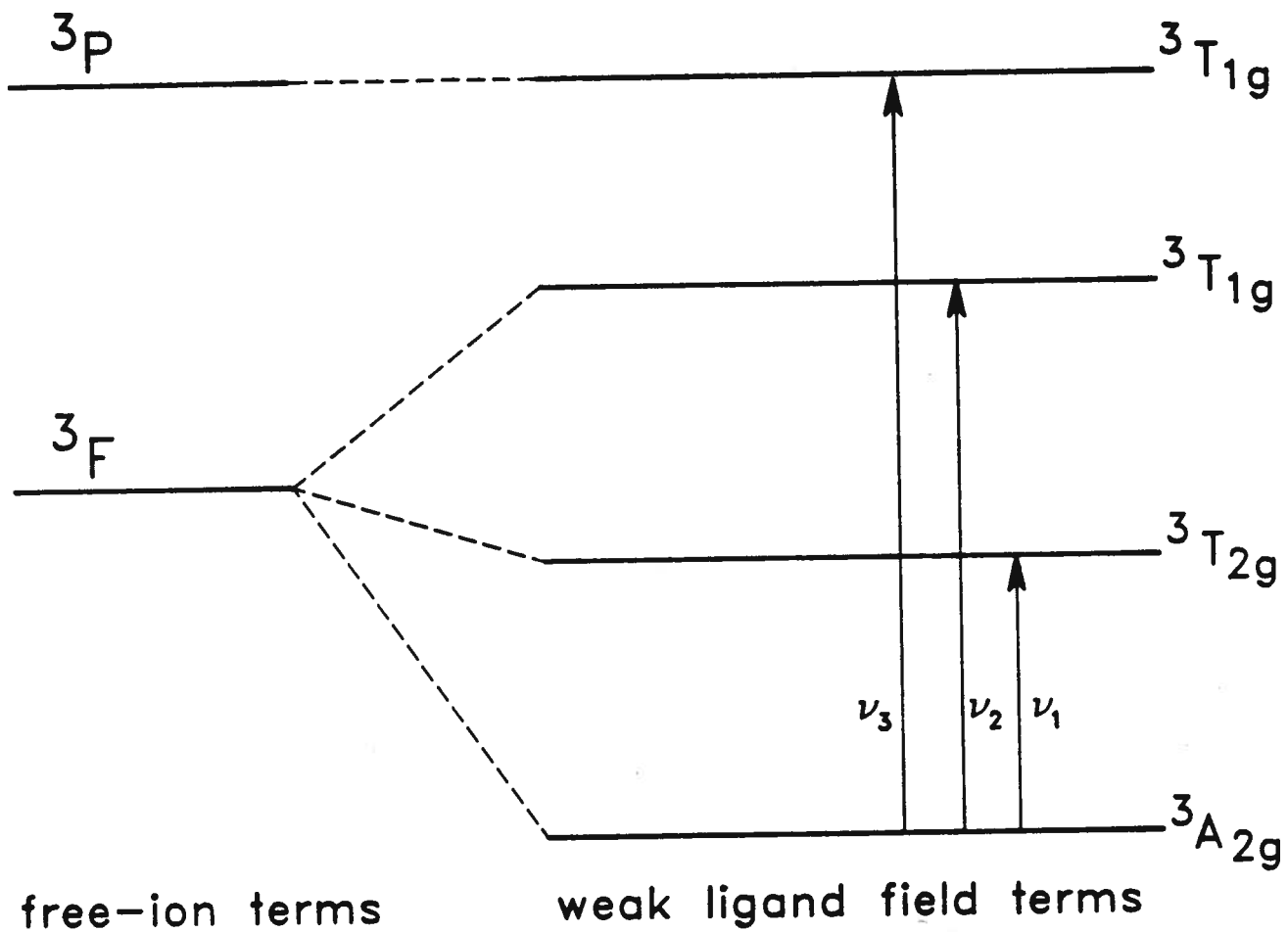


Table 3.3: Electronic Transitions and Ligand Field Parameters for Ni(SbF₆)₂, Pd(SbF₆)₂ and Related Compounds

Compound	Electronic Transition Energy (cm ⁻¹)			10Dq (cm ⁻¹)	B	B/B ^o d	Reference
	ν_1^a	ν_2^b	ν_3^c				
Ni(SbF ₆) ₂	6740	11300	22400	6740	899	0.832	This work
Ni(SO ₃ F) ₂	-	12400	23300	7340	912	0.844	39
Pd(SbF ₆) ₂	11900	18200	26700	11900	613	0.739	This work
Pd(SO ₃ F) ₂	11800	17400	27000	11800	606	0.730	19

a ν_1 : ${}^3A_{2g} \rightarrow {}^3T_{2g}$

b ν_2 : ${}^3A_{2g} \rightarrow {}^3T_{1g}(\text{F})$

c ν_3 : ${}^3A_{2g} \rightarrow {}^3T_{1g}(\text{P})$

d $B/B^o = \beta$, where B^o is the free ion value obtained from Ref. 34(a).

positions for $\text{Ni}(\text{SO}_3\text{F})_2/\text{Ni}(\text{SbF}_6)_2$ and $\text{Pd}(\text{SO}_3\text{F})_2/\text{Pd}(\text{SbF}_6)_2$ pairs suggests similar coordination environments for the Ni^{2+} and Pd^{2+} in the fluorosulfate and hexafluoroantimonate derivatives.

In addition, the Dq and B values reported here also point to a close structural similarity between the two types of compounds. For $\text{Pd}(\text{SO}_3\text{F})_2$ (19), like for most fluorosulfates of divalent metals (18), a layer structure based on the CdCl_2 prototype is postulated. As discussed in Section 3.2, the same structural type is reported for $\alpha\text{-Ag}(\text{SbF}_6)_2$ (14) and implicitly also for $\text{Ni}(\text{SbF}_6)_2$ (11).

Paramagnetic Pd^{2+} complexes with fluorometallate anions have precedents. Complexes of the general type $\text{Pd}[\text{MF}_6]$, with $M = \text{Pd}, \text{Pt}, \text{Ge},$ or Sn , have been known for over 25 years now (31), and their magnetic susceptibility measurements have been reported down to 80 K. The presence of MF_6^{2-} anion would suggest a different structural type, but the coordination environment of Pd^{2+} should again be octahedral.

The ligand field parameters, the octahedral splitting Dq and the interelectronic repulsion term B are obtained by using the appropriate equations (see Appendix A-4) as suggested by Lever (34(b)). The increase in Dq and the decrease in β (defined as B/B^0 , where B^0 is the free ion value) when moving from $\text{Ni}(\text{II}), (3d^8)$ to $\text{Pd}(\text{II}), (4d^8)$ are not unexpected in view of the higher nuclear charge and more spatially diffuse 4d orbitals for palladium (40).

Although no splitting of any of the bands is observable, the broad nature of the bands makes it difficult to confirm or deny the possible existence of distortion in the octahedral coordination sphere of the respective metal centers.

3.3.4 Magnetic Susceptibility Measurements

Magnetic susceptibilities over the temperature range of ~2 to 80 K are recorded for Ni(SbF₆)₂, Pd(SbF₆)₂, and Cu(SbF₆)₂ on a P.A.R. vibrating sample magnetometer. Relevant data are summarized in Tables 3.4, 3.5 and 3.6 respectively, and the plot of the magnetic moments vs. temperature for all three compounds is given in Figure 3.4.

As discussed in the experimental section, attempts to obtain pure α -Ag(SbF₆)₂ in quantities large enough for a bulk magnetic measurement were not successful. The results of measurements made, on what is obviously a mixture of the two valence isomeric forms, allow only limited conclusions, since the small amount of paramagnetic material in the sample did not permit the extension of the measurements to temperature higher than 65 K. Generally, for paramagnetic materials with one or two unpaired electrons, the vibrating sample magnetometer used in this work is useful to ~90 K. In the temperature range of 65-3 K the magnetic moment calculated for α -Ag(SbF₆)₂ appears to be independent of temperature with a shallow maximum at ~6 K before falling off. It is unclear whether the observed dilute magnetic behavior is due to α -Ag(SbF₆)₂, or caused by β -Ag(SbF₆)₂ acting as a diluent.

The diamagnetism of β -Ag(SbF₆)₂ is confirmed by measurements made at room temperature, using the Gouy technique. The measured susceptibility of $-68 \times 10^{-6} \text{ cm}^3 \text{ mol}^{-1}$ is less than the sum of Pascal constants of $-128 \times 10^{-6} \text{ cm}^3 \text{ mol}^{-1}$; however, the Gouy balance used is insufficiently sensitive for a more accurate determination of diamagnetic susceptibilities. In addition, trace amounts of α -Ag(SbF₆)₂ could be responsible for the slight discrepancy, as well as temperature independent paramagnetism (TIP).

As seen in Figure 3.4, the magnetic moment decreases gradually with decreasing temperature for Ni(SbF₆)₂ and Pd(SbF₆)₂, before a steep decline becomes apparent at ~10 K,

Table 3.4: Low Temperature Magnetic Data of Ni(SbF₆)₂

Temperature [K]	$\chi_M^{\text{corr}} \times 10^5$ [cm ³ mol ⁻¹]	μ_{eff} [μ_B]
81.67	750	2.21
77.78	780	2.20
74.08	820	2.20
69.72	870	2.20
65.31	920	2.19
60.15	1000	2.19
54.20	1100	2.18
47.60	1240	2.17
40.05	1450	2.15
30.80	1850	2.14
26.28	2150	2.13
21.17	2610	2.10
16.20	3280	2.06
11.00	4560	2.00
7.72	6060	1.93
5.34	8020	1.85
4.78	8660	1.82
4.32	8990	1.76
3.70	9770	1.70
2.99	10340	1.57
2.50	10730	1.47
2.00	11160	1.34

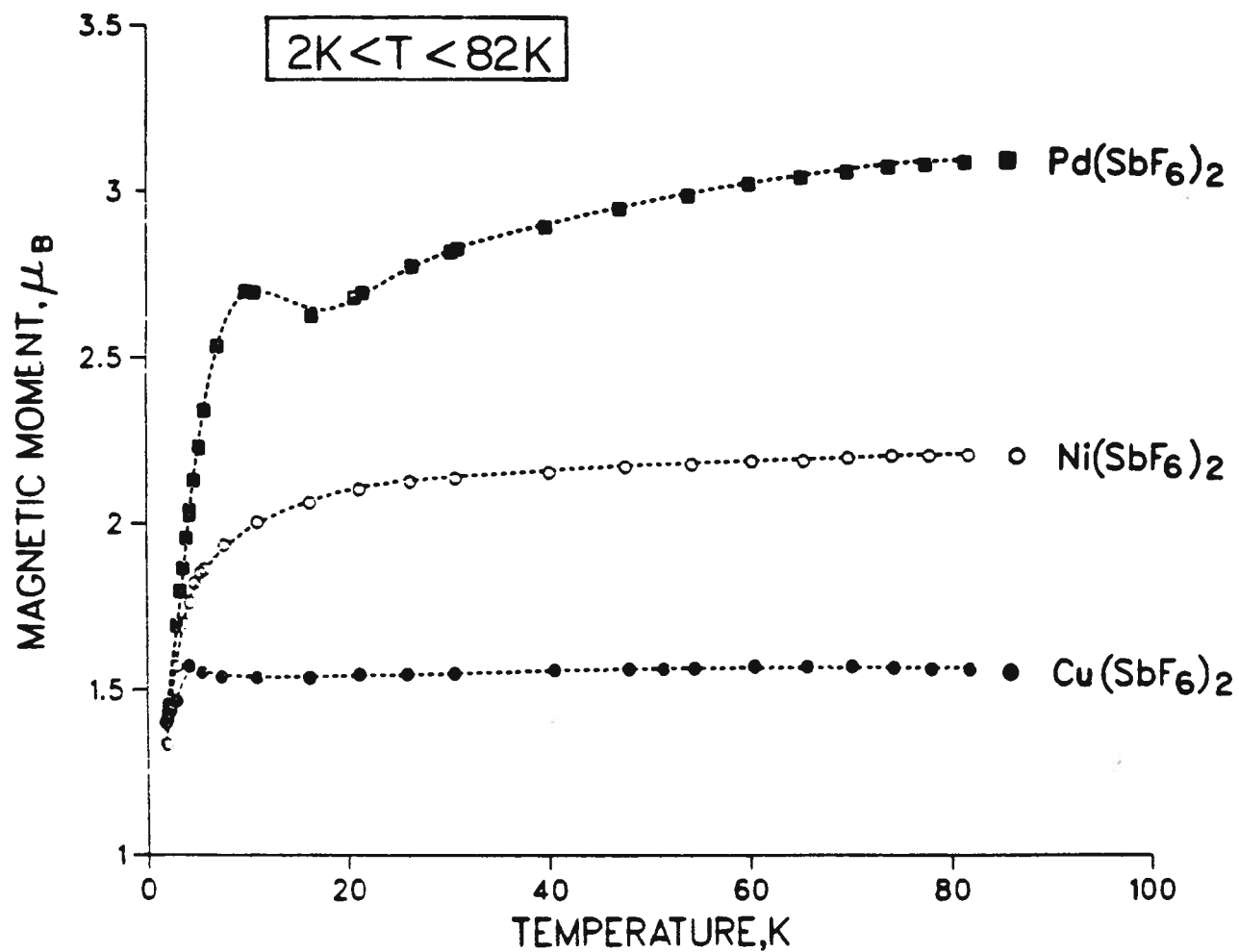
Table 3.5: Low Temperature Magnetic Data of Pd(SbF₆)₂

Temperature [K]	$\chi_M^{\text{corr}} \times 10^5$ [cm ³ mol ⁻¹]	μ_{eff} [μ_B]
81.50	1460	3.09
77.55	1530	3.08
73.91	1600	3.07
69.77	1680	3.06
65.19	1770	3.04
60.03	1900	3.02
54.00	2060	2.99
47.15	2300	2.95
39.80	2630	2.89
31.10	3210	2.83
30.45	3260	2.82
26.55	3620	2.77
21.60	4200	2.69
20.80	4310	2.68
16.50	5220	2.62
10.80	8410	2.70
9.94	9170	2.70
7.12	11270	2.53
5.84	11720	2.34
5.26	11830	2.23
4.76	11910	2.13
4.36	11910	2.04
4.00	11950	1.96
3.64	11950	1.87
3.37	11990	1.80
2.99	11990	1.69
2.29	11990	1.45
2.10	12020	1.42

Table 3.6: Low Temperature Magnetic Data of Cu(SbF₆)₂

Temperature [K]	$\chi_M^{\text{corr}} \times 10^5$ [cm ³ mol ⁻¹]	μ_{eff} [μ_B]
81.83	370	1.56
78.06	390	1.56
74.24	410	1.57
70.11	440	1.57
65.65	470	1.57
60.44	510	1.57
54.45	560	1.56
51.40	590	1.56
47.95	640	1.56
40.55	750	1.56
30.70	980	1.55
26.00	1150	1.55
21.22	1410	1.55
16.25	1820	1.54
11.00	2690	1.54
7.46	3970	1.54
5.56	5420	1.55
4.24	7290	1.57
4.04	7250	1.49
3.02	8890	1.47
2.40	10750	1.44
1.97	12480	1.40
1.86	13230	1.40

Figure 3.4: Magnetic Moment vs. Temperature of $M(\text{SbF}_6)_2$, $M=\text{Ni}$, Pd and Cu



indicative of possible antiferromagnetic ordering. An additional contributing factor to the sharp drop in the magnetic moment values at very low temperatures could come from zero-field splitting of the triplet spin states in the nickel and palladium compounds. It was shown in Section 3.3.3 where the electronic spectra of both $\text{Ni}(\text{SbF}_6)_2$ and $\text{Pd}(\text{SbF}_6)_2$ were discussed that the ground term of Ni^{2+} and Pd^{2+} ions in these two compounds is ${}^3A_{2g}$.

For a d^8 -ion in an octahedral ligand field with ${}^3A_{2g}$ ground term, the magnetic moment can be expressed as follows (41):

$$\mu_{\text{eff}} = (8)^{1/2} \left(1 - \frac{4\lambda}{10Dq} \right) = \mu_{\text{s.o.}} \left(1 - \frac{4\lambda}{10Dq} \right) \quad [3.5]$$

where λ = spin-orbit coupling constant = $\xi/2$ for d^8 .

$10Dq$ = ligand field splitting parameter

$\mu_{\text{s.o.}}$ = spin-only magnetic moment = $[4S(S+1)]^{1/2}$

Since the ground term discussed here is ${}^3A_{2g}$, a first-order orbital contribution to the magnetic moment is not expected. However, through spin-orbit coupling, which is expected to be quite large for second and third row transition metals, the observed magnetic moment is enhanced beyond the spin-only value. In the absence of any magnetic exchange between the paramagnetic centers, the moment calculated is independent of temperature and should depend only on λ and $10Dq$. The sign of λ is negative for transition metals where the d-shell is more than half full, and therefore according to equation [3.5], for Ni^{2+} and Pd^{2+} ions μ_{eff} greater than $\mu_{\text{s.o.}}$ is expected.

For $\text{Pd}(\text{SbF}_6)_2$, using equation [3.5] with $10Dq = 11,900 \text{ cm}^{-1}$ (Table 3.3) and the estimated value of λ for $\text{Pd}^{2+} = 1600/2 \text{ cm}^{-1}$ (42), a temperature independent-moment of $3.59 \mu_B$ is obtained. The observed magnetic moment of $3.09 \mu_B$ at $\sim 82 \text{ K}$ is reasonable when compared

to the predicted value, since the magnetic moment in $\text{Pd}(\text{SbF}_6)_2$ has been lowered by anti-ferromagnetic exchange, as evident from the plot in Figure 3.4.

A slight increase in the magnetic moment is observed in the $\text{Pd}(\text{SbF}_6)_2$ plot (also to a very small extent in $\text{Cu}(\text{SbF}_6)_2$), just before dropping off at very low temperatures. The observed weak effect is reproducible and two possible interpretations are suggested: (a) a phase transition occurs at ~ 10 K and (b) very weak ferromagnetism is responsible for the small effect.

The latter explanation is favored here because there are a number of precedents for simultaneous ferromagnetic and antiferromagnetic ordering in fluoro derivatives of palladium(II). Very weak ferromagnetism is observed in PdF_2 (43), which has a rutile structure (44), and in the ternary fluorides $\text{Pd}(\text{II})\text{Pd}(\text{IV})\text{F}_6$ and $\text{Pd}(\text{II})\text{Pt}(\text{IV})\text{F}_6$ (45). According to a recent crystal structure reported for the latter compound (46), there may even be a close structural relationship: $\text{Pd}(\text{II})\text{Pt}(\text{IV})\text{F}_6$ has a LiSbF_6 structure. For $\text{Pd}(\text{II})(\text{SbF}_6)_2$ a layer structure is suggested, which, as discussed above, is also derived from the LiSbF_6 prototype, with half of the octahedral holes occupied by Pd^{2+} compared to all holes filled for $\text{Pd}(\text{II})\text{Pt}(\text{IV})\text{F}_6$ (46).

Some similarity in magnetic behavior is also evident from the μ_{eff}^{80} values, which are for the ternary palladium(II) fluorides in the range of 2.7 to ~ 3.0 μ_{B} for the series $\text{Pd}(\text{II})\text{M}(\text{IV})\text{F}_6$, with $\text{M} = \text{Pd}, \text{Pt}, \text{Ge}$ or Sn (31a), while for $\text{Pd}(\text{SbF}_6)_2$, where Pd^{2+} is slightly more dilute, a value of 3.09 μ_{B} is found.

Substantially higher magnetic moments (3.30-3.60 μ_{B}) are found for the corresponding fluorosulfato complexes of palladium(II) (19b), where the bulkier fluorosulfate groups appear to prevent antiferromagnetic exchange. It is interesting to note that at low temperatures (~ 20 K) significant ferromagnetism has been observed for two members of this group $\text{Pd}(\text{SO}_3\text{F})_2$ and $\text{Pd}(\text{II})\text{Pd}(\text{IV})(\text{SO}_3\text{F})_6$ (see Chapter 6). The former, like $\text{Pd}(\text{SbF}_6)_2$, has a layer structure, derived

from the CdCl_2 type, and both appear to have the Pd^{2+} ion in very similar electronic environments at room temperature, as reflected in their respective electronic mull spectra (Table 3.3) discussed in Section 3.3.3.

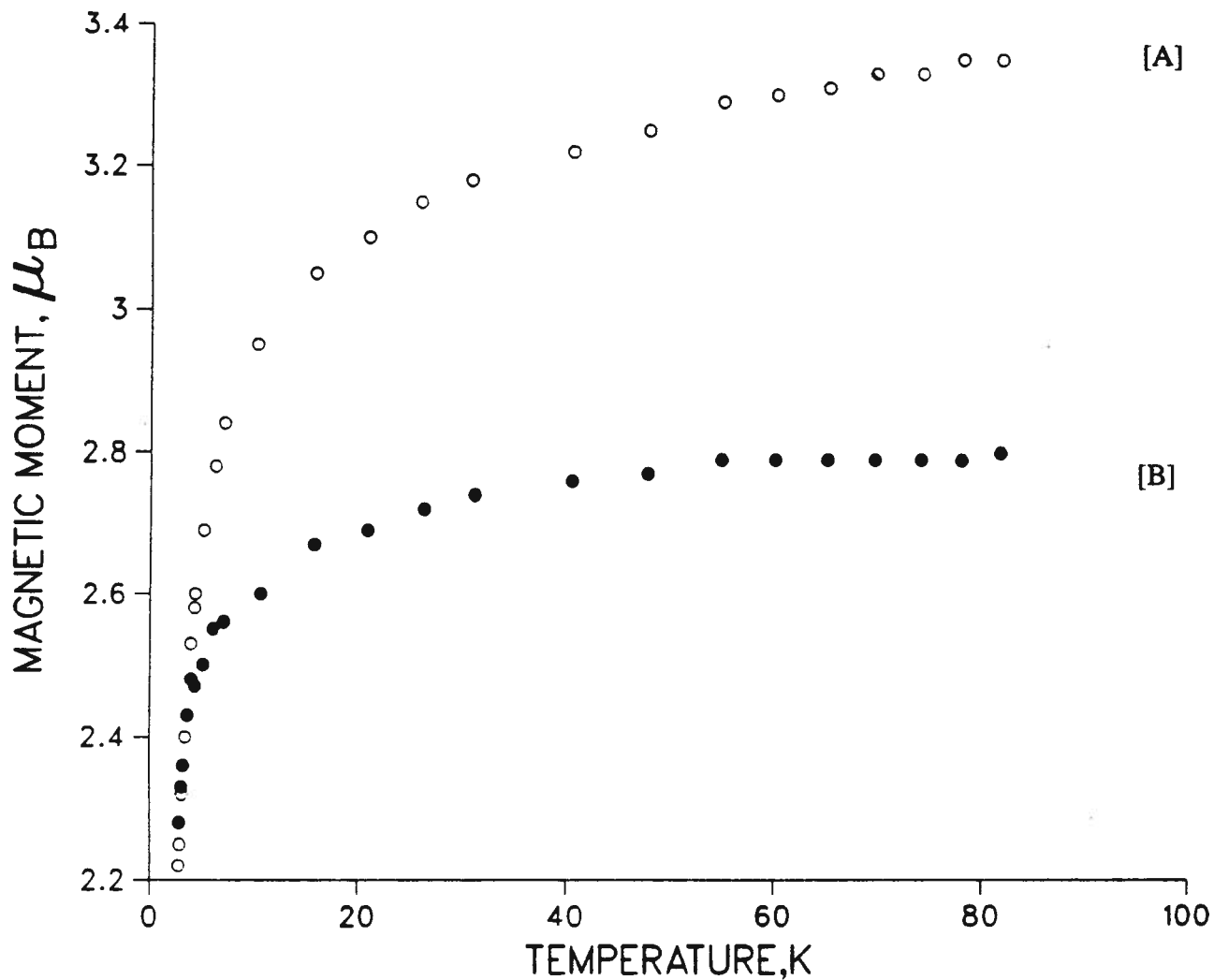
The magnetic moments observed for $\text{Ni}(\text{SbF}_6)_2$ are rather low ($\mu_{\text{eff}} = 2.21 \mu_{\text{B}}$ at $\sim 82 \text{ K}$), even though the moments are reduced by possible antiferromagnetic exchange (see Figure 3.4 and Table 3.7). If there is no magnetic exchange between the paramagnetic Ni^{2+} centers, equation 3.5 can again be utilized to calculate the temperature independent moment. The $10Dq$ value of the compound is 6740 cm^{-1} (Table 3.3), and the estimated value of λ for Ni^{2+} is $644/2 \text{ cm}^{-1}$ (42) which when substituted in equation 3.5 yields a μ_{eff} value of $3.37 \mu_{\text{B}}$.

In order to understand the unusual magnetic results of $\text{Ni}(\text{SbF}_6)_2$, two other $\text{Ni}(\text{SbF}_6)_2$ samples, made by different methods were also investigated for their magnetic properties. A sample was obtained for this study from Dr. Karl O. Christe of Rocketdyne, U.S.A., which was prepared from Ni , SbF_5 and F_2 under high temperature and pressure (11). The second sample was synthesized for this study from NiF_2 and SbF_5 in anhydrous HF according to the published method (14). The low temperature magnetic moment vs. temperature plot of these two samples is given in Figure 3.5 (see Appendices A-5 and A-6 for data).

In addition, magnetic measurements were also taken using a Gouy balance on the solvolysis sample as well as on the above mentioned high temperature fluorination product (11). Results of this high temperature study are given in Table 3.7.

Although all the three samples of $\text{Ni}(\text{SbF}_6)_2$ display the common behavior of temperature dependent low magnetic moments, it is rather puzzling to note that their moments differ so substantially. The plots of μ_{eff} vs. T display very similar slopes which suggests the possible presence of a common magnetic substance at different concentrations in these samples. The

Figure 3.5: Magnetic Moment vs. Temperature of $\text{Ni}(\text{SbF}_6)_2$



[A] Gift sample, from $\text{Ni} + \text{F}_2 + \text{SbF}_5$, Ref. 11

[B] Sample from $\text{NiF}_2 + \text{SbF}_5$ in HF, Ref. 14

Table 3.7: Magnetic Moment Data of Ni(SbF₆)₂ for the Temperature Range ~80 to 295 K

Ni(SbF ₆) ₂ ^a [Ni(SO ₃ F) ₂ + SbF ₅]		Ni(SbF ₆) ₂ ^b [Ni + F ₂ + SbF ₅]	
Temperature (K)	μ _{eff} (μ _B) ^c	Temperature (K)	μ _{eff} (μ _B) ^c
290.5	2.64	293.5	4.25
268.5	2.61	268.8	4.16
251.0	2.61	251.0	4.11
234.5	2.61	234.5	4.07
218.0	2.60	218.0	4.02
200.3	2.58	201.0	3.97
176.0	2.58	177.0	3.90
151.0	2.56	151.5	3.81
126.3	2.45	127.5	3.73
101.8	2.42	103.0	3.61
86.5	2.31	86.5	3.53
78.0	2.26	78.0	3.46

^a This work

^b Gift sample, made according to Ref. 11

^c $\mu_{\text{eff}} = 2.828 [(\chi_{\text{mol}} - \text{TIP})T]^{1/2}$; $\text{TIP} = \frac{8N\beta^2}{10Dq} = 320 \times 10^{-6} \text{ cm}^3 \text{ mol}^{-1}$

solvolysis product from this study appears to have the lowest magnetic moments, whereas the gift fluorination sample exhibits moments which are unexpectedly high for an octahedrally coordinated Ni(II) species (Table 3.7). The sample made using HF as solvent medium has moments (measured up to ~80 K only, Figure 3.5) which fall between the above two sets of values. Furthermore, a Ni(SbF₆)₂ sample made from the oxidation of Ni by SbF₅ in SO₂ solution is reported as having a magnetic moment of 3.16 μ_B at 294 K (12).

It is also important to note here that if the symmetry of the ligand field acting on a d⁸ ion like Ni(II) is allowed to be lower than cubic and this low symmetry component is large enough, then a spin free-spin paired (triplet-singlet) equilibria may occur in the paramagnetic ions of the compound (47,48). This could reduce the magnetic susceptibility of the system, yielding magnetic moments lower than expected. Although this situation is observed mostly in Ni(II) complexes, it is reported to occur almost exclusively in solutions and is dependent on the solvent, concentration and temperature (47). Therefore, this unusual behavior may not be a significant factor in this solid state magnetic study of Ni(SbF₆)₂. However, the existence of such systems in the solid state cannot be ruled out completely.

The temperature dependent low moments obtained for the solvolysis sample may be due primarily to the following factors: (a) possible antiferromagnetic interaction between the Ni(II) centers, which will lead to lower than expected moments; (b) small amounts of nickel ions in oxidation states other than +2 acting as diluents to predominantly octahedral Ni(II) ions in the lattice; and (c) a combination of factors (a) and (b) which will result in lower magnetic moments for the compound.

The contribution of antiferromagnetism toward lower moments can be seen clearly in both Figure 3.5 and Table 3.7, where in the latter tabulation the small contribution (320 x 10⁻⁶ cm³ mol⁻¹) from the temperature independent paramagnetism (TIP) to the susceptibility has

been removed, since this contribution is relatively significant at higher temperatures.

However, as no χ_{\max} is observed in the susceptibility data, antiferromagnetism alone cannot account for such low moments in the solvolysis product. Therefore, the existence of small quantities of other nickel ion species than octahedral Ni(II) in the lattice may have to be considered as a possibility.

Interestingly, two octahedrally coordinated spin paired Ni(III) fluoro compounds, K_3NiF_6 and Na_3NiF_6 have been reported in the literature (49), where the elongation of the $[\text{NiF}_6]^{-3}$ octahedron is ascribed to the Jahn-Teller effect to be expected for the $t_{2g}^6 e_g^1$ configuration. The magnetic moment of K_3NiF_6 is given as 2.51 and 2.12 μ_B at 295 and 90 K respectively (50), although the large temperature dependence of the moments is surprising for an 2E_g ground term, unless thermal equilibrium between low and high spin configurations (49) and/or antiferromagnetism is taken into consideration. It is however still rather difficult to rationalize the generation and hence the presence in the solvolysis product of nickel ions in oxidation states other than +2, since the parent compound $\text{Ni}(\text{SO}_3\text{F})_2$ is well characterized as a Ni(II) octahedral complex, both by electronic spectra (39) and magnetic studies (Chapter 6).

The magnetic moments calculated at higher temperature for the fluorination product (Table 3.7) in contrast, are significantly above the values expected for a d^8 Ni(II) complex. It was shown earlier that equation [3.5] predicts a temperature independent moment of 3.39 μ_B , whereas the moment obtained at room temperature of this compound exceeds this value by nearly one Bohr magneton. As discussed in Section 3.1, the obvious limitation in the high temperature synthesis of $\text{Ni}(\text{SbF}_6)_2$ is that direct fluorination may lead to oxidation of the metal beyond the +2 state. This is possible in nickel where higher oxidation states are accessible and the metal can be oxidized under severe conditions up to the +4 state (40). However, as pointed out above, the known octahedral Ni(III) fluoro compounds are of the spin-paired type (49) and

Ni(IV) derivatives like $(\text{ClF}_2\text{O})_2\text{NiF}_6$ and K_2NiF_6 (51,40) are diamagnetic with the low-spin t_{2g}^6 configuration. Therefore, the origin of the high magnetic moments calculated for this compound is not clear, especially as the compound has been sufficiently characterized using microanalysis, vibrational spectroscopy and X-ray powder diffraction (11). However, a very likely cause of the high magnetic moments for this sample can be Ni metal impurities. Since Ni metal is ferromagnetic, trace amounts of it would cause significantly larger μ_{eff} values for the sample. Furthermore, the metal saturates at relatively low magnetic fields, and as μ_{eff} is proportional to $(\chi_M T)^{1/2}$, this will result in decreasing moments with decreasing temperatures for the compound. Field dependent magnetic susceptibility studies are required to verify this possible ferromagnetic contamination of the samples.

The magnetic moments obtained for $\text{Cu}(\text{SbF}_6)_2$ are given in Table 3.6, and appear to be independent of temperature down to ~ 4 K. It is also of interest to note here that of the four transition metal fluorosulfate precursors used for this study, only $\text{Cu}(\text{SO}_3\text{F})_2$ is magnetically dilute to low temperatures (Chapter 6). The moments of $\text{Cu}(\text{SbF}_6)_2$ are lower than expected for a Cu(II) (d^9) ion in an octahedral ligand field (52). Since the ground term 2E_g has no orbital angular momentum associated with it the moments should be close to the spin only value of $1.73 \mu_B$ in the first approximation. However, spin-orbit coupling can occur between the 2E_g ground term and the higher lying ${}^2T_{2g}$ term, leading to slightly higher moments predicted by the following expression (41):

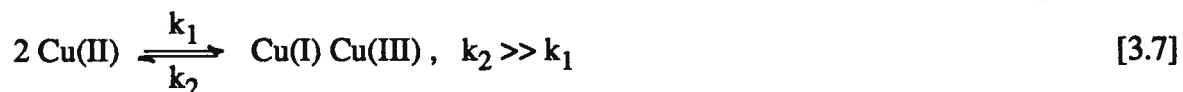
$$\mu_{\text{eff}} = (3)^{1/2} \left(1 - \frac{2\lambda}{10Dq} \right) = \mu_{\text{s.o.}} \left(1 - \frac{2\lambda}{10Dq} \right) \quad [3.6]$$

where the terms used are as in equation [3.5].

It was noted earlier in Section 3.3.2 that the vibrational spectrum of $\text{Cu}(\text{SbF}_6)_2$ made via the solvolysis method is slightly different when compared to that of $\text{CuF}_2 \cdot 2\text{SbF}_5$ (14). This was

taken as a clue to the possible existence of polymorphism in the two forms of $\text{Cu}(\text{SbF}_6)_2$, although to a very limited extent than in the case of $\text{Ag}(\text{SbF}_6)_2$.

Magnetic measurements obtained on several samples of $\text{Cu}(\text{SbF}_6)_2$ also indicate this possibility (Figures 3.6 and 3.7), with Cu(I), Cu(II), and Cu(III) present in an equilibrium of the type:



with the ratio k_2/k_1 differing very slightly relative to the experimental conditions of the formation reaction and the subsequent treatment of the reaction product. Solvolysis of $\text{Cu}(\text{SO}_3\text{F})_2$ in SbF_5 appears to generate small quantities of Cu(I) and Cu(III) ions, in addition to the relatively larger number of Cu(II) ions ($k_2 \gg k_1$). The diamagnetic Cu(I) and Cu(III) ions seem to act as diluents to the paramagnetic Cu(II) centers, thereby lowering the observed magnetic moments of the compound below the expected values. This could also account for the temperature independent magnetic moment behavior of the compound, where the Cu(II) centers are now more dilute than in the corresponding Pd(II) or Ni(II) derivatives.

When the product is treated with anhydrous HF for 3 days, equilibrium [3.7] is shifted further to the left ($k_2 \gg \gg k_1$), resulting in an increase in the Cu(II) ions present in the compound. Consequently, the magnetic susceptibility of the sample is enhanced to a small but significant extent leading to correspondingly higher magnetic moments (Figure 3.6). The opposite effect is found when $\text{Cu}(\text{SbF}_6)_2$ is re-reacted with an excess of SbF_5 for a prolonged period of time, ~6 to 8 weeks (Figure 3.7). In all instances, no weight changes were observed in the vacuum dried products.

Figure 3.6 Magnetic Moment vs. Temperature of HF Treated $\text{Cu}(\text{SbF}_6)_2$

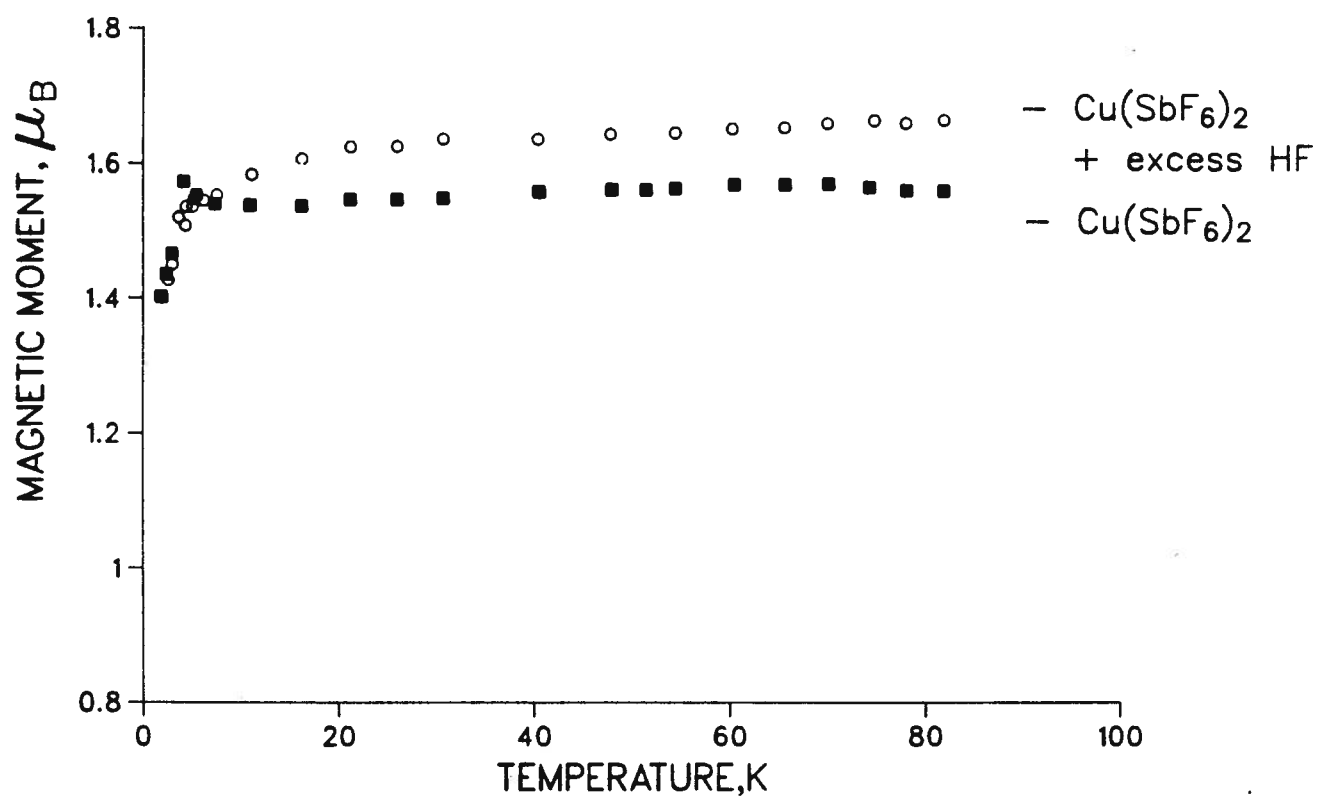
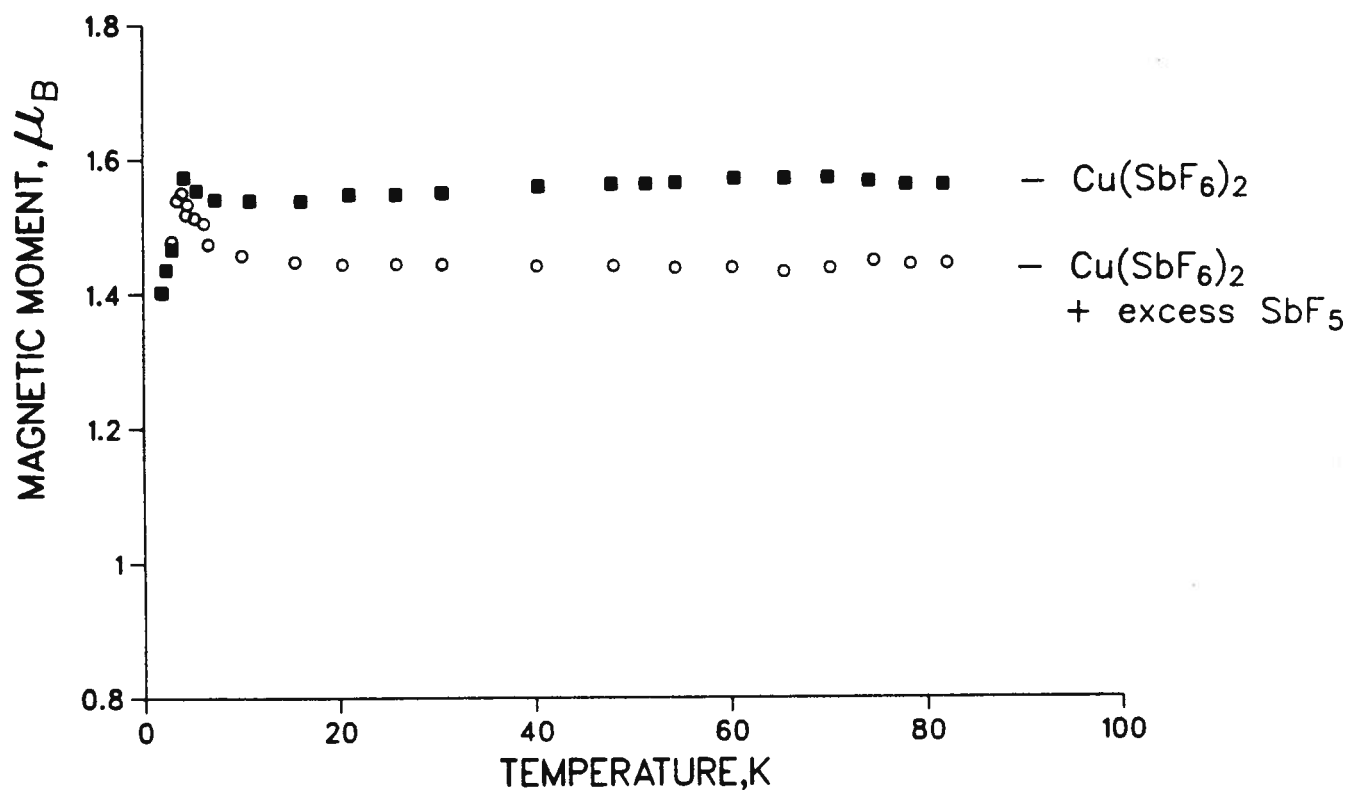


Figure 3.7: Magnetic Moment vs. Temperature of SbF_5 Treated $\text{Cu}(\text{SbF}_6)_2$



The presence of Cu(I) and Cu(III) ions, in addition to Cu(II) in $\text{Cu}(\text{SbF}_6)_2$ is not totally unexpected, since both $\text{Ag}(\text{II})(\text{SO}_3\text{F})_2$ and $\text{Cu}(\text{II})(\text{SO}_3\text{F})_2$, which contain "Jahn-Teller ions" (d^9), could behave in a similar manner toward SbF_5 , generating Ag(I), Ag(III) and to a lesser degree Cu(I), Cu(III) ions in their respective reaction products. As in the case of $\beta\text{-Ag}(\text{SbF}_6)_2$, the Cu(I) and Cu(III) centers could be accommodated in the layer structure of $\text{Cu}(\text{SbF}_6)_2$, with Cu(I) in a linear and Cu(III) in a square planar environment respectively.

3.3.5 X-ray Photoelectron Spectra

Attempts were made to characterize the $\beta\text{-Ag}(\text{SbF}_6)_2$ and $\text{Cu}(\text{SbF}_6)_2$ compounds using X-ray photoelectron measurements. It was hoped that the difference in Binding Energy (BE) between the cations in oxidation states +1, +2, and +3 could be utilized to identify these ions present in the silver compound as Ag(I), Ag(III) and in the copper compound as Cu(I), Cu(II), and Cu(III) respectively. The reported BE values corresponding to these oxidation states (for a given energy level) were reconfirmed by a series of measurements carried out with relevant silver and copper fluoro complexes.

For the XPS study of $\beta\text{-Ag}(\text{SbF}_6)_2$ compound, the $3d_{5/2}$ energy level is chosen, which is found at BE = 366.8 eV in Ag(0). The Ag(I) and Ag(III) BE peaks for the same energy level are expected at ~367.7 and ~371.0 eV respectively (53,54). The sample was scanned in the BE range of 357 to 377 eV. Unfortunately, for the $3d_{5/2}$ level, only a broad band spanning a BE range of ~367.5 to 370 eV is obtainable, with no resolution of the relevant peaks expected for the Ag(I) and Ag(III) species. It is however possible that the two peaks corresponding to the two silver ions are hidden under the broad band centered at ~369 eV. A similar situation is observed when the alternate energy level $3d_{3/2}$ is chosen for the measurements.

The XPS spectra obtained for $\text{Cu}(\text{SbF}_6)_2$ show a more complicated spectral pattern. The energy level $2\text{P}_{3/2}$ located at $\text{BE} = 932.2 \text{ eV}$ for $\text{Cu}(0)$ is chosen, and BE peaks of $\text{Cu}(I)$, $\text{Cu}(II)$ and $\text{Cu}(III)$ corresponding to this energy level are expected at 932.6, 936.1 and 938.0 eV respectively (53,54,55). However, in this compound, only small amounts of $\text{Cu}(I)$ and $\text{Cu}(III)$ ions are expected to be present (see Section 3.3.4), in contrast to the silver compound, where $\text{Ag}(I)$ and $\text{Ag}(III)$ ions are present in equimolar quantities.

The BE range scanned for $\text{Cu}(\text{SbF}_6)_2$ is from 921 to 941 eV, and as in the silver compound, no distinct peaks corresponding to the three oxidation states are observed. The broad band obtained covers an energy range of ~ 932.5 to 938 eV, and is split by several intense satellite lines. This phenomenon is commonly seen in the XPS spectra of cupric compounds, and the number and the splitting of the peaks are found to be sensitive to the chemical environment of the ions (55). This situation is further complicated by the reduction of $\text{Cu}(II)$ ions when subjected to X-rays, and consequently, additional satellite peaks may appear in the spectra (55).

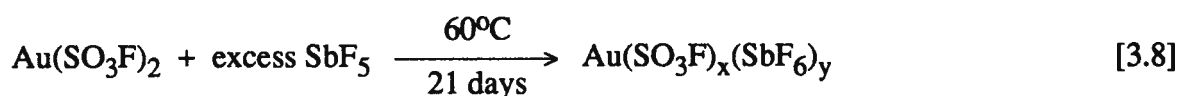
Although no individual peaks at energy level $2\text{P}_{3/2}$ are seen in the spectra, it is again possible to have the less intense $\text{Cu}(I)$ and $\text{Cu}(III)$ peaks hidden under the broad band, since the energy range of the band covers the three BE values of the copper ions $\text{Cu}(I)$, $\text{Cu}(II)$, and $\text{Cu}(III)$ expected in $\text{Cu}(\text{SbF}_6)_2$.

3.3.6 Attempted Synthesis of $\text{Au}(\text{SbF}_6)_2$

Gold(II) fluorosulfate, which was synthesized recently in our group by the reduction of $\text{Au}(\text{SO}_3\text{F})_3$ with either gold powder or CO (56), was selected as the precursor to react with excess SbF_5 in the attempted preparation of the corresponding gold(II) hexafluoro antimonate, $\text{Au}(\text{SbF}_6)_2$. The gold compound has been formulated as a mixed valency, diamagnetic $\text{Au}(I)[\text{Au}(III)(\text{SO}_3\text{F})_4]$ complex, based on magnetic measurements and vibrational spectra (56).

Therefore, it was expected that the resulting binary compound may also have the composition $\text{Au(I)[Au(III)(SbF}_6)_4]$, analogous to the diamagnetic $\beta\text{-Ag(SbF}_6)_2$ compound.

However, in contrast to the other four transition metal fluorosulfate precursors, the reaction of $\text{Au(SO}_3\text{F)}_2$ with excess SbF_5 , carried out in a manner similar to the other preparations discussed in this chapter (equation 3.1), does not yield the anticipated binary product $\text{Au(SbF}_6)_2$. Instead, the synthesis follows the reaction scheme shown below, yielding a ternary compound:

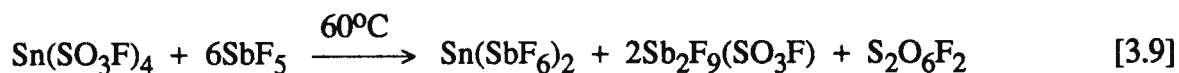


The values of x and y (typically $x = 1$ to 1.5 , and $y = 2-x$), calculated from microanalytical data, seem to vary slightly and appear to depend on the reaction conditions. The bright yellow $\text{Au(SO}_3\text{F)}_2$ gradually turns color to give a dark brown-green powder. When the reaction is performed at elevated temperatures, a dark brown, very viscous liquid which may form due to the melting or decomposition of the lower temperature product, is isolated. Infrared spectra run on several samples clearly show the presence of both SO_3F and SbF_6 groups, and magnetic measurements indicate a diamagnetic compound, as anticipated.

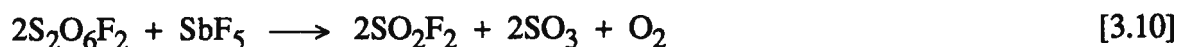
Interestingly, when diamagnetic gold(III) fluorosulfate $\text{Au(SO}_3\text{F)}_3$, which is synthesized by the oxidation of gold powder with $\text{S}_2\text{O}_6\text{F}_2$ in HSO_3F (57), is reacted with excess SbF_5 under the same experimental conditions (equation [3.8]), a dark blue-green powder is isolated, again with composition $\text{Au(SO}_3\text{F)}_x(\text{SbF}_6)_y$, where the values of x and y (typically $x = 2$ to 2.3 and $y = 3-x$), are dependent on the reaction conditions. However, this ternary compound, in contrast, is weakly paramagnetic. The low temperature magnetic data, tabulated in Appendix A-7, yield moments that range from 0.52 to $0.72 \mu_B$ at 82 and 2.7 K respectively. These values are

tentative, since the composition of the compound (and hence the molar mass) cannot be determined accurately. It is important to note here that like in the fluorides, where both AuF and AuF₂ are unknown (33), examples for lower valent fluoro derivatives of gold are so far lacking.

It is conceivable that Au(SO₃F)₃, which is dimeric in the solid state (58) when reacted with SbF₅, may undergo a reduction process to a very slight extent. This reduction of the gold compound may be due to the inability of substituent SbF₆⁻ anions to suitably stabilize the higher oxidation state and hence strongly oxidizing Au(III) species, and consequently, may lead to the formation of small quantities of paramagnetic Au(II) ions in the solid lattice. This observation appears to be valid also for the solvolysis reaction of Sn(IV)(SO₃F)₄ in SbF₅. When about 0.679 g of Sn(SO₃F)₄, made according to a published method (59) is reacted with an excess of SbF₅ for two weeks at 60°C, a white solid that corresponds to the composition Sn(SbF₆)₂ is isolated. The reduction of the Sn(IV) species to Sn(II) could occur according to:



and



The decomposition of S₂O₆F₂ in the presence of SbF₅ (5) leads to byproducts which are all removable in a dynamic vacuum and consequently solid Sn(SbF₆)₂ is obtained in high yield.

3.4 Conclusion

Solvolysis of M(II) fluorosulfates with M = Sn, Ni, Pd, Cu or Ag, in antimony(V) fluoride is found to be a useful synthetic route to the corresponding metal(II) hexafluoro

antimonate compounds. Even though alternate synthetic routes to compounds of the type $M(\text{SbF}_6)_2$ are known, only the solvolysis method leads to the $\text{Pd}(\text{SbF}_6)_2$ and the $\beta\text{-Ag}(\text{SbF}_6)_2$ compounds. The latter complex, unlike a recently reported paramagnetic, blue valence isomer is diamagnetic and based on its chemical and magnetic behavior, formulated as a mixed valency $\text{Ag(I)[Ag(III)(SbF}_6)_4]$ species. Additionally, the copper compound synthesized by this route also appears to be unique, with Cu(II) and, to a lesser extent Cu(I) and Cu(III) ions, all present simultaneously in the lattice of $\text{Cu}(\text{SbF}_6)_2$, as confirmed by low temperature magnetic susceptibility measurements.

The $\text{Ni}(\text{SbF}_6)_2$ compound prepared via solvolysis appears to be structurally similar to the compound obtained by the high temperature fluorination method. However, in the solvolysis sample the nickel centers are predominantly found as Ni(II) ions, whereas in the fluorination product trace Ni metal impurities seem to be present, which is evident from their respective magnetic studies.

Ligand field analyses of the electronic spectra of $\text{Ni}(\text{SbF}_6)_2$ and $\text{Pd}(\text{SbF}_6)_2$ indicate that, like in their fluorosulfate precursors, the Ni(II) and Pd(II) ions are located in approximate octahedral ligand fields with ${}^3\text{A}_{2g}$ ground terms. Both compounds exhibit temperature dependent low magnetic moments, most likely due to antiferromagnetic exchange. Additionally, $\text{Pd}(\text{SbF}_6)_2$ shows very weak ferromagnetism below ~ 10 K.

It appears, based on X-ray powder data and vibrational spectra that a common CdCl_2 -type layer structure is present in all the $M(\text{SbF}_6)_2$ compounds synthesized in this study, although ultimate structural proof will have to come from single crystal X-ray diffraction studies. The lack of solubility of the compounds in suitable solvents like anhydrous HF and their high reactivity toward many of the organic solvents present substantial obstacles to the crystal growth process.

References

1. P.L. Fabre, J. Devynck, and B. Tremillon, Chem. Rev., **82**, 591 (1982), and references therein.
2. S.P. Mallela, S. Yap, J.R. Sams, and F. Aubke, Inorg. Chem., **25**, 4327 (1986).
3. G.A. Olah, G.K.S. Prakash, and J. Sommer, "Superacids", John Wiley and Sons, New York, 1985, and references therein.
4. R.J. Gillespie and R.A. Rothenbury, Can. J. Chem., **42**, 416 (1964).
5. W.W. Wilson and F. Aubke, J. Fluorine Chem., **13**, 431 (1979).
6. P.A. Yeats and F. Aubke, J. Fluorine Chem., **4**, 243 (1974).
7. W.W. Wilson, J.R. Dalziel, and F. Aubke, J. Inorg. Nucl. Chem., **37**, 665 (1975).
8. W.W. Wilson, R.C. Thompson, and F. Aubke, Inorg. Chem., **19**, 1489 (1980).
9. S. Karunanithy and F. Aubke, J. Fluorine Chem., **23**, 541 (1983).
10. S.P. Mallela, S. Yap, J.R. Sams, and F. Aubke, Rev. Chim. Minerale, **23**, 572 (1986).
11. K.O. Christe, W.W. Wilson, R. Bougon, and P. Charpin, J. Fluorine Chem., **34**, 287 (1987).
12. P.A.W. Dean, J. Fluorine Chem., **5**, 499 (1975).
13. T. Birchall, P.A.W. Dean, and R.J. Gillespie, J. Chem. Soc. A, 1777 (1971).
14. D. Gantar, I. Leban, B. Frlec, and J.H. Holloway, J. Chem. Soc. Dalton Trans., 2379 (1987).
15. B. Frlec, D. Gantar, and J.H. Holloway, J. Fluorine Chem., **20**, 385 (1982).
16. B. Frlec, D. Gantar, and J.H. Holloway, J. Fluorine Chem., **19**, 485 (1982).
17. D. Gantar, B. Frlec, D.R. Russell, and J.H. Holloway, Acta Cryst., C, **43**, 618 (1987).
18. C.A. Alleyne, K. O'Sullivan-Mailer, and R.C. Thompson, Can. J. Chem., **52**, 336 (1974).
- 19.a) K.C. Lee and F. Aubke, Can. J. Chem., **55**, 2473 (1977).
- b) K.C. Lee and F. Aubke, Can. J. Chem., **57**, 2085 (1979).

20. P.C. Leung and F. Aubke, Inorg. Chem., **17**, 1765 (1978).
21. M.S.R. Cader, R.C. Thompson, and F. Aubke, Chem. Phys. Lett., **164**, 438 (1989).
22. A.F. Clifford, H.C. Beachell, and W.M. Jack, J. Inorg. Nucl. Chem., **5**, 57 (1957).
23. A.I. Vogel, "Quantitative Inorganic Analysis", 3rd Edition, John Wiley and Sons, New York, 1961.
24. B. Standke and M. Jansen, Angew. Chem. Int. Ed., **25**, 77 (1986).
25. J.A. McMillan, Chem. Rev., **62**, 65 (1962) and references therein.
26. B. Standke and M. Jansen, Angew. Chem. Int. Ed., **24**, 118 (1985).
27. P.C. Leung, K.C. Lee, and F. Aubke, Can. J. Chem., **57**, 326 (1979).
28. L. Helmholtz and R. Levine, J. Am. Chem. Soc., **64**, 354 (1942).
29. W. Klemm, Angew. Chem., **66**, 468 (1954).
30. B.G. Muller, Z. Anorg. Allg. Chem., **553**, 196 (1987) and references therein.
- 31.a) N. Bartlett and R.P. Rao, Proc. Chem. Soc., 393 (1964).
 b) R.P. Rao, Ph.D. Thesis, University of British Columbia, 1965.
32. R. Bougon, T.B. Huy, M. Lance, and H. Abazli, Inorg. Chem., **23**, 3667 (1984).
33. B.G. Muller, Angew. Chem. Int. Ed. Engl., **26**, 1081 (1987).
- 34.a) B.N. Figgis, "Introduction to Ligand Fields", John Wiley and Sons, New York, 1966.
 b) A.B.P. Lever, J. Chem Educ., **45**, 711 (1968).
35. J.H. Burns, Acta Cryst., **15**, 1098 (1962).
36. P. Fischer, G. Roullet, and D. Schwarzenbach, J. Phys. Chem. Solids, **32**, 1641 (1971).
37. B. Frlc and J.H. Holloway, J. Chem. Soc. Dalton Trans., 535 (1975).
38. J. Fawcett, J.H. Holloway, D. Laycock, and D.R. Russell, J. Chem. Soc. Dalton Trans., 1355 (1982).
39. D.A. Edwards, M.J. Stiff, and A.A. Woolf, Inorg. Nucl. Chem. Letters., **3**, 427 (1967).
40. F.A. Cotton and G. Wilkinson, "Advanced Inorganic Chemistry", 5th Edition, John Wiley and Sons, New York, 1989.

41. F.E. Mabbs and D.J. Machin, "Magnetism and Transition Metal Complexes", Chapman and Hall, London, 1973.
42. R.L. Carlin, "Magnetochemistry", Springer-Verlag, Berlin, 1986.
43. R.P. Rao, R.C. Sherwood, and N. Bartlett, J. Chem. Phys., **49**, 3728 (1968).
44. N. Bartlett and R. Maitland, Acta. Cryst., **10**, 63 (1957).
45. J.-M. Dance and A. Tressaud in "Inorganic Solid Fluorides", Ed. P. Hagenmuller, Academic Press, New York, 1985, and references therein.
46. B.G. Muller, Z. Anorg. Allg. Chem., **556**, 79 (1988).
47. B.N. Figgis and J. Lewis, Prog. Inorg. Chem., **6**, 37 (1964).
48. G. Maki, J. Chem. Phys., **28**, 651 (1958).
49. G.C. Allen and K.D. Warren, Inorg. Chem., **8**, 1895 (1969).
50. W. Klemm, W. Brandt, and R. Hoppe, Z. Anorg. Allg. Chem., **308**, 179 (1961).
- 51.a) W.W. Wilson and K.O. Christe, Inorg. Chem., **23**, 3261 (1984).
- b) R. Hoppe in "Inorganic Solid Fluorides", Ed. P. Hagenmuller, Academic Press, New York, 1985.
52. Landolt-Börnstein, Numerical Data and Functional Relationships in Science and Technology, Vol. 2, Magnetic Properties of Coordination and Organometallic Transition Metal Compounds, Springer-Verlag, Berlin, 1966.
53. T.A. Carlson, "Photoelectron and Auger Spectroscopy", Plenum Press, New York, 1975.
54. C.D. Wagner in "Practical Surface Analysis by Auger and X-ray Photoelectron Spectroscopy", Ed. D. Briggs and M.P. Seah, John Wiley and Sons, New York, 1983.
55. D.C. Frost, A. Ishitani, and C.A. McDowell, Mol. Phys., **24**, 861 (1972).
56. H. Willner, F. Mistry, G. Hwang, F.G. Herring, M.S.R. Cader, and F. Aubke, J. Fluorine Chem., **52**, 13 (1991).
57. K.C. Lee and F. Aubke, Inorg. Chem., **18**, 389 (1979).
58. H. Willner, S.J. Rettig, J. Trotter, and F. Aubke, Can. J. Chem., **69**, 391 (1991).
59. S.P. Mallela, K.C. Lee, and F. Aubke, Inorg. Chem., **23**, 653 (1984).

CHAPTER 4

MESITYLENE ADDUCTS OF TIN(II) FLUORO COMPOUNDS,



4.1 Introduction

Arene π -complexes, where low valent post-transition metal centers act as acceptors, and benzene or various alkyl benzenes, function as π -donors, form a small but interesting group of weakly bound complexes. Structural and bonding aspects of these compounds have become more widely known through the work of Amma et al. (1), and Schmidbaur et al. (2). A review on the more general topic of π -complexes of main group elements has also appeared recently (3).

Arene complexes of the post-transition metals are best regarded as donor-acceptor adducts, with the arene π -system being the donor component. For Group 13 metal derivatives, an increased arene donor strength through electron releasing substituents leads to enhanced stability of the complexes. However, as observed in X-ray crystal structure studies, the metal-ligand interactions are not strong enough in these complexes to induce significant distortions of the arene rings (2). Consequently, complexes with low thermal stability are usually isolated (1,2).

Within this group of π -complexes, interest has focussed mainly on arene complexes with univalent metal centers such as Ag(I), Cu(I), Hg(I), Ga(I), In(I) and Tl(I) and comparatively little is known about similar compounds with the Group 14 centers like Sn(II) (4-7) and Pb(II) (1,8). There are commonly two reasons given for the paucity of arene π -complexes in group 14:

a) as exemplified by the structural chemistry of divalent tin (9), the $5s^2$ pair is stereochemically far more active than in compounds of isoelectronic In(I) and consequently the Sn(II) derivatives are apparently less inclined to form π -complexes with arenes (2); b) lattice energies for Sn(II)- and Pb(II)-salts tend to be considerably higher than those of Ga(I), In(I), or Tl(I) salts. The non-polar, π -donating arenes are normally incapable of breaking up such lattices effectively. To reduce the lattice energy and to facilitate complex formation, salts with large, univalent anions are chosen and the majority of arene π -complexes reported so far feature tetrahalometallate (III) anions of the type MX_4^- with M=B, Al, Ga, In or Tl, and X=Cl or Br (1-8) as counter anions; however weakly basic anions like $OTeF_5^-$ appear to be suitable as well (10).

The tin(II)- π -arene complexes reported so far are limited largely to mono-arene complexes with either Sn^{2+} (4) or the chloride bridged moieties such as $(Sn_2Cl_2)^{2+}$ (5) or $(Sn_4Cl_4)^{4+}$ (7) as acceptors, but recently the first bis(arene) complex has been reported as well, $[(\eta^6-C_6H_6)_2SnCl(AlCl_4)]_2$ (6). Benzene functions primarily as donor, bonded to tin in the η^6 -mode, and $AlCl_4^-$ is the counter anion, with Cl atoms bridging to tin. Frequently, however, arenes are also found in the lattice, without being coordinated to tin (4,6,7). Detailed crystal structures (see Appendix A-8) are reported for all compounds (4-7) and have been used in the development of bonding concepts based on the Molecular Orbital theory ((1, 4, 5), Appendix A-9).

The interest in the chemistry of tin for this work stems from the following two specific related objectives: a) the use of ^{119}Sn Mössbauer spectroscopy as a structural tool (this spectroscopic technique has not been applied so far to this small group of tin complexes) and, b) the stabilization of "bare", non - or very weakly coordinated cations like Sn^{2+} (11) or R_2Sn^{2+} (12). As discussed in Chapter 3, two compounds of interest, tin(II)bis(fluorosulfate), $Sn(SO_3F)_2$, and tin(II)bis(hexafluoroantimonate), $Sn(SbF_6)_2$ (13), both originally reported by Gillespie and coworkers (14), appear to be capable of functioning as potential acceptors in arene π -complexes.

Both compounds give rise to broad single line ^{119}Sn Mössbauer spectra with large positive isomer shifts relative to SnO_2 , and, in the case of $\text{Sn}(\text{SO}_3\text{F})_2$, a small resolvable quadrupole splitting (11, 14) suggests non-directional, nearly spherical distribution of the $5s^2$ electron pair. In addition, it had been shown previously, based on ^{119}Sn Mössbauer parameters, that the anions SbF_6^- and $\text{Sb}_2\text{F}_{11}^-$ are extremely weakly basic and the least nucleophilic anions when stabilizing the cation $(\text{CH}_3)_2\text{Sn}^{2+}$ with a linear C-Sn-C group (12). Therefore, it was expected the SbF_6^- anion to be ideally suited to stabilize the "bare" Sn^{2+} ion equally well. The single line ^{119}Sn Mössbauer spectrum with an isomer shift of 4.39 mm s^{-1} relative to SnO_2 obtained for $\text{Sn}(\text{SbF}_6)_2$ (see Chapter 3), which is a shift of about 0.45 mm s^{-1} lower than suggested by calculations for Sn^{2+} (15), indicate that steric factors rather than low nucleophilicity of the counter anion may be important. The list of stannous compounds with single-line ^{119}Sn Mössbauer spectra and isomer shifts higher than the ones observed for $\text{Sn}(\text{SbF}_6)_2$ provides a clue. $\text{Sn}[\text{Sn}(\text{SO}_3\text{F})_6]$, 4.48 (11); $\text{Sn}(\text{ClO}_4)_2 \cdot (15\text{-crown}5)_2$, 4.53 (16); $\text{Sn}(\text{SbF}_6)_2 \cdot 2\text{AsF}_3$, 4.66 (17); and $\text{Sn}[\text{Sn}(\text{SO}_3\text{CF}_3)_6]$ 4.69 mm s^{-1} relative to SnO_2 (18) all approach a true Sn^{2+} more closely than $\text{Sn}(\text{SbF}_6)_2$ and all involve sterically more hindered ligands than SbF_6^- . A crystal structure for $\text{Sn}(\text{SbF}_6)_2 \cdot 2\text{AsF}_3$ (17), where the Lewis base AsF_3 is coordinated to tin as well, indicates 9-coordinate tin. The use of crown ether ligands (16) also supports the view that steric factors play an important role in stabilizing the "bare" Sn^{2+} ion.

Furthermore, the two anions of the compounds, SO_3F^- and SbF_6^- , as seen earlier in Chapter 3, function frequently as weakly coordinating, tridentate ligands towards divalent metal ions giving rise to layer structures, based on the CdCl_2 -prototype. This structural type is commonly found for most sulfonates of divalent metals, and the recently reported structure of $\text{Sn}(\text{SO}_3\text{F})_2$ confirms this structural type, where a three-dimensional framework of SO_3F groups linked by O-Sn-O bridges with the two crystallographically independent fluorosulfates acting as tridentate bridging ligands between the tin atoms is indicated (19). The structure of $\text{Ag}(\text{SbF}_6)_2$ (20) (Chapter 3, Figure 3.2) may serve as an example for the layer structure formed by

$M(\text{SbF}_6)_2$. Both SO_3F^- and SbF_6^- are very weakly basic, and covalent contributions to the lattice energies of their tin(II) salts should be small. Alternatively, both anions may stabilize arene complexes of tin with the help of oxygen or fluorine bridges. As donor, 1,3,5-trimethylbenzene (mesitylene) is chosen, because it is expected and found (2) to be a better donor than benzene. ^{119}Sn Mössbauer spectroscopy is proven to be a useful technique for this investigation. Its application to the study of tin(II) compounds has been reviewed previously (21).

4.2 Experimental

4.2.1 Synthesis

$\text{Sn}(\text{SO}_3\text{F})_2$ was obtained from SnCl_2 and HSO_3F (22) as described (23), and $\text{Sn}(\text{SbF}_6)_2$ was prepared from the solvolysis of $\text{Sn}(\text{SO}_3\text{F})_2$ in an excess of SbF_5 as pointed out in Chapter 3, Section 3.2. Stannocene, $(\eta^5\text{-C}_5\text{H}_5)_2\text{Sn}$, was synthesized from SnCl_2 and NaC_5H_5 . The crude product was purified by sublimation and its purity checked by microanalysis.

4.2.1a Synthesis of $\text{Sn}(\text{SO}_3\text{F})_2 \cdot 1,3,5\text{-(CH}_3)_3\text{C}_6\text{H}_3$

To a one part reactor a sample of $\text{Sn}(\text{SO}_3\text{F})_2$ (1.06 g, 3.35 mmol) was added, and after evacuation of the reactor, dry mesitylene (~7 mL, ~50 mmol) was transferred into the reaction vessel via a distillation bridge. The white suspension was stirred *in vacuo* at room temperature for three days. Excess mesitylene was removed *in vacuo* at -20 to -15°C (ice/NaCl bath) over a period of three days yielding 1.39 g of a white powder, of the composition $\text{Sn}(\text{SO}_3\text{F})_2 \cdot \text{mes}$, with a decomposition point of 97.2-98°C.

Anal calcd. for $C_9H_{12}F_2O_6S_2Sn$: C, 24.74; H, 2.77; F, 8.70; S, 14.67; and Sn, 27.16%.

Found: C, 25.77; H, 2.87; F, 8.53; S, 14.84; and Sn, 27.10%.

An alternate preparation with mesitylene removed *in vacuo* at -5°C gave the following analysis:

Anal. calcd.: C, 24.74; H, 2.77; and S, 14.67%.

Found: C, 24.97; H, 2.80; and S, 14.55%.

IR bands and estimated intensities [cm^{-1}]: 2910w,b, 2860vw, 1760vw, 1604m, 1575w,sh, 1446w, 1337w, 1191vs, 1127w,sh, 1054vs, 888s, 786w, 667w, 589ms, 544m, 507vw, and 405m.

4.2.1b Synthesis of $\text{Sn}(\text{SbF}_6)_2 \cdot 2[1,3,5(\text{CH}_3)_3\text{C}_6\text{H}_3]$

To the bottom portion of a two part reactor, freshly prepared $\text{Sn}(\text{SbF}_6)_2$ (3.11 g, 5.27 mmol) was added. The flask was then fitted to the lower end of a filtration apparatus (24). On the top end of the filtration apparatus a second 100 mL flask was fitted and the entire apparatus was then evacuated. Through a Teflon valve in the bottom chamber of the apparatus mesitylene (15 mL, 108 mmol) was transferred via a distillation bridge. Upon exposure to the mesitylene vapor, the white powder immediately turned yellow and then during the filtration, pale, off-white. When the mesitylene distillation was complete, the suspension was stirred *in vacuo* for 1.5 hours. The apparatus was inverted, and the mixture filtered. The filtrate flask was cooled to -10°C (ice/ NaCl bath) and the mixture was left to filter for 17 hours.

When gravity filtration was complete, the filtrate chamber of the apparatus was evacuated to further dry the solid. The apparatus was refilled with dry nitrogen inside the dry box, and the filtrate chamber was evacuated again. At the end of this drying procedure, a pale,

off-white solid (4.18 g, 5.04 mmol, 95.5% yield) was obtained together with a yellow-green filtrate, which was discarded. The product was transferred to a two part reactor and was further dried *in vacuo* for 24 hours at room temperature. No further weight change was observed. The solid decomposed at 69.5-71.5°C to a greenish yellow liquid.

Anal. calcd. for $C_{18}H_{24}F_{12}Sb_2Sn$: C, 26.03; H, 2.91; F, 27.45; Sb, 29.32; Sn, 14.29%.

Found: C, 26.87; H, 3.00; F, 27.31; Sb, 29.05; Sn, 14.20; Total 100.43%.

IR bands and estimated intensities [cm^{-1}]: 2920mw, 2860w, 1601m, 1580m, 469w, 1384m, 1168vw, 1080vw, 1040vw, 1007w, 960vw,b, 860w, 687s, 671vs, 635s, sh, 580m,b, 544m, 512w, 440w, and 395w.

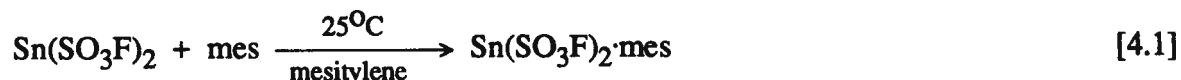
4.3 Results and Discussion

4.3.1 Synthesis

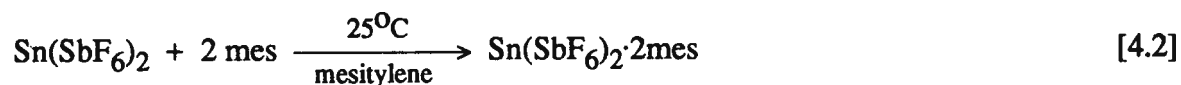
The previously reported synthesis of Sn(II) containing benzene π -complexes (4-7) involves either the reaction of $SnCl_2$ and $AlCl_3$ at different mole ratios and temperatures (4,5), or of molten $Sn(AlCl_4)_2$ (6, 7) with the arene to give either Sn^{2+} , $(Sn_2Cl_2)^{2+}$ or $(Sn_4Cl_4)^{4+}$ containing complexes as colorless crystals. Crystalline material suitable for single crystal X-ray diffraction studies are obtained (4-7) in all instances. The course of the reaction appears to be influenced in part by the mole ratios of the reactants used and in part by the reaction temperature. The different products obtained, with Sn^{2+} or $(Sn_nCl_n)^{n+}$, $n = 2$ or 4 , are not totally surprising since in the binary system $SnCl_2-AlCl_3$, phase studies (9) have revealed the existence of two distinct phases: $SnCl_2 \cdot AlCl_3$ and $SnCl_2 \cdot 2AlCl_3$. It appears that the same two phases crystallize now in the form of π -arene complexes with $AlCl_4^-$ as a coordinated counter ion and in several instances with the lattice arene present (4, 6, 7).

The synthetic reactions reported here differ in a number of ways. Binary rather than tertiary reaction mixtures are used, the reaction temperature is room temperature and the tin(II) substrates are synthesized and characterized prior to their reaction with mesitylene.

Addition of mesitylene occurs smoothly according to:



or



mes = 1,3,5-trimethylbenzene (mesitylene), and the two complexes are formed in nearly quantitative yield. Solid material remains throughout the reaction and in case of $\text{Sn}(\text{SO}_3\text{F})_2$ as acceptor, there is no visible sign of a reaction, except for an increase in the bulk of the solid residue. Complete removal of excess mesitylene *in vacuo* is difficult to judge and the conditions quoted in the experimental section were arrived at by trial and error. It does appear that samples submitted for microanalysis (C, H, and S content) immediately after isolation had small amounts of residual mesitylene trapped while samples sent to Germany for further analysis (S, Sn, Sb, and F content) seemed to have lost the excess reactant.

The reaction of mesitylene with $\text{Sn}(\text{SbF}_6)_2$ differs even further. A 2:1 complex forms and a color change to bright yellow is noted as soon as the tin salt is exposed to mesitylene vapor. However the color of the solid quickly fades during product isolation and an off-white solid is obtained in very high yield together with a yellow-green filtrate. The origin of the initially observed color is unclear. A UV-visible spectrum taken as Nujol mull on a solid sample at this stage shows an intense UV-absorption at ~240 nm tailing off in the visible region

with weak shoulders at 486, 580 and 656 nm respectively.

Observations made during product isolation suggested that the intense color seen was due to a by-product, which was soluble in excess mesitylene. A complex formed by mesitylene and small, residual amounts of SbF_5 becomes a distinct possibility. Furthermore, the addition of mesitylene to pure SbF_5 resulted in an intensely colored dark brown solid, which was not investigated further. There is little doubt that the final product, like other arene complexes of Group 13 and 14 metals (1-8), is a white solid.

The use of gravity filtration as a means of product isolation is important in the case of the $\text{Sn}(\text{SbF}_6)_2 \cdot 2\text{mes}$ synthesis. Attempts to isolate this compound by slow, careful removal of excess mesitylene *in vacuo* or in a stream of dry N_2 at room temperature and at -5°C lead to partial decomposition and materials that analyze as $\text{Sn}(\text{SbF}_6)_2 \cdot 1.5\text{mes}$. In addition, the product has a slight yellow tint.

The thermal stability of both mesitylene complexes described here is limited. $\text{Sn}(\text{SO}_3\text{F})_2 \cdot \text{mes}$ melts with decomposition at $97\text{-}98^\circ\text{C}$ while $\text{Sn}(\text{SbF}_6)_2 \cdot 2\text{mes}$ has a decomposition range of $69.5\text{-}71.5^\circ\text{C}$, where a greenish yellow liquid forms.

Attempts to extend the mesitylene addition reaction to three other tin(II) compounds were unsuccessful. Both SnCl_2 and SnF_2 were recovered unchanged. Both salts have Sn^{2+} in distorted octahedral environments (7) and the structures of SnCl_2 (25) and orthorhombic SnF_2 (14,26), one of the two polymorphic forms, may be regarded as layer structures. It can be concluded that the lattice energies of both compounds are too high and adduct formation does not occur in these two compounds.

Stannocene, $(\eta^5\text{-C}_5\text{H}_5)_2\text{Sn}$, has a molecular structure with a tilted arrangement of the C_5H_5 -rings (27) and presumably a stereochemically active electron pair. Its ^{119}Sn Mössbauer spectrum shows a quadrupole splitting of 0.86 mms^{-1} (28). The compound dissolves in mesitylene, but stannocene is again recovered unchanged after removal of the arene *in vacuo*. The ^1H NMR spectrum of stannocene in mesitylene is studied down to -40°C , but only rather subtle changes are noted. The principle resonance due to stannocene (29) shifts from 5.96 ppm in CDCl_3 to 5.91 ppm relative to TMS in the presence of mesitylene while $J^{1\text{H}} - ^{119/117}\text{Sn}$ changes from 15.76 Hz to 15.16 Hz. Beginning at -20°C and becoming more pronounced at -40°C , a second, smaller and rather broad resonance at 5.88 ppm emerges with a similar separation of the satellite peaks. Mesitylene resonances appear almost in the same position as in pure mesitylene as single lines at 2.28 (CH_3) and 6.78 (C-H) ppm and do not shift with decreasing temperature. While there may be a weak interaction between stannocene and mesitylene at reduced temperature, all attempts to isolate a reaction product by low temperature filtration have failed.

Therefore, it appears that tin(II) is sufficiently acidic only when bulky and very weakly nucleophilic anions like AlCl_4^- , SO_3F^- and SbF_6^- are present, and when lattice energies are reduced in the resulting layer structures. From a correlation of ^{119}Sn Mössbauer data of dimethyltin(IV) salts (12) it seems that SbF_6^- is the weaker nucleophile of the two fluoroanions, and formation of a 2:1 complex with mesitylene is not unexpected, while $\text{Sn}(\text{SO}_3\text{F})_2$ forms a 1:1 complex only. Complex formation by addition of mesitylene to a solid tin(II) salt as described here does not lead to the formation of single crystals suitable for structural studies. Hence evidence for the presence of π -arene complexes has to come from two other sources, i.e. ^{119}Sn Mössbauer and vibrational spectra, to be discussed subsequently.

4.3.2 ^{119}Sn Mössbauer Spectra

Isomer shifts, relative to SnO_2 for tin(II) compounds, fall within the range of ~ 2.1 mm s^{-1} , viewed as the borderline between Sn(II) and Sn(IV), and values of about 5.1 – 7.7 mm s^{-1} for a "bare" Sn^{2+} have been calculated where a spherically distributed $5s^2$ electron pair (9,15) is considered. Experimental values obtained have not reached the ionic limit. The highest values reported so far are 4.69 mm s^{-1} for the tin(II) moiety in $\text{Sn(II)[Sn(IV)(SO}_3\text{CF}_3)_6]$ (18) and 4.66 mm s^{-1} for $\text{Sn(SbF}_6)_2 \cdot 2\text{AsF}_3$ (17), where an X-ray diffraction study reveals a distorted nine-coordinated environment for Sn^{2+} .

In these close approaches to a Sn^{2+} ion no quadrupole splitting is observed (17,18); however, with decreasing isomer shift, first line broadening already evident for $\text{Sn(SbF}_6)_2$, is noted and eventually small but well resolved quadrupole splittings are found (30). Hence ^{119}Sn Mössbauer spectroscopy provides two criteria which determine the ionic character of Sn(II) compounds: (a) the isomer shift which should be high, close to or in excess of 4.69 mm s^{-1} relative to SnO_2 , and (b) the quadrupole splitting which should be zero.

Some ^{119}Sn Mössbauer data of Sn(II) compounds which are of interest to this study are listed in Table 4.1. Of the five tin(II) compounds studied here $\text{Sn(SO}_3\text{F)}_2$ (4.18 mm s^{-1}) and $\text{Sn(SbF}_6)_2$ (4.44 mm s^{-1}) have the highest isomer shifts of those listed and only the former has a small, resolvable quadrupole splitting. Not unexpectedly, the more acidic $\text{Sn(SbF}_6)_2$ is the better acceptor, seemingly capable of coordinating two mesitylene donors, while $\text{Sn(SO}_3\text{F)}_2$ forms a 1:1 complex only.

Upon arene uptake the isomer shift is reduced by 0.17 mm s^{-1} for $\text{Sn(SO}_3\text{F)}_2$ and by 0.40 mm s^{-1} for $\text{Sn(SbF}_6)_2$. This reduction suggests that mesitylene is interacting with Sn(II) and, judging by the magnitude of the shift, that in the case of $\text{Sn(SbF}_6)_2 \cdot 2\text{mes}$ both mesitylene

Table 4.1: ^{119}Sn Mössbauer Parameters of Relevant Tin(II) Compounds at 80K

Compound	Isomer Shift	Quadrupole Splitting	Reference
	δ [mm s^{-1}] rel. to SnO_2	ΔE_Q [mm s^{-1}]	
SnF_2 (orthorhombic)	3.30	2.15	14
SnF_2 (monoclinic)	3.49	1.61	14
$(\eta^5\text{-C}_5\text{H}_5)_2\text{Sn}$	3.74	0.86	28a
$(\Pi\text{-C}_6\text{H}_6)\text{Sn}(\text{AlCl}_4)_2\cdot\text{C}_6\text{H}_6$	3.93	0	4c
SnCl_2	4.08	0.66	15c
$\text{Sn}(\text{SO}_3\text{F})_2$	4.18	0.68	14
$\text{Sn}(\text{SO}_3\text{F})_2\cdot\text{mes}$	4.01	1.04	This work
$\text{Sn}(\text{SbF}_6)_2$	4.44	0	14
$\text{Sn}(\text{SbF}_6)_2\cdot 2\text{mes}$	4.04	1.13	This work

Accuracy limits for δ and ΔE_Q are $\pm 0.03 \text{ mm s}^{-1}$

molecules are probably coordinated to tin. A similar isomer shift of 3.93 mm s^{-1} is reported for $(\pi\text{-C}_6\text{H}_6)\text{Sn}(\text{AlCl}_4)_2\cdot\text{C}_6\text{H}_6$ (4c) but no Mössbauer data appear to have been reported for the two $\text{SnCl}_2\text{-AlCl}_3$ phases (9), which would allow an estimation of the decrease in the isomer shift upon arene addition. The reduction in the isomer shift upon binding to mesitylene is accompanied by an increase in quadrupole splitting to 1.04 mms^{-1} for $\text{Sn}(\text{SO}_3\text{F})_2\cdot\text{mes}$ whereas for $\text{Sn}(\text{SbF}_6)_2\cdot 2\text{mes}$ a slightly asymmetrical doublet (see Figure 4.1) with a ΔE_Q value of 1.13 mm s^{-1} is obtained. These findings are consistent with trends on δ and ΔE_Q summarized above.

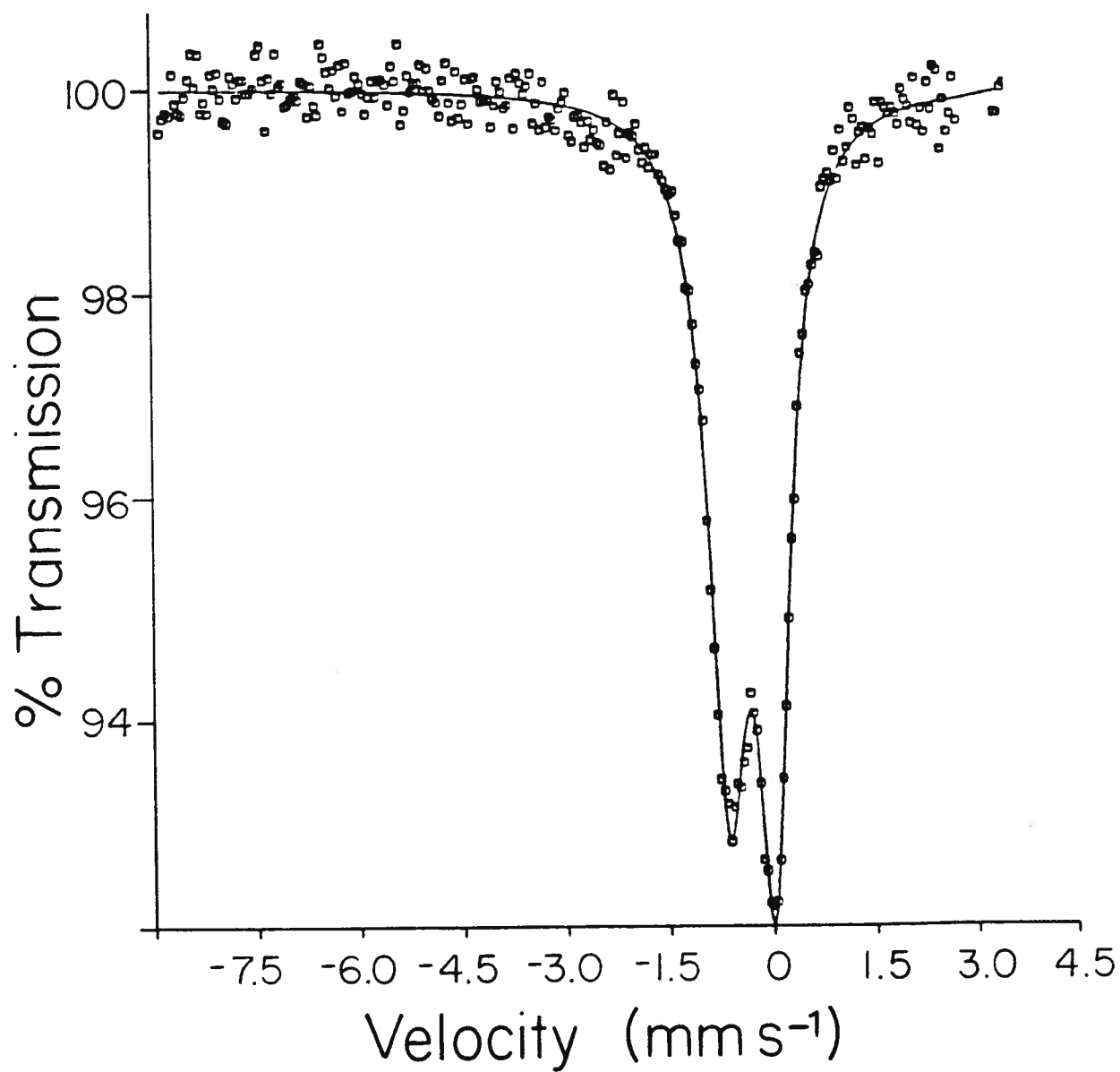
The occurrence of quadrupole splitting suggests an increase in asymmetry in the coordination environment of tin(II) when coordination to only oxygen or fluorine changes to include coordination to the arene as well. For both mesitylene adducts the ^{119}Sn Mössbauer parameters obtained remain well within the range reported for typical tin(II) compounds (21). The addition of mesitylene to Sn^{2+} , as suggested by the ^{119}Sn Mössbauer data, is expected to cause a change in the manner in which the anions SO_3F^- and SbF_6^- coordinate to tin. This change in anion denticity is probed by infrared spectroscopy and discussed in the subsequent section.

4.3.3 Infrared Spectra

Attempts to obtain Raman spectra of both mesitylene adducts are unsuccessful and quick darkening of areas exposed to laser light indicates thermal degradation is occurring even at very low laser power. Hence evidence rests on infrared spectra obtained on solid films between silver halide windows.

Both infrared and Raman spectra for $\text{Sn}(\text{SO}_3\text{F})_2$ (14, 23) and $\text{Sn}(\text{SbF}_6)_2$ (14) have been reported previously, and for tridentate SbF_6^- -groups present in $\text{M}(\text{SbF}_6)_2$ compounds a useful vibrational assignment has been presented (13, 31). As discussed previously in Chapter 3,

Figure 4.1: ^{119}Sn Mössbauer Spectrum of $\text{Sn}(\text{SbF}_6)_2 \cdot 2\text{mes}$ at 77K



Section 3.3.2, to account for the observed spectral complexity in the SbF-stretching region, a subdivision into metal coordinated, through fluorine bridges Sb-F^b, and non-coordinated or terminal Sb-F^t stretches is suggested with the former usually between 550 and 650 cm⁻¹ and the latter above 650 cm⁻¹ (31). Vibrational bands reported for Sn(SbF₆)₂ (14) allow such a division as well, even though a distorted environment around tin introduces additional complexity. Assignments for Sn(SO₃F)₂ have suggested the presence of ionic SO₃F⁻ with the symmetry of the anion reduced from C_{3v} for the free ion to C_s due to coordination to tin (14, 23), but there are still unresolved problems, best reflected in the occurrence of two equally intense bands at ~770 and 830 cm⁻¹ possibly due to νSF(A₁) and a splitting found for δSO₃(A₁). It seems more appropriate here to view the spectrum as being due to two non-equivalent SO₃F-groups with approximately C_{3v} symmetry with some band overlap in the areas of deformation modes. This implies either ionic groups or more likely O-tridentate groups. As mentioned previously, these conclusions are further confirmed by the recently published crystal structure study of Sn(SO₃F)₂ by Adams et al. (19).

Addition of mesitylene to both Sn(II) compounds has two general effects: a) the infrared spectrum is dominated in both instances by bands due to the SO₃F and SbF₆ groups, respectively, with all mesitylene bands of very low intensity, and b) the vibrational spectra of the anions appear to change, and at least the SbF₆ bands reflect a change in anion coordination. Low intensity of vibrational bands due to organic groups is commonly found for organotin(IV) salts (32), and this feature appears to extend to the mesitylene adducts of tin(II) salts as well.

The observed infrared frequencies for the two mesitylene adducts are listed in the experimental section together with estimated relative intensities. The discussion in this section will center around two aspects, (a) the mesitylene bands in neat mesitylene and in the complexes, and (b) the "anion" bands before and after mesitylene addition to Sn(SO₃F)₂ and Sn(SbF₆)₂, respectively. Vibrational bands attributed to mesitylene are listed in Table 4.2 for

Table 4.2: Infrared Bands of Liquid Mesitylene and Bands Attributed to Mesitylene in the Adducts Sn(SO₃F)₂·mes and Sn(SbF₆)₂·2mes

Mesitylene [cm ⁻¹] Int.	Sn(SO ₃ F) ₂ ·mes [cm ⁻¹] Int.	Sn(SbF ₆) ₂ ·2mes [cm ⁻¹] Int.
3018 s		
2921 vs	2910 w,b	2920 mw
2860 s	2860 vw	2860 vw
2730 m		
1760 m-w	1760 vw	
1715 m-w		
1608 vs	1604 m, 1575 w, sh	1601 m, 1580 m
1512 w		
1473 s	1446 w	1469 w
1442 m, sh		
1375 m-s		1384 m
1170 vw		1168 vw
1037 s		1080 vw, 1040 vw, 1007 w
932 vw		960 vw, b
882 vw		860 w
835 vs	786 w	
687 vs	667 w	687 ms
561 w,b		544 m
515 w	507 vw	512 w
443 m		440 w
421 m		
411 m		395 w

See Table 4.3 for abbreviations

both adducts and compared to bands observed for liquid mesitylene. The listing of bands for the adducts is incomplete because of the very low intensity mentioned above which causes medium and weak bands to be unobservable and in case of $\text{Sn}(\text{SO}_3\text{F})_2\cdot\text{mes}$, partial overlap of mesitylene bands with more intense anion bands, in particular in the region of $800\text{-}1300\text{ cm}^{-1}$.

In regions where no anion bands are expected, small band shifts are observed, mostly to lower frequencies. The aromatic C=C stretch at 1608 cm^{-1} in free mesitylene is a good example. This peak is shifted to 1604 and 1601 cm^{-1} for $\text{Sn}(\text{SO}_3\text{F})_2\cdot\text{mes}$ and $\text{Sn}(\text{SbF}_6)_2\cdot 2\text{mes}$ respectively. The lower frequency indicates a very slight withdrawal of π electron density of the aromatic ring towards tin.

Interestingly, some bands assigned to bonded mesitylene appear to be split compared to those of free mesitylene. This is noticeable in the $1570\text{-}1610\text{ cm}^{-1}$ region of both spectra, and especially in the $1000\text{-}1200\text{ cm}^{-1}$ region for $\text{Sn}(\text{SbF}_6)_2\cdot 2\text{mes}$. The splitting can be attributed to a reduction in symmetry of the bonded mesitylene, and/or the presence of two non-equivalent mesitylenes, in particular in $\text{Sn}(\text{SO}_3\text{F})_2\cdot\text{mes}$. However some solid state splitting is possible as well.

All features affecting bands due to mesitylene are subtle, and the observed features are in general consistent with a very weak interaction between the arene and the two Sn(II) salts.

The infrared bands attributed to the anion are summarized in Table 4.3 and are compared to the reported values for the parent compounds $\text{Sn}(\text{SO}_3\text{F})_2$ (14, 23) and $\text{Sn}(\text{SbF}_6)_2$ (14). For $\text{Sn}(\text{SO}_3\text{F})_2\cdot\text{mes}$ the IR spectrum is dominated by an intense broad band centered at 1054 cm^{-1} and two bands at 1191 and 1127 cm^{-1} . These are assigned collectively as SO_3 stretching modes, probably masking some of the less intense motions of the mesitylene component in the adduct.

Table 4.3: Infrared Frequencies for $\text{Sn}(\text{SO}_3\text{F})_2$ and $\text{Sn}(\text{SbF}_6)_2$ and Bands Attributed to the Anions in the Mesitylene Adducts $\text{Sn}(\text{SO}_3\text{F})_2 \cdot \text{mes}$ and $\text{Sn}(\text{SbF}_6)_2 \cdot 2\text{mes}$

$\text{Sn}(\text{SO}_3\text{F})_2^a$ [cm^{-1}] Int.	$\text{Sn}(\text{SO}_3\text{F})_2 \cdot \text{mes}$ [cm^{-1}] Int.	Approximate Band Description for C_{3v}	$\text{Sn}(\text{SbF}_6)_2^b$ [cm^{-1}] Int.	$\text{Sn}(\text{SbF}_6)_2 \cdot 2\text{mes}$ [cm^{-1}] Int.	Assignment ^c
1290s, sh 1240vs 1180s, sh	1337w 1191vs 1127w, sh	νSO_3 (E)	741m, sh 713s 676ms 650s	671vs 635s, sh	νSbF_6 as. (E_{1u})
1062s	1054vs	νSO_3 (A_1)	629s ~613sh ~575sh	580m, b	νSbF_6 (E_{2g})
833s 772s	888s 786w	νSF (A_1)			
606m 592m	589ms	δSO_3 (E)	477w 313sh 292m 271m		SbF_6^- deformations
573s	544m	δSO_3 (A_1)			
554s 403m 395sh	405m	$\delta\text{SO}_3\text{F}$ (E)			

^a Ref. 23

^b Ref. 14

^c Refs. 13 and 31

Abbreviations: s = strong,
v = very,
as = asymmetric,

m = medium,
sh = shoulder,
t = terminal,

w = weak
b = broad
b = bridging

The most noticeable change appears to have occurred in the S-F stretching region. The two intense bands at 772 cm^{-1} and 833 cm^{-1} in $\text{Sn}(\text{SO}_3\text{F})_2$ (Table 4.3) are now replaced by a single strong band at 888 cm^{-1} , with a weak band at 786 cm^{-1} (possibly due to mesitylene).

From this overall band distribution and the increased wave number of the $\nu\text{S-F}$ band, it appears that a change in denticity of the anion has taken place due to mesitylene adduct formation. The findings are consistent with a bidentate, possibly bridging configuration tentatively formulated as $[(\eta^6\text{-mes})\text{Sn}(\text{SO}_3\text{F})_2]_n$ rather than an ionic (perturbed) or tridentate grouping (33).

Compared to the rather complicated pattern observed for $\text{Sn}(\text{SbF}_6)_2$ in the region of $520\text{-}750\text{ cm}^{-1}$ (Table 4.3), the band pattern displayed by the anion in the adduct $\text{Sn}(\text{SbF}_6)_2\cdot 2\text{mes}$ is very simple: a very strong band at 671 cm^{-1} , a sharp, medium band at 635 cm^{-1} , and a weak band at 580 cm^{-1} are found. For a free SbF_6^- anion, a peak at $\sim 660\text{ cm}^{-1}$ is attributed to the asymmetric stretch with Raman active bands observed at ~ 660 again and at 575 cm^{-1} . The pattern observed for $\text{Sn}(\text{SbF}_6)_2\cdot 2\text{mes}$ suggests the presence of a weakly coordinated SbF_6^- anion. Peak splitting in the SbF_6^- stretching region produces bands at 671 and 635 cm^{-1} , with the loss of a symmetry center allowing detection of a Raman active fundamental at 580 cm^{-1} (34).

It appears then that addition of mesitylene has a different effect on the anion bands in $\text{Sn}(\text{SO}_3\text{F})_2\cdot\text{mes}$ and $\text{Sn}(\text{SbF}_6)_2\cdot 2\text{mes}$, respectively. In the former adduct the SO_3F group seems to be still coordinated to tin, but more likely in a bidentate, possibly bridging manner. In $\text{Sn}(\text{SbF}_6)_2\cdot 2\text{mes}$ only weak coordination of the SbF_6^- group is evident and any departure from an ionic SbF_6^- with O_h symmetry is rather slight. It is unfortunate that in particular for this compound support from Raman spectroscopy is lacking due to sample decomposition in the laser light, as mentioned earlier.

The findings for $\text{Sn}(\text{SbF}_6)_2 \cdot 2\text{mes}$ are consistent with the view that both mesitylene groups are coordinated to tin, which in turn is supported also by the ^{119}Sn Mössbauer spectra.

4.4 Conclusion

Direct addition of an arene, in this case mesitylene, to suitable Sn(II) salts like $\text{Sn}(\text{SO}_3\text{F})_2$ and $\text{Sn}(\text{SbF}_6)_2$ at room temperature, and product isolation well below room temperature, allow the high yield synthesis of very weakly bound mesitylene complexes. However, only microcrystalline materials result which precludes structural studies by single crystal X-ray diffraction. The adducts are characterized by chemical analysis and infrared spectra and their formation is followed by ^{119}Sn Mössbauer spectroscopy. This spectroscopic method allows not only product characterization, but also, using the isomer shift and the absence of quadrupole splitting as criteria, the identification of other suitable substrates for complex formation. It is observed that only tin(II) compounds with large, weakly nucleophilic anions are capable of forming mesitylene adducts, while SnCl_2 , SnF_2 and stannocene do not give any indication of adduct formation under similar conditions.

References

1. A.G. Gash, P.F. Rodsiler, and E.L. Amma, Inorg. Chem., **13**, 2429 (1974).
- 2.a) H. Schmidbaur, Angew. Chem. Int. Ed. (English), **24**, 893 (1985).
b) H. Schmidbaur, W. Bublak, B. Haber, and G. Muller, Angew. Chem. Int. Ed. (English), **26**, 234 (1987).
3. P. Jutzi, Adv. Organomet. Chem. **26**, 217 (1986).
- 4.a) Th. Auel and E.L. Amma, J. Am. Chem. Soc., **90**, 5941 (1968).
b) H. Luth and E.L. Amma, J. Am. Chem. Soc., **91**, 7515 (1969).

- c) P.F. Rodsiler, Th. Auel, and E.L. Amma, J. Am. Chem. Soc., **97**, 7405 (1975).
- 5.a) M.S. Weininger, P.F. Rodsiler, A.G. Gash, and E.L. Amma, J. Am. Chem. Soc., **94**, 2135 (1972).
- b) M.S. Weininger, P.F. Rodsiler, and E.L. Amma, Inorg. Chem., **18**, 751 (1979).
6. H. Schmidbaur, T. Probst, B. Huber, O. Steigelmann, and G. Muller, Organomet. **8**, 1567 (1989).
7. H. Schmidbaur, T. Probst, B. Huber, G. Muller, and C. Kruger, J. Organomet. Chem., **365**, 53 (1989).
8. Th. Auel and E.L. Amma, J. Am. Chem. Soc., **90**, 5941 (1968).
9. J.D. Donaldson, Prog. Inorg. Chem., **8**, 287 (1967) and references herein.
10. S.H. Strauss, M.D. Noiroto, and O.P. Anderson, Inorg. Chem., **25**, 3851 (1986).
11. S.P. Mallela, S.T. Tomic, K. Lee, J.R. Sams, and F. Aubke, Inorg. Chem., **25**, 2939 (1986).
12. S.P. Mallela, S. Yap, J.R. Sams, and F. Aubke, Inorg. Chem., **25**, 4327 (1986).
13. M.S.R. Cader and F. Aubke, Can. J. Chem., **67**, 1700 (1989).
14. T. Birchall, P.A.W. Dean, and R. J. Gillespie, J. Chem. Soc. A, 1777 (1971).
- 15.a) J.K. Lees and P.A. Flinn, Phys. Lett., **19**, 186 (1965); and J. Chem. Phys., **48**, 882 (1968).
- b) P.A. Flinn, G.K. Shenoy, F.E. Wagner, Eds., "Mössbauer Isomer Shifts", North-Holland Publishing Co., Amsterdam, 1978, p. 593 ff.
- c) J.D. Donaldson and B.J. Senior, J. Chem. Soc. (A), 1821 (1967).
16. R.H. Herber and G. Carrasquillo, Inorg. Chem., **20**, 3693 (1981).
17. A.J. Edwards and K.I. Khallow, Chem. Comm., 50 (1984).
18. R.J. Batchelor, J.N.R. Ruddick, J.R. Sams, and F. Aubke, Inorg. Chem., **16**, 1414 (1977).
19. D.C. Adams, T. Birchall, R. Faggiani, R.J. Gillespie, and J.E. Vekris, Can. J. Chem., **69**, 2122 (1991).

20. D. Gantar, I. Leban, B. Frlec, and J.H. Holloway, J. Chem. Soc. Dalton Trans., 2379 (1987).
21. R.V. Parish in "Mössbauer Spectroscopy Applied to Inorganic Chemistry", Vol. I, Ed. G.J. Long, Plenum Press, New York, 1984.
22. J. Barr, R.J. Gillespie, and R.C. Thompson, Inorg. Chem., **3**, 1149 (1964).
23. C.S. Alleyne, K. O'Sullivan Mailer, and R.C. Thompson, Can. J. Chem., **52**, 336 (1974).
24. D.F. Shriver, "The Manipulation of Air-Sensitive Compounds", McGraw-Hill, New York, 1969.
25. R.E. Rundle and D.H. Olson, Inorg. Chem., **3**, 596 (1964).
26. J.D. Donaldson, R. Oteng, and B.J. Senior, Chem. Comm., 618 (1965).
27. A. Almenningen, A. Haaland, and T. Motzfeld, J. Organomet. Chem., **7**, 97 (1967).
- 28.a) P.G. Harrison and J.J. Zuckerman, J. Am. Chem. Soc., **92**, 2577 (1970).
b) T.S. Dory and J.J. Zuckerman, J. Organomet. Chem., **264**, 295 (1984).
29. L.D. Dave, D.F. Evans, and G. Wilkinson, J. Chem. Soc., 3684 (1959).
- 30.a) J.G. Stevens and V.E. Stevens in "Mössbauer Effect Data Index", Plenum Press, New York, 1958.
b) J.J. Zuckerman in "Chemical Mössbauer Spectroscopy", Ed. R.H. Herber, Plenum Press, New York, 1984.
31. K.O. Christe, W.W. Wilson, R. Bougon, and P. Charpin, J. Fluorine Chem., **20**, 385 (1982).
32. P.A. Yeats, J.R. Sams, and F. Aubke, Inorg. Chem., **11**, 2634 (1972).
33. W.W. Wilson and F. Aubke, Inorg. Chem., **13**, 326 (1974).
34. A.M. Qureshi, A.H. Hardin, and F. Aubke, Can. J. Chem., **49**, 816 (1971).

CHAPTER 5

A LOW TEMPERATURE MAGNETIC STUDY OF THE MOLECULAR CATIONS O_2^+ , Br_2^+ AND I_2^+

5.1 Introduction

Only a limited number of compounds with paramagnetic homonuclear ions of non-metallic main group elements are known. Of these, compounds with diatomic cations stabilized by very weakly basic fluoroanions are the subject of this study. The cations in this group consist of the dioxygenyl cation O_2^+ , first discovered in $O_2^+[PtF_6]^-$ by Bartlett and Lohmann (1), and the two dihalogen cations I_2^+ and Br_2^+ , first identified in solutions of strong acids and superacids by Gillespie et al. (2,3).

Single crystal X-ray diffraction studies were subsequently reported for $Br_2^+[Sb_3F_{16}]^-$ (4) and $I_2^+[Sb_2F_{11}]^-$ (5), while powder diffraction studies have afforded a more limited structural insight into a number of dioxygenyl salts (6). For the dihalogen cations, electronic spectra of the solvated species (2,3), resonance Raman spectra (7), and magnetic measurements at room temperature (2,4(a)) have allowed some information on the electronic structure, suggesting a $^2\Pi_{3/2g}$ ground state (10). In addition, the study by Herring and McLean (8) has pointed out the close similarity between the solvated cations $I_2^+_{(solv)}$ and $Br_2^+_{(solv)}$ and their gaseous counterparts as studied by photoelectron spectroscopy (9) or molecular spectroscopy (10). This strong resemblance should permit at least an approximation of the energy separation to the nearest excited states, not only for the dihalogen cations, but also for O_2^+ , where a $^2\Pi_{1/2g}$ ground state is indicated (10).

The objectives of the present study which involves low-temperature magnetic susceptibility measurements on suitable compounds containing the three homonuclear diatomic cations can be summarized as follows:

- (i) To investigate the magnetic behavior of what appear to be the only three suitable paramagnetic molecular cations formed by non-metals. Structural and spectroscopic information mentioned previously should help in the interpretation.
- (ii) To explore whether, and to what extent, van Vleck's theory of molecular paramagnetism (11), developed 60 years ago, can be applied to solid-state cations. So far, nitric oxide, NO, has served as the best example; however, useful experimental data for this molecule do not extend into the condensed phase due to intermolecular association.
- (iii) To examine the reasons why the magnetic moments reported so far for O_2^+ salts fall well below the spin-only value of $1.73 \mu_B$. Measurements down to very low temperatures should allow the detection of magnetic behavior consistent with antiferromagnetic exchange, which is a possible cause for reduced magnetic susceptibilities.
- (iv) To compare the magnetic susceptibilities of $I_2^+[Sb_2F_{11}]^-$ and $Br_2^+[Sb_3F_{16}]^-$ below $\sim 80K$, since earlier measurements above that temperature (12) had suggested antiferromagnetic coupling for $I_2^+[Sb_2F_{11}]^-$, but not for $Br_2^+[Sb_3F_{16}]^-$.

5.2 Experimental

Both $Br_2^+[Sb_3F_{16}]^-$ and $I_2^+[Sb_2F_{11}]^-$ were synthesized according to the method reported by Wilson et al. (12). This method involved the oxidation of previously purified Br_2 and resublimed I_2 by bis(fluorosulfonyl) peroxide, $S_2O_6F_2$, at a precise 2:1 mole ratio, and the

subsequent solvolysis of the product mixture in an excess of freshly distilled antimony(V) fluoride. The reactions were followed by weight and the purity checked by melting points.

$\text{Br}_2^+[\text{Sb}_3\text{F}_{16}]^-$ (4.777 g, 5.762 mmol) was obtained from 0.924 g (5.782 mmol) of Br_2 and 0.5724 g (2.891 mmol) of $\text{S}_2\text{O}_6\text{F}_2$ after solvolysis in ~10 g of SbF_5 at room temperature and removal of all volatiles *in vacuo*. The bright red solid melted at $84 \pm 1^\circ\text{C}$ (lit. 85.5°C) (12). $\text{I}_2^+[\text{Sb}_2\text{F}_{11}]^-$ (2.775 g or 3.928 mmol) was synthesized from 0.9986 g (3.934 mmol) I_2 and 0.3895 g (1.967 mmol) of $\text{S}_2\text{O}_6\text{F}_2$ and subsequent solvolysis in ~12 g of SbF_5 at 50°C . The black-blue solid isolated after the removal of all volatiles melted at $129 \pm 1^\circ\text{C}$ (lit. mp. 127°C) (12).

A sample of $\text{O}_2^+[\text{AsF}_6]^-$ was obtained from Dr. Karl O. Christe of Rocketdyne. The compound was synthesized by UV photolysis of O_2 , F_2 , and AsF_5 in quartz. Magnetic field strengths of 7501, 9225, and 9625 G and a temperature range of ~2-124K were used in this study. Molar magnetic susceptibilities, χ_M , were corrected for diamagnetism and for $\text{Br}_2^+[\text{Sb}_3\text{F}_{16}]^-$ and $\text{I}_2^+[\text{Sb}_2\text{F}_{11}]^-$, slightly larger χ_{dia} values were used than reported previously (12). The magnetic moments of the Br_2^+ and I_2^+ compounds were corrected for temperature-independent paramagnetism ($\text{TIP} = 120$ and $68 \times 10^{-6} \text{ cm}^3 \text{ mol}^{-1}$ respectively, calculated as described in the text). The Curie-Weiss law in the form $\chi_M = C_m/T - \theta$ is used throughout.

5.3 Results and Discussion

The discussion of the magnetic behavior of the three cationic species will center around three aspects:

- (i) The selection of suitable compounds for this study in the light of previous magnetic susceptibility studies.

- (ii) The magnetic measurements on $O_2^+[AsF_6]^-$, $I_2^+[Sb_2F_{11}]^-$, and $Br_2^+[Sb_3F_{16}]^-$.
- (iii) An attempted interpretation of these results.

5.3.1 Synthesis

Magnetic measurements on a single compound in the current study require ~300-500 mg of high-purity sample for duplicate measurements when the vibrating sample magnetometer is used, while the Gouy measurements require between 1 and 2 g. All cations are extremely reactive and only I_2^+ is sufficiently stable in H_2SO_4 - SbF_5 solution (2,12), not undergoing disproportionation or further oxidation. This rules out purification by recrystallization as a general procedure for all the three salts. The limited thermal stability reported for all materials has so far precluded purification by sublimation. Hence, synthesis on the desired scale from pure starting materials, with little or no chance for side-reactions and facile product isolation, becomes the only route to the compounds of this study.

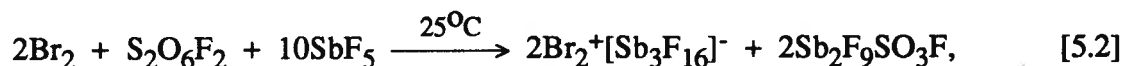
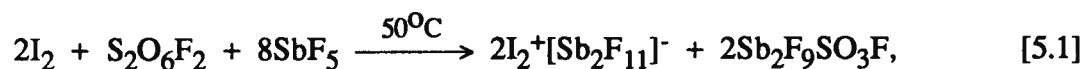
There appears to be no real choice among the Br_2^+ containing compounds, since structural and spectroscopic details on $Br_2^+[AsF_6]^-$ (14), the only other Br_2^+ salt, are not readily available. The original synthesis of $Br_2^+[Sb_3F_{16}]^-$ (4), from BrF_3 , Br_2 , and SbF_5 , did produce a sample suitable for a single-crystal X-ray diffraction study, but judging by the reported physical data, in particular the melting point and a magnetic moment of $\mu_{eff} \sim 1.6 \mu_B$, the product obtained from this method appears to be unsuited for this study.

A similar problem arises in the case of the I_2^+ species as well. The method used for the preparation of single crystals of $I_2^+[Sb_2F_{11}]^-$ (5), the oxidation of I_2 by SbF_5 in SO_2 , is not suited for the preparation on a larger scale, as is evident from the reported analytical data (5). The problem appears to be the quantitative separation of the by-products SbF_3 or $SbF_3 \cdot SbF_5$.

Formation of anions of the type $\text{Sb}_3\text{F}_{14}^-$ becomes a possibility and, in addition, a diamagnetic compound of the composition $\text{I}_4^{2+}[(\text{SbF}_6)(\text{Sb}_3\text{F}_{14})]^{2-}$ has recently been obtained by this synthetic route (15) with reaction conditions only slightly different.

Substitution of SO_2 by AsF_3 as solvent appears to lead to $\text{I}_2^+[\text{Sb}_2\text{F}_{11}]^-$ of a higher purity, but $\text{I}_2^+[\text{Sb}_3\text{F}_{16}]^-$ may form as a by-product as well (16). Any uncertainty in the molar mass of the product will limit the usefulness of a magnetic study. Other materials considered unsuitable for this study, as mentioned in Chapter 1, include the substances formulated as $(\text{SbF}_5)_2\text{I}$ (17) and the insufficiently characterized $\text{I}_2^+[\text{TaF}_6]^-$ (17).

An alternate synthetic route to both $\text{I}_2^+[\text{Sb}_2\text{F}_{11}]^-$ and $\text{Br}_2^+[\text{Sb}_3\text{F}_{16}]^-$, the oxidation of I_2 or Br_2 by stoichiometric amounts of bis(fluorosulfonyl) peroxide and subsequent solvolysis in an excess of SbF_5 according to:



has produced sufficiently large quantities of both compounds for a magnetic study between 298 and 80 K using the Gouy technique (12). With all starting materials readily purified and the volatile byproduct $\text{Sb}_2\text{F}_9\text{SO}_3\text{F}$ (18) easily separated from the product, this method, employed in the present study, was chosen as the most appropriate route to the synthesis of both $\text{I}_2^+[\text{Sb}_2\text{F}_{11}]^-$ and $\text{Br}_2^+[\text{Sb}_3\text{F}_{16}]^-$.

With well over a dozen different O_2^+ salts reported so far, this group of compounds appears to offer a wider choice, but here additional problems surface, which seem to have adversely affected earlier magnetic studies. Some of the reported compounds, $\text{O}_2^+[\text{PtF}_6]^-$ (1),

$O_2^+[PdF_6]^-$ (19), $O_2^+[RuF_6]^-$ (20), or $O_2^+[RhF_6]^-$ (20) have two different paramagnetic centers in the same molecular unit. The initial approach by Bartlett and Beaton (21) involving the subtraction of the molar susceptibilities of $NO^+[PtF_6]^-$ from those obtained for $O_2^+[PtF_6]^-$ has clearly allowed the identification of O_2^+ as a paramagnetic ion; however, magnetic exchange between O_2^+ and Pt(V) (d^5) is a plausible contributing factor for the observed decreasing trend of the magnetic moments attributed to O_2^+ with decreasing temperature. Magnetic ordering due to $O_2^+ \cdots Pt(V)$ exchange has subsequently been reported for this compound (23).

In addition, the high-pressure synthesis of dioxygenyl salts from O_2/F_2 mixtures and either metal fluorides or the metal itself (20,22,24) in metallic reactors has often resulted in materials with ferromagnetic contaminants (19,23). Although monel impurities can be recognized by the characteristic Curie temperature of 335 K and corrections have been attempted (23), such materials remain suspect in magnetic susceptibility studies. This is due to the possible existence of weak antiferromagnetic ordering in such materials contaminated with monel.

UV photolysis in quartz vessels (25) represents a more suitable synthetic method, but a number of O_2^+ salts such as $O_2^+[BF_4]^-$ (26) and $O_2^+[GeF_5]^-$ (27) prepared in this manner show rather limited thermal stability. Nevertheless, a magnetic study of $O_2^+[BF_4]^-$ between 293 and 85 K has been reported (28a), but only limited conclusions were reached.

For the products obtained from the reaction of O_2 and F_2 with SbF_5 by either UV photolysis or high-pressure synthesis, some structural ambiguity has been noticed. This problem arises since in these reactions, a variety of $[Sb_xF_{5x+1}]^-$ type anions may be formed to stabilize the O_2^+ species. Both $O_2^+[SbF_6]^-$ and $O_2^+[Sb_2F_{11}]^-$ are well characterized (6,24), and $O_2^+[Sb_3F_{16}]^-$ has been postulated as well (29). The problems caused by this structural

ambiguity are apparent from magnetic susceptibility studies on " $O_2^+[SbF_6]^-$ " reported in the Soviet literature (28).

To avoid similar problems $O_2^+[AsF_6]^-$ obtained by UV photolysis (25) was chosen for this study. An additional reason for this choice is the availability of structural information on this compound. A phase transition at 255 ± 3 K (30) results in a rhombohedral distortion of the cubic structure found at room temperature (6). This distortion is also evident from ESR studies down to 4 K (23,31). Conclusions reached regarding the ground state of O_2^+ in these ESR studies are useful in the interpretation of our low temperature susceptibility results.

There have been two previous magnetic susceptibility studies of $O_2^+[AsF_6]^-$ down to 4 K, with rather contradictory results. In a study by Grill et al. (32), no magnetic ordering of the O_2^+ cations is observed down to 4 K, while weak $O_2^+ \cdots O_2^+$ exchange is suggested in another study (23) based on the small Weiss constant obtained. However, these conclusions are rendered somewhat tenuous because of ferromagnetic monel impurities in the sample, requiring correction of the susceptibility data (23).

In all previous magnetic susceptibility studies of O_2^+ , the magnetic moments obtained over the whole temperature range are well below the spin-only value of $1.73 \mu_B$, and explanations have varied from suggesting "van-Vleck behavior" (22) in analogy to the behavior of NO (11), to invoking the presence of 17% of an unidentified, magnetically inert impurity in $O_2^+[AsF_6]^-$ (32). Likewise in some studies down to 80 K (28), μ_{eff} values for $O_2^+[SbF_6]^-$ appear to decrease with decreasing temperature, while for the structurally related $O_2^+[AsF_6]^-$, μ_{eff} is said to be invariant with temperature to 4 K (32). It is unclear why there are so many discrepancies and contradictions in previous studies. It is felt, however, that sample identity and purity play a major role here.

5.3.2 Magnetic Measurements

The results of our magnetic susceptibility studies on $\text{Br}_2^+[\text{Sb}_3\text{F}_{16}]^-$ below 80 K, together with results obtained in an earlier study (12) at higher temperatures, are summarized in Table 5.1. Both sets of χ_M and μ_{eff} data have been calculated using the same diamagnetic correction and TIP values (279 and $120 \times 10^{-6} \text{ cm}^3 \text{ mol}^{-1}$, respectively). The agreement between the data sets in the overlap region is excellent for this compound.

The data obtained here for $\text{I}_2^+[\text{Sb}_2\text{F}_{11}]^-$ and $\text{O}_2^+[\text{AsF}_6]^-$ are given in Table 5.2. Because of poor agreement in the 100 K region with the earlier Gouy data (12), the current study was extended with the vibrating sample magnetometer up to 124 K for the I_2^+ compound. Additionally, the measurements for the O_2^+ compound was also extended down to 2 K in the hope (not realized, unfortunately) of observing a maximum in the susceptibility data of this compound at very low temperatures. Pertinent structural and spectroscopic features of the three compounds studied and of the three cations, O_2^+ , Br_2^+ , and I_2^+ , either as solvated or gaseous species, are summarized in Table 5.3.

The contrast in the magnetic properties of the three paramagnetic cationic species studied in this work is clearly evident from the plots of magnetic moment versus temperature shown in Figure 5.1. Two of the compounds, $\text{O}_2^+[\text{AsF}_6]^-$ and $\text{Br}_2^+[\text{Sb}_3\text{F}_{16}]^-$, exhibit Curie-Weiss behavior over a wide temperature range, as is seen by the plots of $1/\chi_M$ vs. T given in Figure 5.2.

5.3.3 $\text{Br}_2^+[\text{Sb}_3\text{F}_{16}]^-$

The magnetic behavior of $\text{Br}_2^+[\text{Sb}_3\text{F}_{16}]^-$ appears to be rather straightforward and will be discussed in detail first. The $1/\chi_M$ versus T plot of this compound indicates Curie-Weiss

Table 5.1: Magnetic Data of Br₂⁺[Sb₃F₁₆]⁻

Temperature ^a (K)	$\chi_M \times 10^6$ (cm ³ mol ⁻¹)	$\mu_{\text{eff}} (\mu_B)^b$
297	1870	2.04
275	2010	2.04
255	2160	2.04
235	2330	2.03
213	2530	2.03
193	2780	2.03
172	3070	2.02
151	3430	2.00
131	3900	1.99
116	4500	2.02
104	4910	2.00
80.0	6130	1.96
81.1	6070	1.96
73.5	6720	1.97
65.7	7440	1.96
55.0	8870	1.96
43.7	10900	1.94
31.4	15000	1.93
21.4	21900	1.93
10.2	45700	1.93
9.88	45900	1.90
4.20	111300	1.93

^a First twelve data points from Ref. 12.

^b Corrected for TIP using $\mu_{\text{eff}} = 2.828 ((\chi_M - \text{TIP})T)^{1/2}$ with $\text{TIP} = 120 \times 10^{-6} \text{ cm}^3 \text{ mol}^{-1}$.

Table 5.2: Magnetic Data of $I_2^+[Sb_2F_{11}]^-$ and $O_2^+[AsF_6]^-$

$I_2^+[Sb_2F_{11}]^-$			$O_2^+[AsF_6]^-$		
Temperature (K)	$\chi_M \times 10^6$ ($cm^3 mol^{-1}$)	μ_{eff}^a (μ_B)	Temperature (K)	$\chi_M \times 10^6$ ($cm^3 mol^{-1}$)	μ_{eff}^b (μ_B)
124.1	3770	1.92	80.1	4170	1.63
117.5	3860	1.89	76.3	4410	1.64
106.5	4290	1.90	72.7	4650	1.64
98.6	4510	1.87	68.5	4950	1.65
90.9	4730	1.84	64.3	5480	1.65
84.3	4900	1.81	59.2	5600	1.63
81.2	5030	1.80	53.2	6170	1.62
76.8	5120	1.76	46.5	6990	1.61
71.8	5300	1.73	42.9	7520	1.61
66.6	5380	1.68	39.1	8200	1.60
63.5	5470	1.66	30.3	10530	1.60
58.4	5560	1.60	25.3	12430	1.59
51.9	5560	1.51	20.5	15100	1.57
44.9	5090	1.34	15.3	19700	1.55
36.9	4910	1.20	10.1	28800	1.52
31.6	4700	1.08	7.12	37500	1.46
27.4	4490	0.98	5.92	44500	1.45
27.1	4520	0.98	5.28	48300	1.43
21.8	4300	0.86	4.78	52200	1.41
11.6	4270	0.62	4.62	52700	1.40
8.64	4290	0.54	4.40	54800	1.39
6.30	4490	0.47	4.04	59400	1.39
4.54	4790	0.41	2.70	70400	1.23
			2.40	75500	1.20
			2.10	81300	1.17

^a Corrected as in Table 3.1 with TIP = $68 \times 10^{-6} cm^3 mol^{-1}$

^b Not corrected for TIP

Table 5.3: Structural and Spectroscopic Information on $O_2^+[AsF_6]^-$, $I_2^+[Sb_2F_{11}]^-$, $Br_2^+[Sb_3F_{16}]^-$, and the Corresponding Ions O_2^+ , Br_2^+ , and I_2^+

Data, X Denotes O, Br, or I	$O_2^+[AsF_6]^-$ or $O_2^+(g)$	$Br_2^+[Sb_3F_{16}]^-$ or $Br_2^+(g)$	$I_2^+[Sb_2F_{11}]^-$ or $I_2^+(g)$
Shortest X...X non-bonding interaction [\AA]	4 to 4.05 ^a (ref. 28b,30)	6.445 (ref. 12, 4b)	4.29 (ref. 12, 6)
van der Waals Radii for X [\AA] (ref. 34)	1.52	1.85	1.98
Ground state of $X_2^+(g)$	$2\Pi_{1/2g}$	$2\Pi_{3/2g}$	$2\Pi_{3/2g}$
Spin orbit coupling const. [cm^{-1}] for $X_2^+(g)$	185 (ref. 52)	2820 ± 40 (ref. 53)	5125 ± 40 (ref. 53)
$\Delta E(2\Pi_{1/2g} - 2\Pi_{3/2g})$	195 (ref. 10)	3141 ± 160 (ref. 55)	5081 ± 60 (ref. 55)
As above for $X_2^+(solv)$ [cm^{-1}]	---	2890 (ref. 12)	5190 (ref. 2)
Diamagnetic Correction (ref. 56) [$10^{-6} \text{ cm}^3 \text{ mol}^{-1}$]	79	279	238

^a Estimated from powder diffraction data

Figure 5.1: Magnetic Moment vs. Temperature of $\text{Br}_2^+[\text{Sb}_3\text{F}_{16}]^-$, $\text{I}_2^+[\text{Sb}_2\text{F}_{11}]^-$, and $\text{O}_2^+[\text{AsF}_6]^-$

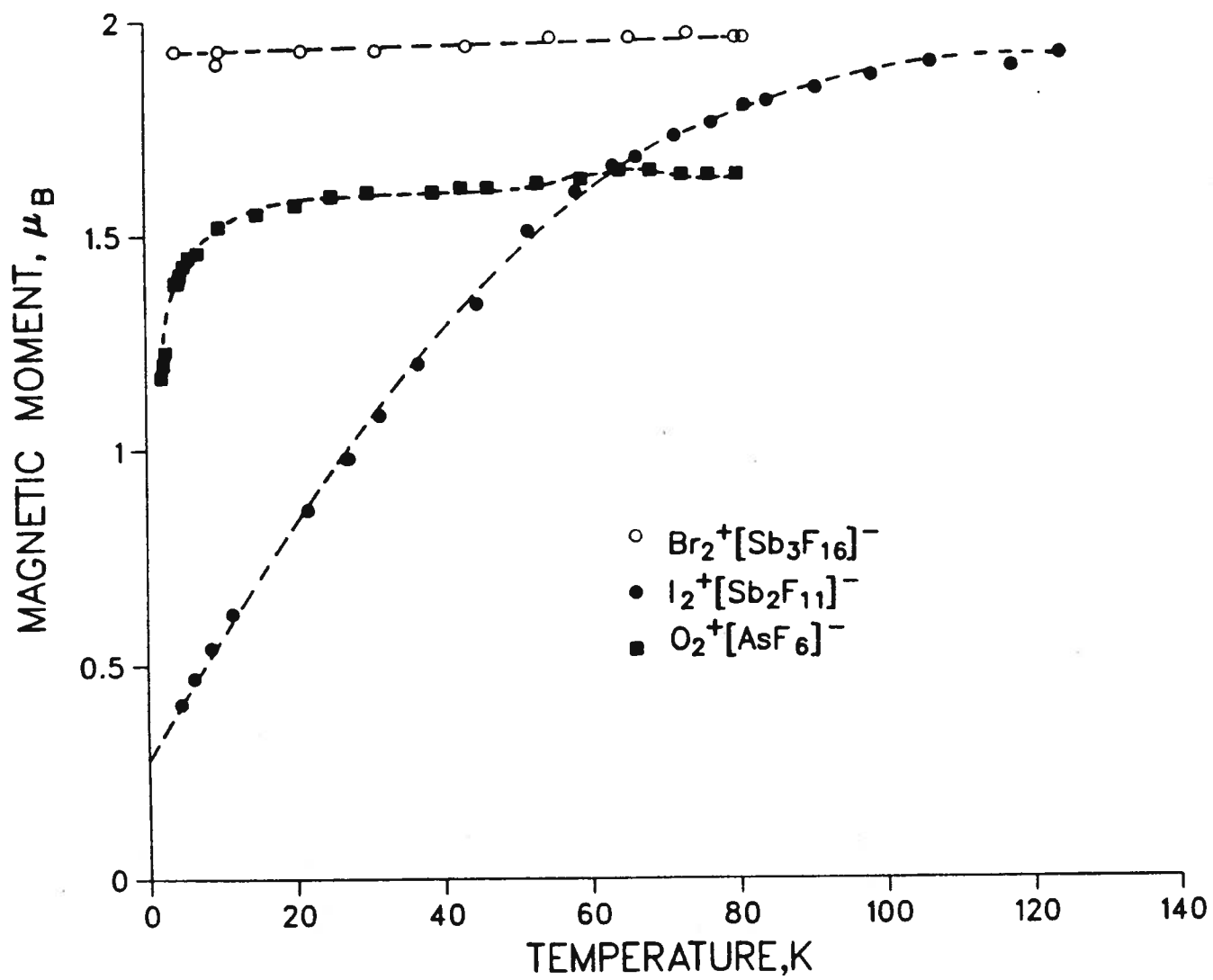
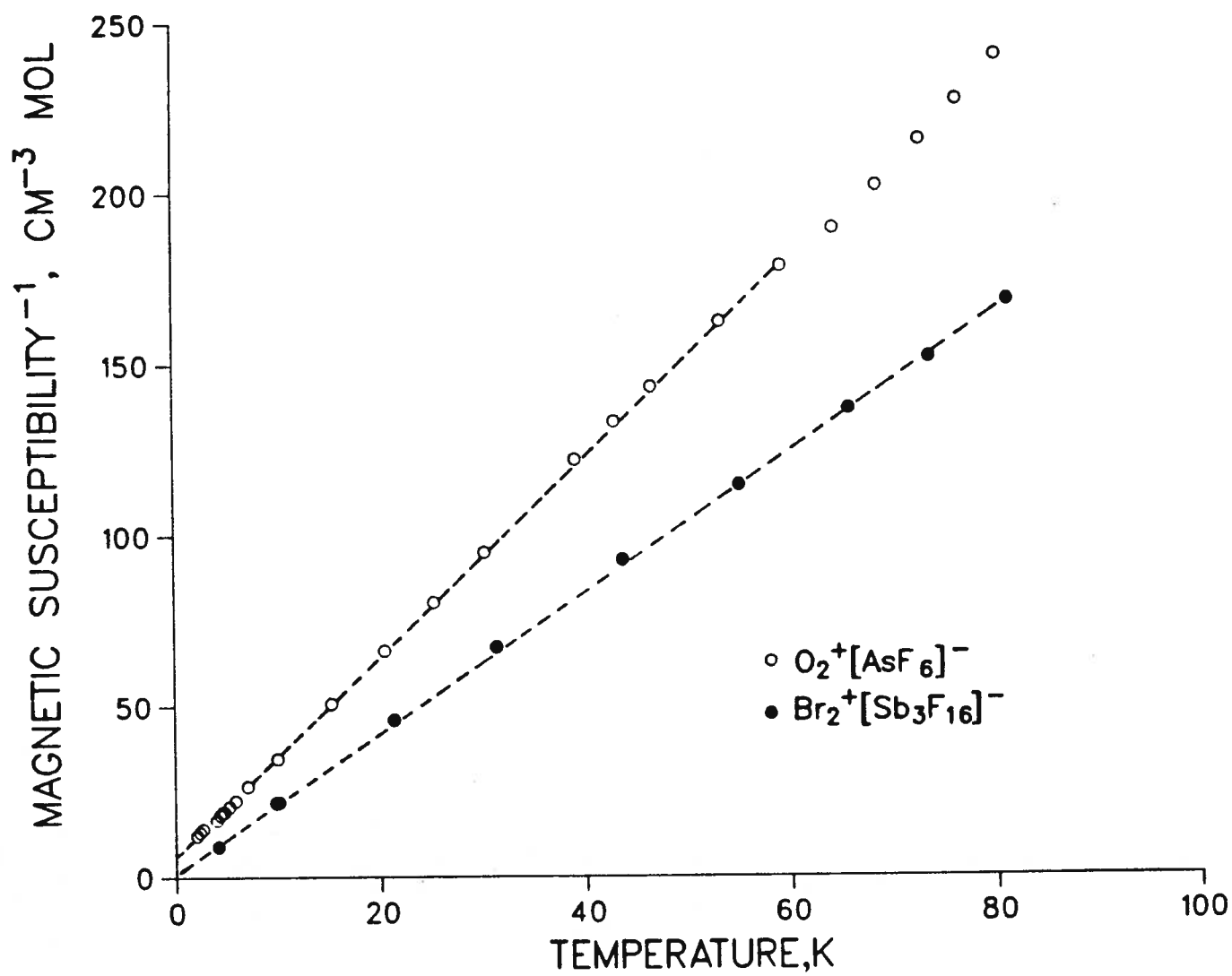


Figure 5.2: Inverse Susceptibility vs. Temperature of $O_2^+[AsF_6]^-$ and $Br_2^+[Sb_3F_{16}]^-$

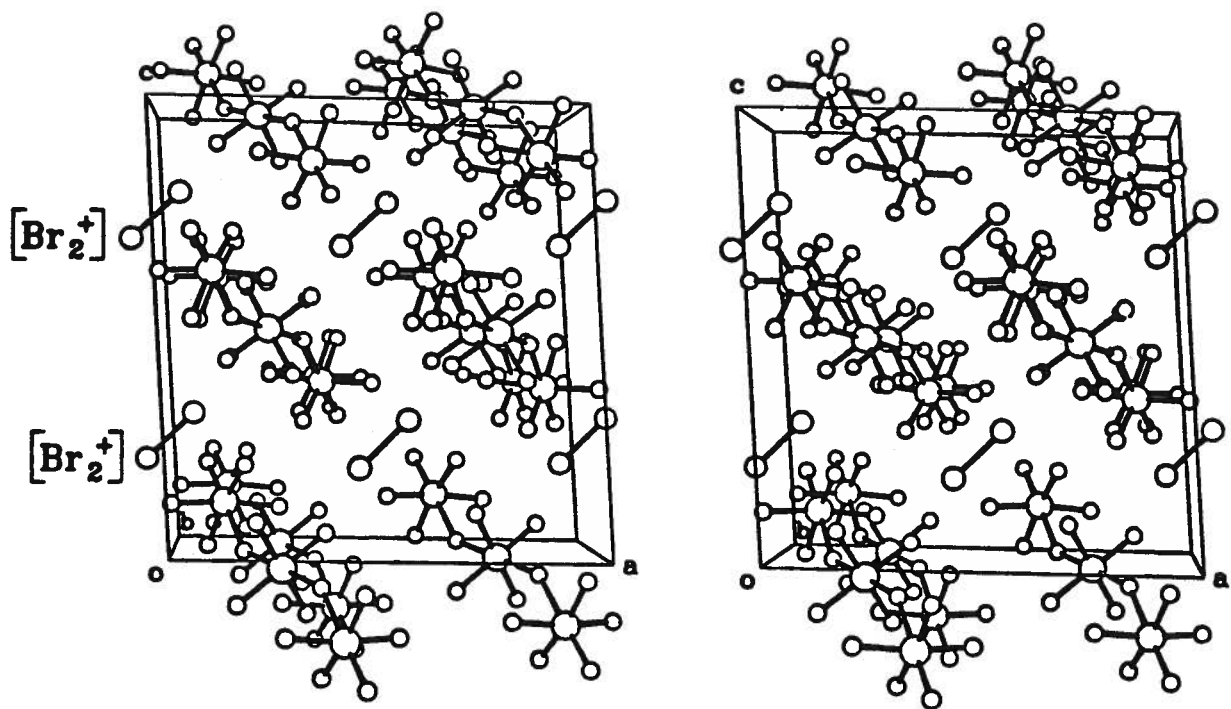


behavior over the temperature range from 80-4 K ($C_m = 0.49 \pm 0.01 \text{ cm}^3 \text{ mol}^{-1} \text{ K}$, $\theta = -0.74 \pm 0.01 \text{ K}$). The magnetic moments (even when corrected for TIP) decrease slightly with temperature. A TIP correction had been arbitrarily assigned in the earlier work (12) in order to bring the magnetic moments in the high-temperature region into agreement with the value of $2.0 \mu_B$ predicted by theory (11) for a species with a $^2\Pi_{3/2g}$ ground state and no thermally accessible excited state (see Table 5.3).

The correction for TIP in the present study was taken as $4N\beta^2/3\Delta E$ (33), where ΔE is the energy separation between the ground $^2\Pi_{3/2g}$ and the next excited $^2\Pi_{1/2g}$ state with which it is mixing. The ΔE value for Br_2^+ is the spin-orbit coupling constant, λ , and for this species, estimated at 2890 cm^{-1} for the solvated ion (Table 5.3), and using this value a TIP of $120 \times 10^{-6} \text{ cm}^3 \text{ mol}^{-1}$ is calculated. Magnetic moments calculated using this TIP correction are within $\pm 2\%$ of the theoretical value of $2.0 \mu_B$ over the wide temperature range of 297-55 K (Table 5.1).

The cause of the very small drop in the moment, particularly at very low temperatures (corresponding to the effect of a Curie-Weiss rather than Curie law behavior) is not certain. Although the shortest non-bonding $\text{Br}\cdots\text{Br}$ contact at 6.445 \AA (4b) is too long to invoke significant direct magnetic interaction (Figure 5.3), $\text{F}\cdots\text{Br}$ contacts ranging from $2.86\text{-}3.34 \text{ \AA}$, comparable to or shorter than the sum of the van der Waals radii of 3.32 \AA (34), suggest the possibility of very weak exchange via bridging anions. However, the effect is very minor and it is reasonable to conclude that in $\text{Br}_2^+[\text{Sb}_3\text{F}_{16}]^-$ the Br_2^+ cation is in a thermally isolated $^2\Pi_{3/2g}$ ground state and there is no conclusive evidence for any magnetic exchange between paramagnetic centers down to 4.2 K. In this regard $\text{Br}_2^+[\text{Sb}_3\text{F}_{16}]^-$ is somewhat unique, since for all other paramagnetic main group species, including O_2^- (35), the recently studied ozonides, KO_3 , RbO_3 , and CsO_3 (36), and solid O_2 (37), as well as I_2^+ and O_2^+ (discussed below), at least weak antiferromagnetic coupling has been suggested.

Figure 5.3: Crystal Structure of $\text{Br}_2^+[\text{Sb}_3\text{F}_{16}]^-$ (redrawn using data from ref. 4b)



$$r_{\text{Br}_2^+ - \text{Br}_2^+} = 6.445 \text{ \AA}$$

$\text{Br}_2^+\text{Sb}_3\text{F}_{16}^-$	
	<i>Monoclinic</i>
a	$13.58 \pm 0.02 \text{ \AA}$
b	$7.71 \pm 0.01 \text{ \AA}$
c	$14.33 \pm 0.02 \text{ \AA}$
β	$93.7 \pm 0.2^\circ$
V	1497 \AA^3
D _{calc}	3.68 g cm^{-3}
z	4
X-X, bond length	2.15 \text{ \AA}
X ... F, closest contact	2.86 \text{ \AA}
r _{Sb-F(terminal)}	1.83 \text{ \AA}
r _{Sb-F(bridging)}	2.10; 1.97 \text{ \AA}
R = r _{bridg} /r _{ter}	1.11

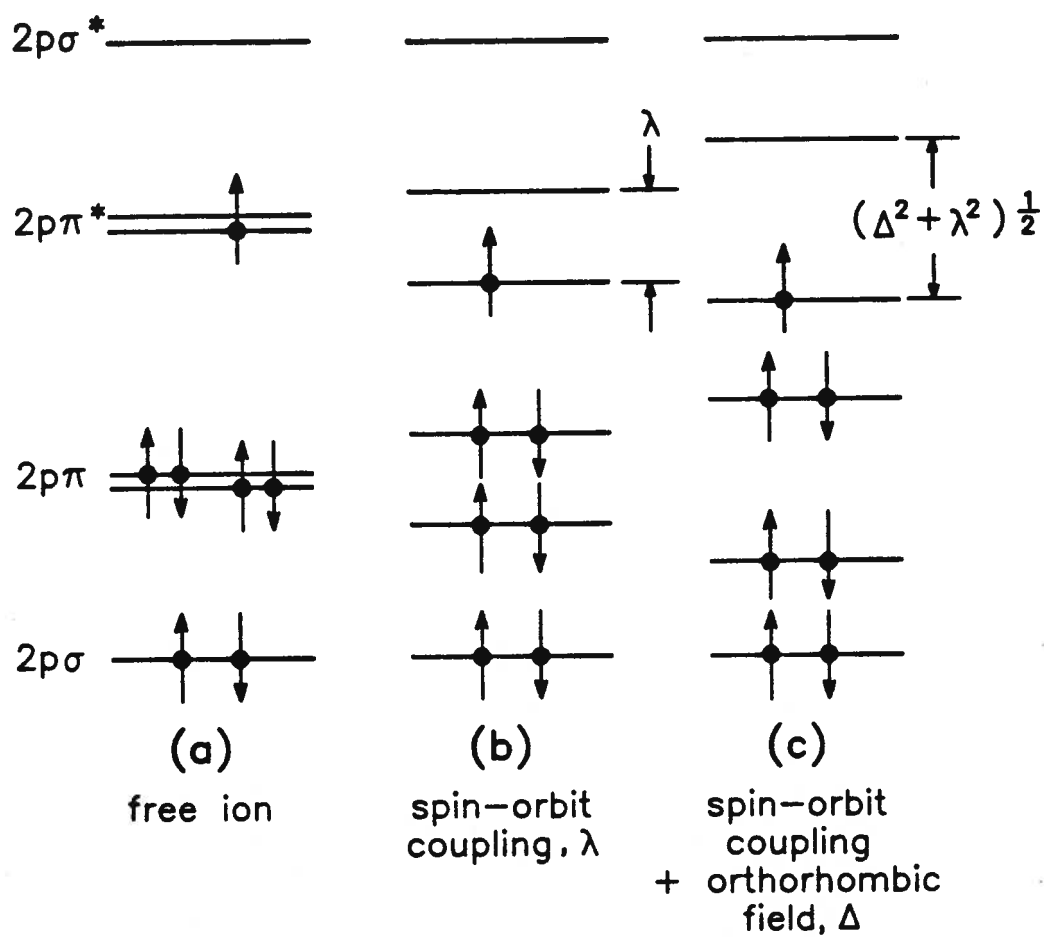
5.3.4 $O_2^+[AsF_6]^-$

The magnetic properties of $O_2^+[AsF_6]^-$ are similar to those of the Br_2^+ compound in that Curie-Weiss behavior is followed (Figure 5.2), although over a more limited temperature range of 60-2 K. Here the Curie constant C_m , is significantly smaller and the absolute value of the Weiss constant, $|\theta|$, greater ($C_m = 0.34 \pm 0.01 \text{ cm}^3 \text{ mol}^{-1} \text{ K}$, $\theta = -1.90 \pm 0.01 \text{ K}$). Consequently, the effective magnetic moments are significantly smaller for $O_2^+[AsF_6]^-$ and show a stronger temperature dependence, particularly in the low temperature region (Figure 5.1). A slight departure from linear behavior in the Curie-Weiss plot is noted (Figure 5.2) above 60 K. This may be significant, as it coincides with the observed broadening of the ESR line (23), possibly caused by tumbling motions of O_2^+ in the crystal lattice.

These findings are at variance with a previous report by Grill et al. (32), who observed Curie-Weiss behavior for O_2^+ with a positive θ value (according to our formulation of the law) of 0.7 K. The results of our study are in reasonable agreement with those of DiSalvo et al. (23), who obtained $C_m = 0.309 \text{ cm}^3 \text{ mol}^{-1} \text{ K}$ and $\theta = -0.8 \text{ K}$ (sign changed from (23) to conform to our formulation of the law), although it must be taken into consideration that a temperature-independent paramagnetism contribution as well as corrections for ferromagnetic impurities were made in the earlier work.

In this work the susceptibilities of O_2^+ were not corrected for TIP. A crystal-field analysis of ESR data for $O_2^+[AsF_6]^-$ suggests the separation between the ground and first electronic excited state to be 1480 cm^{-1} (Figure 5.4), caused by both spin-orbit coupling and crystal-field splitting due to O_2^+ being in a site of orthorhombic or lower symmetry (31). In this case one is clearly not dealing with pure $^2\Pi_{1/2g}$ and $^2\Pi_{3/2g}$ states and it is not clear what the TIP correction should be. In any event, the large separation between the states means such a correction will be small, and hence ignoring it should not significantly affect the conclusions.

Figure 5.4: Energy Level Diagram of the Dioxygenyl Ion with the σ and π -Bonding 2p Orbitals (Ref. 31)



When considering the magnitude of the magnetic moment, it is observed that for $\text{O}_2^+[\text{AsF}_6]^-$ the measured magnetic moments in the range of $1.6 \mu_B$ at the higher temperature region agree well with values predicted using the average g values, g_{av} , of 1.89 (23) and 1.905 (31) obtained by ESR. Using the equation for the magnetic moment of a single electron $\mu_B = g[S(S+1)]^{1/2}$, values of 1.64 and $1.65 \mu_B$ are obtained respectively for the above two g_{av} data.

As described by Goldberg et al. (31), both crystal-field splitting and spin-orbit coupling contribute to the ground state in $\text{O}_2^+[\text{AsF}_6]^-$. In a pure ${}^2\Pi_{1/2g}$ ground state the spin and orbital contributions cancel, and there is no first-order paramagnetism associated with this state (33). If this were the case for O_2^+ with negligible thermal population of excited states, only temperature-independent paramagnetism would be present. This is clearly not the case here. The crystal-field interactions have the effect of quenching the orbital contribution, although not completely, resulting in a μ_{eff} value slightly below the spin-only value. Quite the opposite effect is observed for the alkali metal superoxides, MO_2 with $M = \text{Na}, \text{K}, \text{Rb}, \text{Cs}$ (35). Here the ground state is ${}^2\Pi_{3/2g}$ and in all instances the μ_{eff} values are well above the spin-only value of $1.73 \mu_B$, as was found for $\text{I}_2^+[\text{Sb}_2\text{F}_{11}]^-$ and $\text{Br}_2^+[\text{Sb}_3\text{F}_{16}]^-$ (12).

The decrease in μ_{eff} values with decreasing temperature for $\text{O}_2^+[\text{AsF}_6]^-$, particularly significant below ~ 20 K, requires further consideration. With a splitting of 1480 cm^{-1} separating the ground state from the nearest excited state, the variation in the effective magnetic moment with temperature observed here cannot be accounted for by the sort of van Vleck behavior observed for gaseous NO (33). The existence of antiferromagnetic exchange between paramagnetic centers must be considered as a possibility.

The limited structural information available on $\text{O}_2^+[\text{AsF}_6]^-$ (25,31,38) derived from powder diffraction data does not permit an accurate determination of the shortest O...O non-bonding contact distance. Estimates of 4.00 (30b) and 4.05 \AA (32) respectively, which were

used to argue against O··O interaction, are simply half the unit cell length $a\sqrt{2}$ for the room-temperature phase (25,31,38). The distance $a\sqrt{2}$ describes the separation between the mass centers of the O_2^+ cations, which are assumed to be in the most probable sites. The low-temperature phase, which is directly relevant to this study, has a powder diffraction pattern that has not been successfully indexed (30); hence the conclusion (32) that there can be no antiferromagnetic exchange in $O_2^+[AsF_6]^-$ because the O_2^+ ions are too far apart is most likely invalid.

For $O_2[Mn_2F_9]$, where a single crystal X-ray diffraction study at room temperature and at -150°C is reported (39), non-bonding O··O contacts of 3.86 \AA are detected at -150°C with values of 3.98 \AA observed at room temperature. However, the anion is described as a double chain of cis-bridged MnF_6^- octahedra with O_2^+ cations between the anion layers, and the resulting structure is not comparable with that of $O_2^+[AsF_6]^-$. Moreover, susceptibility studies on this material would not be suitable for the purposes of this work as the magnetism would be complicated by the presence of Mn^{4+} , a second paramagnetic center.

With the sum of the van der Waals radius 3.02 \AA for two oxygen atoms, one would reasonably expect distances of $3.2\text{-}3.3 \text{ \AA}$ as the limit for significant direct antiferromagnetic exchange. This estimation is corroborated by recent reports on the structures of the alkali metal ozonides KO_3 (40,41,42), RbO_3 (40,41) and CsO_3 (43), all of which exhibit significant antiferromagnetism (34) than $O_2^+[AsF_6]^-$, and where O··O non-bonding contacts range between $3.01\text{-}3.15 \text{ \AA}$ for KO_3 and $3.01\text{-}3.30 \text{ \AA}$ for RbO_3 , respectively. For CsO_3 , where antiferromagnetic exchange is rather weak (36), only powder data are reported (43) and indexed, suggesting CsO_3 to be iso-structural with RbO_3 . The unit-cell dimensions indicate slightly longer O··O contacts for this compound (42). Contact distances of the order of those observed in the ozonides could be present in $O_2^+[AsF_6]^-$ and this could account for its observed magnetic properties.

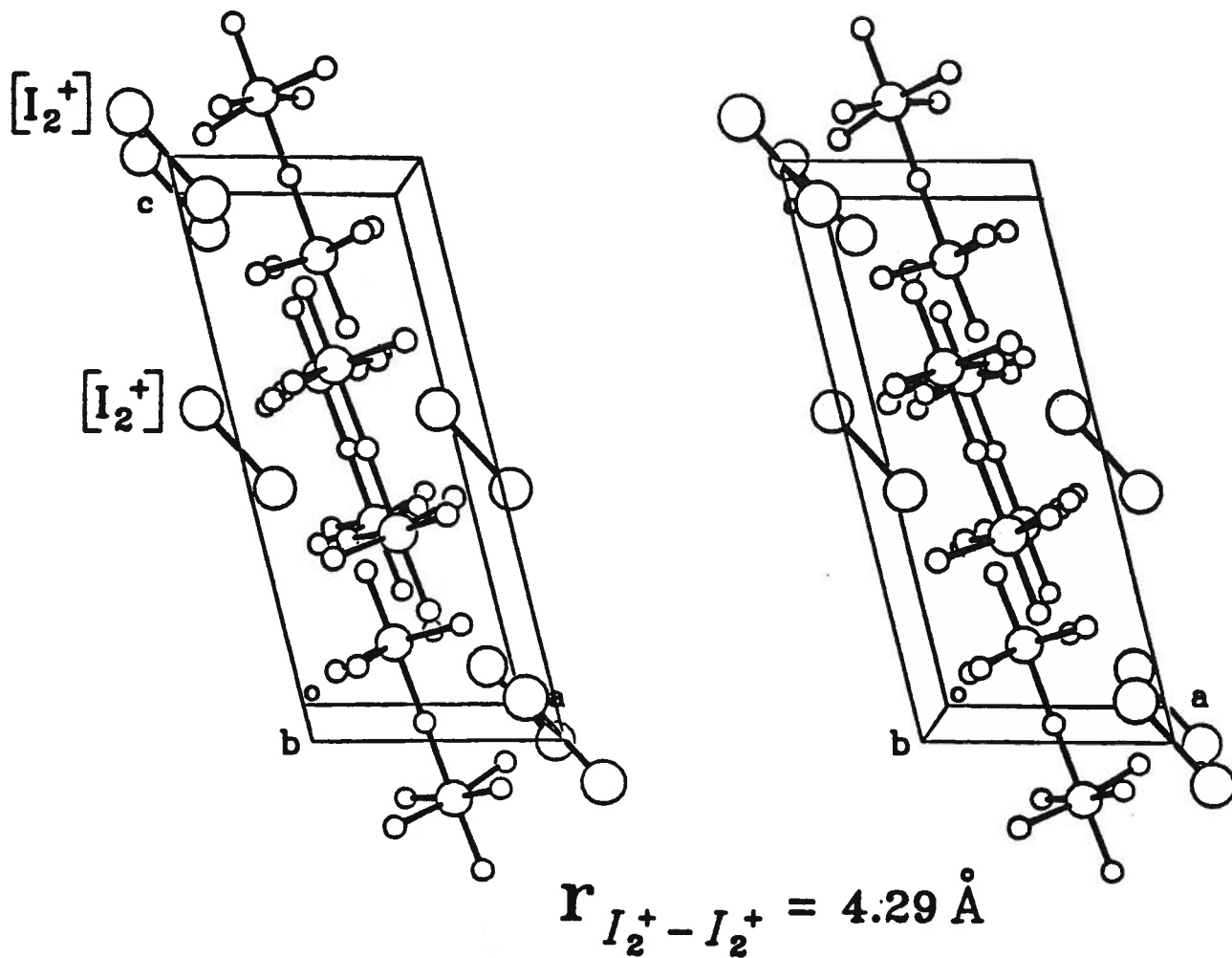
5.3.5 $I_2^+[Sb_2F_{11}]^-$

In a previous report from our group on $I_2^+[Sb_2F_{11}]^-$ it was shown that a TIP correction in excess of that assumed for the Br_2^+ compound was required to bring the experimental room-temperature moment into agreement with the value of $2.0 \mu_B$ predicted by theory (12). In addition, it was suggested in the earlier work that the observed decrease in the magnetic moment on decreasing the temperature to 80 K may arise from antiferromagnetic exchange between contiguous I_2^+ cations in the crystal lattice, where the shortest I...I non-bonding contact distance (5) is found to be 4.29 \AA (Figure 5.5). Magnetic measurements on $I_2^+[Sb_2F_{11}]^-$ down to 4.2 K reported here confirm the presence of antiferromagnetic coupling. The susceptibility rises to a maximum at ~ 54 K, then decreases on further cooling (Figure 5.6). The rise again in susceptibility on cooling below ~ 10 K is probably due to trace amounts of paramagnetic structural impurity, as is often observed in antiferromagnetically coupled systems (13).

In view of the clear evidence that this system is exchange-coupled, there is no justification for arbitrarily reducing the room-temperature moment to $2.00 \mu_B$ with an appropriate TIP correction, as was done previously (12). Indeed, in view of the fact that the $^2\Pi_{3/2g} - ^2\Pi_{1/2g}$ separation is significantly greater in the I_2^+ compound compared to Br_2^+ (see Table 5.3), any TIP would be expected to be smaller in the former. TIP for I_2^+ (calculated as described above for Br_2^+) is $68 \times 10^{-6} \text{ cm}^3 \text{ mol}^{-1}$ and magnetic moments calculated employing this value are given in Table 5.2. The decrease in μ_{eff} with decreasing temperature is consistent with antiferromagnetic coupling; interestingly though, the absolute values in the high-temperature region are in excess of the theoretically predicted value of $2.0 \mu_B$ (11).

An attempt is made here to analyze the magnetic susceptibility data of I_2^+ (including the data from 295-130 K from ref. (12)) according to three theoretical models for antiferromagnetic exchange in one-dimensional systems. For a magnetically concentrated system with spins S_i

Figure 5.5: Crystal Structure of $I_2^+[Sb_2F_{11}]^-$ (redrawn using data from ref. 5)

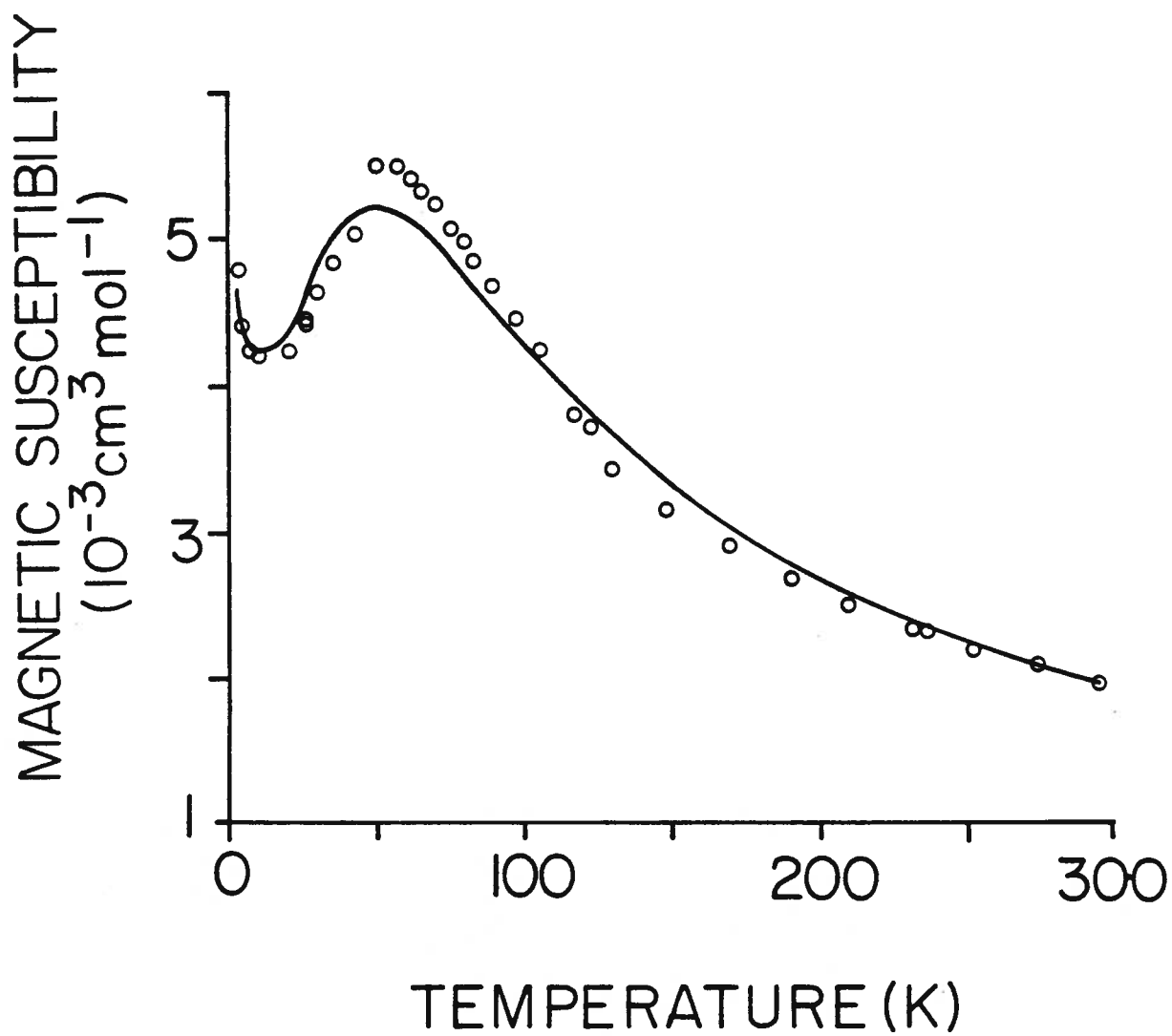


$I_2^+Sb_2F_{11}^-$	
<i>Monoclinic</i>	
a	13.283(5) Å
b	8.314(3) Å
c	5.571(2) Å
β	103.75(2)°
V	597.5 Å ³
D _{calc}	3.92 g cm ⁻³
z	2
X-X, bond length	2.557(4) Å
X...F, closest contact	2.89 Å
r _{Sb-F} (terminal)	1.85 Å
r _{Sb-F} (bridging)	2.00 Å
R = r _{bridg} /r _{ter}	1.08

Figure 5.6: Magnetic Susceptibility vs. Temperature of $I_2^+[Sb_2F_{11}]^-$.

(Circles are experimental data; Solid line is the best fit to the Ising

$S' = 1/2$ model)



and S_j , the nearest neighbor exchange coupling is given by the Hamiltonian H_{ex} (44):

$$H_{\text{ex}} = -2J \sum_{i \leq j}^N \alpha S_i^z S_j^z + \beta S_i^x S_j^x + \gamma S_i^y S_j^y \quad [5.3]$$

where S_i^x , S_i^y and S_i^z are the components of the spin vector S_i of the i th atom, N the number of magnetic atoms and J , the exchange coupling constant, which can either have a positive or negative value, i.e. ferromagnetic or antiferromagnetic interaction. The values of α , β and γ in equation (4.3) define the nature of the exchange coupling. When $\alpha = \beta = \gamma = 1$, the isotropic Heisenberg exchange Hamiltonian results. In the extreme situation where $\alpha = 1$ and $\beta = \gamma = 0$, the Ising model is described (anisotropic coupling).

The isotropic Heisenberg Hamiltonian has been extensively examined but no exact solutions are presently known. However, results of many approximate methods exist (45). For the Ising model Hamiltonian, closed-form solutions are available for both the parallel and perpendicular magnetic susceptibilities of the $S = 1/2$ system (46).

Considering the ${}^2\Pi_{3/2g}$ ground state of I_2^+ as having an effective spin $S' = 3/2$ (47), our data were fitted to an isotropic Heisenberg model developed by Weng (48), employing the following polynomial expression and appropriate coefficients given by Hiller et al. (49) for the molar susceptibility:

$$\chi_M = \frac{Ng^2\beta^2}{kT} [A + Bx^2][1 + Cx + Dx^3]^{-1} \quad [5.4]$$

where $x = kT/J$.

In the above equation (and equations [5.6] and [5.7], see below) g is the Lande splitting factor, β the Bohr Magneton, N the number of spins in the lattice, k Boltzmann constant, T the temperature and J the exchange coupling constant. The values of the coefficients for $S=1/2$ and $S=3/2$ are as follows:

S	A	B	C	D
1/2	0.2500	0.18297	1.5467	3.4443
3/2	1.2500	17.041	6.7360	238.47

Allowance was made for paramagnetic impurity by modelling it as a Curie paramagnet with a g value equal to that of the bulk sample, i.e. $\chi_{\text{para}} = Ng^2\beta^2S(S+1)/3kT$. Expressing χ_M from equation [5.4] as χ_{chain} , the susceptibility expression including paramagnetic impurity is $\chi = [1-P]\chi_{\text{chain}} + P\chi_{\text{para}}$. The experimental data were fitted to this expression using g , J , and P as fitting parameters. The best fit was considered to be that set of fitting parameters which gave the minimum value of the function F (50):

$$F = \left[\frac{1}{n} \sum_i^n (\chi_{\text{calcd}}^i - \chi_{\text{obs}}^i / \chi_{\text{obs}}^i)^2 \right]^{1/2} \quad [5.5]$$

where n is the number of data points, and χ_{calcd}^i and χ_{obs}^i are the calculated and observed susceptibilities, respectively. For $S' = 3/2$, the best fit of the data for I_2^+ was with $J = -7.2 \text{ cm}^{-1}$, the effective $g = 1.23$, $P = 0.0035$, and $F = 0.0560$. In view of the molecular anisotropy of the magnetic species, the anisotropic Ising model should be examined as well. Unfortunately, while an exact solution exists for the parallel susceptibility of the Ising $S = 3/2$ case (51), there is no solution for the perpendicular case and hence one cannot analyze the powder data according to

this model.

An alternative approach to the data analysis is to consider the possibility that the four-fold degeneracy of the ground ${}^2\Pi_{3/2g}$ state has been lifted by second- or higher-order interactions with excited states, leaving a thermally isolated Kramer's doublet as the only significantly thermally populated ground level. In this case one needs to consider an effective spin, $S' = 1/2$, and here both Heisenberg and Ising models are available. Employing again the Weng model and equation [5.4], a best fit between theory and experiment was obtained with $J = -28 \text{ cm}^{-1}$, effective $g = 2.72$, $P = 0.0061$, and $F = 0.0487$.

As mentioned earlier, exact solutions for both the parallel and perpendicular susceptibilities for the anisotropic Ising $S' = 1/2$ case are available, and the data were analyzed using the equations of Fisher (46):

$$\chi_{\parallel} = \left(\frac{Ng^2\beta^2}{4kT} \right) \exp. \left(\frac{2|J|}{kT} \right) \quad [5.6]$$

$$\chi_{\perp} = \left(\frac{Ng^2\beta^2}{8|J|} \right) \left[\tanh \left(\frac{|J|}{kT} \right) + \frac{|J|}{kT} \operatorname{Sech}^2 \left(\frac{|J|}{kT} \right) \right] \quad [5.7]$$

Assuming $\chi_{\text{powder}} = 1/3\chi_{\parallel} + 2/3\chi_{\perp}$, the best fit was generated with $J = -38 \text{ cm}^{-1}$, effective $g = 2.61$, $P = 0.0054$, and $F = 0.0368$. The agreement between experiment and theory for this Ising $S' = 1/2$ case is illustrated in Figure 5.6 where the solid line is calculated from theory. The agreement between experiment and theory for the other two models is visually very similar to that shown in Figure 5.6, although in both cases the agreement is slightly poorer, as is indicated by the higher F values. In all three cases, as the temperature is lowered the experimental susceptibilities rise more steeply to a higher maximum value and then decrease more steeply

when compared to the calculated susceptibilities.

The analysis of the magnetic susceptibility data clearly indicates that in the lattice of $I_2^+[Sb_2F_{11}]^-$ contiguous I_2^+ ions are relatively strongly antiferromagnetically coupled, although it does not provide a clear answer to the question of whether or not the thermally occupied ground state at low temperatures is a pure $^2\Pi_{3/2g}$ state. Measurements of magnetic susceptibilities at low temperatures on suitably oriented single crystals to obtain $\chi_{||}$ values (47) would be informative, but would require the synthesis of relatively large crystals of the material.

It is important to note that the antiferromagnetic coupling observed here for $I_2^+[Sb_2F_{11}]^-$ is distinctly different from the dimerization process suggested for $I_2^+_{(solv)}$ in HSO_3F (2), just as the solid-state structure of $I_2^+[Sb_2F_{11}]^-$ differs from the structures of $I_4^{2+}[AsF_6^-]_2$ and $I_4^{2+}[(SbF_6)(Sb_3F_{14})]^{2-}$ (15) where square planar, diamagnetic I_4^{2+} cations are found.

5.4 Conclusion

Magnetic susceptibility measurements to 4.2 K are reported for $O_2^+[AsF_6^-]$, $Br_2^+[Sb_3F_{16}]^-$, and $I_2^+[Sb_2F_{11}]^-$. The data are interpreted utilizing previous results from photoelectron spectroscopy of the gaseous cations, known crystal structures, magnetic studies on the superoxide ion and the ozonide ion, and in the case of $O_2^+[AsF_6^-]$, previous ESR studies.

The magnetic properties of the three materials are quite different. $Br_2^+[Sb_3F_{16}]^-$ obeys Curie-Weiss law between 80 and 4 K: $C_m = 0.49 \pm 0.01 \text{ cm}^3 \text{ mol}^{-1} \text{ K}$ and $\theta = -0.74 \pm 0.01 \text{ K}$ (with $TIP = 120 \times 10^{-6} \text{ cm}^3 \text{ mol}^{-1}$). The magnetic moment decreases slightly from $2.04 \mu_B$ at room temperature to $1.93 \mu_B$ at 4 K. $I_2^+[Sb_2F_{11}]^-$ exhibits relatively strong antiferromagnetic coupling with a maximum in χ_M observed at 54 K. the magnetic moment (corrected for a TIP contribution of $68 \times 10^{-6} \text{ cm}^3 \text{ mol}^{-1}$) decreases from $1.92 \mu_B$ at 124 K to $0.41 \mu_B$ at 4 K.

Experimental susceptibilities for this compound over the range 300-4 K have been compared to values calculated using three different theoretical models for extended chains of antiferromagnetically coupled paramagnetic compounds.

The major difference in magnetic behavior between Br_2^+ and I_2^+ is due to structural difference between $\text{Br}_2^+[\text{Sb}_3\text{F}_{16}]^-$ and $\text{I}_2^+[\text{Sb}_2\text{F}_{11}]^-$. Magnetic exchange through contiguous I_2^+ ions is suggested by the crystal structure of $\text{I}_2^+[\text{Sb}_2\text{F}_{11}]^-$. The shortest I...I non-bonding contact is 4.29 Å, comparable to the sum of the van der Waals radii of 3.96 Å. In $\text{Br}_2^+[\text{Sb}_3\text{F}_{16}]^-$ the shortest Br...Br contact is 6.445 Å, about 2.8 Å longer than the van der Waals distance, and direct magnetic exchange becomes improbable as discussed above.

$\text{O}_2^+[\text{AsF}_6]^-$ exhibits Curie-Weiss behavior over the range 60-2 K ($C_m = 0.34 \pm 0.01 \text{ cm}^3 \text{ mol}^{-1} \text{ K}$, $\theta = -1.90 \pm 0.01 \text{ K}$). The magnetic moment, uncorrected for TIP, varies from 1.63 μ_B at 80 K to 1.17 μ_B at 2 K.

Finally, in the $\text{O}_2^+[\text{AsF}_6]^-$, there appears to be weak antiferromagnetic coupling that may involve either super-exchange through intervening AsF_6^- anions (the smallest anion of the three encountered in this study) or even direct weak O...O interaction.

References

- 1.a) N. Bartlett and D.H. Lohmann, Proc. Chem. Soc., 115 (1962).
- b) N. Bartlett and D.H. Lohmann, J. Chem. Soc., 5253 (1962).
2. R.J. Gillespie and J.B. Milne, Inorg. Chem., 5, 1577 (1966).
- 3.a) R.J. Gillespie and M.J. Morton, Chem. Comm., 1565 (1968).
- b) R.J. Gillespie and M.J. Morton, Inorg. Chem., 11, 586 (1972).

- 4.a) A.J. Edwards, G.R. Jones, and R.J. Sills, Chem. Comm., 1527 (1968).
- b) A.J. Edwards and G.R. Jones, J. Chem. Soc. A, 2318 (1971).
5. C.G. Davies, R.J. Gillespie, P.R. Ireland, and J.M. Sowa, Can. J. Chem., **52**, 2048 (1974).
6. R.J. Gillespie and J. Passmore, Adv. Inorg. Radiochem., **17**, 49 (1975) and references therein.
7. R.J. Gillespie and M.J. Morton, J. Mol. Spectrosc., **30**, 178 (1969).
8. F.G. Herring and R.A.N. McLean, Inorg. Chem., **11**, 1667 (1972).
9. D.W. Turner, C. Baker, A.D. Baker, and C.R. Brundle, "Molecular Photoelectron Spectroscopy", Wiley, New York, 1970.
10. G. Herzberg, "Spectra of Diatomic Molecules", van Nostrand, New York, 1950.
11. J.H. Van Vleck, "The Theory of Electric and Magnetic Susceptibilities", Oxford University Press, Oxford, 1932.
12. W.W. Wilson, R.C. Thompson, and F. Aubke, Inorg. Chem., **19**, 1489 (1980).
13. J.S. Haynes, K.W. Oliver, S.J. Rettig, R.C. Thompson, and J. Trotter, Can. J. Chem., **62**, 891 (1984).
14. A. Smalc, Inst. Josef Stefan, I.J.S. Report R. 612, 1 (1972); Chem. Abstr. **79**, 13032t (1973).
15. R.J. Gillespie, R. Kapoor, R. Faggiani, C.J.L. Lock, M.J. Murchie, and J. Passmore, Chem. Comm., 8 (1983).
16. J. Passmore, E.K. Richardson, and P. Taylor, J. Chem. Soc. Dalton Trans., 1006 (1976).
17. R.D.W. Kemmitt, M. Murray, V.M. McRay, R.D. Peacock, M.C.R. Symons, and T.A. O'Donnell, J. Chem. Soc. A, 862 (1968).
18. W.W. Wilson and F. Aubke, J. Fluorine Chem., **13**, 431 (1979).
19. W.E. Falconer, F.J. DiSalvo, A.J. Edwards, J.E. Griffiths, W.A. Sunder, and M.J. Vasile, J. Inorg. Nucl. Chem. Suppl., 59 (1976).

20. A.J. Edwards, W.E. Falconer, J.E. Griffiths, W.A. Sunder, and M.J. Vasile, J. Chem. Soc. Dalton Trans., 1129 (1974).
21. N. Bartlett and S.P. Beaton, Chem. Comm., 167 (1966).
22. J.B. Baal, Jr., C. Pupp, and W.E. White, Inorg. Chem., **8**, 828 (1969).
23. F.J. DiSalvo, W.E. Falconer, R.S. Hutton, A. Rodriguez, and J.V. Waszczack, J. Chem. Phys., **62**, 2575 (1975).
24. I.V. Nikitin and V. Ya. Rosolovskii, Russ. Chem. Rev. (Engl. Trans.) **40**, 889 (1971); Usp. Khim. **40**, 1913 (1971) and references therein.
25. J. Shamir and J. Binenboym, Inorg. Chim. Acta, **2**, 37 (1968); Inorg. Synth., **14**, 39 (1973).
26. J.N. Keith, I.J. Solomon, I. Sheft, and H.H. Hyman, Inorg. Chem., **7**, 230 (1968).
27. K.O. Christe, R.D. Wilson, and I.B. Goldberg, Inorg. Chem., **15**, 1271 (1976).
- 28.a) V.I. Belova, Ya.K. Syrkin, D.V. Bantov, and V.F. Sukhoverkhov, Russ. J. Inorg. Chem. (Engl. Trans.) **13**, 765 (1968).
- b) V.I. Belova, V.Ya. Rosolovskii, and E.K. Nikitina, Russ. J. Inorg. Chem (Engl. Trans.), **16**, 772 (1971).
29. D.R. Slim, Ph.D. Thesis, University of Birmingham, 1974.
- 30.a) P. Rigny and W.E. Falconer, J. Chem. Phys., **62**, 2581 (1975).
- b) C. Naulin and R. Bougon, J. Chem. Phys., **64**, 4155 (1976).
31. I.B. Goldberg, K.O. Christe, and R.D. Wilson, Inorg. Chem., **14**, 152 (1975).
32. A. Grill, M. Schieber, and J. Shamir, Phys. Rev. Lett., **25**, 747 (1970).
33. R.J. Myers, "Molecular Magnetism and Magnetic Resonance Spectroscopy", Prentice-Hall Inc., Englewood Cliffs, New Jersey, 1973.
34. A. Bondi, J. Phys. Chem., **68**, 441 (1964).
35. A. Zumsteg, M. Ziegler, W. Kanzig, and M. Bosch, Phys. Cond. Matter, **17**, 267 (1974).
36. K. Lueken, M. Deussen, M. jansen, W. Hesse, and W. Schnick, Z. Anorg. Allg. Chem., **553**, 179 (1987).

37. D.E. Cox, E.J. Samuelson, and K.H. Beckurts, Phys. Rev. **B7**, 3102 (1973).
38. A.R. Young, II, T. Hirata, and S.I. Morrow, J. Am. Chem. Soc., **86**, 20 (1964).
39. B.G. Mueller, J. Fluorine Chem., **17**, 409 (1981).
40. W. Schnick and M. Jansen, Angew. Chem. Int. Ed. (English), **97**, 54 (1985).
41. W. Schnick and M. Jansen, Z. Anorg. Allg. Chem., **532**, 37 (1986).
42. W. Schnick and M. Jansen, Rev. Chem. Miner., **24**, 446 (1987).
43. M. Jansen, and W. Hesse, Z. Anorg. Allg. Chem., **560**, 47 (1988).
44. J.S. Miller, Ed. "Extended Linear Chain Compounds", Vol. 3, Plenum Press, New York, 1983.
45. J.D. Johnson, J. Appl. Phys., **52**, 1991 (1981).
46. M.E. Fisher, J. Math. Phys., **4**, 124 (1963).
47. R.L. Carlin, "Magnetochemistry", Springer-Verlag, Berlin, 1986.
48. C.H. Weng, Ph.D. Dissertation, Carnegie-Mellon University, Pittsburgh, PA, (1968).
49. W. Hiller, J. Strahle, A. Datz, M. Hanack, W.E. Hatfield, L.W. ter Haar, and P. Gutlich, J. Am. Chem. Soc., **106**, 329 (1984).
50. W.V. Cicha, J.S. Haynes, K.W. Oliver, S.J. Rettig, R.C. Thompson, and J. Trotter, Can. J. Chem., **63**, 1055 (1985).
51. M. Suzuke, B. Tsujiyama, and S. Katsura, J. Math Phys., **8**, 124 (1976).
52. O. Edquist, E. Lindholm, L.E. Selin, and L. Asbrink, Phys. Scripta, **1**, 25 (1970).
53. A.B. Cornford, D.C. Frost, C.A. McDowell, J.L. Ragle, and I.A. Stenhouse, J. Chem. Phys., **54**, 2651 (1971).
54. P. Venkateswarlu, Can. J. Phys., **47**, 2525 (1969).
55. P. Venkateswarlu, Can. J. Phys., **48**, 2525 (1969).
56. Landolt-Börnstein, Numerical data and functional relations in science and technology, Vol. 2, Magnetic properties of coordination and organometallic transition metal compounds, Springer-Verlag, Berlin, 1966.

CHAPTER 6

MAGNETIC EXCHANGE IN M(II) SULFONATES,

M(II) = Ni(II), Pd(II) AND Ag(II)

6.1 Introduction

The sulfonates described in this Chapter include the metal(II) fluorosulfates $\text{Ni}(\text{SO}_3\text{F})_2$, $\text{Pd}(\text{SO}_3\text{F})_2$, $\text{Ag}(\text{SO}_3\text{F})_2$ and " $\text{Pd}(\text{SO}_3\text{F})_3$ ", more appropriately formulated as the mixed valency compound $\text{Pd}(\text{II})[\text{Pd}(\text{IV})(\text{SO}_3\text{F})_6]$, and the metal(II) trifluoromethylsulfates $\text{Ni}(\text{SO}_3\text{CF}_3)_2$, $\text{Pd}(\text{SO}_3\text{CF}_3)_2$, and $\text{Ag}(\text{SO}_3\text{CF}_3)_2$. These compounds can also be considered as transition metal derivatives of the strong sulfonic acids HSO_3F and HSO_3CF_3 respectively. The anions SO_3F^- and SO_3CF_3^- have the potential to coordinate to the metal ions as bidentate or tridentate bridging ligands (1-5), and consequently polymeric, layered materials with paramagnetic metal centers are formed. As pointed out in Chapter 3, only a limited number of paramagnetic binary fluoro compounds of divalent nickel, palladium and silver has been synthesized so far, and therefore it is of interest to study the magnetic properties of the above sulfonates which are rare binary fluoro derivatives of the respective divalent metals.

Several transition metal fluorosulfate and trifluoromethylsulfate compounds have been studied previously for their magnetic properties in the higher temperature range, usually down to ~ 80 K only (1-4,6-15). Interestingly, it appears that among the fluorosulfates, only $\text{Ir}(\text{SO}_3\text{F})_4$ and its derivative $\text{Cs}_2[\text{Ir}(\text{SO}_3\text{F})_6]$ (11) are magnetically concentrated, and in the trifluoromethylsulfates magnetic exchange is detected only in $\text{Fe}(\text{SO}_3\text{CF}_3)_3$ (14) and $\text{Ag}(\text{SO}_3\text{CF}_3)_2$ (4). The exchange coupling observed in all four of these derivatives is reported as antiferromagnetic. This is significant and not totally unexpected, since the majority of the magnetically concentrated transition metal fluoro compounds exhibit antiferromagnetism rather than ferro- or

ferrimagnetism (16).

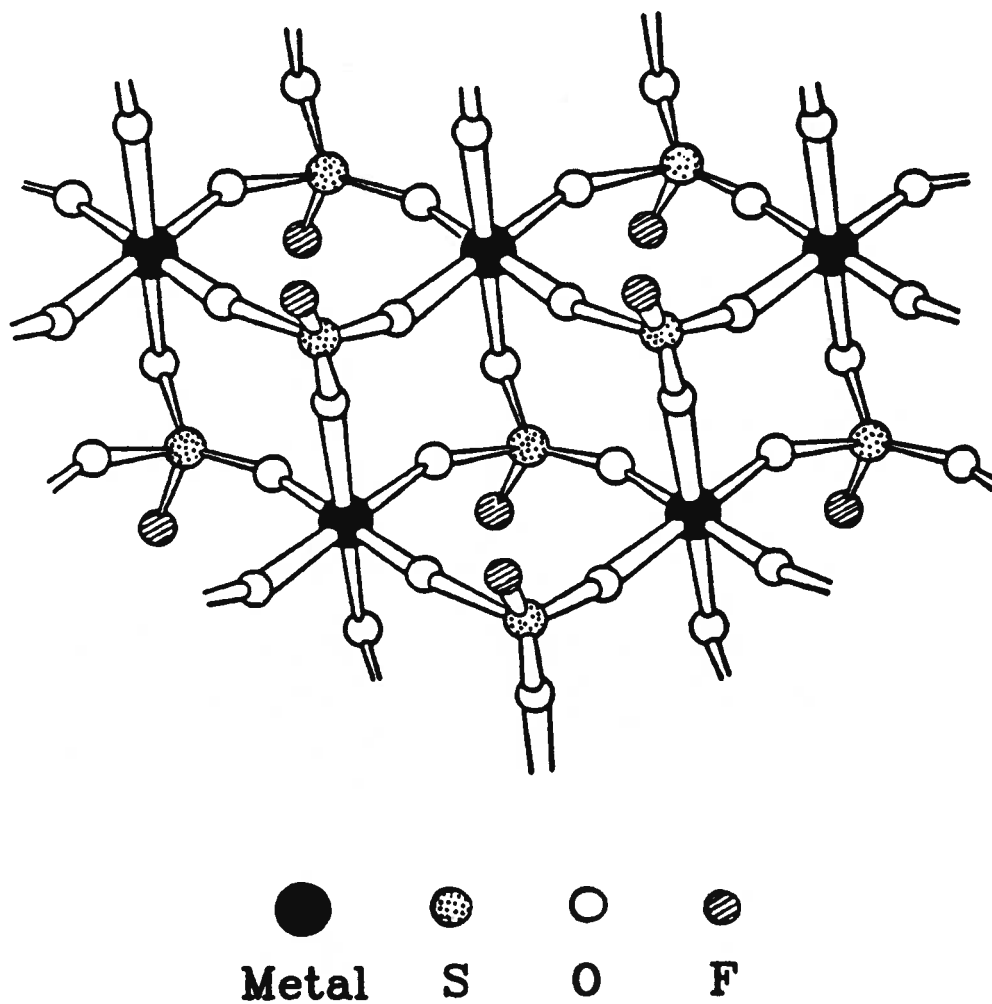
Ferromagnetic ordering is hence a rare phenomenon in ionic solids, and is largely confined to small groups of transition (d-block) and lanthanide metal -oxides, -chalcogenides and -halides with distinct structural features that permit one, two or three dimensional exchange via monoatomic anions (17, 18). However, in contrast the four metal(II) fluorosulfate compounds studied here contain the polyatomic SO_3F^- anion and show significant ferromagnetic exchange at low temperatures. Previous magnetic measurements down to ~ 80 K on the binary fluorosulfates $\text{Pd}(\text{SO}_3\text{F})_2$ (2), $\text{Ag}(\text{SO}_3\text{F})_2$ (3) and " $\text{Pd}(\text{SO}_3\text{F})_3$ " (2), showed that the compounds were relatively magnetically unconcentrated in that temperature range, and their susceptibilities followed the Curie-Weiss law closely with small positive Weiss constants.

The three metal(II) trifluoromethylsulfate compounds $\text{Ni}(\text{SO}_3\text{CF}_3)_2$, $\text{Pd}(\text{SO}_3\text{CF}_3)_2$ and $\text{Ag}(\text{SO}_3\text{CF}_3)_2$ investigated here for their magnetic behavior have all been synthesized previously (4, 5, 19) although no variable temperature susceptibility studies have been reported for the $\text{Ni}(\text{SO}_3\text{CF}_3)_2$ and $\text{Pd}(\text{SO}_3\text{CF}_3)_2$ compounds until now. A previous high temperature study on the $\text{Ag}(\text{SO}_3\text{CF}_3)_2$ compound indicated that the Ag(II) ions in the sample were coupled antiferromagnetically (4). Therefore, the two analogous nickel and palladium derivatives were investigated in this work to determine whether these compounds are also magnetically concentrated with antiparallel spins. In addition, magnetic measurements were run on the $\text{Ag}(\text{SO}_3\text{CF}_3)_2$ compound at lower temperatures to verify the previously reported higher temperature susceptibility data.

It is significant to note here that the metal(II) fluorosulfates and the trifluoromethylsulfate analogs described in this Chapter are assumed to have the common CdCl_2 -type structure, which is also seen in the metal(II) hexafluoroantimonates discussed in Chapter 3. Layered structures of the type seen in $\text{Sn}(\text{SO}_3\text{F})_2$ (20a) and $\text{Ca}(\text{SO}_3\text{CH}_3)_2$ (20b) have been previously

proposed for a number of divalent metal sulfonates (6, 10, 13, 15), on the basis of magnetic properties and vibrational spectra. It was proposed that these compounds adopt a polymeric two-dimensional structure, where each metal site is surrounded by an octahedral arrangement (tetragonally distorted in the silver derivatives) of oxygen ligands, as illustrated for $\text{Pd}(\text{SO}_3\text{F})_2$ in Figure 6.1.

Figure 6.1: Proposed Structure of $\text{Pd}(\text{SO}_3\text{F})_2$



6.2 Experimental

The synthetic procedures for the preparation of metal(II) fluorosulfates $\text{Ni}(\text{SO}_3\text{F})_2$ (13), $\text{Pd}(\text{SO}_3\text{F})_3$ (2), $\text{Ag}(\text{SO}_3\text{F})_2$ (3), " $\text{Pd}(\text{SO}_3\text{F})_3$ " (2), and the metal(II) trifluoromethylsulfates $\text{Ni}(\text{SO}_3\text{CF}_3)_2$ (19), $\text{Pd}(\text{SO}_3\text{CF}_3)_2$ (5) and $\text{Ag}(\text{SO}_3\text{CF}_3)_2$ (4) have been described in detail previously. These methods were followed in the present study as well. Attempts were made to synthesize " $\text{Pd}(\text{SO}_3\text{CF}_3)_3$ ", the corresponding trifluoromethylsulfate derivative of " $\text{Pd}(\text{SO}_3\text{F})_3$ ", but in all instances the solvolysis of " $\text{Pd}(\text{SO}_3\text{F})_3$ " in excess HSO_3CF_3 (5) led to the binary $\text{Pd}(\text{SO}_3\text{CF}_3)_2$ compound only.

All the reactions were monitored by weight, and the purity of the products was determined by elemental analysis and IR spectroscopy. Magnetic data were corrected for Temperature Independent Paramagnetism (TIP) using the following reported 10Dq values [cm^{-1}]: $\text{Ni}(\text{SO}_3\text{F})_2$, 7340 (1); $\text{Pd}(\text{SO}_3\text{F})_2$, 11770 (1); $\text{Ag}(\text{SO}_3\text{F})_2$, 16600 (3) and $\text{Ni}(\text{SO}_3\text{CF}_3)_2$, 7350 (19).

6.3 Results and Discussion

The magnetic data obtained on the M(II) sulfonates with $\text{M}=\text{Ni}$, Pd and Ag , clearly indicate two distinct types of magnetic exchange present in the two groups of compounds. All the M(II) fluorosulfates studied here exhibit strong ferromagnetic exchange at lower temperatures, whereas the M(II) trifluoromethylsulfates show antiferromagnetism with varying degrees of magnetic concentration over a wider temperature range. Therefore, the discussion of the magnetic results can be conveniently divided into two parts, ferromagnetism and antiferromagnetism of the respective sulfonate derivatives. Ferromagnetism will be discussed first and in greater detail, since this phenomenon is rare and unusual in transition metal fluoro compounds.

6.3.1 Ferromagnetism of M(II) fluorosulfates $\text{Ni}(\text{SO}_3\text{F})_2$, $\text{Pd}(\text{SO}_3\text{F})_2$, $\text{Pd}(\text{II})[\text{Pd}(\text{IV})(\text{SO}_3\text{F})_6]$ and $\text{Ag}(\text{SO}_3\text{F})_2$

Previous magnetic susceptibility measurements on the three palladium and silver fluorosulfates investigated here indicate that the compounds are relatively magnetically dilute down to ~ 80 K (2,3). No detailed magnetic study exists in the case of $\text{Ni}(\text{SO}_3\text{F})_2$. Therefore, measurements on $\text{Pd}(\text{SO}_3\text{F})_2$, $\text{Ag}(\text{SO}_3\text{F})_2$ and " $\text{Pd}(\text{SO}_3\text{F})_3$ " are extended down to ~ 4 K (~ 2 K for $\text{Pd}(\text{SO}_3\text{F})_2$) and $\text{Ni}(\text{SO}_3\text{F})_2$ is studied in the temperature range of ~ 291 to 2 K. The pertinent magnetic data obtained with the vibrating sample magnetometer in the lower temperature range are presented in Tables 6.1, 6.2, 6.3 6.4, and the Gouy measurements of $\text{Ni}(\text{SO}_3\text{F})_2$ from ~ 291 to 79 K are given in Table 6.5. A summary of the relevant magnetic parameters on all four fluorosulfates is listed in Table 6.6 (see Appendices B-1 to B-3 for additional magnetic data).

For $\text{Pd}(\text{SO}_3\text{F})_2$, " $\text{Pd}(\text{SO}_3\text{F})_3$ " and $\text{Ag}(\text{SO}_3\text{F})_2$, previous higher temperature measurements were presented as plots of $1/\chi_M$ vs. T, which were linear, and had positive Weiss constants (Table 6.6), indicative of Curie-Weiss behavior. The magnetic moments calculated for the three compounds (1-3) were in good agreement with expected values for approximately octahedrally coordinated Pd(II)(d^8) and Ag(II)(d^9) species. A similar situation is observed in the case of $\text{Ni}(\text{SO}_3\text{F})_2$, where the inverse susceptibility vs. temperature graph in the higher temperature region also gives a straight line plot (Figure 6.2). However, the Weiss constant obtained here 0.41 K is relatively small and hence $\text{Ni}(\text{SO}_3\text{F})_2$ appears to be magnetically dilute down to ~ 80 K. The μ_{eff} value of about $3.27 \mu_B$ (Table 6.5) in this temperature range is not unexpected for $\text{Ni}(\text{SO}_3\text{F})_2$, with the Ni(II) ions located in octahedral ligand sites (13,21; see also Chapter 3).

Table 6.1: Low Temperature Magnetic Data of Ni(SO₃F)₂

Temperature (K)	$\chi_M^{\text{corr}} \times 10^6$ (cm ³ mol ⁻¹)	μ_{eff} (μ_B) ^a
81.72	15520	3.16
77.72	16370	3.16
74.02	17250	3.17
69.72	18370	3.18
65.19	19740	3.18
59.86	21590	3.19
54.40	23880	3.20
47.60	27390	3.21
40.40	32800	3.24
31.25	43800	3.30
26.23	54310	3.37
20.65	71640	3.43
15.98	100200	3.57
11.17	170500	3.90
7.60	329600	4.47
6.30	502700	5.03
5.08	670900	5.22
4.24	766000	5.10
4.12	775700	5.05
3.37	839100	4.75
2.60	880500	4.28
2.30	900000	4.07

^a $\mu_{\text{eff}} = 2.828 [(\chi_M^{\text{corr}} - \text{TIP})T]^{1/2}$; $\text{TIP} = 8N\beta^2/10Dq = 285 \times 10^{-6} \text{ cm}^3 \text{ mol}^{-1}$
Magnetic field = 9225 G.

Table 6.2: Low Temperature Magnetic Data of Pd(SO₃F)₂

Temperature (K)	$\chi_M^{\text{corr}} \times 10^6$ (cm ³ mol ⁻¹)	μ_{eff} (μ_B) ^a
82.06	19010	3.52
79.89	19560	3.52
78.33	20060	3.53
76.60	20610	3.54
74.47	21250	3.54
72.55	21950	3.55
70.28	22640	3.55
67.95	23520	3.56
65.77	24640	3.59
63.40	25740	3.60
60.73	27060	3.61
58.00	28620	3.63
55.00	30600	3.66
51.40	33020	3.67
47.90	36130	3.71
44.50	39870	3.76
40.60	45170	3.82
31.23	66750	4.08
21.35	127300	4.66
16.50	211800	5.29
11.25	574900	7.19
8.11	1015000	8.11
5.99	1162000	7.46
4.32	1215000	6.48
3.88	1236000	6.19
3.30	1248000	5.74
2.70	1258000	5.21
1.74	1271000	4.20

^a $\mu_{\text{eff}} = 2.828 [(\chi_M^{\text{corr}} - \text{TIP})T]^{1/2}$; $\text{TIP} = 8N\beta^2/10Dq = 177 \times 10^{-6} \text{ cm}^3 \text{ mol}^{-1}$
Magnetic field = 7501 G.

Table 6.3: Low Temperature Magnetic Data of Pd(II)[Pd(IV)(SO₃F)₆]

Temperature (K)	$\chi_M^{\text{corr}} \times 10^6$ (cm ³ mol ⁻¹)	$\mu_{\text{eff}} (\mu_B)^a$
82.28	21220	3.74
78.73	22130	3.73
74.64	23460	3.74
70.34	24860	3.74
65.88	26750	3.75
60.60	29130	3.76
55.00	32420	3.78
48.00	37180	3.78
44.20	40610	3.79
40.60	44880	3.82
31.65	60000	3.90
27.23	73720	4.01
21.75	98300	4.14
16.34	155000	4.50
11.17	355300	5.63
7.94	581500	6.08
5.98	663400	5.63
5.08	681600	5.26

^a $\mu_{\text{eff}} = 2.828 [\chi_M^{\text{corr}} \times T]^{1/2}$
Magnetic field = 7501 G.

Table 6.4: Low Temperature Magnetic Data of Ag(SO₃F)₂

Temperature (K)	$\chi_M^{\text{corr}} \times 10^6$ (cm ³ mol ⁻¹)	μ_{eff} (μ_B) ^a
82.06	7950	2.27
78.28	8450	2.29
74.53	9070	2.32
70.34	9840	2.35
65.82	10840	2.38
60.50	12300	2.43
55.00	14270	2.50
47.95	17560	2.59
44.35	20080	2.66
40.55	23560	2.76
30.85	40400	3.15
26.58	58350	3.52
21.23	110400	4.33
16.34	277000	6.02
10.53	605800	7.14
7.40	688000	6.38
5.08	730300	5.45
4.54	735300	5.17

^a $\mu_{\text{eff}} = 2.828 [(\chi_M^{\text{corr}} - \text{TIP})T]^{1/2}$; $\text{TIP} = 4N\beta^2/10Dq = 63 \times 10^{-6} \text{ cm}^3 \text{ mol}^{-1}$
Magnetic field = 7501 G.

Table 6.5: Magnetic Data of Ni(SO₃F)₂ for the Temperature Range 291 to 79 K

Temperature (K)	$\chi_M^{\text{corr}} \times 10^6$ (cm ³ mol ⁻¹)	$\mu_{\text{eff}} (\mu_B)^a$
291.3	4840	3.26
271.0	5240	3.28
253.1	5580	3.27
235.7	5970	3.27
219.0	6420	3.28
201.7	6940	3.28
177.6	7860	3.28
152.0	9120	3.28
127.5	10920	3.29
103.0	13250	3.27
87.0	15690	3.27
79.0	17100	3.26

^a $\mu_{\text{eff}} = 2.828 [(\chi_M^{\text{corr}} - \text{TIP})T]^{1/2}$; $\text{TIP} = 8N\beta^2/10Dq = 285 \times 10^{-6} \text{ cm}^3 \text{ mol}^{-1}$
Magnetic field = 8000 G.

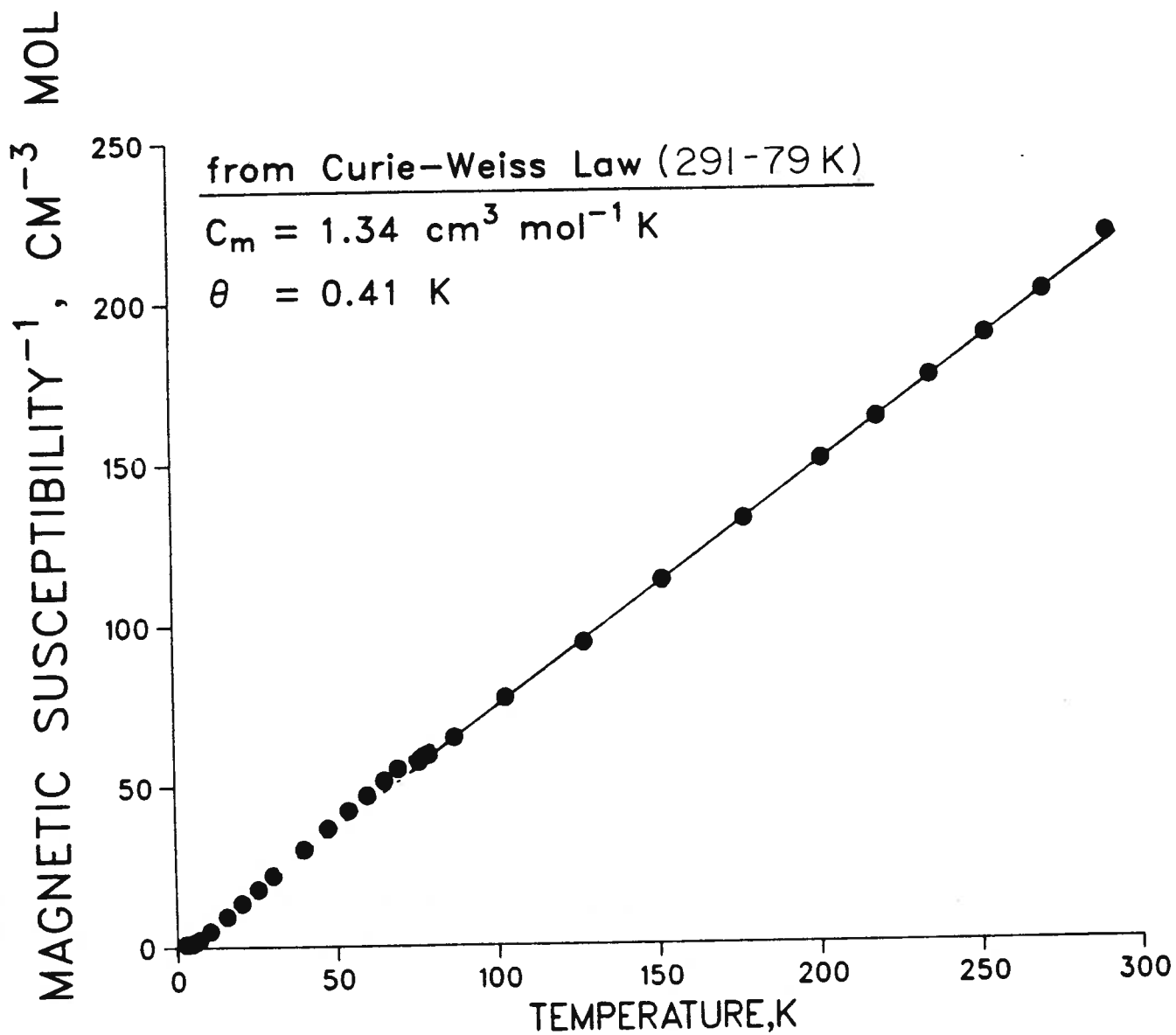
Table 6.6: Magnetic Parameters of Ni(SO₃F)₂, Pd(SO₃F)₂, Pd(II)[Pd(IV)(SO₃F)₆] and Ag(SO₃F)₂

Compound	Temperature Range (K)	Weiss Const. θ (K)	$\mu_{\text{eff}}^{\text{a}}$ (μ_{B})	$\mu_{\text{eff}}^{\text{b}}$ (max) ^b (μ_{B})	$T_{\text{max}}(\mu_{\text{eff}}^{\text{b}} \text{max})^{\text{b}}$ (K)	Reference
Ni(SO ₃ F) ₂	291–79 81.7–2.3	0.41±2	3.27	5.27	4.78	This work
Pd(SO ₃ F) ₂	299–103 82.1–1.7	13±4	3.34	8.11	8.11	(1) This work
"Pd(SO ₃ F) ₃ "	334–107 82.3–5.1	10±2	3.45	6.08	7.94	(1) This work
Ag(SO ₃ F) ₂	301–80 82.1–4.5	20±2	1.92	7.14	10.53	(3) This work

^a Values for 290 K.

^b Values for magnetic field = 7501 G.

Figure 6.2: Inverse Susceptibility vs. Temperature of Ni(SO₃F)₂



The low temperature plots of $1/\chi_M$ vs. T for $\text{Pd}(\text{SO}_3\text{F})_2$, " $\text{Pd}(\text{SO}_3\text{F})_3$ " and $\text{Ag}(\text{SO}_3\text{F})_2$ are shown in Figure 6.3. Extrapolation of the higher temperature linear portion ($\text{Pd}(\text{SO}_3\text{F})_2$ and " $\text{Pd}(\text{SO}_3\text{F})_3$ " > 11 K, $\text{Ag}(\text{SO}_3\text{F})_2$ > 14 K) of these plots produces intercepts on the temperature axis in excellent agreement with the values reported earlier (Table 6.6). In the lower temperature region all four compounds show a temperature independent $1/\chi_M$ (and therefore χ_M) behavior as the temperature is lowered. This change in the temperature dependence of the magnetic susceptibility at low temperature is illustrated for $\text{Pd}(\text{SO}_3\text{F})_2$ and " $\text{Pd}(\text{SO}_3\text{F})_3$ " in Figures 6.4 and 6.5, where the field dependence of the susceptibility in this region is also shown for the two compounds.

The approximate maximum susceptibilities expected for these compounds can be calculated with the following (spin only) expression given by Carlin (22):

$$M_{\text{sat}} = Ng\mu_B S \quad [6.1]$$

where M_{sat} = saturation magnetic moment ($M_{\text{sat}}/H = \chi_{\text{sat}}$)

N = Avogadro's number

g = Lande splitting factor

μ_B = Bohr magneton

S = Spin system, S=1 (Pd(II)) and S=1/2 (Ag(II))

The maximum or saturation magnetization situation corresponds to the alignment of all the magnetic spins parallel to the external field (H), where the magnetization becomes independent of field and temperature. The saturation susceptibility values calculated using equation [6.1] are compared with the observed maximum susceptibilities for $\text{Ni}(\text{SO}_3\text{F})_2$, $\text{Pd}(\text{SO}_3\text{F})_2$, " $\text{Pd}(\text{SO}_3\text{F})_3$ " and $\text{Ag}(\text{SO}_3\text{F})_2$ in Table 6.7.

Figure 6.3: Inverse Susceptibility vs. Temperature of $\text{Pd}(\text{SO}_3\text{F})_2$, $\text{Pd}(\text{II})[\text{Pd}(\text{IV})(\text{SO}_3\text{F})_6]$ and $\text{Ag}(\text{SO}_3\text{F})_2$

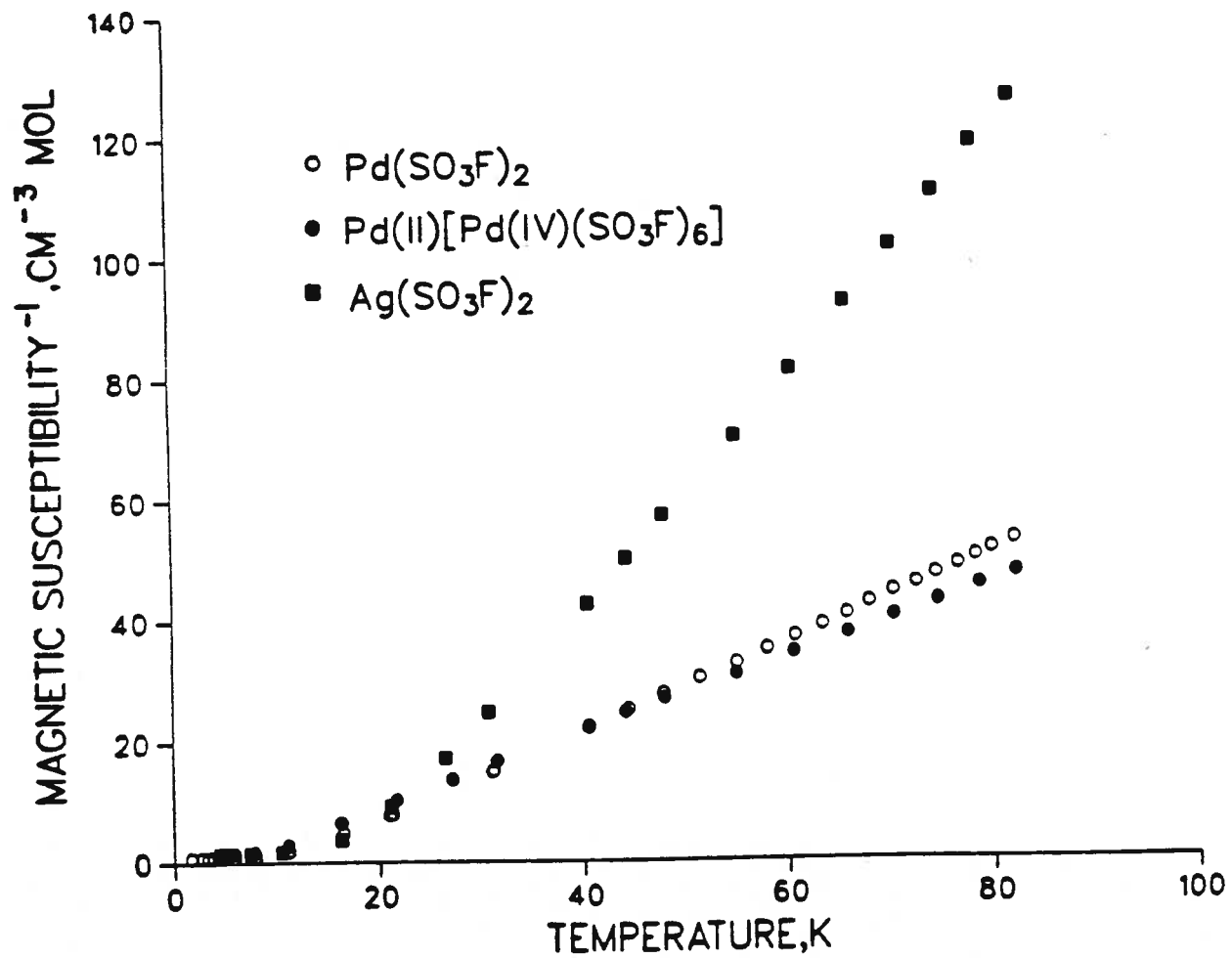


Figure 6.4: Magnetic Susceptibility vs. Temperature for Pd(SO₃F)₂ at 7501 and 9625 G

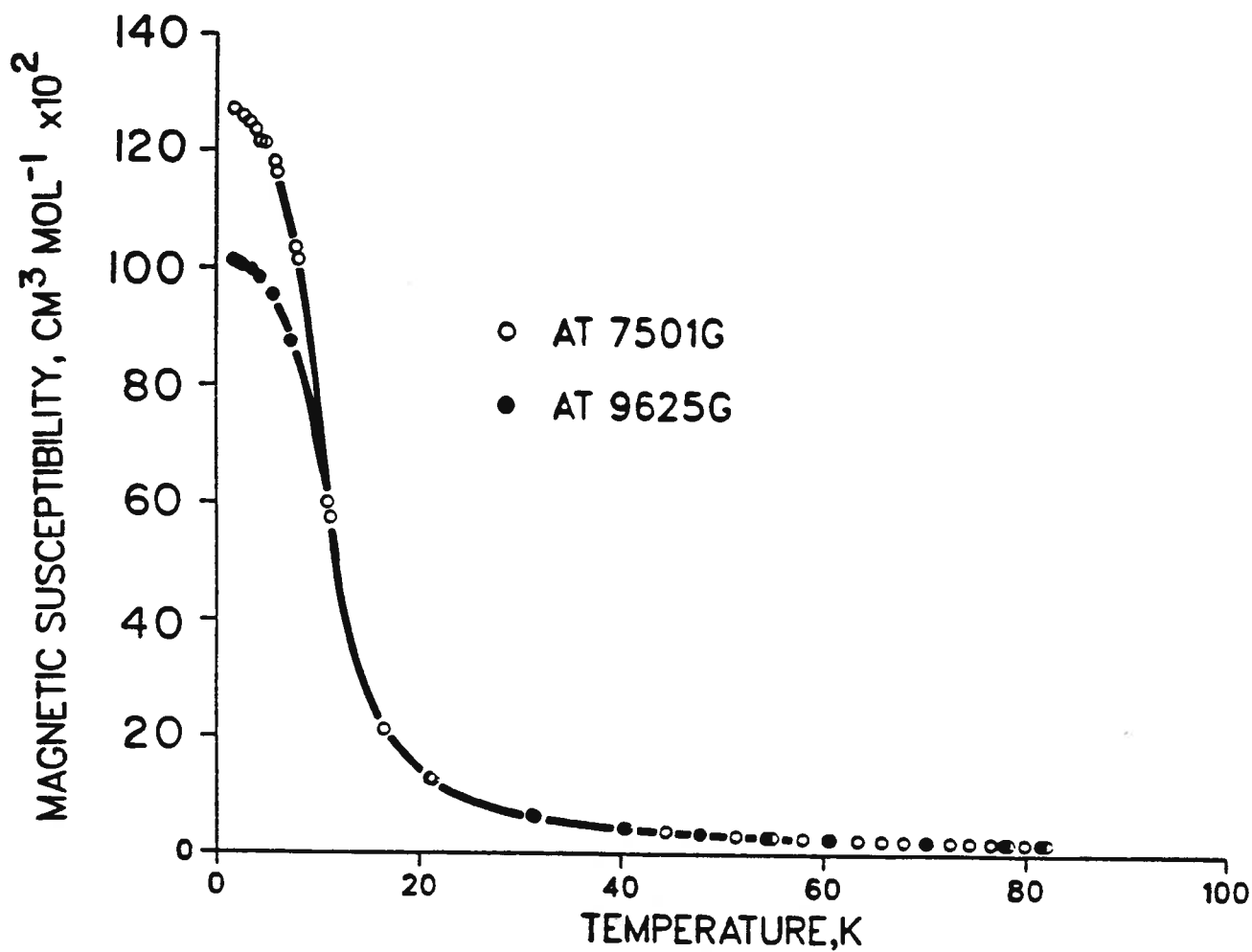


Figure 6.5: Magnetic Susceptibility vs. Temperature for Pd(II)[Pd(IV)(SO₃F)₆] at 7501 and 9625 G

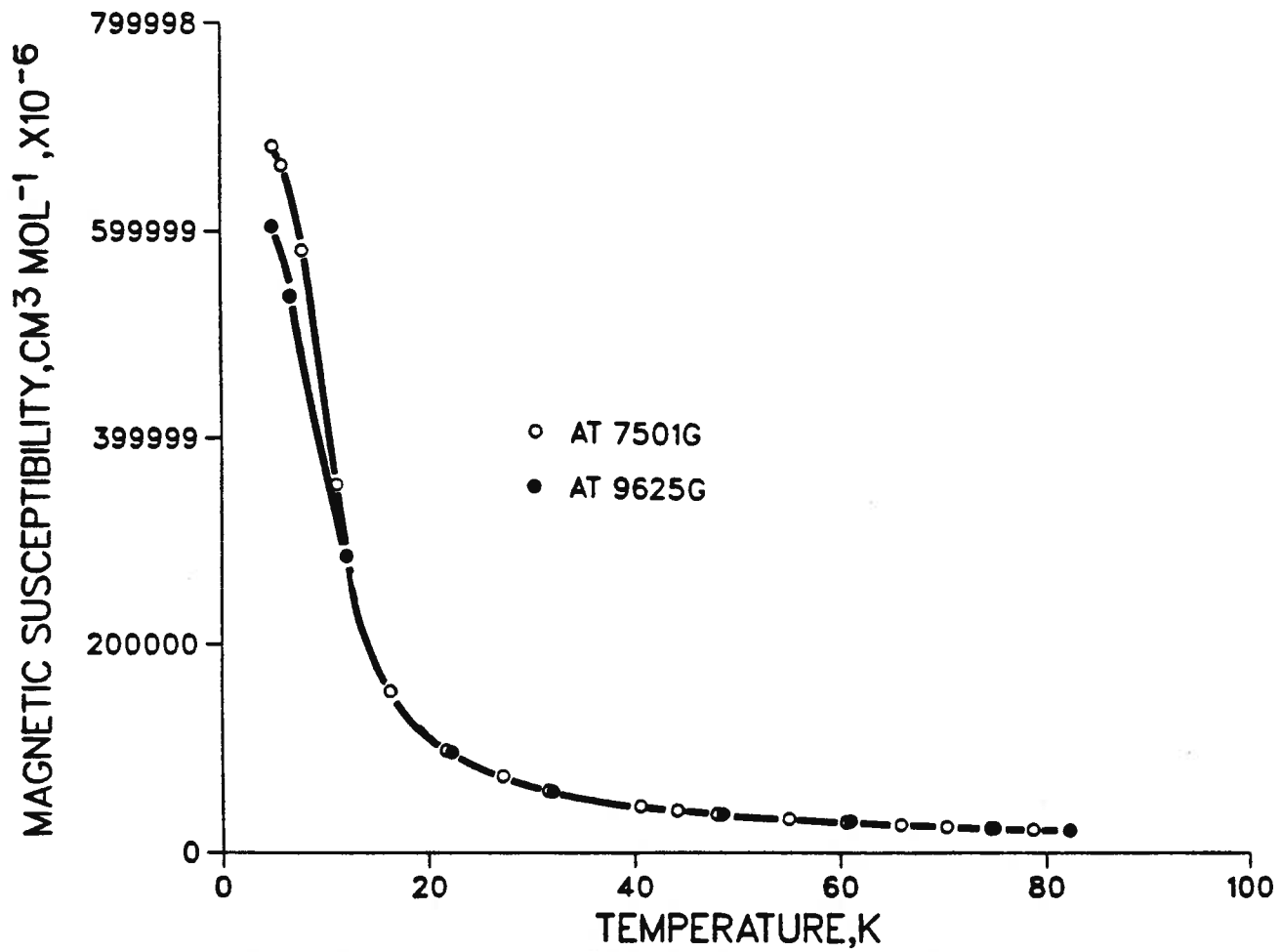


Table 6.7: Experimental and Calculated Saturation Magnetic Susceptibilities of Ni(SO₃F)₂, Pd(SO₃F)₂, Pd(II)[Pd(IV)(SO₃F)₆] and Ag(SO₃F)₂

Compound	χ_M , sat. calculated ^a (cm ³ mol ⁻¹)	χ_M , max. observed ^a (cm ³ mol ⁻¹)	Temp. (χ_M , max) (K)	% saturation = $\frac{\chi_M, \text{max.}}{\chi_M, \text{sat.}} \times 100$
Ni(SO ₃ F) ₂	1.488	1.041	2.69	70
Pd(SO ₃ F) ₂	1.488	1.271	1.74	85
"Pd(SO ₃ F) ₃ "	1.488	0.682	5.08	46
Ag(SO ₃ F) ₂	0.744	0.735	4.54	99

^a Susceptibility data for magnetic field = 7501 G.

It appears from the data in Table 6.7 that the magnetic behavior observed at lower temperature in $\text{Ni}(\text{SO}_3\text{F})_2$, $\text{Pd}(\text{SO}_3\text{F})_2$ and $\text{Ag}(\text{SO}_3\text{F})_2$ may be largely a result of saturation magnetization. As a consequence, the magnetic moments of these compounds are temperature dependent and pass through maxima at ~ 5 , ~ 8 , and ~ 10.5 K respectively (Table 6.6). This is illustrated in the magnetic moment vs. temperature plot for $\text{Pd}(\text{SO}_3\text{F})_2$ and $\text{Ag}(\text{SO}_3\text{F})_2$ in Figure 6.6. Spin saturation in the mixed valent " $\text{Pd}(\text{SO}_3\text{F})_3$ " may be achieved at higher magnetic fields, since closer approach to saturation magnetization would be expected at stronger applied fields. Even at a field of 7501 G, the magnetic moments of this compound shows temperature dependent behavior and has a maximum at ~ 8 K.

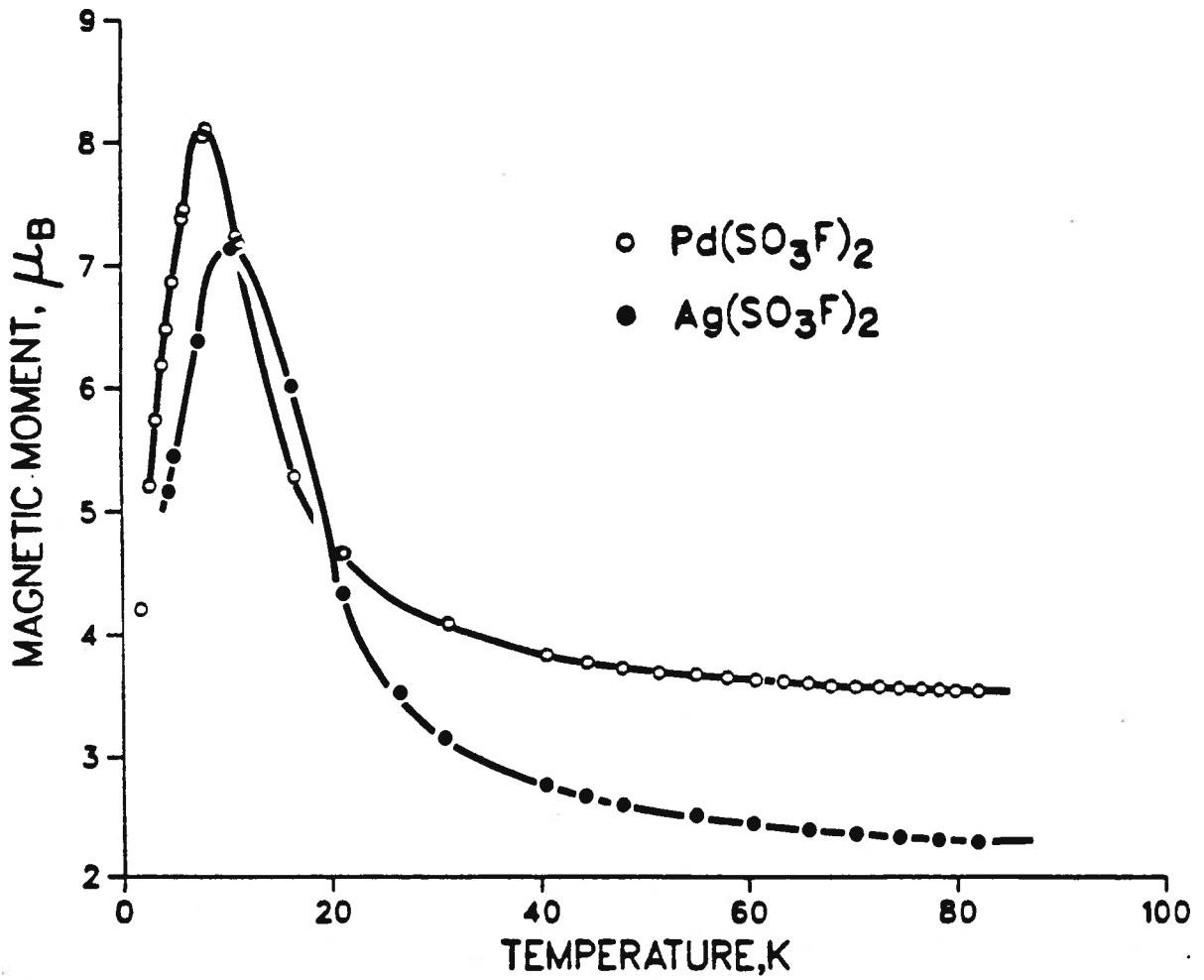
In the $\text{Ni}(\text{SO}_3\text{F})_2$, $\text{Pd}(\text{SO}_3\text{F})_2$ and " $\text{Pd}(\text{SO}_3\text{F})_3$ " compounds, the paramagnetic Ni(II) and Pd(II) ions have been shown to be in octahedral environments with $^3A_{2g}$ ground states (1,2,21). Although there is no orbital contribution to the susceptibility associated with this state, to first order, zero-field splitting via second order spin orbit coupling could lift the triplet spin degeneracy which can significantly affect the magnetic properties of such systems, particularly at low temperatures.

The average susceptibility $\langle \chi \rangle$ of powder samples ($\langle \chi \rangle = (\chi_{11} + 2\chi_{\perp})/3$) in the presence of zero-field splitting for $S=1$ spin systems is obtained from the expression (22):

$$\langle \chi \rangle = \frac{2Ng^2\mu_B^2}{3kT} \left[\frac{(2/x - 2 \exp(-x))/(x + \exp(-x))}{1 + 2 \exp(-x)} \right] \quad [6.2]$$

where $x = D/kT$, D = zero-field splitting parameter, k = Boltzmann's constant, and N , g and μ_B as defined for equation [6.1].

Figure 6.6: Magnetic Moment vs. Temperature of $\text{Pd}(\text{SO}_3\text{F})_2$ and $\text{Ag}(\text{SO}_3\text{F})_2$



In general, the value of D is only a few wavenumbers, and with $kT \sim 205 \text{ cm}^{-1}$ at room temperature, $D/kT \ll 1$. However, at lower temperatures D/kT becomes significant, thereby affecting the measured susceptibilities of these samples. The sign of D could be either positive or negative, and in the case of nickel, both signs have been observed (22).

Attempts were made to fit the magnetic susceptibility data to equation [6.2]. However, only very poor fits were obtained, which indicates clearly that this effect cannot explain the magnetic behavior exhibited by the nickel and palladium complexes. Moreover, the magnetic behavior of $\text{Ag}(\text{SO}_3\text{F})_2$ cannot be rationalized by this effect, since in $\text{Ag}(\text{II})$ ions with $^2\text{B}_{1g}$ ground states, the possibility of zero-field splitting does not exist.

The magnetic properties observed in these four fluorosulfate compounds bear a strong resemblance to those reported for the binary chlorides FeCl_2 , CoCl_2 and NiCl_2 by Starr et al. (23). Neutron-diffraction studies on the iron and cobalt compounds have revealed ferromagnetic coupling between the metal centers within each layer (intralayer exchange), and weak antiferromagnetic coupling between layers (interlayer exchange) (24). This magnetic behavior, termed metamagnetism, has been extensively reviewed for other compounds as well (25). Interestingly, the binary chlorides mentioned above have the typical CdCl_2 -type structure, with each layer of the metal atoms separated by two layers of chlorine atoms from the next metal atom layer. Each metal atom layer forms a two-dimensional hexagonal network in which every metal atom has six near neighbours (26).

Furthermore, in a number of layer type fluorides containing Jahn-Teller ions, the intralayer ferromagnetic couplings are found to be much stronger than the interlayer antiferromagnetic couplings, and as a result ferromagnetism is observed in these compounds (17). Similar interactions may be present in "the Jahn-Teller compound" $\text{Ag}(\text{SO}_3\text{F})_2$ studied in this work as well.

Similar crystal and magnetic structures are possible for the M(II) fluorosulfates examined in this work. Indeed, layer structures based on the CdCl_2 prototype have also been proposed for the compounds discussed here, as mentioned in the introductory section of this chapter (see also Figure 6.1). The apparent lack of solubility of these metal fluorosulfates in a suitable solvent such as fluorosulfuric acid, HSO_3F , has so far precluded single crystal X-ray diffraction studies as well as magnetic measurements on oriented crystals leading to studies on paramagnetic anisotropy.

It is significant to note that octahedral Pd(II) ions with a $^3A_{2g}$ ground state is found only in $\text{Pd}(\text{SbF}_6)_2$ (Chapter 3), PdF_2 (27), $\text{Pd}(\text{SO}_3\text{F})_2$, $\text{Pd}(\text{SO}_3\text{CF}_3)_2$, and in some of their cationic and anionic derivatives, just as AgF_2 (28), $\text{Ag}(\text{SO}_3\text{F})_2$ and $\text{Ag}(\text{SO}_3\text{CF}_3)_2$ have remained the only simple binary compounds of Ag(II) with a d^9 configuration. However, the fluorides AgF_2 (28), PdF_2 (27), and NiF_2 (30) are essentially antiferromagnetic compounds, and compare more appropriately with the trifluoromethylsulfate derivatives discussed in the next section. In PdF_2 , NiF_2 , and AgF_2 , weak ferromagnetism is observed due to a canting of the spins (27,28,30).

The ternary $\text{Pd}(\text{II})[\text{Pd}(\text{IV})\text{F}_6]$ is reported to have a significant ferromagnetic component at low temperatures, although the complex is weakly ferromagnetic over a wide temperature range (17, 18, 29). In contrast, the structurally similar $\text{Pd}(\text{II})[\text{Pd}(\text{IV})(\text{SO}_3\text{F})_6]$ is found here as a strongly ferromagnetically coupled compound. The fluorosulfate ligand seems to bond strongly to the Pd(IV) center and weakly to Pd(II), in an "anisobidentate" bonding mode (1,2). A large number of $\text{M}(\text{II})\text{M}'(\text{IV})\text{F}_6$ type fluorides with both M and M' transition metals such as Pd, Pt and Ni, have been studied for their ferromagnetic contribution (17,18) as already noted above in the case of the Pd_2F_6 compound. Ferromagnetism in these compounds may be associated with cationic ordering, which is observed in Pd_2F_6 from neutron diffraction measurements (29). Magnetic ordering at low temperatures is explained in these ternary species by a mechanism where the spins of the e_g^2 electrons of the divalent metals ($t_{2g}^6e_g^2$) are ferromagnetically

coupled via a superexchange interaction involving the 2p fluorine orbitals and the empty e_g orbitals of the tetravalent cations (17,18).

Therefore, it has been shown that when cationic ordering in M(II) and empty e_g orbitals on the transition metal M(IV) are present, ferromagnetism can occur in these bimetallic compounds. This may be applicable to the Pd(II)[Pd(IV)(SO₃F)₆] complex as well, although the much larger SO₃F⁻ anion may significantly affect the extent of ferromagnetic interaction. Interestingly, when the tetravalent cation is replaced by a non-transition metal ion such as Sn(IV) or Ge(IV), magnetic ordering is not observed even at 4.2 K (17). This observation appears to be valid for the ternary bimetallic fluorosulfates as well. A number of previously synthesized fluorosulfate derivatives with three different divalent metals where the tetravalent cation is Sn(IV) were studied for their low temperature magnetic properties in this work. The compounds chosen were Ni(II)[Sn(IV)(SO₃F)₆] (31), Cu(II)[Sn(IV)(SO₃F)₆] (31) and Ag(II)[Sn(IV)(SO₃F)₆] (3). The magnetic measurements obtained for these three samples are given in Appendices B-4, B-5, and B-6. It is clear from these data that the compounds are relatively magnetically dilute to ~4 K.

Furthermore, previous high temperature magnetic measurements on Pd(II)[Sn(IV)(SO₃F)₆] (2) and Ag(II)[Sn(IV)(SO₃F)₆] (3) indicated Curie-Weiss behavior for the compounds down to liquid nitrogen temperature. However, stronger magnetic exchange interactions may be present at lower temperatures in Ag(II)[Pt(IV)(SO₃F)₆] (3) and Pd(II)[Pt(IV)(SO₃F)₆] (2), where the tetravalent cation is a transition metal ion, i.e. Pt(IV), although no magnetic exchange is observed in the two samples down to ~80 K (3,2).

Even though the above described superexchange mechanism may be valid for the Pd(II)[Pd(IV)(SO₃F)₆] complex, for the binary Ni(SO₃F)₂, Pd(SO₃F)₂, and Ag(SO₃F)₂ compounds detailed magneto-structural relationships cannot be made, especially in the absence of

structural evidence from single crystal X-ray studies. This is also true in the case of the corresponding trifluoromethylsulfate derivatives discussed below.

Crystal growth was, however, attempted for $\text{Pd}(\text{SO}_3\text{F})_2$, " $\text{Pd}(\text{SO}_3\text{F})_3$ " and $\text{Ag}(\text{SO}_3\text{F})_2$, utilizing the method employed to obtain single crystals of $\text{Au}(\text{SO}_3\text{F})_3$, the structure of which was reported recently by our group (32). Unfortunately, the highly polymeric compounds formed only microcrystalline materials, unsuitable species for single crystal measurements.

In the following section, antiferromagnetic behavior in the divalent nickel, palladium and silver trifluoromethylsulfates will be discussed in some detail.

6.3.2 Antiferromagnetism of M(II) trifluoromethylsulfates $\text{Ni}(\text{SO}_3\text{CF}_3)_2$, $\text{Pd}(\text{SO}_3\text{CF}_3)_2$ and $\text{Ag}(\text{SO}_3\text{CF}_3)_2$

It was mentioned in the introduction that in previous magnetic susceptibility studies to ~80 K, the only four sulfonates which had detectable magnetic exchange all showed antiferromagnetism, which is observed more frequently than ferromagnetism in magnetically concentrated transition metal compounds (16,33).

In this study, the magnetic measurements on $\text{Ag}(\text{SO}_3\text{CF}_3)_2$ were extended down to ~4 K to complete the earlier Gouy work, and also to detect unusual magnetic properties, if any, at lower temperatures. The results of the low temperature study are given in Table 6.8, together with the previous Gouy data obtained for the compound. Similarly, the $\text{Pd}(\text{SO}_3\text{CF}_3)_2$ and $\text{Ni}(\text{SO}_3\text{CF}_3)_2$ complexes are investigated here for their possible antiferromagnetic behavior, and pertinent low temperature data for the two compounds are shown in Tables 6.9 and 6.10 respectively. The nickel compound is also measured in the higher temperature range of ~292 to 80 K by the Gouy method, and the results of this work are presented in Table 6.11.

Table 6.8: Magnetic Data of $\text{Ag}(\text{SO}_3\text{CF}_3)_2$ for the Temperature Range 304 to 4 K

Temperature (K) ^a	$\chi_M^{\text{corr}} \times 10^6$ ($\text{cm}^3 \text{mol}^{-1}$)	$\mu_{\text{eff}} (\mu_B)^b$
304	1100	1.64
278	1150	1.60
254	1200	1.56
226	1270	1.52
204	1320	1.47
179	1380	1.41
154	1420	1.32
128	1430	1.21
108	1390	1.10
82.06	650	0.66
78.28	630	0.63
70.34	620	0.59
65.82	610	0.57
60.38	570	0.53
47.80	550	0.46
40.40	540	0.42
31.85	540	0.37
26.35	520	0.33
21.40	520	0.30
16.55	510	0.26
11.20	510	0.21
8.04	510	0.18
5.34	510	0.15
4.39	510	0.13

^a First nine data points from Ref. 4.

^b Not corrected for TIP; $\mu_{\text{eff}} = 2.828 [\chi_M^{\text{corr}} \times T]^{1/2}$

Table 6.9: Low Temperature Magnetic Data of Pd(SO₃CF₃)₂

Temperature (K)	$\chi_M^{\text{corr}} \times 10^6$ (cm ³ mol ⁻¹)	$\mu_{\text{eff}} (\mu_B)^a$
123.2	6950	2.62
118.0	7220	2.61
112.8	7460	2.59
108.2	7730	2.59
103.0	8030	2.57
97.97	8330	2.55
93.46	8690	2.55
88.31	9020	2.52
84.81	9350	2.52
81.95	9670	2.52
78.33	9970	2.50
74.47	10180	2.46
70.23	10540	2.43
68.46	10630	2.41
65.59	10990	2.40
60.40	11530	2.36
54.45	12190	2.30
51.40	12550	2.27
47.92	13030	2.24
44.20	13510	2.19
40.32	14140	2.14
31.60	15700	1.99
20.88	17970	1.73
16.00	19020	1.56
10.75	20220	1.32
7.52	21060	1.13
5.78	21330	0.99
5.62	21630	0.99
4.32	21720	0.87
3.70	21330	0.79
2.99	21270	0.71
2.40	21270	0.64
2.10	21240	0.60

^a Not corrected for TIP; $\mu_{\text{eff}} = 2.828 [(\chi_M^{\text{corr}} \times T)]^{1/2}$

Table 6.10: Low Temperature Magnetic Data of Ni(SO₃CF₃)₂

Temperature (K)	$\chi_M^{\text{corr}} \times 10^6$ (cm ³ mol ⁻¹)	μ_{eff} (μ_B) ^a
81.78	16620	3.27
77.72	17360	3.26
74.19	18200	3.26
69.72	19240	3.25
65.19	20570	3.25
60.15	22160	3.24
54.00	24290	3.22
47.60	27270	3.21
40.10	31970	3.19
30.80	41390	3.18
25.93	48220	3.15
20.70	58650	3.11
15.90	74230	3.07
10.42	105700	2.96
7.16	140000	2.83
5.92	159800	2.75
4.85	181500	2.65
4.78	182100	2.64
3.96	200300	2.52
3.29	213900	2.37
3.11	220000	2.34
2.79	230400	2.27
2.60	234600	2.21
2.50	236200	2.17

^a $\mu_{\text{eff}} = 2.828 [(\chi_M^{\text{corr}} - \text{TIP})T]^{1/2}$; $\text{TIP} = 8N\beta^2/10Dq = 284 \times 10^{-6} \text{ cm}^3 \text{ mol}^{-1}$

Table 6.11: Magnetic Data of Ni(SO₃CF₃)₂ for the Temperature Range 292 to 80 K

Temperature (K)	$\chi_M^{\text{corr}} \times 10^6$ (cm ³ mol ⁻¹)	$\mu_{\text{eff}} (\mu_B)^a$
291.8	5270	3.41
286.2	5390	3.42
269.3	5700	3.42
251.7	6050	3.41
234.5	6450	3.40
218.0	6890	3.39
200.3	7380	3.37
175.7	8310	3.36
150.0	9540	3.33
125.5	11320	3.33
103.0	13510	3.30
86.5	15740	3.27
79.6	16890	3.25

^a $\mu_{\text{eff}} = 2.828 [(\chi_M^{\text{corr}} - \text{TIP})T]^{1/2}$; $\text{TIP} = 8N\beta^2/10Dq = 284 \times 10^{-6} \text{ cm}^3 \text{ mol}^{-1}$

The previous magnetic report on $\text{Ag}(\text{SO}_3\text{CF}_3)_2$ where antiferromagnetic behavior was seen with χ_{max} at ~ 138 K (4) is further confirmed by the present low temperature study. The magnetic moments decrease continuously with decreasing temperature, and the susceptibility also follows a similar trend, falling rapidly in value below the Néel temperature (Table 6.8). The very small magnetic moments observed down to ~ 4 K indicate that the compound has no ferromagnetic component present in the low temperature region. This behavior of $\text{Ag}(\text{SO}_3\text{CF}_3)_2$ is in contrast to the magnetic behavior of AgF_2 , in which ferromagnetism is detected below 163 K (28).

Therefore, it seems that structural differences in AgF_2 and $\text{Ag}(\text{SO}_3\text{CF}_3)_2$ play significant roles in determining the extent of antiferromagnetic coupling, although the exact exchange mechanism remains still unclear in the $\text{Ag}(\text{SO}_3\text{CF}_3)_2$ compound. It has been shown that in octahedrally coordinated transition metal d^9 fluorides, the Jahn-Teller effect leads to two crystallographic distortions, termed ferro and antiferrodistortive ordering, with the former favoring antiferromagnetism and the latter ferromagnetism (34). In AgF_2 , the ferromagnetic units are coupled antiparallel, which give a bulk 3D antiferromagnetism to the compound, although spin canting produces a small ferromagnetic component below 163K (28). However, in layer type fluoride structures with Jahn-Teller ions, the intralayer ferromagnetic couplings are much stronger than the interlayer antiferromagnetic couplings, as postulated in the case of $\text{Ag}(\text{SO}_3\text{F})_2$ discussed earlier, leading to ferromagnetism (17). But in contrast, the magnetic behavior observed in $\text{Ag}(\text{SO}_3\text{CF}_3)_2$ may arise from strong interlayer antiparallel coupling of the spins with weak intralayer exchange, resulting in a bulk 3D antiferromagnetism for the compound.

The magnetic data obtained for $\text{Pd}(\text{SO}_3\text{CF}_3)_2$ also clearly indicate antiferromagnetic behavior, where the magnetic moments calculated in the temperature range ~ 123 to 2K show typical temperature dependent low values (Table 6.9). The moments decrease with decreasing temperature, and a sharp decline becomes apparent below ~ 40 K, as seen in the magnetic

moment vs. temperature plot for the compound illustrated in Figure 6.7. From a previously unpublished study in our group, the room temperature magnetic moment for $\text{Pd}(\text{SO}_3\text{CF}_3)_2$ was found as $2.90 \mu_{\text{B}}$ (35). This value seems to be reasonable when compared with the μ_{eff} of $2.62 \mu_{\text{B}}$ obtained at 123 K in this study (Table 6.9), and it also confirms the continuous decreasing trend of the magnetic moments with decreasing temperatures. The higher temperature μ_{eff} value is not unexpected for an octahedrally coordinated Pd(II), where the moments are lowered by antiferromagnetic exchange.

The magnetic susceptibility vs. temperature plot of $\text{Pd}(\text{SO}_3\text{CF}_3)_2$, shown in Figure 6.8, has a χ_{max} at approximately 4K. This is conclusive evidence, as in $\text{Ag}(\text{SO}_3\text{CF}_3)_2$, that the spins in the palladium compound are coupled antiferromagnetically. The appearance of χ_{max} at a very low temperature, in contrast to the χ_{max} observed at 138 K in $\text{Ag}(\text{SO}_3\text{CF}_3)_2$ (4), indicates that in the palladium compound the antiferromagnetic interaction is much weaker than in the corresponding silver species. It is not uncommon however, to observe stronger spin couplings in a d^9 -Jahn-Teller system than in a d^8 -octahedral system.

Significant differences are also noted between the magnetic behavior of $\text{Pd}(\text{SO}_3\text{CF}_3)_2$ and its fluoride derivative PdF_2 . The difluoride, although antiferromagnetic with a Néel temperature of $\sim 217\text{K}$, shows a ferromagnetic magnetization component ("weak ferromagnetism") below this temperature (27). Consequently, the magnetic moment of $1.84 \mu_{\text{B}}$ found at room temperature has a much larger value at lower temperatures. This magnetic behavior of PdF_2 , as in the case of AgF_2 (28), is accounted for by Moriya's theory of single-ion magnetocrystalline anisotropy (30), where the preferred direction of magnetization is different for the nonequivalent magnetic ions, leading to a canting of the spins.

This is in contrast to the magnetic properties of $\text{Pd}(\text{SO}_3\text{CF}_3)_2$, in which a continuous decreasing trend of the magnetic moments with decreasing temperatures is observed (Figure

Figure 6.7: Magnetic Moment vs. Temperature of $\text{Pd}(\text{SO}_3\text{CF}_3)_2$

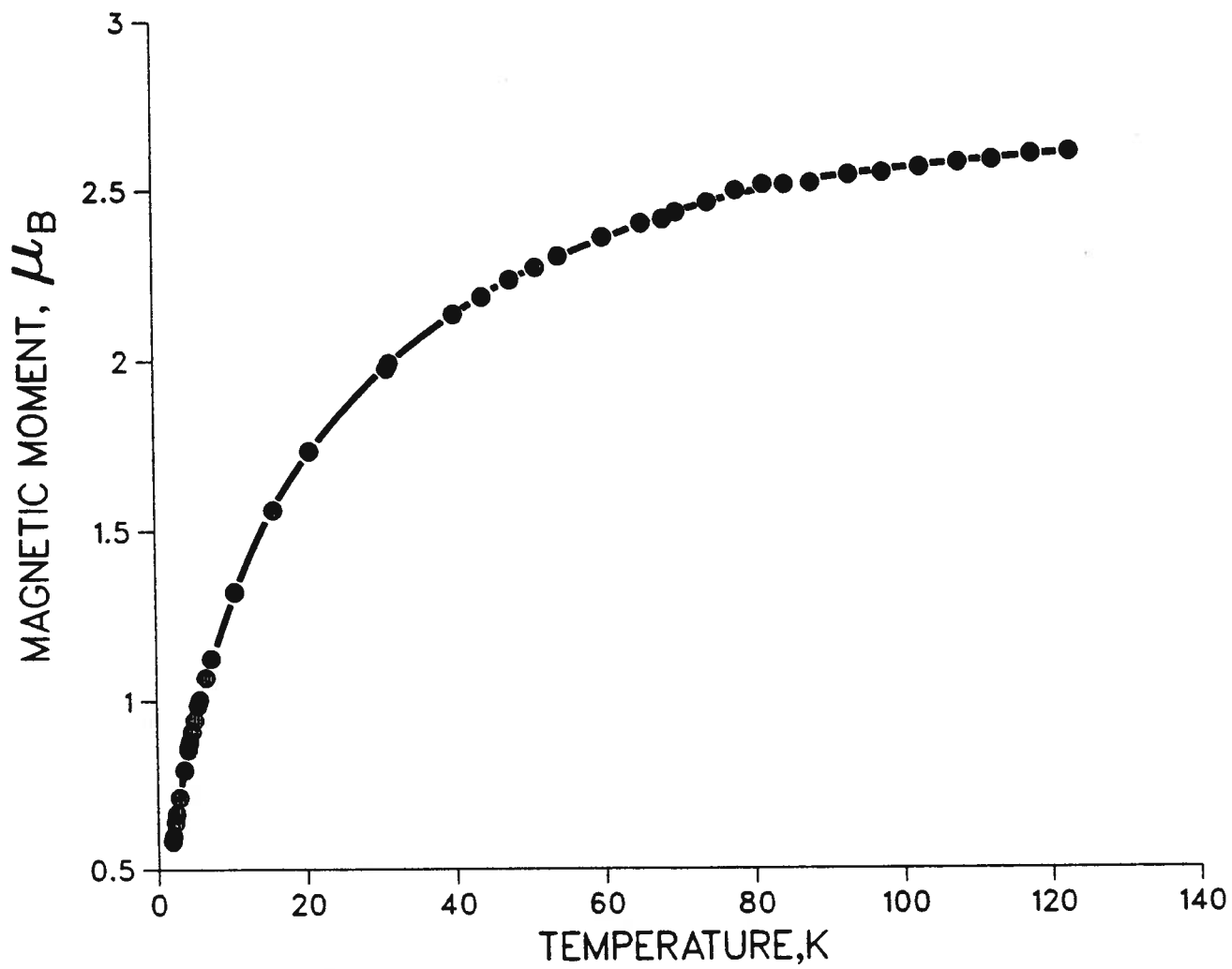
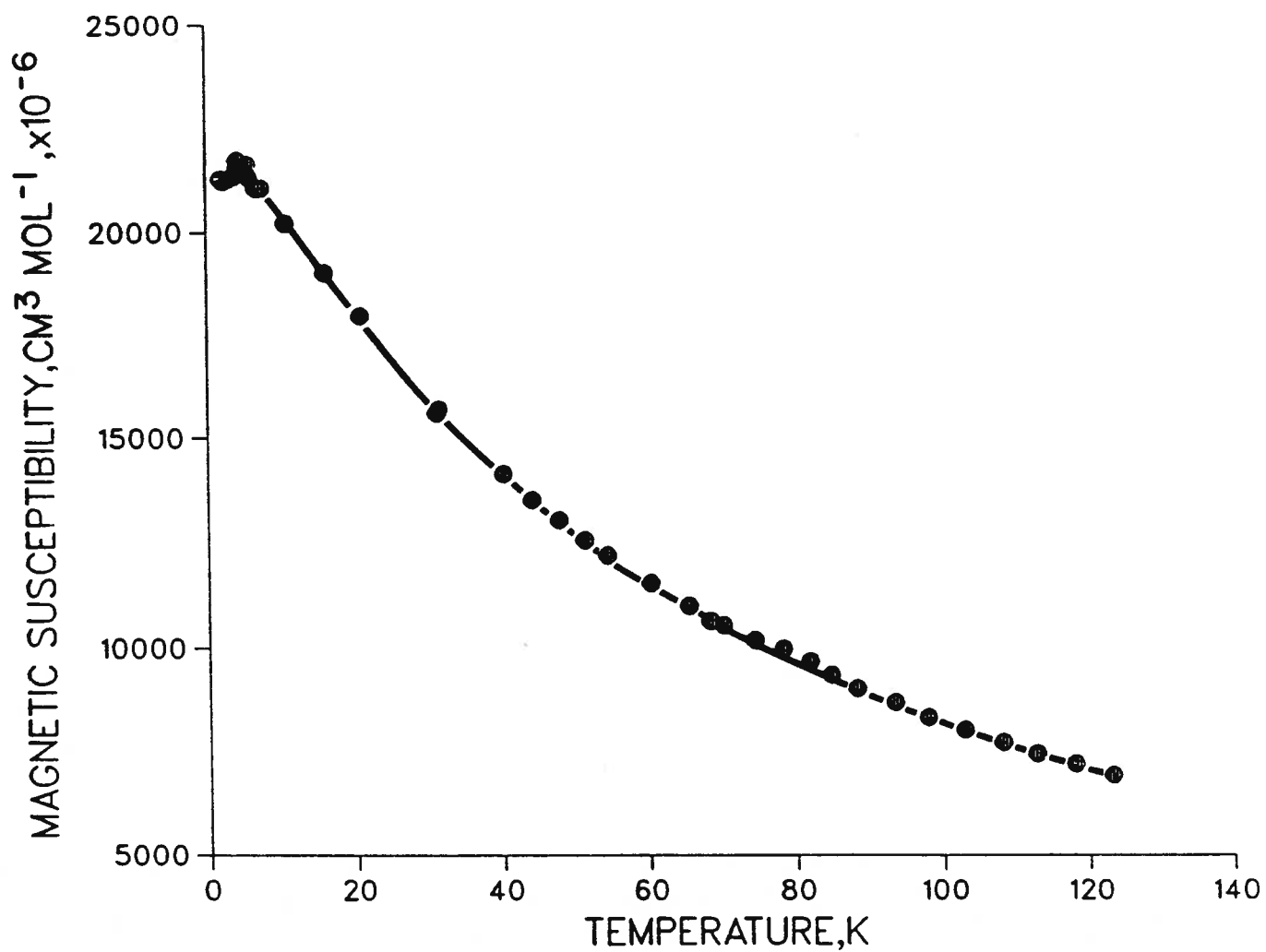


Figure 6.8: Magnetic Susceptibility vs. Temperature of $\text{Pd}(\text{SO}_3\text{CF}_3)_2$



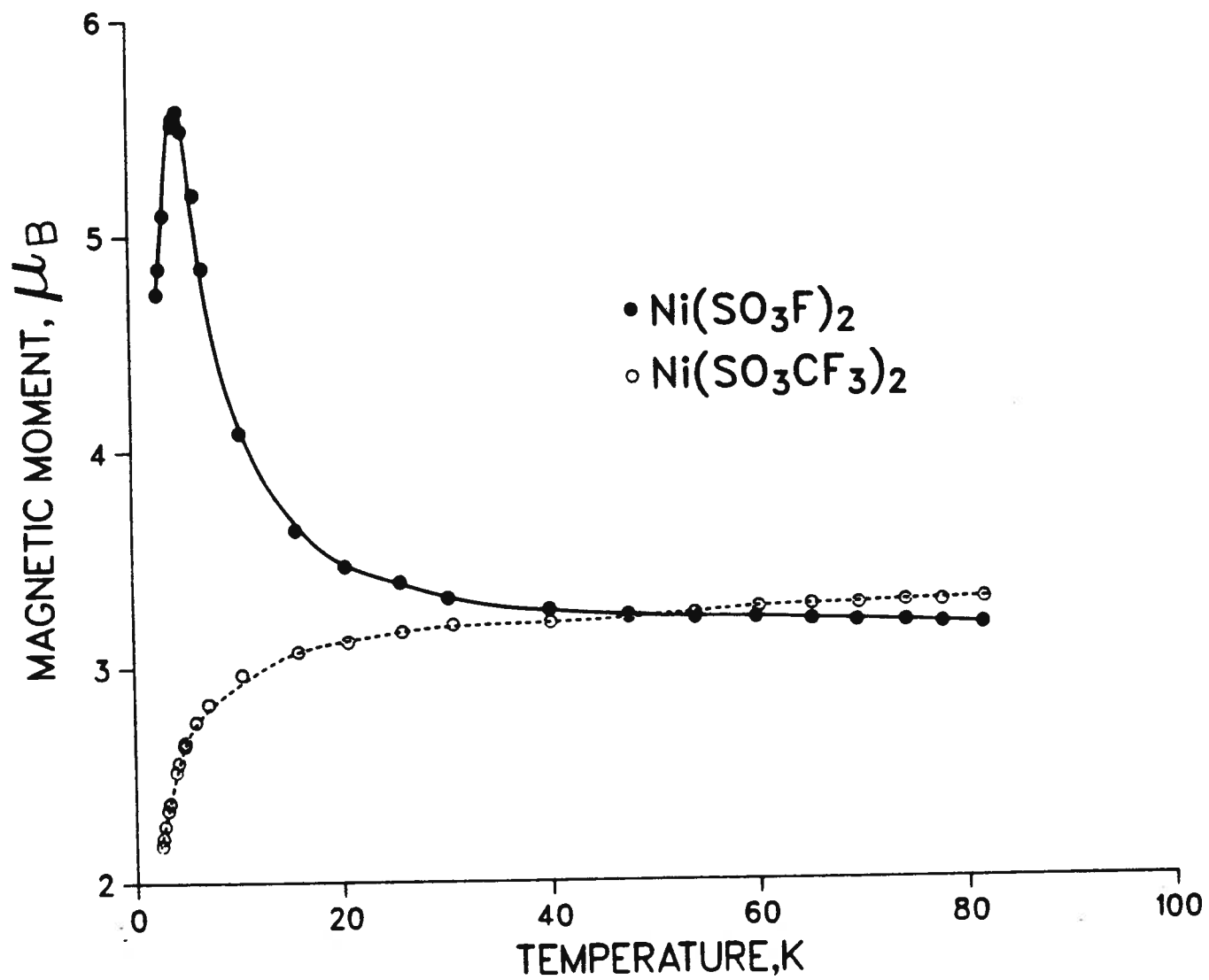
6.7), with the susceptibility also falling off below the Néel temperature of ~ 4 K (Figure 6.8). It appears from these observations that in $\text{Pd}(\text{SO}_3\text{CF}_3)_2$ the dominant magnetic interaction is antiferromagnetic and unlike PdF_2 , weak ferromagnetism is not seen at lower temperatures in the trifluoromethylsulfate compound.

The magnetic results of $\text{Ni}(\text{SO}_3\text{CF}_3)_2$, illustrated in Tables 6.10 and 6.11, show temperature dependent magnetic moments that decrease with the gradual lowering of the temperature, indicative of antiferromagnetic interaction among the Ni(II) centers. Excellent agreement is noted between the Gouy and the vibrating sample magnetometer data for the overlap region. The Gouy data (Table 6.11) in the temperature range 292 to 80 K are plotted as $1/\chi_M$ vs. T, and the following Weiss and Curie constants are obtained respectively: $\theta = -12.56$ K and $C_m = 1.52$ $\text{cm}^3 \text{mol}^{-1}$ K. The negative Weiss constant is characteristic of antiferromagnetism, and this behavior in $\text{Ni}(\text{SO}_3\text{CF}_3)_2$ is further confirmed by the low temperature magnetic data given in Table 6.10.

The μ_{eff} of $3.41 \mu_B$ calculated at room temperature falls within the expected range for an octahedrally coordinated Ni(II) species. However, curiously this value is slightly larger than the moment of $3.26 \mu_B$ found at the same temperature for the corresponding $\text{Ni}(\text{SO}_3\text{F})_2$ (Table 6.5), although both compounds appear to have similar electronic environments for the respective Ni(II) ions with near identical $10Dq$ values (1,21,19). Furthermore, the antiferromagnetic $\text{Ni}(\text{SO}_3\text{CF}_3)_2$ is expected to have a lower moment at room temperature than its ferromagnetic fluorosulfate derivative, analogous to the palladium and silver derivatives discussed previously.

Interestingly, when the low temperature magnetic moments are plotted against temperature, the effects of magnetic coupling interactions for $\text{Ni}(\text{SO}_3\text{CF}_3)_2$ and $\text{Ni}(\text{SO}_3\text{F})_2$ become observable nearly at the same temperature, but are of opposite nature, as illustrated in Figure 6.9.

Figure 6.9: Magnetic Moment vs. Temperature of $\text{Ni}(\text{SO}_3\text{CF}_3)_2$ and $\text{Ni}(\text{SO}_3\text{F})_2$



In contrast to $\text{Pd}(\text{SO}_3\text{CF}_3)_2$ and $\text{Ag}(\text{SO}_3\text{CF}_3)_2$, the nickel derivative does not have a χ_{max} in its susceptibility data. Therefore, the decrease of the moment values with decreasing temperature is less pronounced in the case of $\text{Ni}(\text{SO}_3\text{CF}_3)_2$ (Table 6.10).

These observations indicate that the antiferromagnetic interaction in the nickel species is relatively weak in comparison to that in the palladium and silver derivatives. The magnetic behavior observed in $\text{Ni}(\text{SO}_3\text{CF}_3)_2$ differs also from the reported antiferromagnetism of the corresponding binary fluoride NiF_2 , where a weak ferromagnetic moment is detected below the Néel temperature of 73.2 K, which is attributed, as in AgF_2 and PdF_2 discussed previously, to spin canting (30). The theoretical basis of this phenomenon has been developed extensively by Moriya in his study of the magnetic behavior of NiF_2 (30).

In concluding this discussion on the magnetic exchange interactions of the M(II) sulfonates, a few comments will be made here regarding the magnetic behavior of the corresponding copper derivatives. A previous magnetic study of $\text{Cu}(\text{SO}_3\text{F})_2$ and $\text{Cu}(\text{SO}_3\text{CF}_3)_2$ (down to 100 and 127 K respectively) indicated that the salts are essentially magnetically dilute with moments normally observed for hexacoordinated copper(II) (15). For this work, the magnetic measurements on the $\text{Cu}(\text{SO}_3\text{F})_2$ is extended down to ~4 K, and a summary of the data is given in Appendix B-7. The compound was synthesized according to the method described by Alleyne et al. (13). The magnetic moments calculated are independent of temperature and remain close to the expected value of $\sim 2.0 \mu_{\text{B}}$ down to ~4 K. Good agreement is also noted in the overlap region between the previous high temperature μ_{eff} values and the low temperature moments of this study. The reason for this magnetically dilute behavior of $\text{Cu}(\text{SO}_3\text{F})_2$ is not clear, and it is rather surprising to note that while $\text{Ag}(\text{SO}_3\text{F})_2$ shows strong magnetic exchange below ~10 K, the corresponding Group 11 copper derivative is magnetically dilute down to very low temperatures. Interestingly, the copper(II) difluoride is antiferromagnetic with a Néel temperature of 69 K, and as seen previously in AgF_2 , PdF_2 and NiF_2 , spin canting produces a

weak ferromagnetic moment below the Néel temperature in CuF_2 as well (37).

In summary, it may be envisioned that in the layer type metal(II) sulfonates discussed in this Chapter, magnetic exchange may occur preferentially via one of two possible spin interactions: ferromagnetism in the fluorosulfate compounds could arise from strong intralayer parallel spin coupling, while in the corresponding trifluoromethylsulfate derivatives predominant interlayer spin coupling could lead to an antiparallel arrangement of the spins in the lattice. Alternatively, the O-S-O bridging angle in the two types of sulfonates may favor ferromagnetism and antiferromagnetism for the fluorosulfates and trifluoromethylsulfates respectively. Although the exchange pathway cannot be stated clearly in these compounds due to a lack of X-ray crystal data, it is interesting to note that in the divalent sulfates FeSO_4 , NiSO_4 and CuSO_4 which also have oxygen bridging extended 3D lattice structures, antiferromagnetic ordering is postulated to occur through the O-S-O bridges (38,39). Furthermore, neutron diffraction data obtained on FeSO_4 and NiSO_4 indicate magnetically ordered sheet-type structures, and the structurally similar CrVSO_4 appears to have ferromagnetically ordered sheets which stack antiferromagnetically (38). In other examples involving sulfate derivatives, the compounds are found as linear chains, and their magnetic properties have been analyzed utilizing either the Ising or Heisenberg exchange coupling models (40).

In the case of the sulfonates discussed here, however, analyzing the magnetic data is made difficult by several factors. The choice of either the Ising or Heisenberg 2-D model is usually not appropriate for the metal(II) sulfonates. These models do not apply to a system where three-dimensional interactions are also present in the lattice structure. The one dimensional models of the type used in Chapter 5 cannot be utilized for the sulfonates for the same reason. The available 2-D Heisenberg model is not applicable in this instance, as this model only takes into account interactions between one paramagnetic center and only the four (but not six) nearest neighbors in a square array. In contrast, for the metal(II) sulfonates, the

proposed structure consists of each metal center being surrounded by six nearest neighbours (see Figure 6.1). It appears that the degree and sign of magnetic exchange in these compounds is a function of the O-S-O bridging angle, the M-O and S-O bond distances and the steric and electronic properties of the CF₃ and F groups. Unfortunately, in the absence of any X-ray single crystal data it is rather difficult to make detailed magneto-structural correlations for these sulfonates in order to explain the observed magnetic interactions.

6.4 Conclusion

The paramagnetic divalent fluorosulfates Ni(SO₃F)₂, Pd(SO₃F)₂, Pd(II)[Pd(IV)(SO₃F)₆], and Ag(SO₃F)₂ and their corresponding trifluoromethylsulfate derivatives Ni(SO₃CF₃)₂, Pd(SO₃CF₃)₂ and Ag(SO₃CF₃)₂ investigated for their magnetic properties show significant magnetic exchange, and except in Ag(SO₃CF₃)₂, the effects of magnetic exchange become observable at low temperatures. Two types of magnetic interactions are seen in the respective groups of compounds. The fluorosulfates exhibit ferromagnetism at all temperatures, whereas the trifluoromethylsulfates couple antiferromagnetically with the spin interactions noted over a wider temperature range.

The fluorosulfates Pd(SO₃F)₂, "Pd(SO₃F)₃" and Ag(SO₃F)₂ were initially described as relatively magnetically dilute down to ~80 K, and similarly, the Ni(SO₃F)₂ compound studied here in the temperature range ~291 to 2 K also follows the Curie-Weiss law between ~291 and 79 K with $C_m = 1.34 \pm 0.01 \text{ cm}^3 \text{ mol}^{-1} \text{ K}$ and $\theta = 0.41 \pm 2 \text{ K}$. For the ferromagnetic M(II) fluorosulfates, the following field dependent maximum magnetic moments are obtained in the temperature range ~5 to 10.5 K: Ni(SO₃F)₂ 5.22 μ_B (5 K), Pd(SO₃F)₂ 8.11 μ_B (8 K), "Pd(SO₃F)₃" 6.08 μ_B (8 K), and Ag(SO₃F)₂ 7.14 μ_B (10.5 K). Furthermore, the maximum magnetic susceptibility values of Ni(SO₃F)₂, Pd(SO₃F)₂ and Ag(SO₃F)₂ appear to indicate, for the magnetic fields used, saturation magnetization where all the magnetic spins align parallel to

the external magnetic field. Although the mixed valency fluorosulfate "Pd(SO₃F)₃" shows significant ferromagnetism at low temperatures, the structurally similar bimetallic fluorosulfates Ni(II)[Sn(IV)(SO₃F)₆], Cu(II)[Sn(IV)(SO₃F)₆] and Ag(II)[Sn(IV)(SO₃F)₆] are found to be magnetically dilute down to ~4 K with calculated temperature independent magnetic moments of ~3.3, ~2.0, and ~1.8 μ_B respectively.

In contrast to the fluorosulfates, the divalent trifluoromethylsulfate derivatives couple antiferromagnetically, and maxima in the susceptibility vs. temperature plots are noted for Pd(SO₃CF₃)₂ and Ag(SO₃CF₃)₂ at ~4 and ~138 K respectively. However, Ni(SO₃CF₃)₂ does not show a χ_{max} in its susceptibility plot, indicative of a weaker magnetic concentration in the compound. The magnetic moments of the three compounds decrease continuously with decreasing temperatures, and hence no ferromagnetic contribution to the magnetic moments is detected at lower temperatures. Therefore, the antiferromagnetic behavior observed in Ni(SO₃CF₃)₂, Pd(SO₃CF₃)₂, and Ag(SO₃CF₃)₂ seems to differ from that seen in the corresponding antiferromagnetic fluorides NiF₂, PdF₂, and AgF₂, where a ferromagnetic magnetization component due to spin canting is detected at lower temperatures.

Although the exchange pathways of the divalent sulfonates cannot be explained adequately due to a lack of X-ray single crystal data, the common layer type structure appears to indicate a possible intralayer vs. interlayer spin interaction, leading to predominantly parallel and antiparallel spin arrangements in the respective fluorosulfate and trifluoromethylsulfate lattices. However, the magnetic behavior observed in these sulfonates may be dependent on the O-S-O bridge angle, which may result in ferro- or antiferromagnetism for the respective groups of compounds investigated in this study.

References

1. K.C. Lee and F. Aubke, Can. J. Chem., **55**, 2473 (1977).
2. K.C. Lee and F. Aubke, Can. J. Chem., **57**, 2058 (1979).
3. P.C. Leung and F. Aubke, Inorg. Chem., **17**, 1765 (1978).
- 4.a) P.C. Leung, K.C. Lee, and F. Aubke, Can. J. Chem., **57**, 326 (1979).
b) P.C. Leung, Ph.D. Thesis, University of British Columbia (1979).
5. S.P. Mallela, J.R. Sams, and F. Aubke, Can. J. Chem., **63**, 3305 (1985).
6. J.R. Sams, R.C. Thompson, and T.B. Tsin, Can. J. Chem., **55**, 115 (1977).
7. J. Goubeau and J.B. Milne, Can. J. Chem., **45**, 2321 (1967).
8. P.C. Leung and F. Aubke, Can. J. Chem., **62**, 2892 (1984).
9. P.C. Leung, G.B. Wong, and F. Aubke, J. Fluorine Chem., **35**, 607 (1987).
10. J.M. Taylor and R.C. Thompson, Can. J. Chem., **49**, 511 (1971).
11. K.C. Lee and F. Aubke, J. Fluorine Chem., **19**, 501 (1982).
12. K.C. Lee and F. Aubke, Can. J. Chem., **59**, 2835 (1981).
13. C.S. Alleyne, K.O. Mailer, and R.C. Thompson, Can. J. Chem., **52**, 336 (1974).
14. J.S. Haynes, J.R. Sams, and R.C. Thompson, Can. J. Chem., **59**, 669 (1981).
15. A.L. Arduini, M. Garnett, R.C. Thompson, and T.C.T. Wong, Can. J. Chem., **53**, 3812 (1975).
- 16.a) G. Muller, Angew. Chem. Int. Ed. Engl., **26**, 1081 (1987).
b) L.N. Mulay in "Theory and Applications of Molecular Paramagnetism", Eds. E.A. Boudreaux and L.N. Mulay, John Wiley and Sons, New York, 1976.
17. J.-M. Dance and A. Tressaud in "Inorganic Solid Fluorides", Ed. P. Hagenmuller, Academic Press, New York, 1985.
18. A. Tressaud, J.-M. Dance, and P. Hagenmuller, Israel J. Chem., **17**, 126 (1978).
19. M.T. Jansky and J.T. Yoke, J. Inorg. Nucl. Chem., **41**, 1707 (1979).

- 20.a) D.C. Adams, T. Birchall, R. Faggiani, R.J. Gillespie, and J.E. Vekris, Can. J. Chem., **69**, 2122 (1991).
- b) F. Charbonnier, R. Faure, and H. Loiseleur, Acta Cryst., **B33**, 1478 (1977).
21. D.A. Edwards, M.J. Stiff, and A.A. Woolf, Inorg. Nucl. Chem. Letters, **3**, 427 (1967).
22. R.L. Carlin, "Magnetochemistry", Springer-Verlag, New York, 1986.
23. C. Starr, F. Bitter, and A.R. Kaufmann, Phys. Rev., **58**, 977 (1940).
24. M.K. Wilkinson, J.W. Cable, E.O. Wollan, and W.C. Koehler, Phys. Rev., **113**, 497 (1959).
25. E. Stryjewski and G. Giordano, Adv. in Physics, **26**, 487 (1977).
26. C. Starr, Phys. Rev., **58**, 984 (1940).
- 27.a) N. Bartlett and P.R. Rao, Proc. Chem. Soc., 393 (1964).
- b) P.R. Rao, R.C. Sherwood, and N. Bartlett, J. Chem. Phys., **49**, 3728 (1968).
- 28.a) E. Gruner and W. Klemm, Naturwissenschaften, **59**, 25 (1937).
- b) P. Charpin, A.J. Dianoux, H. Marquet-Ellis, and C.R. Nguyen-Nghi, Acad. Sci. Fr., **C264**, 1108 (1967).
- c) P. Charpin, P. Plurien, and P. Meriel, Bull. Soc. Fr. Mineral Cristollogr., **93**, 7 (1970).
- d) P. Fischer, G. Roult, and D. Schwarzenbach, J. Phys. Chem. Solids, **32**, 1641 (1971).
29. A. Tressaud, M. Wintenberger, N. Bartlett, and P. Hagenmuller, C.R. Acad. Sci. Fr., **C282**, 1069 (1976).
- 30.a) T. Moriya, Phys. Rev., **117**, 635 (1960).
- b) L.M. Matarrese and J.W. Stout, Phys. Rev., **94**, 1792 (1954).
31. S.P. Mallela, K. Lee, P.F. Gehrs, J.I. Christensen, J.R. Sams, and F. Aubke, Can. J. Chem., **65**, 2649 (1987).
32. H. Willner, S.J. Rettig, J. Trotter, and F. Aubke, Can. J. Chem., **69**, 391 (1991).
33. W.E. Hatfield, W.E. Estes, W.E. Marsh, M.W. Pickens, L.W. ter Haar, and R.R. Weller in "Extended Linear Chain Compounds", Ed. J.S. Miller, Plenum Press, New York, 1983.

34. D. Reinen and C. Friebel in "Structure and Bonding", Eds. J.D. Dunitz, P. Hemmerich, C.K. Jorgensen, and D. Reinen, Vol. 37, Springer-Verlag, Berlin, 1979.
35. S.P. Mallela and F. Aubke, unpublished results.
36. F.A. Cotton and G. Wilkinson, "Advanced Inorganic Chemistry", 5th Edition, John Wiley and Sons, New York, 1989.
37. R.J. Joenk and R.M. Bozorth, J. Appl. Phys., 36, 1167 (1965).
38. B.C. Frazer and P.J. Brown, Phys. Rev., 125, 1283 (1962).
39. I. Almodovar, B.C. Frazer, J.J. Hurst, D.E. Cox, and P.J. Brown, Phys. Rev., 138, A153 (1965).
40. H.T. Witteveen and J. Reedijk, J. Solid State Chem., 10, 151 (1974).

preparation. The solvolysis product show temperature dependent low μ_{eff} values, whereas the fluorination sample has unexpectedly high magnetic moments, which also decrease with decreasing temperature.

As a preparative method, there appears to be a wide synthetic potential for this solvolysis route to the corresponding metal hexafluoro antimonates, since a large number of well characterized transition metal fluorosulfates are available as precursors.

The transition metal precursors of the hexafluoro antimonates, the divalent fluorosulfates $\text{Ni}(\text{SO}_3\text{F})_2$, $\text{Pd}(\text{SO}_3\text{F})_2$, $\text{Ag}(\text{SO}_3\text{F})_2$, and the ternary " $\text{Pd}(\text{SO}_3\text{F})_3$ " all exhibit ferromagnetic exchange at lower temperatures. Additionally, the three binary fluorosulfate compounds indicate saturation magnetization at very low temperatures. In contrast, the corresponding trifluoromethylsulfates $\text{Ni}(\text{SO}_3\text{CF}_3)_2$, $\text{Pd}(\text{SO}_3\text{CF}_3)_2$ and $\text{Ag}(\text{SO}_3\text{CF}_3)_2$ couple antiferromagnetically, and for the last two compounds χ_{max} are also found in their susceptibility vs. temperature plots. The antiferromagnetism observed in these compounds differ from that seen in the corresponding binary fluorides, in that no ferromagnetic magnetization component due to spin canting is detected even at very low temperatures. Interestingly, both the divalent hexafluoro antimonates and the sulfonates studied in this work have a common layered structure which is based on the CdCl_2 prototype.

Furthermore, the two post-transition metal layered compounds $\text{Sn}(\text{SO}_3\text{F})_2$ and $\text{Sn}(\text{SbF}_6)_2$, which are structurally similar to their transition metal derivatives mentioned above, form π -arene adducts with mesitylene(mes) to give the weakly bound complexes $\text{Sn}(\text{SO}_3\text{F})_2 \cdot \text{mes}$ and $\text{Sn}(\text{SbF}_6)_2 \cdot 2\text{mes}$ in high yield. The reduction of the lattice energies in the layer structures of the parent tin compounds by the weakly nucleophilic anions SbF_6^- and SO_3F^- appear to facilitate adduct formation, with the weaker nucleophile SbF_6^- been the more effective of the two ions, leading to the 2:1 complex with the arene. Mössbauer data of the adducts indicate

partial back-donation of the 5s electrons of tin to the antibonding π^* orbitals of mesitylene to further stabilize the tin-arene bond, giving rise to synergic bond characteristics.

The remaining group of non-transition metal fluoro complexes, the molecular species $O_2^+[AsF_6]^-$, $Br_2^+[Sb_3F_{16}]^-$ and $I_2^+[Sb_2F_{11}]^-$, which were investigated for their low temperature magnetic behavior, exhibit magnetic properties that are quite different for the three derivatives. This is reflected in the magnetic data of the respective complexes, measured down to $\sim 4K$. Of the halogen compounds, $Br_2^+[Sb_3F_{16}]^-$ is magnetically dilute to low temperatures, whereas $I_2^+[Sb_2F_{11}]^-$ show relatively strong antiferromagnetic coupling with a χ_{max} at 54K. As in $Br_2^+[Sb_3F_{16}]^-$, the $O_2^+[AsF_6]^-$ compound also exhibits Curie-Weiss behavior down to low temperatures, but weak antiferromagnetic exchange seems to be present in the very low end of the temperature region. In $Br_2^+[Sb_3F_{16}]^-$, the shortest non-bonding $Br \cdots Br$ distance is too large to invoke direct orbital overlap, but in $I_2^+[Sb_2F_{11}]^-$ magnetic exchange can occur via contiguous I_2^+ ions, where the non-bonding $I \cdots I$ distance is comparable to the sum of the van der Waals radii. The low μ_{eff} values observed for $O_2^+[AsF_6]^-$, which are below the spin only magnetic moment value, result from crystal field interactions in the solid lattice that partially quench the orbital contribution to the magnetic susceptibility.

APPENDICES

APPENDIX A

A-1: Standard Reduction Potentials of Selected (M/Mⁿ) Couples*

Electrode	Potential (V)
$\text{Ni}^{+2} + 2\text{e} \rightarrow \text{Ni}$	-0.250
$\text{Pd}^{+2} + 2\text{e} \rightarrow \text{Pd}$	+0.987
$\text{Cu}^{+} + \text{e} \rightarrow \text{Cu}$	+0.521
$\text{Cu}^{+2} + 2\text{e} \rightarrow \text{Cu}$	+0.337
$\text{Cu}^{+2} + \text{e} \rightarrow \text{Cu}^{+}$	+0.153
$\text{Ag}^{+} + \text{e} \rightarrow \text{Ag}$	+0.7991
$\text{Ag}^{+2} + \text{e} \rightarrow \text{Ag}^{+}$	+1.980
$\text{Au}^{+} + \text{e} \rightarrow \text{Au}$	+1.691
$\text{Au}^{+3} + 3\text{e} \rightarrow \text{Au}$	+1.498
$\text{Sn}^{+2} + 2\text{e} \rightarrow \text{Sn}$	-0.136
$\text{Sn}^{+4} + 2\text{e} \rightarrow \text{Sn}^{+2}$	+0.15
$\text{Sb}_2\text{O}_5 + 6\text{H}^{+} + 4\text{e} \rightarrow 2\text{SbO}^{+} + 3\text{H}_2\text{O}$	+0.581
$\text{Sb}_2\text{O}_5 + 2\text{H}^{+} + 2\text{e} \rightarrow 2\text{Sb}_2\text{O}_4 + \text{H}_2\text{O}$	+0.479
$\text{O}_2 + 4\text{H}^{+} + 4\text{e} \rightarrow 2\text{H}_2\text{O}(\text{l})$	+1.229
$\text{O}_2 + 4\text{H}^{+} + 4\text{e} \rightarrow 2\text{H}_2\text{O}(\text{g})$	+1.185

* From J.E. Huheey, "Inorganic Chemistry", 2nd Ed., Harper and Row, New York, 1978.

A-2: Frequency Range of Vibrational Fundamentals for Fluorosulfate Group

Symmetry		Frequency Range (cm ⁻¹)	
Bonding or Coordination Mode	Stretching Band	Deformation Band	
C _{3v}	COVALENT TRIDENTATE	$\nu_{\text{sym}}(\text{S-O})$ <input type="checkbox"/> $\nu_{\text{sym}}(\text{S-O})$ <input type="checkbox"/> $\nu(\text{S-F})$ <input checked="" type="checkbox"/>	$\delta_{\text{sym}}(\text{SO}_3)$ <input type="checkbox"/> $\delta_{\text{sym}}(\text{SO}_3)$ <input type="checkbox"/> ρ_{rect} <input type="checkbox"/>
	PURELY IONIC	$\nu_{\text{sym}}(\text{S-O})$ <input type="checkbox"/> $\nu_{\text{sym}}(\text{S-O})$ <input type="checkbox"/> $\nu(\text{S-F})$ <input checked="" type="checkbox"/>	$\delta_{\text{sym}}(\text{SO}_3)$ <input type="checkbox"/> $\delta_{\text{sym}}(\text{SO}_3)$ <input type="checkbox"/> ρ_{rect} <input type="checkbox"/>
C _s	IONIC PERTURBED	$\nu_{\text{sym}}(\text{SO}_2)$ <input checked="" type="checkbox"/> $\nu_{\text{sym}}(\text{SO}_2)$ <input checked="" type="checkbox"/> $\nu(\text{S-O})$ <input type="checkbox"/> $\nu(\text{S-O})$ <input type="checkbox"/> $\nu(\text{S-F})$ <input checked="" type="checkbox"/>	$\delta_{\text{band}}(\text{SO}_2)$ <input type="checkbox"/> $\tau_{\text{rect}}(\text{SO}_2)$ <input type="checkbox"/> $\tau_{\text{rect}}(\text{SO}_2\text{F})$ <input type="checkbox"/> $\tau_{\text{rect}}(\text{S-F})$ <input type="checkbox"/> $\tau(\text{SO}_2\text{F})$ <input type="checkbox"/>
	COVALENT MONODENTATE	$\nu_{\text{sym}}(\text{SO}_2)$ <input type="checkbox"/> $\nu_{\text{sym}}(\text{SO}_2)$ <input type="checkbox"/> $\nu(\text{S-O})$ <input checked="" type="checkbox"/> $\nu(\text{S-O})$ <input checked="" type="checkbox"/> $\nu(\text{S-F})$ <input type="checkbox"/>	$\tau_{\text{rect}}(\text{SO}_2)$ <input type="checkbox"/> $\delta_{\text{band}}(\text{SO}_2)$ <input type="checkbox"/> $\tau_{\text{rect}}(\text{S-F})$ <input type="checkbox"/> $\tau(\text{SO}_2\text{F})$ <input type="checkbox"/>
COVALENT BIDENTATE	$\nu(\text{S-O})$ <input type="checkbox"/> $\nu_{\text{sym}}(\text{SO}_2)$ <input checked="" type="checkbox"/> $\nu_{\text{sym}}(\text{SO}_2)$ <input checked="" type="checkbox"/>	$\delta_{\text{band}}(\text{SO}_2)$ <input type="checkbox"/> $\tau_{\text{rect}}(\text{SO}_2)$ <input type="checkbox"/> $\tau_{\text{rect}}(\text{S-F})$ <input type="checkbox"/> $\tau(\text{SO}_2\text{F})$ <input type="checkbox"/>	$\tau_{\text{rect}}(\text{SO}_2)$ <input type="checkbox"/> $\delta_{\text{band}}(\text{SO}_2)$ <input type="checkbox"/> $\tau_{\text{rect}}(\text{S-F})$ <input type="checkbox"/> $\tau(\text{SO}_2\text{F})$ <input type="checkbox"/>

A-3: X-ray Powder Data for Ni(SbF₆)₂

[Ni(SO ₃ F) ₂ + SbF ₅] ^a		[Ni + F ₂ + SbF ₅] ^b		[NiF ₂ + SbF ₅] ^c	
d-space (Å), Intensity		d-space (Å), Intensity		d-space (Å), Intensity	
4.60	m-s	4.61	m-s	4.56	m
4.17	s	4.24	s	4.26	m
		4.03	w	4.17	m
3.71	s	3.75	s	3.68	s
2.702	m	2.744	m-s	3.58	m
2.534	m-w	2.576	m-w	2.70	m
2.344	m-w	2.363	m	2.51	w
2.273	m-s	2.252	s	2.33	w
2.224	m	2.207	m-w	2.22	m
2.167	m	2.125	m-w	2.10	w
1.859	m	1.881	m	1.86	m
1.841	m	1.819	m		
1.768	w	1.746	w		
1.714	m-s	1.728	s		
1.704	m	1.681	m	1.70	m
1.648	m	1.646	m		
		1.625	w	1.61	m
1.553	vw	1.550	vw		
1.534	m-w	1.521	m	1.50	w
1.493	m	1.491	m	1.47	w
1.465	m	1.447	m-w	1.44	w
1.426	w	1.420	m-w		
1.398	w	1.377	w		
1.352	w	1.332	m		

^a This work

^b Christe et al., *J. Fluorine Chem.*, **34**, 287 (1987)

^c Gantar et al., *J. Chem. Soc. Dalton Trans.*, 2379 (1987)

A-4: The Assignments and Energies of Octahedral Ni(II) and Pd(II) (d⁸) Ligand Field Spectra, According to Lever,* are as Follows:

$${}^3A_{2g} \rightarrow {}^3T_{2g} \quad \nu_1 = 10Dq$$

$${}^3A_{2g} \rightarrow {}^3T_{1g}(F) \quad \nu_2 = 7.5B + 15Dq - 1/2(225B^2 + 100Dq^2 - 180DqB)^{1/2}$$

$${}^3A_{2g} \rightarrow {}^3T_{1g}(P) \quad \nu_3 = 7.5B + 15Dq + 1/2(225B^2 + 100Dq^2 - 180DqB)^{1/2}$$

$$\text{and, } \nu_3 + \nu_2 - 3\nu_1 = 15B$$

* A.B.P. Lever, J. Chem. Educ., **45**, 711 (1968).

[see also: Yu-Sheng Dou, J. Chem. Educ., **67**, 134 (1990)].

A-5: Low Temperature Magnetic Data of Ni(SbF₆)₂ Made from Ni, F₂ and SbF₅

Temperature [K]	$\chi_M^{\text{corr}} \times 10^6$ [cm ³ mol ⁻¹]	μ_{eff} [μ_B] ^a
81.83	17140	3.35
78.06	17930	3.35
74.19	18740	3.33
69.72	19830	3.33
65.19	21030	3.31
60.15	22660	3.30
55.00	24620	3.29
47.90	27610	3.25
40.60	32010	3.22
30.80	41040	3.18
26.00	47840	3.15
21.00	57360	3.10
15.90	73240	3.05
10.30	105600	2.95
7.16	140500	2.84
6.30	153800	2.78
5.18	174200	2.69
4.40	191900	2.60
3.96	201700	2.53
3.46	207900	2.40
3.11	215800	2.32
2.89	219900	2.25
2.79	221800	2.22

^a Uncorrected for TIP

A-6: Low Temperature Magnetic Data of Ni(SbF₆)₂ Made from NiF₂ and SbF₅ in HF

Temperature [K]	$\chi_M^{\text{corr}} \times 10^6$ [cm ³ mol ⁻¹]	μ_{eff} [μ_B] ^a
81.83	12000	2.80
78.06	12490	2.79
74.19	13170	2.79
69.72	14000	2.79
65.19	14900	2.79
60.15	16130	2.79
55.00	17750	2.79
47.90	20070	2.77
40.60	23450	2.76
31.23	30160	2.74
26.40	35040	2.72
21.00	43070	2.69
15.90	55980	2.67
10.75	78900	2.60
7.16	114600	2.56
6.15	132600	2.55
5.16	151700	2.50
4.40	173500	2.47
4.04	190700	2.48
3.70	199400	2.43
3.29	211000	2.36
3.11	218100	2.33
2.89	225600	2.28

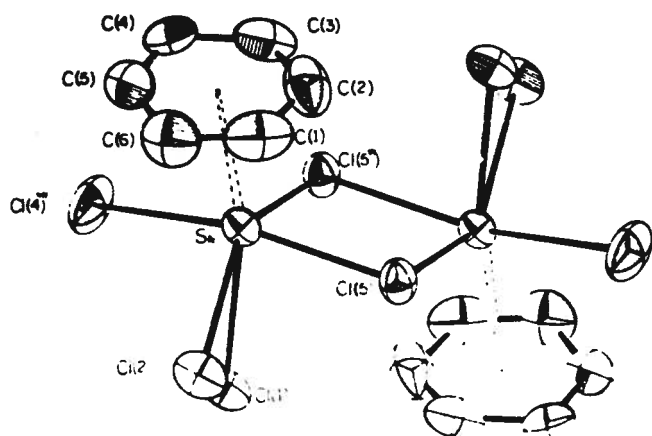
^a Uncorrected for TIP

A-7: Low Temperature Magnetic Data of $\text{Au}(\text{SO}_3\text{F})_x(\text{SbF}_6)_y$

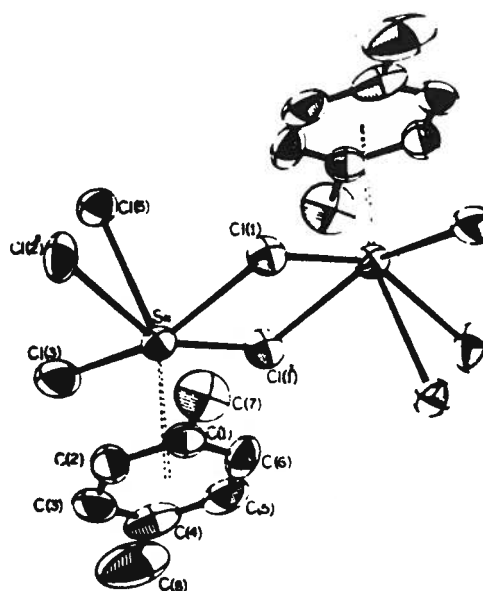
Temperature [K]	$\chi_M^{\text{corr}} \times 10^6 [\text{cm}^3\text{mol}^{-1}]^a$	$\mu_{\text{eff}} [\mu_B]$
81.78	410	0.52
74.24	460	0.52
69.72	560	0.56
65.25	630	0.58
60.21	690	0.58
54.20	820	0.60
47.40	980	0.61
40.00	1250	0.63
30.85	1820	0.67
25.60	2340	0.69
20.60	3070	0.71
15.85	4240	0.73
10.30	7010	0.76
6.84	11500	0.79
6.30	14800	0.86
4.32	20570	0.84
4.20	21090	0.84
3.37	22170	0.77
2.69	24300	0.72

^a Experimental MW of compound = 734.88 g mol⁻¹

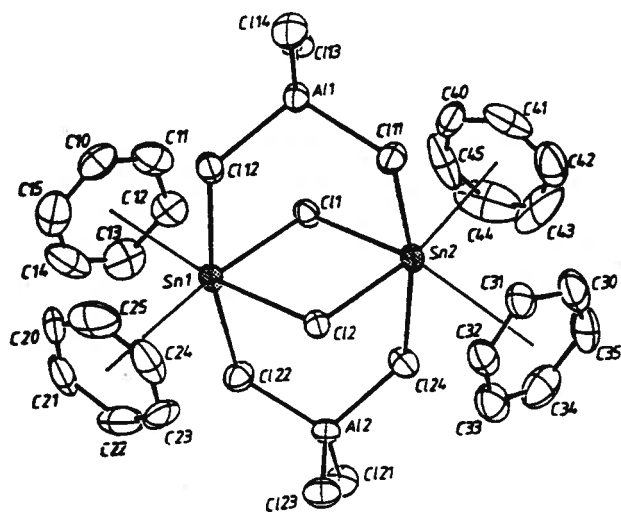
A-8: Crystal Structures of Some Arene-Sn(II) Complexes



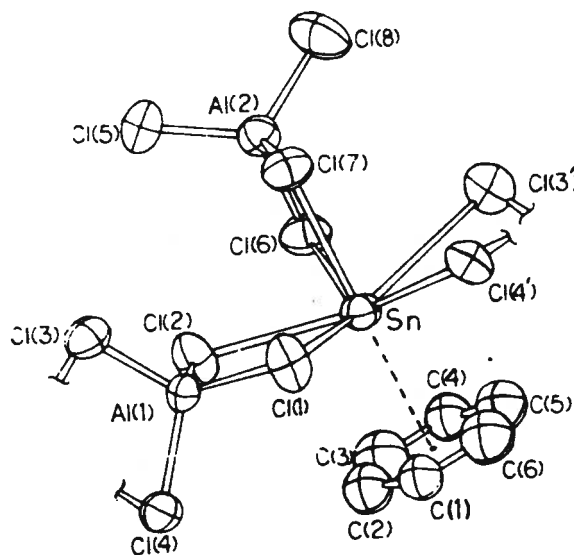
(a) $C_6H_6SnCl(AICl_4)$



(b) $p-(CH_3)_2C_6H_4SnCl(AICl_4)$

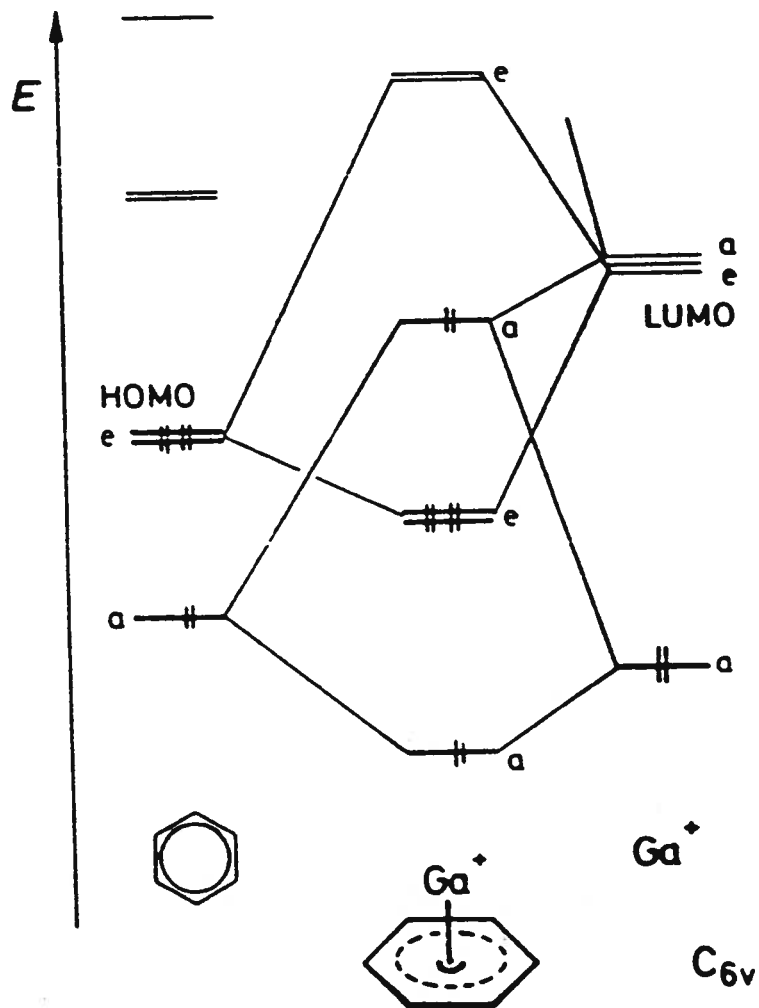


(c) $[(C_6H_6)_2SnCl(AICl_4)]_2$



(d) $C_6H_6Sn(AICl_4)_2 \cdot C_6H_6$

A-9: Qualitative MO Diagram of [(arene)Ga]⁺ Complex (C_{6v} Symmetry)



APPENDIX B

B-1: Low Temperature Magnetic Data of Ni(SO₃F)₂ at Magnetic Field = 7501 G

Temperature [K]	$\chi_M^{\text{corr}} \times 10^6$ [cm ³ mol ⁻¹]	μ_{eff} [μ_B] ^a
81.61	15470	3.18
77.72	16310	3.18
74.19	17180	3.19
69.49	18380	3.20
65.19	19700	3.21
59.86	21590	3.22
54.00	23950	3.22
47.60	27460	3.23
40.02	33160	3.26
30.35	45210	3.31
25.75	55730	3.39
20.48	73180	3.46
15.75	104700	3.63
10.42	200000	4.08
7.04	417400	4.85
6.30	534400	5.19
5.18	726200	5.49
4.78	813200	5.58
4.40	873100	5.54
4.32	879100	5.51
3.37	963100	5.10
2.89	1017000	4.85
2.69	1041000	4.73

^a Uncorrected for TIP

B-2: Low Temperature Magnetic Data of Pd(SO₃F)₂ at Magnetic Field = 9625 G

Temperature [K]	$\chi_M^{\text{corr}} \times 10^6$ [cm ³ mol ⁻¹]	μ_{eff} [μ_B] ^a
81.50	18900	3.51
77.89	19840	3.52
70.17	22590	3.56
60.50	27090	3.62
54.40	30610	3.65
47.90	36090	3.72
40.30	45460	3.83
31.50	64760	4.04
7.42	875200	7.21
5.64	955100	6.56
4.32	984400	5.83
3.54	998000	5.32
2.60	1006000	4.57
2.20	1010000	4.22
1.84	1013000	3.86

^a Uncorrected for TIP

**B-3: Low Temperature Magnetic Data of Pd(II)[Pd(IV)(SO₃F)₆] at
Magnetic Field = 9625 G**

Temperature [K]	$\chi_M^{\text{corr}} \times 10^6$ [cm ³ mol ⁻¹]	μ_{eff} [μ_B] ^a
82.33	21070	3.73
74.98	23360	3.74
61.00	30070	3.83
48.60	38330	3.86
32.10	59150	3.90
22.30	96310	4.14
12.15	285700	5.27
6.84	537300	5.42
5.08	604400	4.96

^a Uncorrected for TIP

B-4: Low Temperature Magnetic Data of Ni(II)[Sn(IV)(SO₃F)₆]

Temperature [K]	$\chi_M^{\text{corr}} \times 10^6$ [cm ³ mol ⁻¹]	μ_{eff} [μ_B] ^a
81.56	16610	3.29
77.83	17460	3.30
73.91	18470	3.30
69.49	19560	3.30
65.02	20830	3.29
59.98	22600	3.29
53.85	24950	3.28
47.45	28330	3.28
40.30	33300	3.28
30.70	43750	3.28
25.85	51580	3.27
21.05	63720	3.28
15.50	85710	3.26
10.06	134900	3.30
6.44	223400	3.39
4.46	321200	3.39
4.24	340600	3.40

^a Uncorrected for TIP
Magnetic field = 7501 G

B-5: Low Temperature Magnetic Data of Cu(II)[Sn(IV)(SO₃F)₆]

Temperature [K]	$\chi_M^{\text{corr}} \times 10^6$ [cm ³ mol ⁻¹]	μ_{eff} [μ_B] ^a
81.50	6540	2.06
77.83	6830	2.06
74.08	7100	2.05
69.83	7550	2.05
65.31	8010	2.05
60.09	8600	2.03
54.10	9520	2.03
47.55	10700	2.02
40.00	12730	2.02
30.80	16280	2.00
26.10	19360	2.01
21.35	23630	2.01
16.15	30650	1.99
10.48	46260	1.97
7.19	66730	1.96
5.84	82150	1.96
5.00	95270	1.95
4.78	98560	1.94
4.32	109700	1.95
3.02	140500	1.84
2.40	168800	1.80

^a Uncorrected for TIP
Magnetic field = 9225 G

B-6: Low Temperature Magnetic Data of Ag(II)[Sn(IV)(SO₃F)₆]

Temperature [K]	$\chi_M^{\text{corr}} \times 10^6$ [cm ³ mol ⁻¹]	μ_{eff} [μ_B] ^a
81.61	5010	1.81
77.55	5230	1.80
73.68	5490	1.80
69.26	5970	1.82
64.90	6330	1.81
59.68	6890	1.81
53.12	7710	1.81
46.94	8730	1.81
40.20	10300	1.82
30.36	13640	1.82
25.30	16640	1.83
20.18	20070	1.80
15.05	26320	1.78
9.76	39680	1.76
6.44	57840	1.73
6.15	61370	1.74
5.34	68870	1.72
4.62	77760	1.70
3.96	91000	1.70
3.37	103600	1.67
2.69	112400	1.56
2.50	116200	1.52

^a Uncorrected for TIP
Magnetic field = 9225 G

B-7: Magnetic Data of Cu(SO₃F)₂ for the Temperature Range 312 to 4 K

Temperature [K] ^a	$\chi_M^{\text{corr}} \times 10^6$ [cm ³ mol ⁻¹]	μ_{eff} [μ_B] ^b
312	1830	2.08
300	1900	2.08
287	1970	2.07
272	2090	2.08
240	2350	2.08
211	2660	2.08
181	3060	2.07
152	3620	2.07
123	4460	2.07
100	5460	2.07
81.78	6500	2.05
78.06	6850	2.05
74.36	7290	2.07
69.94	7780	2.07
65.77	8320	2.08
59.98	8950	2.06
55.00	9880	2.07
48.10	11180	2.06
41.60	13100	2.08
31.80	17280	2.09
26.65	20600	2.09
21.83	25170	2.09
16.90	33010	2.11
11.13	52110	2.15
8.70	71180	2.22
5.91	77690	1.91
4.20	85130	1.69

^a First ten data points from Ref. 15, Chapter 6.

^b Corrected for TIP (TIP = 100×10^{-6} cm³ mol⁻¹, Ref 15, Chapter 6)

Magnetic Field = 9225 G